Analysis of Two Pore Channel Proteins in *Dictyostelium* Development.

A thesis submitted to the Board of the Medical Science Division, University of Oxford, in partial fulfilment of the requirements for the degree of Doctor of Philosophy

Fu-Sheng Chang

University College

Michaelmas Term 2016

Abstract

Analysis of Two Pore Channel Proteins in *Dictyostelium* Development.

Fu-Sheng Chang, University College

A thesis submitted for the degree of Doctor of Philosophy in Michaelmas Term 2016

Calcium is a ubiquitous intracellular signal responsible for controlling numerous cellular responses including development and proliferation. Calcium (Ca^{2+}) is stored in both neutral and acidic stores and its release through gated channels has been implicated in regulating development in *Dictyostelium discoideum*. This thesis aims to understand the roles of the calcium channel proteins, in particular the two-pore channel proteins (TPCs), found on acidic stores in Ca^{2+} signalling during *Dictyostelium* development.

Bioinformatic analysis indicates conservation of a gene encoding an orthologue of TPC2 in *Dictyostelia* and, similar to plant TPCs, a Ca^{2+} sensing domain is predicted along with a novel potential calmodulin binding site. To investigate the role of intracellular Ca^{2+} channels, a series of strains was generated, disrupted in one or more of genes encoding the channels TPC2 and mucolipin (TRP-ML), predicted to be located on acidic stores, and IplA, located on neutral stores. All disrupted strains, including one lacking all three channels, are able to complete development. However, strains lacking TPC2 show a pronounced delay in early development, correlating with reduced expression of some early developmental genes. Vesicles derived from *tpc2*-null cells show normal Ca^{2+} release compared to parental cells but an increased rate of Ca^{2+} uptake. During early development, the pH of acidic vesicles is increased in the absence of TPC2. However development of *tpc2*-null cells showed increased sensitivity to weak bases in producing fewer aggregates but resistance to sodium chloride and weak bases in later development suggesting a complex role for TPC during development.

In vivo cytosolic Ca^{2+} responses were analysed in strains expressing an ultra-sensitive Ca^{2+} indicator YC-Nano 15. Growing *tpc2*$^{-}$ and *iplA*$^{-}$ cells have lower basal cytosolic Ca^{2+} than parental Ax2 cells. Intercellular Ca^{2+} waves were observed in aggregates from Ax2, *mcln*$^{-}$ and *tpc2*$^{-}$ cells but were greatly reduced in *iplA*$^{-}$ aggregates, as was the increase in cytosolic Ca^{2+} in response to extracellular cAMP. In *tpc2*$^{-}$ aggregates, wave frequencies were reduced and the response to cAMP addition abolished after treatment with caffeine, a known adenylyl cyclase inhibitor in *Dictyostelium*.

This work demonstrates that TPC2 plays a role in the early stages of *Dictyostelium* development. TPC2 is important for pH regulation in acidic vesicles and cytosolic Ca^{2+} levels, either or both of which could influence development either directly or via changes in early developmental gene expression.

Acknowledgements

Firstly, I would like to thank my dearest supervisor Catherine Pears. I am grateful for all your warm support and guidance throughout the journey of my DPhil. Thank you for always being so kind and patient. I could not imagine that I would have finished this thesis without you! Thank you Antony Galione, Julian Gross and Nick Lakin for your kind support and supervision. You always gave me nice advice and encouragement, thank you!

Thank you Clive Garnham, Anthony Morgan and Lianne Davies for your kind help at Department of Pharmacology. Your teaching, support and help have made this thesis possible.

I would also like to thank my dear friends and colleagues in the laboratory, Anne-Marie Couto, Peggy Paschke, Li-Yao Huang, Laura Matthews, Lena Kolb, Huajiang Xiong, Duen-Wei Hsu, Alina Rakhimova, Alastair Gunn, George Ronson, Ellie Warren, Iza Bombik, Eric Liang, Anna Motnenko, Guifeng Wei, Tianyi Zhang, Seiji Ura, and Amanda Unsworth. Also thank you, Keiko Watanabe, for guiding me through the details of experiments and giving me good advice for initiating my research.

I gratefully acknowledge my dearest friends, Zhiqiao Wang, Na Wu, Ruby Chen, Yu-Fen Chang, Min-Wen Chung, Chloe Tsai, Porky Fan, Elizabeth Huang, Yung-Kang Peng, Bo-Shiuan Li and I-Chun Yeh for your warm support, company and friendship, which provided the strength and fortitude for me to complete this journey.

I would also like to thank my College Chaplain, Andrew Gregory, and my College Domestic Bursar, Angela Unsworth, who kindly provided me support both emotionally and financially when I was facing the darkest and most difficult period of my life and bereavement. I will remember this forever, thank you.

This thesis is to dedicate to the memory of my father, Hung-Ping Chang, who always believed in me, and that I could succeed in the path of academia. To fulfill my dream of studying abroad, he had provided me all the best things he could do. You are gone but you are always there in my heart. I would also like to dedicate this thesis to my dearest mother, Ning-Ling Ju, and sister, Jung-Wen Chang. You are always my best family and the purpose that I am carrying on. I love you and thank you!

ABBREVIATIONS

AA	arachidonic acid
acaA	adenylyl cyclase A
ATP	adenosine 5'-triphosphate
BLAST	basic local alignment search tool
BSA	bovine serum albumin
bsR	blasticidin resistance
cADPR	cyclic adenosine diphosphate ribose
CaM	calmodulin
cAMP	adenosine 3', 5'- cyclic monophosphate
CAR	cAMP receptor
cDNA	complementary DNA
cGMP	cyclic guanosine 3', 5' monophosphate
CAX	Ca^{2+}/H^{+} cation exchanger
CICR	calcium-induced calcium release
CMA	concamycin A
CRAC	calcium-release activated calcium channel
CV	contractile vacuole
DAG	diacylglycerol
DIF	differentiation inducing factor
DMSO	dimethyl sulfoxide
DTT	dithiothreitol
dscA	discoidin A

EDTA	ethylenediaminetetra-acetic acid
EGTA	ethyleneglycol-bis-(β-amino ethyl ether)-N,N,N',N' tetra-acetic acid
ER	endoplasmic reticulum
FA	fatty acid
FBS	foetal bovine serum
gDNA	genomic DNA
G418	geneticin
GFP	green fluorescent protein
GPCR	G protein-coupled receptor
HEPES	N-2-hydroxyethyylpiperazine-N'-2-ethanesulphonic acid
IP_3	inositol 1,4,5-trisphosphate
IplA	IP_3 receptor–like protein
IPTG	isopropyl β-D-thiogalactopyranoside
IP_3R	inositol 1,4,5-trisphosphate receptor
kDa	kilodaltons
LGCC	ligand-gated calcium channel
LvsA	large volume sphere A
Mb	megabases
MBS	m-maleimidobenzoyl-N-hydroxysuccinimide ester
MCR	mutiple cloning site
mRNA	messenger RNA
MW	molecular weight

mucolipin	TRPML channel
NAADP	nicotinic acid adenine dinucleotide phosphate
NADP	nicotinamide adenine dinucleotide phosphate
NCKX	Na^+/Ca^{2+}-K^+ exchangers
NCXs	Na^+/Ca^{2+} exchangers
NLS	nuclear localization signal
NP-40	nonidet P-40
ORF	open reading frame
PAT1	P-type Ca^{2+} ATPase 1
PBS	phosphate buffered saline
PCR	polymerase chain reaction
PIP_2	phosphatidylinositol 4,5-bisphosphate
PIP_3	phosphatidylinositol 3,4,5-trisphosphate
PI3K	phosphatidylinositol-3-kinase
PKA	cAMP-dependent protein kinase A
PLA_2	phospholipase A2
PLC	phospholipase C
PldB	phospholipase D homologue
PMCAs	plasma membrane Ca^{2+}-ATPases
pdsA	cAMP phosphodiesterase
PTP3	protein tyrosine phosphatase-3
P2X	ATP-gated P2X Receptor Cation Channel
PUFAs	polyunsaturated fatty acids
RNA	ribonucleic acid

ROC	receptor-operated channel
RT	reverse transcriptase
RyR	ryanodine receptor
SDS	sodium dodecyl sulphate
SDS-PAGE	sodium dodecyl sulphate polyacrylamide gel
SERCA	sarco (endo) plasmic reticulum calcium ATPase
SMOC	second messenger operated Ca^{2+} channel
SOC	store-operated channel
SOCE	store-operated calcium entry
SPCAs	secretor-pathway Ca^{2+}-transport ATPases
SPF	rabbit specific pathogen free rabbit
STIM	stromal interaction molecule
TAE	Tris-acetate-EDTA buffer
tBHQ	tert-Butylhydroquinone
Tg	thapsigargin
TGN	trans Golgi network
TKR	tyrosine-kinase receptors
TMD	transmembrane domains
TPC	Two-pore channel
Tris	2-amino-2-(hydroxymethyl-)1,2-propanediol
TRP	transient receptor potential
TRPA	transient receptor potential ankyrin

TRPC	transient receptor potential canonical
TRPM	transient receptor potential melastatin
TRPN	transient receptor potential no mechanoreceptor potential C
TRPP	transient receptor potential polycystin
TRPV	transient receptor potential vanilloid
VGCC	voltage-gated calcium channel
XeC	xestospongin C
X-gal	5-bromo-4-chloro-3-indolyl- β-D-galactoside
yakA	*Dictyostelium* protein kinase yakA
YC-Nano 15	Yellow Cameleon Nano 15

Table of Contents

CHAPTER 1: General Introduction

1.1 Calcium signalling

Calcium (Ca^{2+}) has emerged as one of the most essential and versatile second messengers for regulating a wide spectrum of cellular functions early in evolution of eukaryotes (Berridge *et al.*, 2000; Plattner and Verkhratsky, 2013). Calcium signalling involves transient increases in cytosolic calcium and is essential for a large number of cellular responses including cell division, cell growth, cell motility, differentiation and morphogenesis (Poloz and O'Day, 2012; Tu *et al.*, 2004). Many organisms have evolved a wide range of ion channels, pumps and exchangers to allow precise and versatile Ca^{2+} signals to be generated. Many proteins respond to changes in calcium levels including, but not limited to, those equipped with a domain that binds calcium known as an EF-hand domain, such as calmodulin, and troponin C. The conformational change caused by binding of Ca^{2+} can activate these proteins and trigger a plethora of cellular responses that effect downstream signalling essential for cell physiology such as apoptosis, muscle contraction, cell movement, exocytosis, metabolism, proliferation, secretion, fertilization and transcription(Berridge *et al.*, 2003) . Figure 1.1 shows Ca^{2+} channels, pumps and exchangers located on the plasma membrane and/or membranes of intracellular organelles responsible for orchestrating a complex system of Ca^{2+} signalling.

1.1.1 Ca^{2+} homeostasis

The calcium concentration in the cytosol is normally maintained at a low level. Ca^{2+} is efficiently removed from the cytosol unlike other similar ions such as Mg^{2+}. The main reason for this might be that Ca^{2+} has a tendency to precipitate phosphates, such as ATP and nucleic acids, which would be incompatible with life, so it is avidly excluded from the cytosol. It has been proposed that cells probably firstly evolved strategies for

binding or excluding calcium to reduce its level in the cytosol, and these later evolved to be used for signal transduction in eukaryotic cells (Clapham, 1995).

Maintaining a low level of intracellular Ca^{2+} requires Ca^{2+} pumps and exchangers to extrude Ca^{2+} to the extracellular space or sequester it into intracellular stores. The following section contains a brief review of the intracellular Ca^{2+} stores and the pumps and exchangers which cells use for maintaining a low basal cytosolic Ca^{2+} level, $[Ca^{2+}]c$.

1.1.1.1 Intracellular Ca^{2+} stores

A number of organelles are used as calcium stores inside eukaryotic cells. Based on the luminal pH and the presence of Ca^{2+} ions, the organelles can be categorised as acidic and neutral Ca^{2+} stores. Acidic stores include acidocalcisomes, vacuoles, endosomes, lysosomes, lysosome-related organelles, secretory granules and the Golgi complex (Patel and Docampo, 2010). On the other hand, Ca^{2+} stores that have relatively neutral pH are called neutral stores and include the endoplasmic reticulum (ER), sarcoplasmic reticulum (SR) in muscle cells and the nuclear envelope (Koch, 1990; Petersen *et al.*, 1998). Calcium uptake into acidic calcium stores is mediated by either calcium pumps or exchangers. Calcium stores also possess several calcium-permeable channels such as members of the transient receptor potential superfamily, the two-pore channels (TPCs) and inositol-1,4,5-trisphosphate (IP_3) and ryanodine (RyR) receptors in order to effect calcium release.

Mitochondria are essential for cell function as they generate ATP. However, they also serve as an important cytosolic Ca^{2+} buffer. Their Ca^{2+} channels, voltage dependent

anion channels (VDAC) and the calcium uniporter (MCU) are able to take up Ca^{2+} released from other stores, for example from IP_3 receptors (IP_3R) on the ER (Figure 1.1). This is important for the function of IP_3Rs since this prevents negative feedback by $[Ca^{2+}]c$ and, thus, IP_3R activity can be sustained and Ca^{2+} release from the ER is prolonged. After Ca^{2+} is taken up by the mitochondria, it regulates important functions such as aerobic metabolism and autophagy (Rizzuto *et al.*, 2012).

1.1.1.2 Intracellular Ca^{2+} pumps and ion exchangers

A series of P type Ca^{2+} ATPases, such as the plasma membrane Ca^{2+}-ATPase (PMCA), sarco/endoplasmic reticulum Ca^{2+}-ATPase (SERCA) and secretory pathway Ca^{2+} ATPase (SPCA), act as pumps to remove Ca^{2+} from the cytosol or into the Ca^{2+} stores (Carafoli, 1991).

There are also a variety of ion exchangers, in particular the cation/Ca^{2+} (CaCA) superfamily of exchangers that are specialised calcium transporters, which play an essential role in calcium signalling via regulating the concentrations of Ca^{2+} and other cations between two cellular compartments. These exchangers including K^+-independent Na^+/Ca^{2+} exchangers (NCXs), K^+-dependent Na^+/Ca^{2+} exchangers (NCKX), cation/Ca^{2+} exchangers (CCX) and Ca^{2+} / H^+ exchanger (CAX). CaCA superfamily members have been identified in bacteria, archaea, fungi, animals and plants (Cai and Lytton, 2004; Lytton, 2007) (Figure 1.1).

Ion exchangers are not only found on the plasma membrane but also on acidic stores. For example, as with plant vacuoles, the large concentration gradient of protons across the lysosomal/endosomal membrane can drive calcium ions into the lumen via an

antiport mechanism (Patel and Docampo, 2010). In yeast and plant vacuoles, as well as the contractile vacuoles of *Dictyostelium*, this process is mediated by CAXs (Cunningham and Fink, 1996; Hirschi *et al.*, 1996; Rooney and Gross, 1992). Interestingly, although the genes encoding CAXs are present in the genomes of some animals (e.g. amphibians and fish), they are absent from mammalian genomes (Shigaki *et al.*, 2006). Thus, the net Ca^{2+}/H^{+} exchange activities measured in mammalian endosomes most likely results from the concerted activity of Na^{+}/H^{+} exchangers and Na^{+}/Ca^{2+} exchangers.

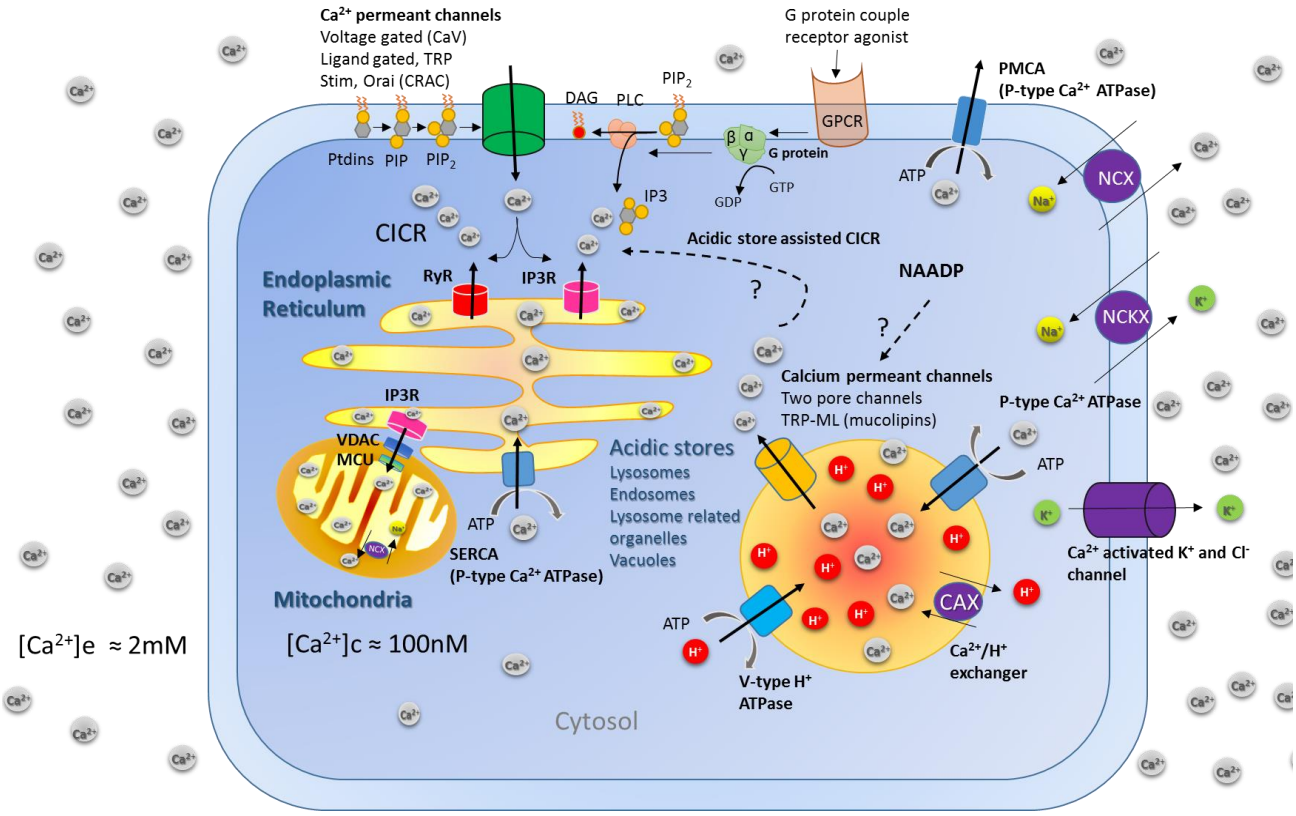

Figure 1.1 Overview of intracellular Ca^{2+} signalling.
The endoplasmic reticulum (ER) and acidic stores (lysosomes, endosomes, lysosomal related organelles and vacuoles) function as Ca^{2+} stores in the centre of Ca^{2+} signalling. The cytosolic Ca^{2+} level is low in resting cells, which is usually maintained at 100 nM by extrusion via plasma membrane Ca^{2+} ATPase (PMCA) and sarco/endoplasmic reticulum Ca^{2+} ATPase (SERCA) transporters. The Na/Ca^{2+} exchanger (NCX), acts as a major secondary regulator of [Ca^{2+}] via exchanging 3 Na^+ ions for 1 Ca^{2+}. Intracellular Ca^{2+} hyperpolarizes cells by activating K^+ channels, and in some cells, Cl^- channels. This decreases CaV channel activity but increases the driving force across active Ca^{2+}-permeant channels. In excitatory Ca^{2+} signalling system, plasma membrane ion channels are triggered to open by changes in voltage, or extra- or intracellular ligand binding. Initial increases in [Ca^{2+}] trigger more release, primarily from ER via Ca^{2+}-sensitive ryanodine receptors (RyR), termed Ca^{2+}-induced Ca^{2+} release (CICR). G protein-coupled receptor (GPCR) or receptor tyrosine kinase (RTK) -mediated activation of PLC cleaves PIP_2 into inositol (1,4,5) trisphosphate (IP_3) and diacylglycerol (DAG). IP_3 is a ligand for the intracellular IP_3R channel which spans the ER membrane. GPCRs catalyse the exchange of guanosine diphosphate (GDP) for GTP on Gα subunits, releasing active Gα and Gβγ subunits that in turn activate PLCβ. RTKs dimerize upon ligand binding, autophosphorylate, and interact with other signalling proteins to activate PLCγ. The acidic stores are another major Ca^{2+} store, sequestering cytosolic Ca^{2+} via P-type ATPase. The acid stores contain V-type H^+ ATPases to maintain a lower pH. Ca^{2+}/H^+ exchanger regulates the homeostasis of Ca^{2+} and H^+ in the lumen. Ca^{2+} ions are release from channels including TPC and TRP-ML, which are proposed to be activated by nicotinic acid adenine dinucleotide phosphate (NAADP) directly or indirectly, which releases Ca^{2+} and is proposed to assist the priming of CICR from ER and RyR. Mitochondria are important for maintaining Ca^{2+} homeostasis by taking up Ca^{2+} released from the ER. Important mitochondrial channels are shown, where cytoplasmic Ca^{2+} ions released by ER enter the mitochondria through voltage dependent anion channels (VDAC) and calcium uniporter (MCU). Modified from (Clapham, 2007).

1.1.2 Ca^{2+} influx through plasma membrane

In order to introduce extracellular Ca^{2+} into the cytosol, the plasma membrane is equipped with many types of ion channels that are named and categorised by their mechanisms of activation. For example, Ca^{2+} channels which are activated by changes in membrane potential are named voltage-operated Ca^{2+} channels (VOCs), also VGCCs or CaVs. Similarly, Ca^{2+} channels that are activated by ligand-receptor binding are called receptor-operated channels (ROCs) or ligand-gated Ca^{2+} channels (LGCCs). The distribution of Ca^{2+} channels in the plasma membrane reflects the nature of cells and whether they are electrically excitable (e.g. neurons, cardiomyocytes, smooth muscle cells) or non-excitable (e.g. T-lymphocytes). In excitable cells, VGCCs comprise the major route for Ca^{2+} influx, with some contribution from LGCCs. In non-excitable cells, Ca^{2+} entry is achieved largely by store-operated calcium channels (SOCs), which are activated by depletion of the intracellular calcium stores within the ER/SR through Ca^{2+}-release activated channels (CRACs), STIM1/Orai complex, and second-messenger operated Ca^{2+} channels (SMOCs) (Berridge *et al.*, 2003). However, the distribution of VGCCs and SOCCs is not mutually exclusive, since SOCCs are also found in muscle cells (Lyfenko and Dirksen, 2008) and VGCCs are found in T-lymphocytes (Kotturi and Jefferies, 2005) although to a lesser extent.

Human cells have genes encoding plasma membrane Ca^{2+} channels that are gated by different mechanisms, including VGCC that are activated by plasma membrane depolarization, and transient receptor potential (TRP) channels which are often regulated by different sensory inputs such as cold, heat and mechanical stress. Moreover, there are a group of channels operated by agonists, which are called agonist-operated channels (AOCs), such as cyclic nucleotide-gated channels (CNGCs),

belonging to the SMOCs, that are typically opened by cAMP or cGMP, and glutamate receptor channels, belonging to LGCCs and responding to the extracellular presence of the amino acid glutamate (Figure 1.2)

The mechanisms by which Ca^{2+} can enter the cell through plasma membrane Ca^{2+} channels are briefly described below.

1.1.2.1 Store-operated Ca^{2+} entry (SOCE)

When the intracellular Ca^{2+} stores, such as the ER, are depleted of Ca^{2+}, SOCE is triggered. SOCE, also called capacitative Ca^{2+} entry, was a concept firstly proposed (Putney, 1986) in which the concerted control of both Ca^{2+} release from intracellular stores and Ca^{2+} influx from the extracellular space orchestrates Ca^{2+} homeostasis. Ca^{2+} influx is modulated by the capacity of the cell to hold Ca^{2+} ions. Entry of extracellular Ca^{2+} upon store depletion was later suggested to be mediated by CRACs (Hoth and Penner, 1992). More recently, essential components of this process such as STromal Interaction Molecule 1 (STIM) and Orai were identified (Roos *et al.*, 2005; Zhang *et al.*, 2006; Zhang *et al.*, 2005), which enable the reconstitution of CRAC channels that mediate SOCE. (Zhang *et al.*, 2006)

STIM1 is located on the membrane of the ER/SR as the intracellular CRAC component that acts as the Ca^{2+} sensor. The plasma membrane protein Orai1 forms the pore of the CRAC channel. In basal conditions, the intraluminal EF-hand of STIM1 is occupied by Ca^{2+}. Upon Ca^{2+} depletion from the ER/SR, STIM1 molecules aggregate closer to Orai1 channels on plasma membrane. STIM1 then activates Orai1 via the STIM1-Orai activating region or CAD to facilitate Ca^{2+} influx (Feske and Prakriya, 2013). Ca^{2+}

influx is essential for regulating a number of kinetically distinct processes involving gene regulation, exocytosis, enzyme control, cell growth and proliferation, and apoptosis. Capacitative Ca^{2+} entry appears to also be a major means of signal transduction.

Recently, another mechanism of calcium influx has been found to cause inhibition of some types of VGCCs such as L-type CaV1.2 (Park *et al.*, 2010; Wang *et al.*, 2010) and T-type CaV3.1 channels (Nguyen *et al.*, 2013). This emergent mechanism is via "store-inhibited channels (SIC)" (Moreno and Vaca, 2011).

1.1.2.2 Ca^{2+} entry through voltage gated Ca^{2+} channels (VGCC)

VGCCs form one of the major routes for Ca^{2+} influx in excitable cells, in response to membrane potential changes. This leads to intracellular Ca^{2+} transients that then initiate many important physiological events such as generation of excitation-contraction coupling in cardiac, skeletal and smooth muscle cells (Catterall, 2011; Navedo and Santana, 2013; Tuluc and Flucher, 2011), and fast neurotransmission at nerve terminals (Bezprozvanny *et al.*, 1995). There are 10 members of the VGCC family in mammals, which play distinct roles in cellular signal transduction. The overall VGCC structure is similar for all family members consisting of a multimeric complex. The main component is the pore forming α1 subunit coupled together with a number of VGCC-associated subunits (α2, β, δ and γ) (Figure 1.3). The Ca_V1 subfamily initiates regulation of gene expression, secretion, contraction, integration of synaptic input in neurons, and synaptic transmission at ribbon synapses in specialized sensory cells. The Ca_V2 subfamily is chiefly responsible for initiation of synaptic transmission at fast

synapses. The Ca_V3 subfamily is essential for repetitive firing of action potentials in rhythmically firing cells such as cardiac myocytes and thalamic neurons (Table 1.1).

It is noteworthy that the CaV1.1 L-type Ca^{2+} channel acts significantly differently from other CaV1 family members. In skeletal muscle, CaV1.1, somewhat strangely, exerts a stimulatory effect without gating Ca^{2+} across the sarcolemma. Instead, the channel acts indirectly by activating the type 1 ryanodine receptors (RyR1s) to release Ca^{2+} from the SR. Upon membrane depolarization, the L-type channel undergoes a conformational change that is transferred to the RyR1 through a direct protein-protein interaction. This conformational coupling mechanism ensures that membrane depolarization results in a very rapid activation of the RyR1s to release the Ca^{2+} signal activating muscle contraction (Berridge, 2014). In smooth and cardiac muscle, the other CaV1 isoforms serve as conventional voltage-gated Ca^{2+} channels. For example, in heart cells, the CaV1.2 L-type channels play an important role in the process of excitation-contraction coupling by providing a brief pulse of Ca^{2+} that is responsible for activating the underlying RyR2s via the process of Ca^{2+}-induced Ca^{2+} release (CICR). The initial brief trigger pulse of Ca^{2+} has been called a sparklet and can be clearly seen at the leading edge of the larger Ca^{2+} spark (Berridge, 2014).

Table 1.1 Voltage-gated Ca^{2+} channels (VGCCs) consist of three families.

VGCC	Subunit and gene	Pharmacology	Tissue distribution	Conductance (pS)	Activation threshold (mV)
Ca_V1 family					
$Ca_V1.1$ L-type	α_{1S} subunit	Dihydropyridine	Skeletal muscle and CNS	11-25	~ −30
$Ca_V1.2$ L-type	α_{1C} subunit *CACNA1C*	Dihydropyridine	Heart, CNS and endocrine cells	11-25	~ −30
$Ca_V1.3$ L-type	α_{1D} subunit	Dihydropyridine	CNS and endocrine cells	11-25	~ −30
$Ca_V1.4$ L-type	α_{1F} subunit		Retina	11-25	~ −30
Ca_V2 family					
$Ca_V2.1$ P/Q-type	α_{1A} subunit	ω-Agatoxin	CNS, neuromuscular junction	10-20	~ −30
$Ca_V2.2$ N-type	α_{1B} subunit	ω-Conotoxin	CNS, neuromuscular junction	16	~ −30
$Ca_V2.3$ R-type	α_{1E} subunit	SNX-482	CNS, neuromuscular junction	12	~ −30
Ca_V3 family					
$Ca_V3.1$ T-type	α_{1G} subunit	Kurotoxin	CNS, heart, smooth muscle	7	~ −60 to −70
$Ca_V3.2$ T-type	α_{1H} subunit	Kurotoxin, Mibefradil	CNS, heart, liver, kidney, zona glomerulosa	5	~ −60 to −70
$Ca_V3.3$ T-type	α_{1L} subunit		CNS	11	~ −60 to −70

Summary of the terminology, classification and properties of voltage-gated Ca^{2+} channels (VGCCs). The Ca_v1 family of L-type channels, the Ca_v2 family of N-type, P/Q type and R-type channels, and the Ca_v3 family of T-type channels. CNS, central nervous system. Adapted from (Berridge, 2014).

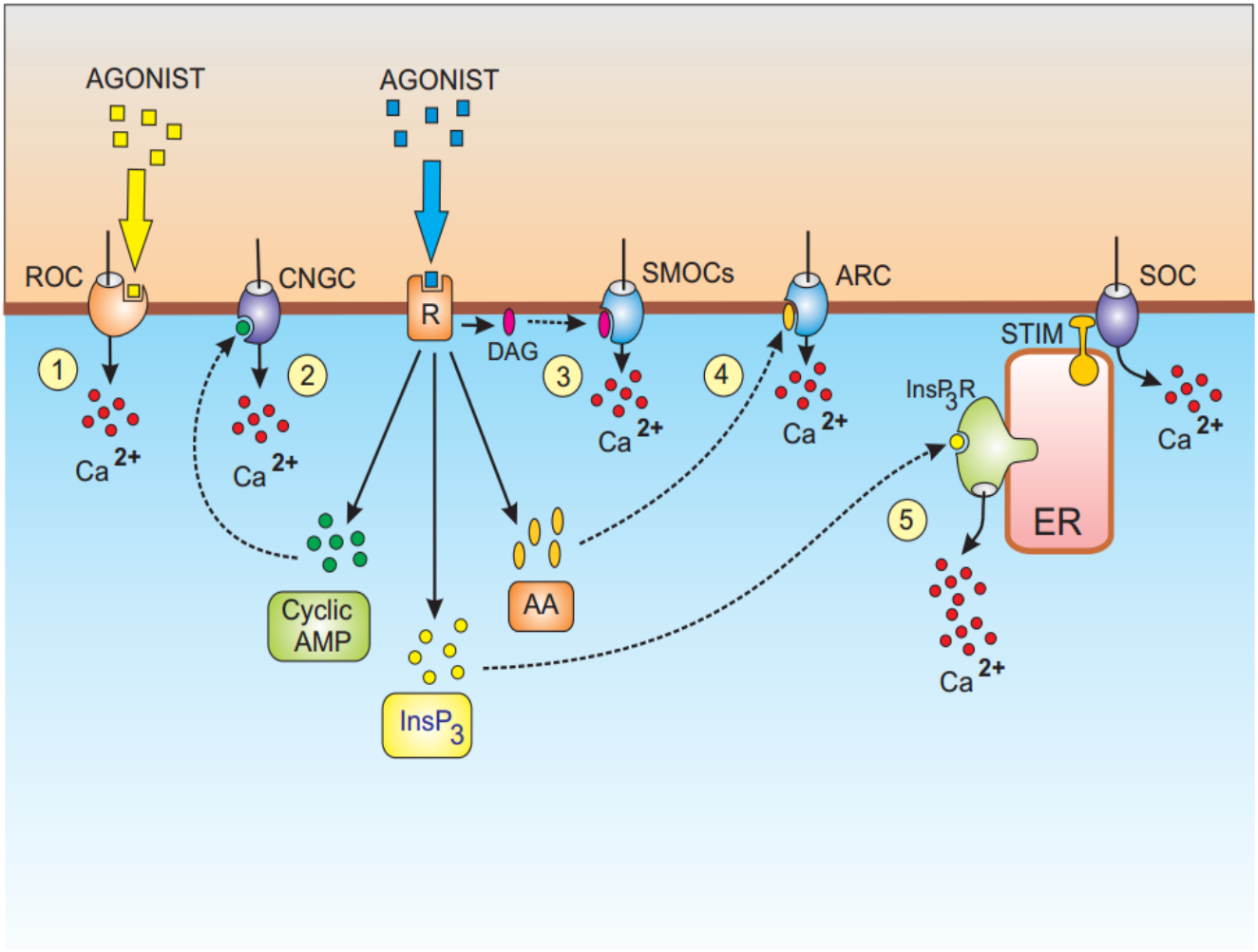

Figure 1.2 Entry of Ca^{2+} through agonist-operated channels.
Entry of external Ca^{2+} can be activated by stimuli arriving at the cell surface or by signals generated within the cell. The most direct mechanism occurs in the receptor-operated channels (ROCs), where the agonist binds directly to the ion channel. Agonists can also activate entry indirectly by recruiting various internal signalling pathways to activate second messenger-operated channels (SMOCs) or a store-operated channel (SOC) as described in the text. CNGC, cyclic nucleotide gated channels, ARC, arachidonic acid-regulated Ca^{2+} channels. AA, arachidonic acid. The diagram is adapted from (Berridge, 2014).

A.

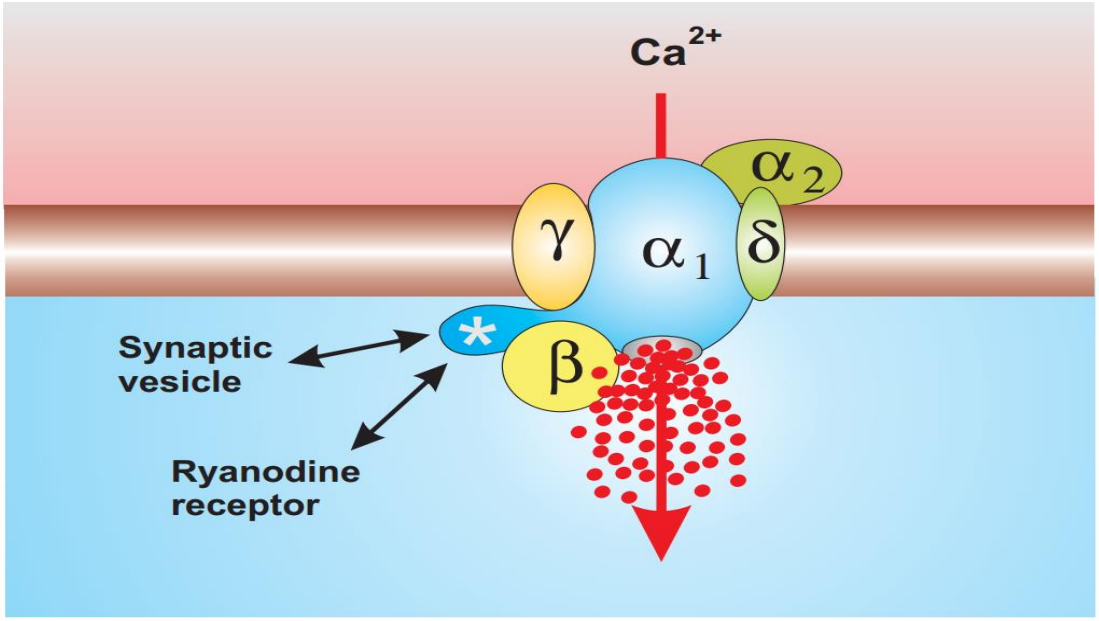

B.

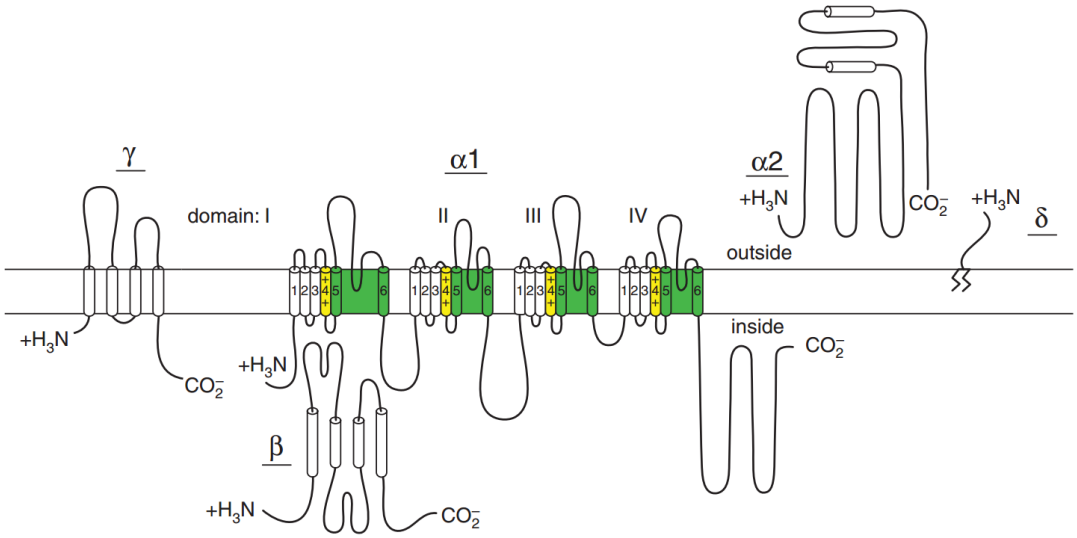

Figure 1.3 Subunit structure of voltage-gated Ca^{2+}channels (VGCCs).
(A) Structural organization of the VGCC subunits. The channel complex is based on the large α1 subunit, which contains the pore region, voltage sensor and binding sites for Ca^{2+} and drugs such as dihydropyridine (DHP). The large cytoplasmic loop (∗) on some α1 subunits links channels to synaptic vesicles or type 1 ryanodine receptor (RYR1) of skeletal muscle. The extracellular α2 subunit has numerous glycosylation sites and is linked through a disulphide bond to a δ subunit that has a single transmembrane region. The variable γ subunit is another transmembrane protein. Finally, there is an intracellular β subunit, which seems to alter the function of different channels and is the target of some of the modulatory signalling pathways. (B) Subunit structure of Ca^{2+} channels illustrated as transmembrane folding models; predicted α helices are depicted as cylinders; the lengths of lines correlate approximately to the lengths of the polypeptide segments represented; and the zigzag line on the δ subunit illustrates its glycophosphatidylinositol anchor. Adapted from (Berridge, 2014; Catterall, 2011).

1.1.2.3 Ca^{2+} entry through TRP channels

Transient receptor potential channels (TRP channels) are a group of ion channels located largely on the plasma membrane in many cell types. TRP channels are expressed and functional in a variety of organisms, including human, mice, worms, fruit flies, zebrafish and *Dictyostelium* (Venkatachalam and Montell, 2007; Wilczynska *et al.*, 2005). Many of these channels mediate a variety of sensations like vision, taste, olfaction, hearing, touch, and thermo- and osmo-sensation (Venkatachalam and Montell, 2007). The TRP superfamily is divided into groups 1 and 2, which can be further divided into seven subfamilies (Figure 1.4). Group 1 includes TRPC (canonical), TRPV (vanilloid), TRPM (melastatin), TRPN, and TRPA. In group 2, there are TRPP (polycystin) and TRPML (mucolipin). There is an eighth subfamily, TRPY, which consists of yeast TRPs that are distantly related to the group 1 and group 2 TRPs, and indicate that the origin of TRP channels predates the emergence of metazoan organisms (Venkatachalam and Montell, 2007).

The group 1 TRPs contain several conserved domains and sequence elements that are similar to other ion channels. The most conserved region spans the six transmembrane segments, including the pore loop located between the fifth and sixth (Figure 1.4 A). TRPC, TRPM, and TRPN channels also contain a TRP domain, which follows the sixth transmembrane segment (Figures 1.4 A). There are only two subfamilies TRPP and TRPML of the group 2 TRPs, which are distantly related to the group 1 TRPs. The TRPP and TRPML proteins share sequence homology over the transmembrane segments and contain a large loop separating the first two transmembrane domains (Figure 1.4B). The TRPP subfamily may be the most ancient, as members of this subfamily extend from yeast to mammals (Palmer *et al.*, 2005). Of relevance to this

thesis, it should be noted that *Dictyostelium discoideum* only has genes encoding group 2 TRP channels in its genome, which are TRPML (mucolipin) and TRPP (polycystin) (Figures 1.4 C) (Wilczynska *et al.*, 2005).

Gating mechanisms and functions of the TRPC family are diverse (Clapham, 2007). It is known TRP channels can be activated by molecules related to phospholipase C (PLC) signalling, such as phosphoinositide-4,5-bisphosphate (PIP_2), phosphatidylinositol 3,4,5-trisphosphate (PIP_3) and diacylglycerol (DAG) as well as polyunsaturated fatty acids (PUFAs), such as arachidonic acid (AA). For example, TRPC channels are mainly potentiated by PLC, activated by G protein-coupled receptors (GPCRs) or tyrosine-kinase receptors (TKRs). TRPC2, 3, 6 and 7 have been shown to be activated through a DAG-dependent mechanism. TRPV channels respond to environmental signals including pH, heat and light. On the other hand, some of the TRP channels are also activated by the environment. For example, TRPV1 is activated by capsaicin and heat, and TRPV2, 3 and 4 are also heat activated (Venkatachalam and Montell, 2007). TRPM2 is suggested to act as a sensor of intracellular oxidation/reduction. TRPM5 is a Ca^{2+}- activated non-selective cation channel found in taste receptor cells, and is involved in the production of taste sensations (Perez *et al.*, 2002). TRPA and TRPN are characterized by long chains of Ankyrin repeats which are domains that usually mediate protein-protein interactions (Hardie, 2007).

A.

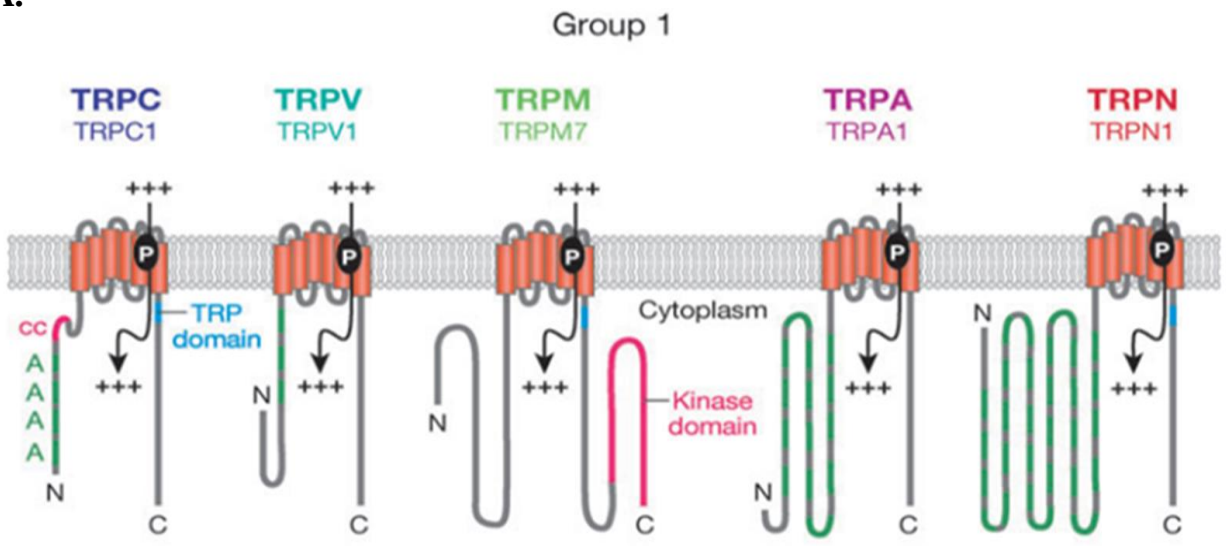

B.

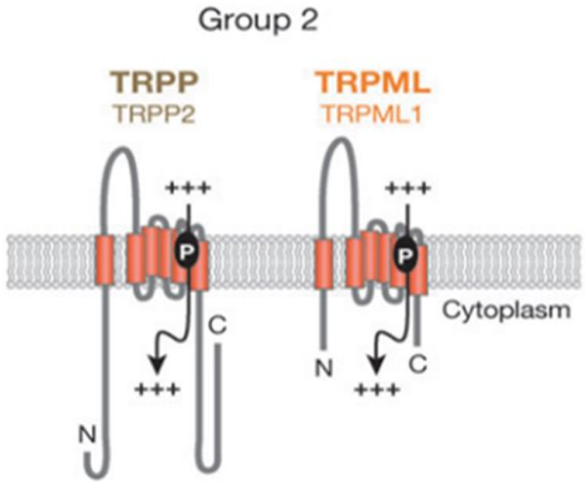

C.

	Worms	Files	Mice	Humans	*Dictyostelium*
TRPC	3	3	7	6[1]	0
TRPV	5	2	6	6	0
TRPM	4	1	8	8	0
TRPA	2	4	1	1	0
TRPN	1	1	0	0	0
TRPP[2]	1	1	3	3	1
TRPML	1	1	3	3	1
Total	17	13	28	27	2

Figure 1.4 The TRP superfamily.
(A) Single members from each of the five group 1 subfamilies. (B) Single members from each of the two group 2 subfamilies. The following domains are indicated: A, ankyrin repeats; cc, coiled-coil domain; protein kinase domain; TRP domain. Also shown are transmembrane segments (*vertical rectangles*) and pore loop (P), allowing the passage of cations (+++). (C) Composition of the TRP superfamily in worms, flies, mice, and humans. 1 Human *TRPC2* is a pseudogene and is not included. 2 TRPP1-like proteins are not included. Modified from (Venkatachalam and Montell, 2007).

1.1.2.4 Ca^{2+} entry through agonist-operated channels (AOCs)

Upon agonist arriving at the cell surface, ligand binding can also trigger Ca^{2+} influx through the plasma membrane (Figure 1.2). Receptor-operated channels include P2X receptors that bind agonists such as ATP. Neurotransmitters such as acetylcholine, glutamate and 5-hydroxytryptamine (5-HT) can interact with surface receptors that have intrinsic channel activity or interact with other receptors that trigger the production of second messengers, such as cAMP, DAG, IP_3 and AA, that in turn activate second messenger-operated channels (SMOCs). Intracellular cAMP can activate the CNGCs that operate in sensory systems (gustatory, olfactory and visual signalling pathways). DAG acting in the plane of the plasma membrane stimulates an entry channel that appears to be transient receptor potential canonical 6 (TRPC6) (Graham *et al.*, 2010). AA activates an arachidonic acid-regulated Ca^{2+} (ARC) channel (Shuttleworth, 2009).

1.1.3 Intracellular Ca^{2+} channels

On receipt of a signal Ca^{2+} can be released from intracellular stores via a number of calcium channels found on intracellular organelles, for example the IP_3R and RyR, on the ER (Berridge *et al.*, 2000), transient receptor potential – mucolipins (TRPML) channels on the endolysosomal system and plasma membrane (Puertollano and Kiselyov, 2009) and two-pore channel proteins (TPCs) on acidic stores (Calcraft *et al.*, 2009; Davis and Galione, 2013).

1.1.3.1 IP_3 receptors

The second messenger IP_3 and downstream Ca^{2+} signalling control a great number of cellular processes. For example this signalling pathway can be initiated by ligands binding to GPCRs activating the Gq alpha subunit, which stimulates PLCβ activity to hydrolyse the precursor lipid phosphatidylinositol 4,5-bisphosphate ($PI4,5P_2$ or PIP_2) to produce both IP_3 and DAG. The IP_3 that is released into the cytoplasm then functions as a second messenger to mobilize Ca^{2+} from the ER by acting on IP_3Rs which are ligand-gated Ca^{2+} channels (Berridge, 2014).

The discovery of the IP_3Rs was a great breakthrough in the field of Ca^{2+} signalling. It has been more than 30 years since the first studies described a ^{32}P-IP_3 binding activity (Spat *et al.*, 1986), soon followed by purification of IP_3Rs from cerebellum (Maeda *et al.*, 1988; Supattapone *et al.*, 1988) and then the first IP_3R subtype (IP_3R1) was cloned (Furuichi *et al.*, 1989; Mignery *et al.*, 1989). IP_3Rs are large proteins, comprising tetramers of closely-related subunits, each with about 2,700 amino acid residues. In humans there are three different IP_3Rs (IP_3R1, IP_3R2 and IP_3R3), which share a high degree of similarity in primary sequence and properties. However, different cells express them in different proportions and in different cellular locations (Berridge, 2014). The domain structure of one of the subunits reveals that the receptor is organized into three main regions. The transmembrane (TM) and pore domain embeds the receptor in the ER membrane. Similar to many ion channels, there are six TM domains, with the pore loop located between TM5 and TM6. The luminal loops of the pore are glycosylated. There is a fairly long N-terminal region that has an IP_3R-binding domain at the end, which is connected to TM1 by the modulatory domain. This modulatory loop has two important functions. Firstly, it has to transmit the conformational change

that is induced by the binding of IP_3 and Ca^{2+} down to the transmembrane region to open the pore. Secondly, it is the site where many of the modulators act to alter the properties of the release of Ca^{2+} (Berridge, 2014).

IP_3R channels are not only regulated by IP_3 but also by cytosolic Ca^{2+} in a biphasic manner (Finch *et al.*, 1991; Iino, 1987, 1990; Marshall and Taylor, 1993; Parys *et al.*, 1992). The term biphasic regulation means that low increases in cytosolic Ca^{2+} concentration enhance responses to IP_3, while higher concentrations (above about 300 nM) cause inhibitory effects. This dual control of the IP_3R by both IP_3 and Ca^{2+} is central to Ca^{2+} oscillations that are important for multiple aspects in cell signalling. The fact that the opening of the IP_3R depends upon the presence of both IP_3 and Ca^{2+} has suggested a possible role as a neuronal coincident detector (Nakamura *et al.*, 1999). However, the structural basis for Ca^{2+}-regulation of IP_3R is still not fully resolved. It may be either direct, via Ca^{2+} binding to a site intrinsic to the IP_3R or via an accessory Ca^{2+}-binding protein (Taylor *et al.*, 2004).

1.1.3.2 Ryanodine receptors

Ryanodine receptors (RyRs) in many ways are similar to IP_3Rs. Firstly, they are both localised mostly on the membrane of ER/SR. Secondly, they are also present as three isoforms, RyR1, RyR2 and RyR3. They are also very large proteins (more than 5,000 amino acids) almost twice the size of IP_3Rs (2,700 amino acids). Moreover, functional channels are also formed when four subunits associate to form homotetramers. RyRs are proposed to be activated by the ligand cyclic ADPribose (cADPR) analogous to IP_3R gating by IP_3. A critical character of both of these channels, IP_3Rs and RyRs, is that they are activated by Ca^{2+} that is derived either from outside the cell through

voltage-operated or receptor-operated channels or from internal stores via neighbouring internal channels, as occurs when these release channels release Ca^{2+} to excite each other to create intracellular Ca^{2+} waves (Berridge, 2014).

The type 1 ryanodine receptor (RyR1) is expressed predominantly in skeletal muscle, but has also been described in certain neurons such as the cerebellar Purkinje cells (Ohashi *et al.*, 2014). The major function of RyR1 is in excitation-contraction coupling in skeletal muscle. This coupling depends upon the CaV1.1 L-type channel in the T-tubule membrane that makes direct contact with RyR1 located in the underlying SR membrane. The gap is spanned by the large cytoplasmic head of RyR1, which makes contact with four L-type channels. Depolarising the T-tubule induces a conformational change in the L-type Ca^{2+} channels which then act to open the RyR1 channel through a direct protein--protein interaction. This opening process is quite remarkable since Ca^{2+} entry through Cav1.1 is not required which is different from other conventional calcium channels (Proenza *et al.*, 2002).

Type 2 ryanodine receptors (RyR2) form one of the major Ca^{2+} release channels that functions in a broad range cell types, such as cardiac muscle, smooth muscle, and many neuronal cells. Like the other RyRs, the functional channel is a homotetramer, with the C-terminal transmembrane domains embedding the subunits in the ER/SR membrane and the large N-terminal region forming a bulbous head that functions as a scaffolding protein that binds a large number of regulatory components. The cAMP signalling pathway has been implicated in the modulation of RyR2 activity, where the cyclic AMP dependent protein kinase A (PKA) interacts with RyR2 to phosphorylate Ser-

2809. Dephosphorylation is carried out by phosphatases that are also in a complex with this channel (Marx *et al.*, 2000).

Compared to RyR1 and RyR2, much less is known about type 3 ryanodine receptor (RyR3). Recently, a study indicated that RyR3 is the major isoform expressed in neural stem cells in the hippocampus (Chung *et al.*, 2016). In the case of the interstitial cells of Cajal, it may play a role in the initiation of the cytosolic Ca^{2+} oscillator (Berridge, 2014).

Recent studies have observed that not only cytosolic but also the luminal concentration of Ca^{2+} in the ER/SR seems to play an important role in regulating the activity of both IP_3Rs and RyRs. The major consequence of this luminal effect is to adjust the sensitivity of these two release channels to the stimulatory effect of Ca^{2+} (Berridge, 2014). In the past, it was believed that cardiac calsequestrin (CASQ2), an SR luminal Ca^{2+}-binding protein, as well as junctin and triadin, serves as the key SR luminal Ca^{2+} sensor (Gyorke *et al.*, 2004; Gyorke and Terentyev, 2008). However, RyR2 in CASQ2-null cardiomyocytes still senses changes in SR luminal Ca^{2+}, which indicates that other luminal Ca^{2+}-sensing mechanisms exist (Knollmann *et al.*, 2006). The mechanisms by which the effects of luminal Ca^{2+} are sensed continued to be obscure until Chen and colleagues recently (2014) identified the site of the luminal Ca^{2+} sensor, postulated to lie close to the helix bundle crossing region that constitutes the gate of RyR2 (Chen *et al.*, 2014). They found the key RyR2 residues (D4868, E4872 and R4874) involved in store Ca^{2+} sensing are also conserved in all IP_3R isoforms, raising the intriguing possibility that IP_3R luminal Ca^{2+} sensitivity may also be governed by a store-sensing gate.

1.1.3.3 TRPML channels

TRP channels are a large family of ion channels that are members of the voltage-gated ion channel superfamily. TRPMLs (also known as mucolipins) belong to this large TRP superfamily of distantly related cation channels involved in the transduction of sensory stimuli. TRPML together with the TRP polycystins, constitute the group 2 TRP channel (Venkatachalam and Montell, 2007). For a more general discussion of TRP channels see section 1.1.2.3: this section will be focused on TRPML.

Mucolipins are so named because mutation of the gene encoding mucolipin was found to cause the lysosomal storage disease mucolipidosis IV, which is a developmental neurodegenerative disorder characterised by severe neurologic and ophthalmologic abnormalities (Bargal *et al.*, 2000; Sun *et al.*, 2000). TRPMLs are mainly expressed within the endocytic pathway, where they are involved in regulation of membrane traffic and/or degradation (Puertollano and Kiselyov, 2009). Mammals encode three isoforms of the proteins that are TRPML1, TRPML2 and TRPML3. Subcellular localisation studies have shown that TRPML1 is expressed in the late endosomes/lysosomes, TRPML2 expressed in recycling endosomes, late endosomes/lysosomes and the plasma membrane, and TRPML3 throughout the endolysosomal system and plasma membrane (Puertollano and Kiselyov, 2009).

When TRPML1 is expressed in *Xenopus* oocytes, the TRPML1-containing lysosomes translocate to the plasma membrane in response to ionomycin, a Ca^{2+} ionophore, causing an increase of intracellular Ca^{2+} level (Liu and Hermann, 1978). They further confirmed that the Ca^{2+} ionophore promotes the exocytosis of the MLN1-containing

lysosomes (LaPlante *et al.*, 2002). This suggests that the TRPML1 channels may be involved in Ca^{2+} transport across lysosomal membranes reported in the past (Lemons and Thoene, 1991) as well as in Ca^{2+}-dependent fusion between the plasma membrane and lysosomes during the exocytotic stage of the membrane trafficking process.

TRPML1 has also been linked to pH regulation. A study indicates that TRML1 is a non-selective cation channel whose function is inhibited by a decrease in pH (Raychowdhury *et al.*, 2004). However, the pH regulation and Ca^{2+} permeability of TRPML1 are contentious. TRPML1 has been reported to be a monovalent cation-permeable channel (Kiselyov *et al.*, 2005) which fluxes H^{+}, thereby providing a leak pathway for protons, regulating intra-lysosomal pH. Moreover, TRPML-null cells showed enhanced lysosomal acidification which is consistent with the fact that the channel is proton permeable (Soyombo *et al.*, 2006).

In recent years, nicotinic acid adenine nucleotide diphosphate (NAADP) has been shown to be one of the most potent Ca^{2+} mobilizing messengers targeting the acidic stores (Galione, 2011). Therefore, it would be interesting to ask if TRPML1 mediates NAADP signalling in acidic Ca^{2+} stores. This hypothesis was based on the findings that NAADP-activated channel activity in a lipid bilayer reconstituted with lysosomal membranes was inhibited by an anti-TRPML1 antibody (Zhang *et al.*, 2009; Zhang and Li, 2007), by immunodepletion with a second anti-TRPML1 antibody or by treating the cells with TRPML1 siRNA prior to isolation of lysosomal membranes for reconstitution (Zhang *et al.*, 2009). However, in 2011, Yamaguchi and colleagues (2011) found overexpression of TRPML1 did not enhance NAADP-mediated Ca^{2+} signals whereas overexpression of TPCs did. Moreover, a dominant negative TRPML1

(D471K) had no effect on endogenous NAADP-mediated Ca^{2+} signals. TRPML1 contributed nothing to the single channel properties of NAADP-activated TPC2delN. Moreover, NAADP-evoked Ca^{2+} oscillations were shown the same in wild-type and TRPML1-null pancreatic acinar cells (Yamaguchi *et al.*, 2011). Another study conducted by Ruas and colleagues (2015) found expression of the TRPML1 in Tpcn1/2$^{-/-}$ mouse embryonic fibroblasts (MEFs) failed to rescue the NAADP-induced Ca^{2+} response (Ruas *et al.*, 2015). These results indicated that NAADP does not gate TRPML.

Interestingly, it is noteworthy that PI(3,5)P_2, an endolysosome-specific lipid, has been shown to elicit Ca^{2+} responses in TRPML channels, which is in agreement with other groups who have confirmed PI(3,5)P_2 as an emerging intracellular signalling molecule for TRPML (Dong *et al.*, 2010; Feng *et al.*, 2014). It would be an interesting signalling pathway since PI(3,5)P_2 also triggers opening of other Ca^{2+} channels such as mammalian TPCs and RyRs (Ruas *et al.*, 2015; Touchberry *et al.*, 2010; Wang *et al.*, 2012) .

1.1.3.4 Two pore channel (TPC) proteins

Similar to TRPML, Two Pore Channels (TPCs) are also members of the voltage-gated ion channel superfamily (Patel, 2015). TPCs are characterised by a duplicated domain architecture where 2 × 6 trans-membrane regions are in a tandem arrangement (Figure 1.5 and 1.6). It is interesting to note that these channels tend to form dimers and thus form the four-fold symmetry typical of voltage-gated ion channels. Recently, it was reported that the function of the plant TPC1 depends on dimerization by its carboxy-terminal helix (CTH). Disruption of this CTH domain in TPC1 causes impediment of

dimerization and cation transport (Larisch *et al.*, 2016). This dimer structure is not only similar to the voltage-gated ion channels but also reminiscent of other Ca^{2+} channels that also form a four subunit (tetramer structure) such as IP_3Rs and RyRs (see sections 1.1.3.1 and 1.1.3.2). Figure 1.6A shows that the structure of TPCs are intermediate between CatSper \ Kv channels, which require four subunits to form a functional tetrameric channel, and Cav and Nav channels with four domains (DI to DIV). Such an intermediate structure is thought to be an evolutionary intermediate between one- and four-domain channels (Patel, 2015).

TPCs exist in protist, animal and plant kingdoms suggesting that this is a rather ancient channel family. There are three related families of TPCs (for example in sea urchins) but many species, including mice and humans only have genes encoding TPC1 and TPC2. Interestingly, TPCs seem to be lost altogether in some organisms in the process of evolution, such as *C. elegans*, flies and mosquitos. On the contrary, other insects such as honeybees and silkworms still preserve the genes encoding TPCs. However this protein is not essential for maintaining life (Zhu *et al.*, 2010).

In plants, there is only one type of TPC, a TPC1, which is localised to the tonoplast (vacuole membrane) and mediates slow-vacuolar currents, therefore it is also called the SV channel in plants. Recently, two structural studies of plant TPC1 have revealed much information (Guo *et al.*, 2016; Kintzer and Stroud, 2016), which will be discussed and compared with *Dictyostelium* TPC2 in detail in Chapter 3. The TPC1 channel plays an important part in plant physiology, such as regulating stomatal movement, germination and salt stress-induced Ca^{2+} waves (Choi *et al.*, 2014). Since the major players of Ca^{2+}-induced Ca^{2+} release (CICR) in animals, such as IP_3Rs and RyRs, are

missing in the genome of land plants=, TPC1 has been thought to mediate CICR in plants. Therefore, the discovery of Choi and colleagues (2014) might reveal a different paradigm for organellar Ca^{2+} release is required in plants. Moreover, the finding that the ubiquitous TPC channels are permeable to Ca^{2+} ions led to the model that TPC1 could be part of a distinct mechanism mediating CICR in plants (Ward and Schroeder, 1994). However it is still debatable if TPC1 can actually mediate CICR (Bewell *et al.*, 1999; Pottosin *et al.*, 1997). Direct biological evidence for SV channel-mediated CICR remains elusive.

In animals, TPCs localise to the endo-lysosomal system and are proposed to be activated by the Ca^{2+} mobilising messenger NAADP as well as the phosphoinositide $PI(3,5)P_2$ to control numerous Ca^{2+}-dependent events in cells. The channel is permeable to cations including Ca^{2+}, Na^{+}, and H^{+} ions. Figure 1.6 C to E shows the progression of our understanding of TPC activation (Pitt *et al.*, 2010b). TPCs have been proposed to be activated by NAADP as, for example, NAADP-dependent Ca^{2+} release is lost in MEFS from transgenic mice lacking the genes encoding both TPC1 and TPC2 (Ruas et. al., 2015) and this response was restored by exogenous TPC expression. This is supported by evidence from various studies of ion channel activity (Pitt *et al.*, 2010b; Pitt *et al.*, 2014; Rybalchenko *et al.*, 2012). TPCs are not thought to bind NAADP directly but activation is via an unknown binding protein (Ruas *et al.*, 2010; Walseth *et al.*, 2012). Some studies using cells from different null mice had suggested that TPCs are Na^{+} channels regulated by $PI(3,5)P_2$ but not NAADP (Cang *et al.*, 2013; Wang *et al.*, 2012), however it has been proposed that these mice have residual TPC activity as the gene disruption allowed expression of truncated protein (Morgan and Galione, 2014; Ruas *et al.*, 2014).

TPCs and/or NAADP have been implicated in a large number of cellular responses in mammals including histamine-induced secretion in human endothelial cells (Esposito *et al.*, 2011), skeletal muscle differentiation (Aley *et al.*, 2010), T cell function (Davis *et al.*, 2012) and loss of TPC2 in mice has been associated with susceptibility to fatty liver disease (Grimm *et al.*, 2014).

Clearly mammalian cells express a large number of Ca^{2+} channels and changes in cytosolic Ca^{2+} are used to signal a wide variety of processes. The interplay between the different Ca^{2+} stores, and the channels that regulate Ca^{2+} release is complex to study as so many channels are present. Although, for example, mice disrupted in genes encoding TPC proteins exist, it is challenging to investigate the role of multiple channels in complicated physiological processes such as development. Therefore it can be beneficial to study these processes in simpler eukaryotic systems with a more limited range of channels and physiological processes, to shed light on mechanisms conserved in higher eukaryotes.

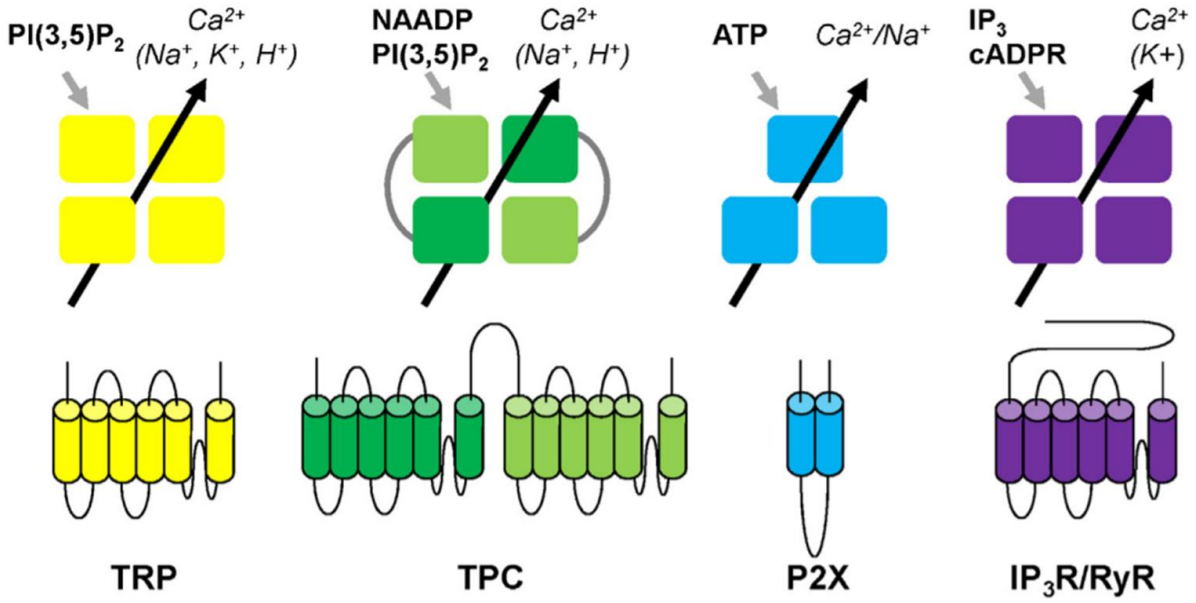

Figure 1.5 Schematic representation of Ca^{2+} channels found on intracellular Ca^{2+} stores. Quaternary structure (top panel) and tertiary structure (bottom panel). Activating ligands and permeant ions are shown. TRP channels are voltage-gated ion channels (Venkatachalam and Montell, 2007), including TRP-ML (mucolipin) which have been identified in *Dictyostelium* and in other systems and have been proposed as targets for *nicotinic acid adenine dinucleotide phosphat*e NAADP and phosphatidylinositol 3,5-bisphosphate ($PI(3,5)P_2$) (Zhang and Li, 2007). TPCs are also voltage-gated ion channels suggested to be targeted by NAADP (Calcraft *et al.*, 2009), which are located throughout the endolysosomal system. P2X receptors are ATP-gated ion channels expressed on the plasma membrane, and are permeable to Ca^{2+} and Na^{+}. In *Dictyostelium* P2X receptor orthologues (P2XA-E) are found on the contractile vacuole (Fountain *et al.*, 2007). IP_3 and ryanodine receptors are Ca^{2+} release channels on the ER and SR. IP_3 is the second messenger mediating response from IP_3 receptors, and cADP ribose is the second messenger for ryanodine receptors. Adapted from (Patel and Cai, 2015).

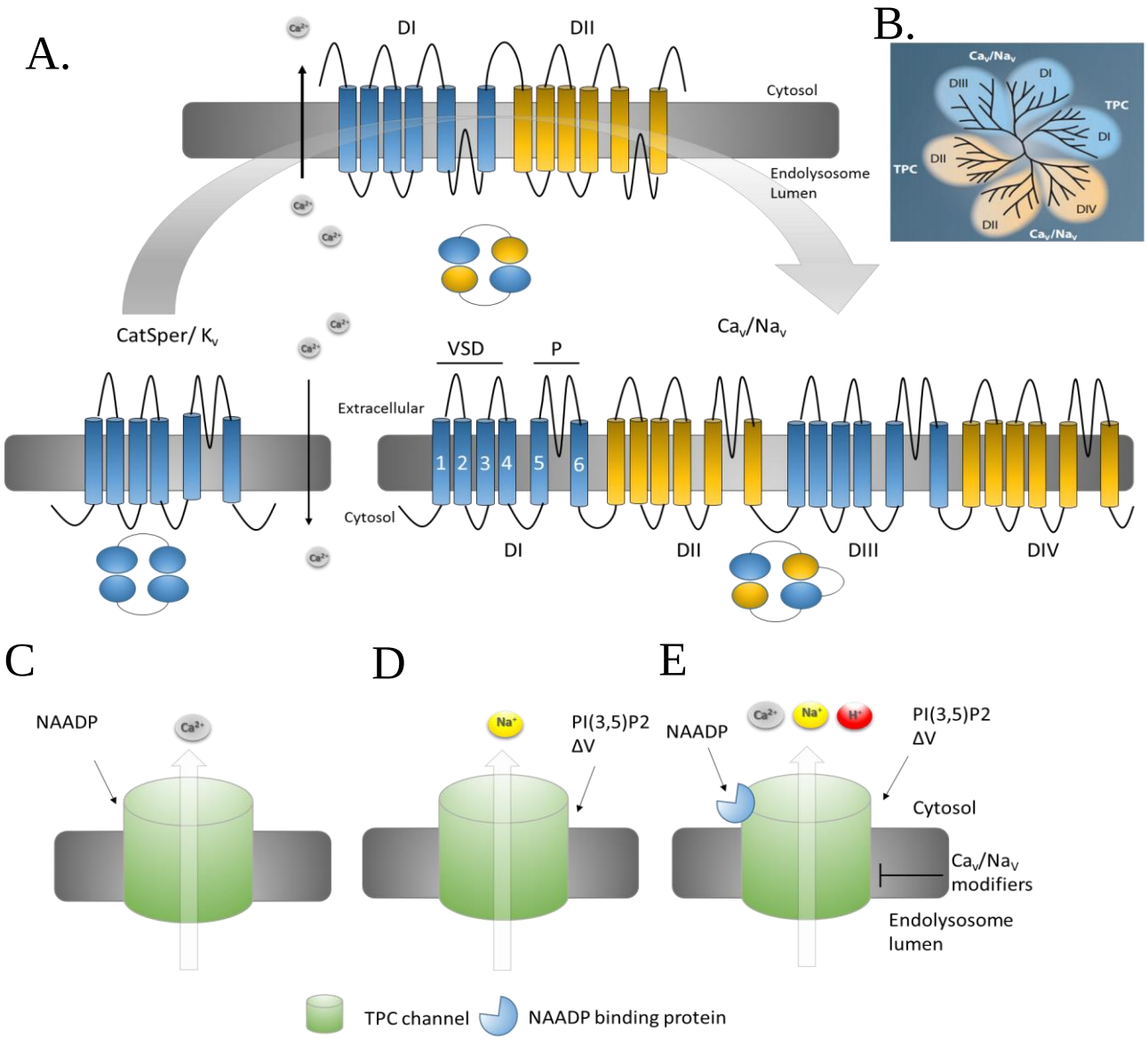

Figure 1.6 Schematic representation of the functional role of TPCs from an evolutionary perspective and their latest models of action.

(A) TPCs are an evolutionary intermediate from one to four domain ion channels. Predicted structure of individual (cylindrical) and assembled (circular) TPC subunits in relation to one- and four-domain channels. The grey curved arrow represents evolution from channels with one domain through TPCs with two domains to Ca_v and Na_v channels with four domains (DI to DIV). CatSper and Kv channels require four subunits to form a functional tetrameric channel, TPCs form a pseudotetramer by association of two subunits, and Ca_v and Na_v channels form a pseudotetramer with a single subunit. Similarity in domains is indicated by the two colours. (B) Phylogenetic relationships between individual channel domains of TPCs, Ca_v and Na_v. The blue areas denote DI and DIII and the orange areas denote DII and DIV in a phylogeny tree. Adapted from (Rahman *et al.*, 2014). (C to E) shows the development of understanding of activation of TPC2. (C) Original model based on evidence that TPCs are NAADP-gated Ca^{2+}-permeable channels. (D) Alternative model that is based on evidence that TPCs are $PI(3,5)P_2$-gated Na^+ channels. (E) Mixture model suggesting that TPCs are Na^+, Ca^{2+} (and H^+)–permeable channels co-regulated by NAADP (through associated NAADP-binding proteins) and $PI(3,5)P_2$, blocked by Ca_v and Na_v modifiers. Modified from (Patel, 2015).

1.2 *Dictyostelium discoideum* (*Dictyostelium*)

1.2.1 Life cycle of *Dictyostelium*

Dictyostelium discoideum is an unusual haploid, eukaryotic organism that lives in the soil and feeds on bacteria as single cells. The developmental life cycle is triggered when food sources are depleted. Some cells then start to secrete cyclic AMP (cAMP) and other cells then aggregate by chemotaxis to cAMP to form a multicellular organism that develops into a fruiting body containing two major cell types, spore and stalk cells (Figure 1.7). Therefore, *Dictyostelium* is a good model organism to study chemotaxis, development and differentiation.

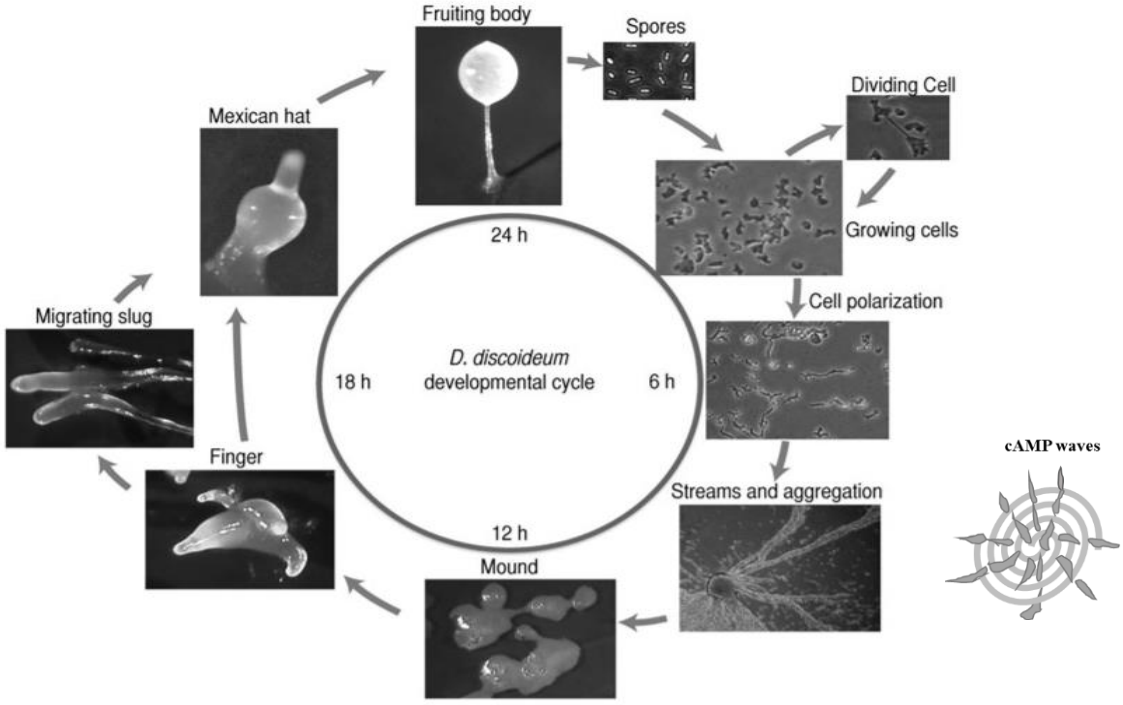

Figure 1.7 Life cycle of *Dictyostelium discoideum*.
Representative photographs of vegetative cells and developed structures. Starving *Dictyostelium* amoebae secrete pulses of cyclic adenosine monophosphate (cAMP, indicated by grey spiral waves) that cause the chemotactic aggregation of cells into mounds. Cells in the mound move up the cAMP gradient in response to continued cAMP emission, causing the formation of a tipped mound that then forms a finger and an optional slug phase which can migrate. This stage the prespore and prestalk cells are spatially separated. Finally, the structure culminates, undergoing fruiting body formation, during which the different cell types migrate to specified locations and ultimately differentiate into spores, stalk cells and the structures that support the stalk and spore head. After their dispersal to nutrient-rich habitats, spores germinate and resume proliferation as individual amoebae. Modified from (Muñoz-Braceras *et al.*, 2013)

1.2.2 Early development

Dictyostelium cells have evolved complex mechanisms to sense the environment (e.g. food sources), modulate cell behaviour and to control multicellular development. Figure 1.8 shows the major signalling molecules known to be involved at different stages of development.

Even before the food sources are depleted, cells secrete proteins, such as AprA and CfaD, to control proliferation. These proteins serve as a brake to prevent the cells proliferating too much. The developmental consequence of not expressing these proteins is a decreased ability to form spores since the cells have enhanced proliferation (cell number) at the expense of growth (cell size) (Gomer *et al.*, 2011).

In order to prepare for developmental transition, cells monitor the ratio of cell density to food density. The vegetative cells secrete a glycoprotein, known as prestarvation factor (PSF) (Clarke *et al.*, 1988). PSF activates a signalling pathway involving the protein kinase YakA (Figure 1.8B) to regulate expression of genes encoding proteins expressed in early development, many of which are involved in aggregation such as discoidin-I, cAMP receptor cAR1, lysosomal protein α-mannose and cell adhesion protein gp24 (Clarke *et al.*, 1992; Schatzle *et al.*, 1993; Schatzle *et al.*, 1991). PSF continues to be expressed at a level which is too low to activate these genes until cells are four generations from exiting exponential growth (Clarke *et al.*, 1987). Therefore PSF is able to regulate transcription based upon cell density. Once the cells starve, secretion of PSF drops rapidly (Rathi *et al.*, 1991). Moreover, PSF activity is inhibited by the presence of bacteria, which allows its activity to be modulated by available food sources (Clarke *et al.*, 1987). Thus, PSF acts as an ideal factor for regulating the

initiation of aggregation via monitoring the ratio of cell density to food density in actively growing cells.

Dictyostelium has evolved a mechanism that ensures that cells only aggregate when the cell density is high enough to generate aggregates of sufficient size to make effective fruiting bodies (Gomer *et al.*, 2011). Cells sense the population density via a factor known as Conditioned Medium Factor (CMF). *Dictyostelium* cells starved at low cell densities cannot aggregate unless they are incubated in starvation buffer previously conditioned by cells starved at high density (Gomer *et al.*, 1986a; Gomer *et al.*, 1986b; Grabel and Loomis, 1978; Kay, 1982; Mehdy and Firtel, 1985). This indicates that starving *Dictyostelium* cells are able to sense each other, and are able to make a developmental decision based upon the information contained in the surrounding environment. This ability is not dependent upon cell to cell contact, but involves a secreted, soluble factor, CMF (Mehdy and Firtel, 1985). The gene that encodes CMF has been cloned, and CMF is an 80 kDa glycoprotein with optimal activity at 0.3 ng/ml. Cells lacking CMF cannot aggregate unless exogenous CMF is added. CMF is secreted at a steady rate from starving cells, as expected for a quorum-sensing molecule, since its extracellular concentration is dependent upon the number of cells secreting it (Clarke *et al.*, 1992; Clarke and Gomer, 1995; Yuen and Gomer, 1994).

CMF also regulates the cAMP signalling system. CMF controls cAMP-dependent gene expression through the CMF receptor CMFR1 (Deery *et al.*, 2002; Deery and Gomer, 1999). Cells lacking CMF show a strong inhibition of Ca^{2+} influx, activation of adenylyl cyclase, and guanylyl cyclase in response to a pulse of extracellular cAMP, but are rescued by as little as 10 seconds exposure of cells to CMF (Yuen *et al.*, 1995).

Thus, CMF coordinates development by regulating cAMP signal transduction so that cells will not respond to cAMP and begin development until a sufficient number of cells are starving, as detected by high levels of extracellular CMF. The proposed pathway linking CMF and cAMP signalling is shown in Figure 1.9B.

The concerted action of these early developmental signals allows cells to become responsive to extracellular cAMP that then co-ordinates aggregation by acting as a chemoattractant, as well as inducing changes in developmental gene expression to promote aggregation. Extracellular cAMP interacts with cell surface GPCRs, such as cAR1, and activates a number of signalling pathways in the cell (some are shown in Figure 1.9A and B). One of the responses to cAMP is to activate an adenylyl cyclase, ACA, which generates more cAMP to be secreted and relay the signal. The co-ordinated action of this, along with an extracellular phosphodiesterase to degrade cAMP, leads to waves of cAMP passing through the field of aggregating cells that are generated around every 6 minutes in early aggregation (reviewed in Loomis, 2014).

A.

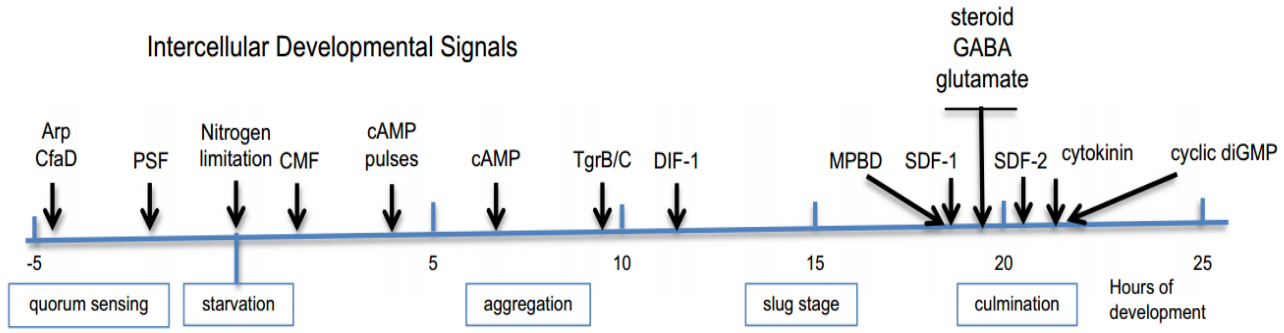

B.

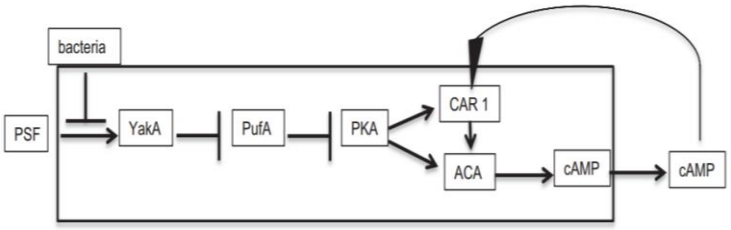

D.

1. Early developmental genes

Gene[a]	Product or function	GenBank accession no.[b]
Pulse independent		
carA	cAMP receptor	167683
gpaB	Gα2	167794
pdsA	cAMP phosphodiesterase	862416
Pulse dependent		
acaA	Adenylyl cyclase	167658
csaA	Adhesion protein gp80	167803
cbpA	Calcium binding protein	577004
cbpB	Calcium binding protein	1322367
cbpD	Calcium binding protein	9864389
cbpF	Calcium binding protein	4336199
cbpG	Calcium binding protein	15375419
SSL579	CbpB related	5181123
dia-2	Growth to differentiation	3983657
pgmA	Phosphoglucomutase	1408295
lagC	gp150 adhesion protein	5161855
lagC2	gp150 related	5834504
lagC2-like	Unknown	4883221
SLD188	Unknown	4882207
SSG481	Unknown	3218777

C.

Intercellular Signals	Structure
PSF	87 kD glycoprotein
Arp CfaD	138 kD complex
CMF	80 kD protein and peptides
cAMP (5 nM)	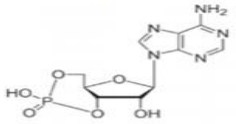
TgrB/C	Dimer of gp150 kD subunits
DIF-1 (5 nM)	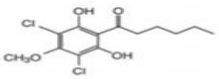
MPBD (5 nM)	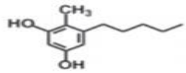
SDF-1 (kemptide phosphate; 1 pM)	Peptide: LRRASpLG

Intercellular Signals	Structure
Steroid (hydrocortisone; 5 nM)	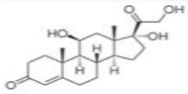
GABA (1 nM)	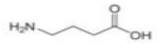
Glutamate (100 nM)	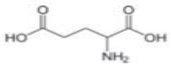
SDF-2 (processed AcbA; 0.01 pM)	Peptide: PSNDELLSLYGLYK-QGTDGDCNISEPWAVQVEAK
Cytokinin (discadenine; 10 nM)	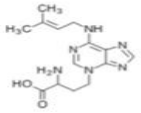
cyclic- diGMP (100 nM)	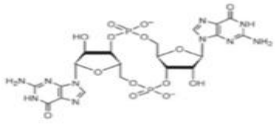

Figure 1.8 Developmental signals and genes of *Dictyostelium*.
Figure A shows signalling during *Dictyostelium* development. The signals used to integrate development of *Dictyostelium* are indicated at the stages at which they act. In the 5 hrs preceding the initiation of development, while the cells are still growing, secreted proteins function as quorum sensors. Morphogenesis occurs over 24 h following the initiation of development by nitrogen limitation; the stages are indicated below the temporal line. The structure of each signal is given in C. Figure B shows the known response to prestarvation factor (PSF) at initiation of development. D lists some of the genes involved in early development, categorised by the dependency on cAMP pulses, adapted from (Iranfar *et al.*, 2003). Adapted from (Loomis, 2014).

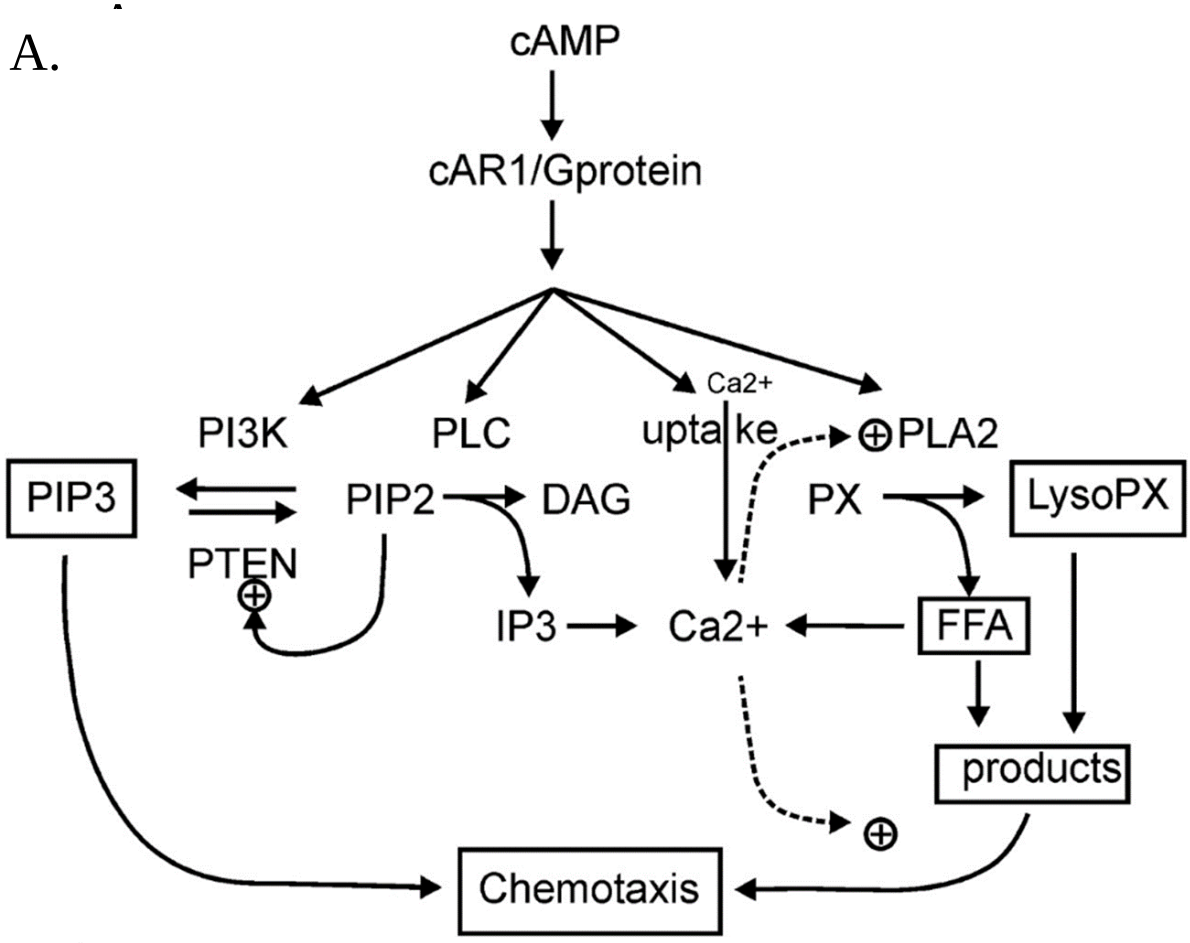

Figure 1.9A Model of signalling cascades activated by cAMP leading to *Dictyostelium* chemotaxis.

cAMP activates multiple pathways. The PI3K and PLA_2 pathways are parallel mediators of chemotaxis: either one can mediate chemotaxis, but chemotaxis is blocked nearly completely when both pathways are inhibited. PIP_3 is the likely mediator of the PI3K pathway, by recruiting PH domain-containing proteins modulating the actin cytoskeleton. The messenger of the PLA_2 pathway controlling chemotaxis is unknown. The PI3K pathway appears to be controlled by the PLC pathway, presumably at the level of PIP_2 degradation, leading to a reduction of membrane-associated PTEN that degrades PIP_3. The PLA_2 pathway is dependent on cytosolic Ca^{2+}, but it is unknown whether this occurs at the level of PLA_2 activation or the action of downstream messengers on the chemotaxis system. Cytosolic Ca^{2+} is potentially regulated by Ca^{2+} influx from the medium (which is both G protein dependent and independent), free fatty acid (FFA)–mediated Ca^{2+} release from acidic stores, and the IP_3 receptor–mediated Ca^{2+} release from the endoplasmic reticulum. Adapted from (van Haastert *et al.*, 2007).

B.

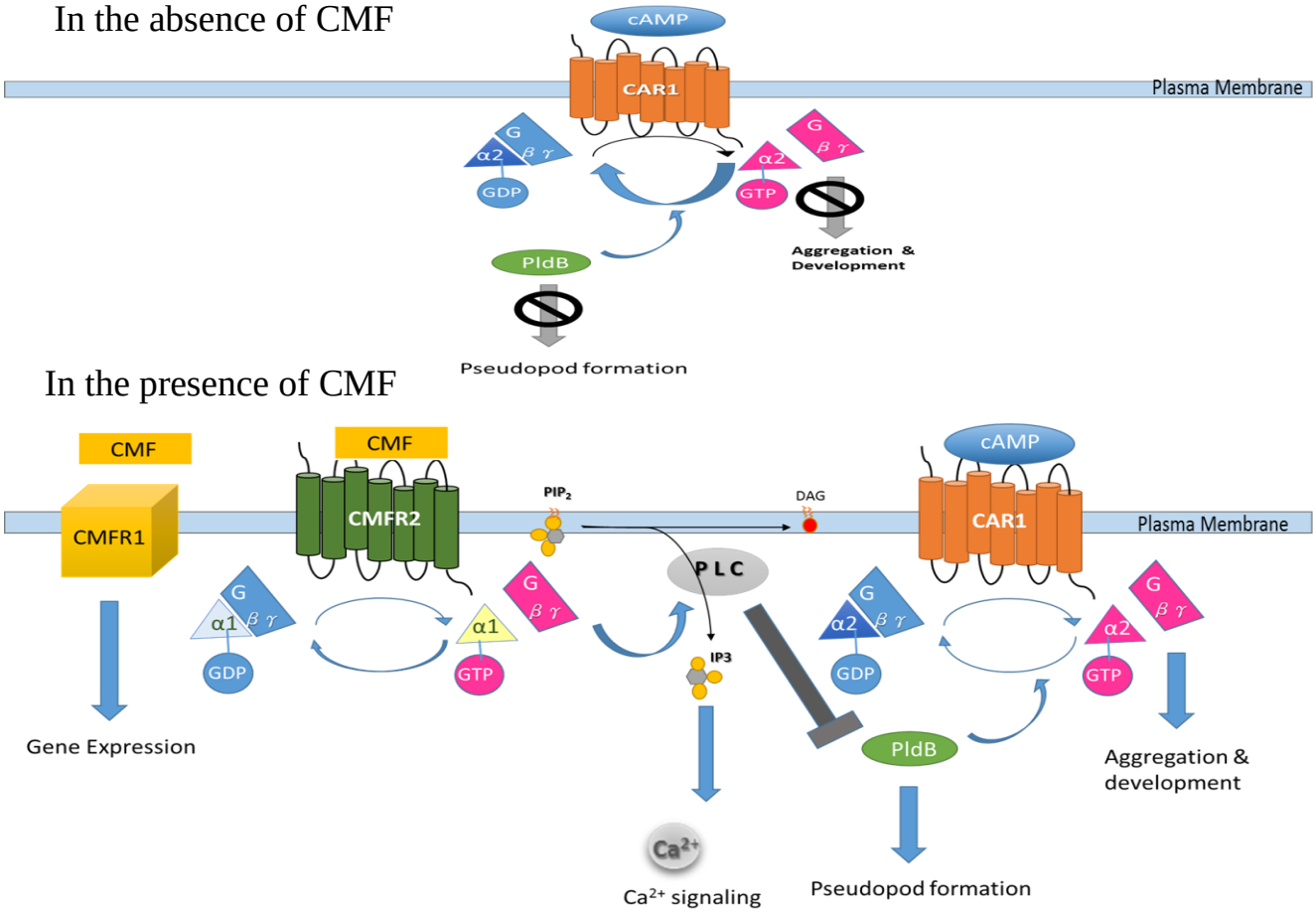

Figure 1.9B Model of quorum sensor CMF, cAMP receptor and Ca^{2+} signalling.
Model of cAMP signalling in the absence (upper panel) and presence (lower panel) of CMF. CMF exerts its effect on cAMP signalling through a G protein signalling pathway of its own. Specifically, CMF binds a G protein coupled receptor associated with Gα1. This pathway activates phospholipase C (PLC), an enzyme that converts the phosphoinositide PIP_2 to inositol 1,4,5-trisphosphate (IP_3) and diacylglycerol (DAG) (Brazill *et al.*, 1998). CMF stimulates IP_3 production, and this effect is lost in cells lacking phospholipase C, Gα1, or Gβ. RpkA, an unusual G-protein coupled receptor, appears to regulate Gα1 but may not be the CMF receptor itself (Bakthavatsalam *et al.*, 2007). Most importantly, PLC is required for CMF to regulate the GTPase activity of Gα2, as well as for the activation of guanylyl and adenylyl cyclase. This pathway was further delineated when it was found that the phospholipase D orthologue, PldB, regulates CMF signalling. Cells lacking pldB aggregate at low cell density, as if the CMF signal transduction pathway is constitutively on. Conversely, cells overexpressing pldB do not aggregate at all, as though the CMF pathway is constitutively off (Chen *et al.*, 2005). Both cell lines are insensitive to added CMF, suggesting that PldB is involved in the CMF quorum sensing pathway. Much like phospholipase C, PldB is required for CMF to regulate the GTPase activity of Gα2, as CMF can no longer decrease the GTPase activity of Gα2 in cells lacking PldB (Ray *et al.*, 2011). Finally, this system might link early development to the Ca^{2+} signalling system as the production of IP_3 is involved. CAR1, cAMP receptor. CMFR, CMF receptor. PLC, phospholipase C. PldB, phospholipase D orthologue. Adapted and modified from (Gomer *et al.*, 2011).

1.2.3 The role of Ca^{2+} and H^{+} in early development of *Dictyostelium*.

It is known that both cytoplasmic Ca^{2+} and H^{+} concentrations in vegetative cells have an effect on cell fate choice in later development (Jang and Gomer, 2011; Kubohara and Okamoto, 1994). It is intriguing to investigate if intracellular Ca^{2+} and H^{+} also have a role in early development.

1.2.3.1 Ca^{2+} in early development of *Dictyostelium*

Activation of cAR1 by cAMP is known to release IP_3 and fatty acids via activation of PLC and PLA_2 activities (Chen *et al.*, 2007), which have the potential to open Ca^{2+} channels and it is known that cAMP causes a cytosolic Ca^{2+} response (Abe *et al.*, 1988). CMF has also been proposed to activate PLC activity (Figure 1.9B) with the potential to release Ca^{2+} consistent with Ca^{2+} playing an important part in early development.

1.2.3.2 pH in development.

A role for intracellular pH playing a role in early development is supported by the observation that weak bases such as ammonia or imidazole inhibit aggregation. These can cross membranes when deprotonated and then pick up protons acting to neutralise acidic compartments in cells. Developmental effects are consistent with weak bases acting on acidic compartments to inhibit aggregation (Davies *et al.*, 1993).

The hypothesis for acidic vesicles also playing a role in late *Dictyostelium* development is based on the following evidence: Neutral red (a weak base) stains large intracellular acidic vesicles, and a number of smaller acidic compartments found in prestalk cells in the slug (Gross, 2009). Examination of the expression patterns of reporter constructs

revealed that the regions of prestalk- and prespore-specific gene expression correspond closely to the neutral red staining and non-staining zones, respectively. Also mutants with defects in the V-type H^+-ATPase are defective in developmental signalling (Aubry *et al.*, 1993). These changes in acidic compartments have been hypothesized to act through changes in Ca^{2+} signalling. Vesicle acidification is coupled to Ca^{2+} sequestration. Rooney and Gross (1992) characterised the acidic vesicles in *Dictyostelium* and found a substantial reduction in Ca^{2+} uptake in the acid vesicle fractions when the proton pump or proton gradient were inhibited or collapsed by bafilomycin and protonophore nigericin, respectively. Uptake was sensitive to vanadate, indicating that it depended on a Ca^{2+}-ATPase rather than a simple H^+/Ca^{2+} antiporter. It was also inhibited by concanamycin (CMA) and ammonia and was therefore dependent on the transport of protons into the vesicles by a vacuolar-type H^+-ATPase. Subsequent work in other laboratories has established that the enzyme is PAT1, which is distinct from the activity found on endoplasmic reticulum (ER) Ca^{2+} stores that is sensitive to thapsigargin (TG), a well-established sarcoplasmic/endoplasmic-type Ca^{2+}-ATPase inhibitor, and resistant to bafilomycin and vanadate (Flaadt *et al.*, 1993).

1.2.4 Known Ca^{2+} mobilising agents in *Dictyostelium*

A number of signalling molecules are known to elicit a Ca^{2+} response in intact cells of *Dictyostelium*. These signalling molecules are cAMP (Abe *et al.*, 1988), ATP (Ludlow *et al.*, 2009; Ludlow *et al.*, 2008), ADP (Ludlow *et al.*, 2008), Differentiation inducing factor (DIF) (Traynor and Kay, 2016), cyclic-di-GMP (Traynor and Kay, 2016), gamma amino butyric acid (GABA) (Traynor and Kay, 2016) and arachidonic acid (Schaloske *et al.*, 1998). These signalling molecules are valuable tools for Ca^{2+} research

but the pathways leading to Ca^{2+} release are not well characterised for any of these molecules.

1.2.5 Ca^{2+} stores in *Dictyostelium*

In *Dictyostelium* two non-mitochondrial Ca^{2+} stores have been described, one of which is sensitive to the second messenger IP_3 in permeablised amoebae (possibly the ER) (Europe-Finner and Newell, 1986) and another that is acidic (Flaadt *et al.*, 1993; Rooney and Gross, 1992).

1.2.5.1 Endoplasmic reticulum (ER)

The ER has been implicated in the cAMP-induced Ca^{2+} response in *Dictyostelium*. By using mutants that lack Ca^{2+} ER storage proteins (calnexin and calreticulin), Wilczynska and colleagues (2005) found that although cytosolic Ca^{2+} responses were enhanced, the influx of Ca^{2+} from the extracellular medium into the mutant cells was smaller. They concluded that Ca^{2+} release from the ER in the mutants thus contributes more to the total cytosolic Ca^{2+} response while influx from the extracellular medium contributes less, which provided the first evidence that release of Ca^{2+} from the ER contributes to cytosolic Ca^{2+} responses in *Dictyostelium* (Wilczynska *et al.*, 2005).

Presenilins are a protein family predominantly localised at the ER and have both proteolysis-dependent functions, as components of the γ-secretase complex, and proteolysis-independent functions in cell signalling. Ludtmann and colleagues (2014) reported that *Dictyostelium* presenilins, PsenA and PsenB, also localised in the ER and ablation of the genes encoding these causes enhanced cAMP-induced calcium release,

which suggests that presenilins regulate Ca^{2+} signalling via neutral stores in *Dictyostelium* (Ludtmann *et al.*, 2014).

1.2.5.2 Acidic Stores

A number of potential acidic Ca^{2+} stores have been described in *Dictyostelium.* These include contractile vacuoles (CVs) which are rich in some proteins important for ion transportation, such as vacuolar proton pumps (V-type H^+-ATPase) (Fok *et al.*, 1993; Heuser *et al.*, 1993; Nolta *et al.*, 1993), Ca^{2+} pumps (P-type ATPase) (Moniakis *et al.*, 1995), P2X channels (Fountain *et al.*, 2007) and Ca^{2+}/H^+ exchanger (CAX) (Rooney and Gross, 1992) and calmodulin (Zhu *et al.*, 1993).

There are also a group of dense granules which contain large amounts of phosphorus, magnesium, and calcium that are thought to be homologous to the acidocalcisomes described in protozoan parasites and are functionally linked to the contractile vacuole (Marchesini *et al.*, 2002).

1.2.6 Intracellular Ca^{2+} channels in *Dictyostelium*

Dictyostelium has a relatively small but well equipped Ca^{2+} signalling kit, which makes it a very good system to study Ca^{2+} signalling (Figure 1.10). The genome of *Dictyostelium* contains only three genes encoding putative calcium channels predicted to be expressed at the cell surface or in endocytic compartments (*mcln, pkd2, tpc2*), and a single mechanosensing-like channel (*mscS*) (Lima *et al.*, 2012; Lima *et al.*, 2014; Wilczynska *et al.*, 2005). In addition the genome encodes only one IP_3-like receptor (IplA) (potentially present in the ER), and five P2X receptors (P2xA-E) restricted to the

contractile vacuole (Baines *et al.*, 2013; Fountain *et al.*, 2007; Parkinson *et al.*, 2014) and no orthologue of Ryanodine receptors. This reduced complement of ion channels facilitates analysis of their role in development. Figure 1.11 shows a summary of known components, including Ca^{2+} stores, pumps and channels in *Dictyostelium*.

1.2.6.1 IP_3 receptor-like protein A (IplA)

There is one gene encoding a putative inositol-1,4,5-triphosphate receptor homologue (*iplA*) found in *Dictyostelium* although the protein has not been demonstrated to have to IP_3-gated channel activity. The subcellular location of IplA is in cytoplasmic vesicular membranes and to a lesser extent the plasma membrane (Lusche *et al.*, 2012). The *iplA* mRNA transcript is expressed at low levels during growth and peaks at 9 hours of development before declining. *iplA*$^-$ cells lack cAMP-stimulated Ca^{2+} uptake from the extracellular medium, however, their ability to chemotax towards cAMP is unaffected (Traynor *et al.*, 2000). Further analysis of *iplA*$^-$ cells (Schaloske *et al.*, 2005) shows that while influx of extracellular Ca^{2+} is largely reduced, release of stored Ca^{2+} into the cytoplasm is intact. Inhibition of capacitative Ca^{2+} entry does in fact impair the ability of cells to chemotax towards cAMP. Moreover, *iplA* null cells show defects in Ca^{2+}-mediated chemotaxis (Lusche et al., 2012), and a reduced capacity to reorient in the direction of the aggregation centre to the onset of cAMP waves. These results suggest that IplA has a role in Ca^{2+} chemotaxis and the authors hypothesize that transient Ca^{2+} gradients formed between cells at the onset of natural cAMP waves help the cells to reorient towards the aggregation centre.

iplA$^-$ cells are also inhibited in autophagic cell death, suggesting that cell death may require Ca^{2+} flux. Moreover, *iplA*/*atg1* double null cells show a variable and partial

inhibition of necrotic cell death, which suggests a minor role for IplA in this kind of cell death (Lam *et al.*, 2008).

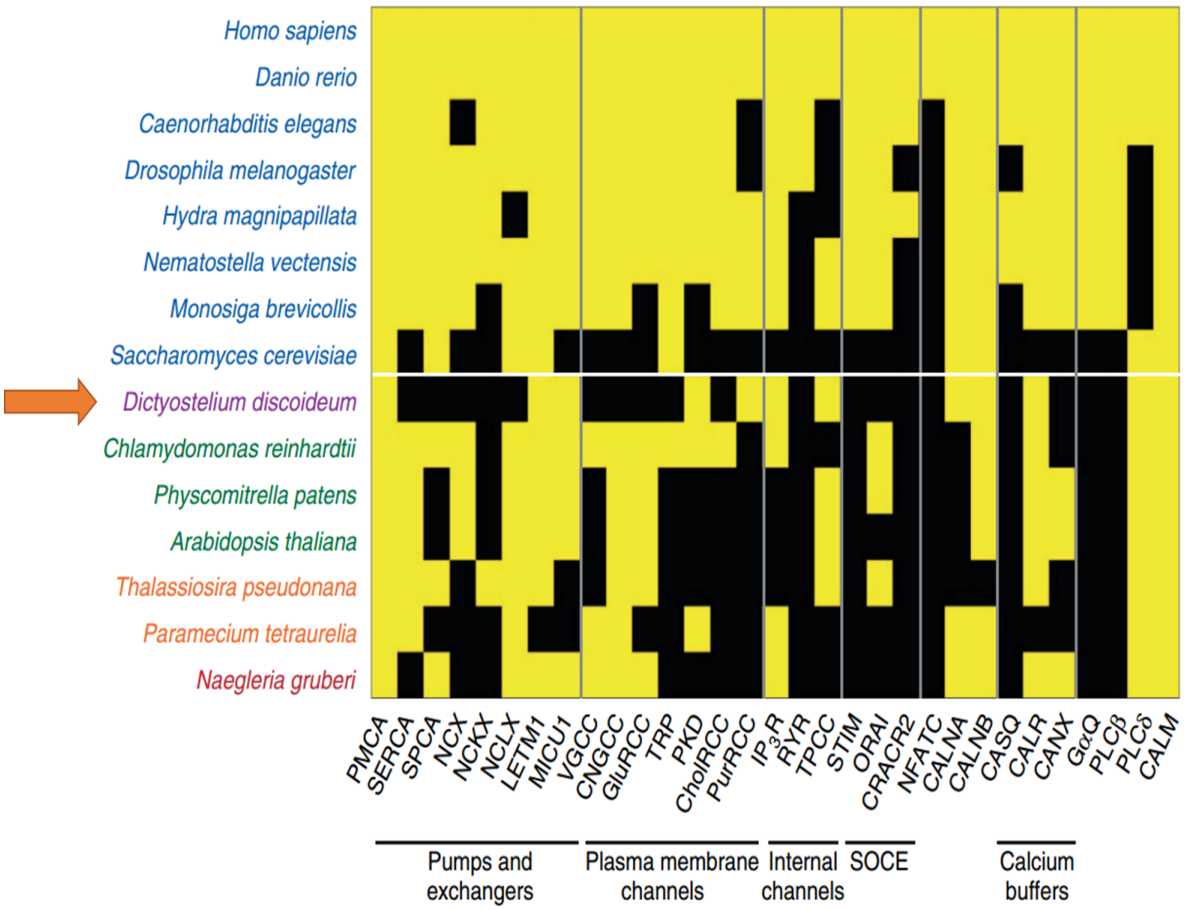

Figure 1.10 Ca^{2+} tool kit components in *Dictyostelium* compared to other organisms. A representative set of species with sequenced genomes are labelled on the left. Human and *Dictyostelium* gene families are listed underneath. Note that STIM includes the genes STIM1 and STIM2, and TRP-ML (mucolipin) is not shown in the diagram. Yellow indicates evidence for the presence of a homologue of a human gene family in a particular species, and black indicates the lack of an apparent homologue. Adapted from (Collins and Meyer, 2011).

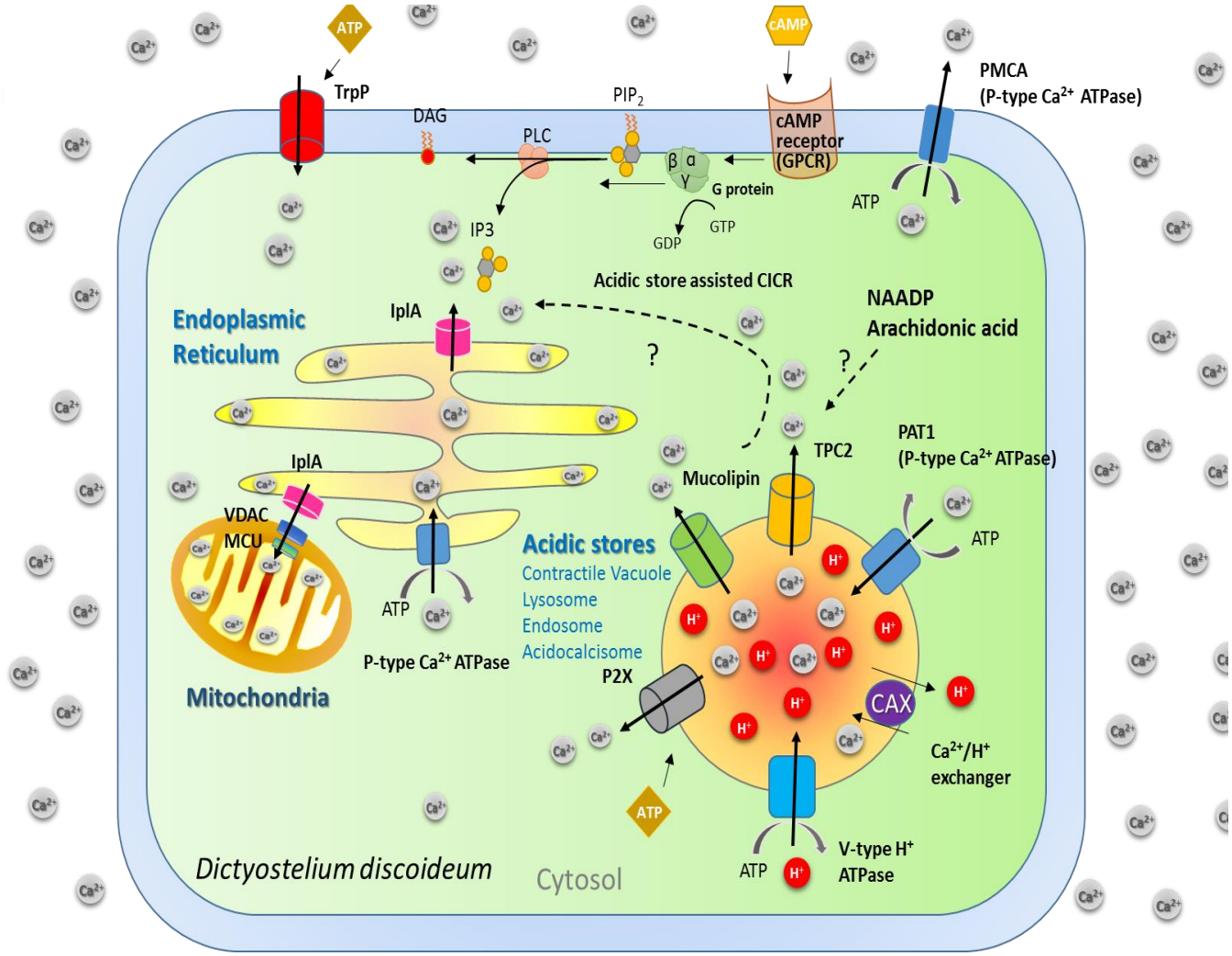

Figure 1.11 Summary of known components of intracellular Ca^{2+} signalling in *Dictyostelium*.
Dictyostelium possess a series of Ca^{2+} channels and pumps that are suitable for investigating Ca^{2+} in development. The most studied GPCR system in *Dictyostelium* are the cAMP receptors that mediate activation of many signalling pathways including a PLC and a putative downstream Ca^{2+} signalling pathway as shown in (Figure 1.1) and chemotaxis (not shown). Putative IP_3 receptor IplA, located on the ER. Putative TPC2, P2X receptors and TRP-ML (also known as mucolipin) are located on the acidic stores (contractile vacuoles and lysosomes in *Dictyostelium*). TrpP channel (polycystin-type transient receptor potential channel, also known as PKD2) which is gated directly or indirectly by ATP and is located on the plasma membrane (Traynor and Kay, 2016).

1.2.6.2 TRP channels: TRPP and TRPML

There are genes encoding two TRP channels proteins, TRPML (mucolipin) and TRPP (polycystin, also known as PKD2), found in the genome of *Dictyostelium*, both of them belonging to group 2 (Wilczynska *et al.*, 2005).

TRPP is important for rheotaxis, as *trpP*$^{-}$ null cells were unable to respond to a flow-induced shear stress, and a wild type phenotype was restored by complementation with expression of a full-length PKD2. This is the first time that TRPP has been implicated as a molecular player in mechanotaxis (Lima *et al.*, 2014). Recently, Traynor and Kay have shown that the *Dictyostelium* TRPP channel is required for ATP-dependent Ca^{2+} responses and is located on the plasma membrane (Traynor and Kay, 2016).

Disruption of the gene encoding mucolipin (*mcln*) causes dysregulation of post lysosomes and alters calcium homeostasis (Lima et al., 2012). However, the endosomal pH is unaffected. The *mcln*$^{-}$ cells also show a significant, though limited, reduction in mechanosensing (Lima et al., 2014).

1.2.6.3 P2X receptors

There are five genes encoding P2X receptors in *Dictyostelium*. However, unlike their counterparts in mammals that are found on the plasma membrane, in *Dictyostelium* they are localised on the membrane of contractile vacuoles and have a role in osmoregulation (Fountain *et al.*, 2007; Sivaramakrishnan and Fountain, 2012). They are not involved in ATP-induced Ca^{2+} influx as this is normal in cells in which all five genes have been deleted (Ludlow *et al.*, 2009). However Ca^{2+} efflux through P2XA is

required for localised down-regulation of activity of the small G protein Rab11a and efficient vacuole fusion (Parkinson *et al.*, 2014).

1.2.6.4 TPC2

Dictyostelium has one gene encoding a protein predicted to be a homologue of human TPC2. A *tpc2*$^{-}$ strain has been generated and shows no significant phenotype in terms of mechanosensing (Lima *et al.*, 2014). However no further analysis has been reported.

1.3 Overall Aims

The limited number of Ca^{2+} channels present in *Dictyostelium* and the viability of cells lacking these channels offers an ideal opportunity to study their role in development. In particular, there is evidence for the importance of acidic compartments in development and any developmental defects in cells lacking channels predicted to be on acidic stores have not been characterized. The aim of this thesis is to determine the role of two pore channel (TPC2) on acidic Ca^{2+} stores, in intracellular Ca^{2+} signalling and early development of *Dictyostelium* in comparison to other putative channels such as mucolipin and IplA.

Specific aims:-

1. To generate strains of *Dictyostelium* in which genes encoding for the calcium channels TPC2, mucolipin and IplA have been disrupted in the same genetic background to ask whether calcium channels found on acidic stores play a role in early development.

2. To investigate the role of TPC2 by in acidic vesicles of *Dictyostelium*, by establishing and characterising a vesicle system to study Ca^{2+} uptake and release *in vitro* to determine the effects of gene disruption or pharmacological inhibitors. The sensitivity to weak bases in development assays and the pH of vesicles will shed more light on the role of TPC2 in acidic vesicles.

3. To investigate if the Ca^{2+} response is altered in cells lacking TPC2 channels, mucolipin or IplA. I will establish a real-time Ca^{2+} detection system using living cells expressing ultrasensitive the Ca^{2+} indicator, yellow cameleon-Nano, to analyse calcium uptake and release from intracellular stores *in vivo*.

This work will help understand if TPCs work as Ca^{2+} channels located on acidic stores and have a role in early development in *Dictyostelium*. More importantly, this will also help us to understand common mechanisms shared by many organisms, including humans, to better understand the role of this ion channel in development.

CHAPTER 2: Materials and Methods

2.1 Materials

All solutions were prepared using distilled water and sterilized either by autoclaving for 15 min at 125 ^{0}C or filtration through 0.2 μm filter (Nalgene).

2.1.1 Solutions and media

HL5 (Formedium)

53 mM maltose

1.4% bactopeptone

0.7% yeast extract

4 mM Na_2HPO_4

3.5 mM KH_2PO_4

340 μM dihydrostreptomycin sulphate

74 μM vitamin B12

82 μM biotin

532 μM riboflavin

Adjusted to pH 6.5

Autoclaved

LoFlo medium (Formedium)

11 g Glucose

0.68 g KH_2PO_4

5 g Casein Peptone

26.8 g NH_4Cl

37.1 g $MgCl_2$

1.1 g $CaCl_2$

8.31 g $FeCl_3$

4.84 g Na_2-EDTA

2.3 g $ZnSO_4$

1.11 g H_3BO_3

0.51 g $MnCl_2.4H_2O$

0.17 g $CoCl_2$

0.15 g $CuSO_5.5H_2O$

0.1 g $(NH_4)_6Mo7O_{24}.4H_2O$

Suspend 16.8 gram powdered medium in 1 litre distilled water

Adjust to pH 6.5

Filtered

SM agar

1% bactopeptone

56 mM glucose

0.1% yeast extract

16 mM KH_2PO_4

5.5 mM K_2HPO_4

4 mM $MgSO_4$

1.7% agar

Autoclaved

KK2

19 mM KH_2PO_4

3.6 mM K_2HPO_4

Autoclaved

LB agar

1% bactotryptone

0.5% yeast extract

85 mM NaCl

1.5% agar

Autoclaved

LB broth

1% bactotryptone

0.5% yeast extract

85 mM NaCl

Autoclaved

2xSDS gel loading buffer

50 mM Tris pH 6.8

4% SDS

20% glycerol

0.2% bromophenol blue

100 mM dithiothreitol

SDS-PAGE Running buffer

25 mM Tris

250 mM Glycine

Adjusted to pH 8.3

0.1% SDS

SDS-PAGE Transfer buffer

50 mM Tris

500 mM Glycine

Adjusted to pH 8.3

0.1% SDS

20% methanol

Phosphate-Buffered Saline (PBS)

137 mM NaCl

2.7 mM KCl

10 mM Na_2HPO_4

1.8 mM KH_2PO_4

Adjusted to pH 7.4

Autoclaved

Lower Pad Solution (LPS) Development buffer

1.5 g KCl

0.5 g Streptomycin sulfate

0.5 g $MgCl_2$ $6H_2O$

3.750 g NaH_2PO4

3.375 g Na_2HPO_4

Suspend in 1 litre distilled water

Adjusted to pH 7.0

Filtered

Store at 5 °C in a dispensing jug

Allowed it to come up to room temperature before use

HKC-LoCa Development buffer

10 mM HEPES

10 mM KCl

250 μM $CaCl_2$

Adjusted to pH 7.0

Filtered

MM-HiCa Development buffer

5 mM MES

5 mM $MgCl_2$

5 mM $CaCl_2$

Adjusted to pH 6.5

Filtered

2.2 Methods

2.2.1 Cell culture

Dictyostelium discoideum axenic strain Ax2 was used for all the experiments presented. Cells were grown on SM agar plates in association with *Klebsiella aerogenes* or axenically in HL5 media in shaking suspension at 220 rpm or in Petri dishes at 22 ^{0}C. Ax2 strain was used as a parental cell line. *Dictyostelium* cells were harvested at the exponentially growing stage, washed and resuspended at a density of 2 - 5x10^5 cells/ml in HL5.

2.2.2 Genetically modified cell lines

Ax2 cells were transformed with plasmid vectors designed to confer resistance to the antibiotics blasticidin S (BS). Blasticidin-resistant (bsR) strains were selected for and maintained in HL5 medium containing 10 μg/ml BS.

2.2.3 Molecular Cloning and Gene Disruption

2.2.3.1 Plasmid construction

pLPBLP vector containing a blasticidin resistant cassette was chosen for experiments. The *PstI* and *BamHI* restriction enzyme sites at the 3'end of the bsR cassette (3' arm) and the *KpnI* and *HindIII* sites at the 5' of the bsR cassette (5' arm) were chosen as the cloning sites. Successful plasmids containing two arms were linearised using *KpnI* and *BamHI*, or using *ApaI* and *SacII* for the *iplA* disruption plasmid, pTLB, liberating the disruption fragments for electroporation.

The disruption plasmid for *iplA* (pTD5) previously used to successfully disrupt this gene (Traynor *et al.*, 2000) was obtained from the *Dictyostelium* Stock Center. The original bsR region of the pTD5 plasmid was replaced by the bsR cassette from pLPBLP flanked by two *loxP* sites, by utilising *HindIII* and *NotI* restriction sites, to generate pTLB (See Chapter 3 Figure 3.15). All the cloning enzymes were bought from New England Biolabs. Resulting disruption fragments were used for electroporation to the cells for homologous recombination-mediated gene disruption.

2.2.3.2 Electroporation procedure

Dictyostelium cells were harvested at the exponentially growing stage, washed three times with the ice-cold electroporation buffer (20 mM HEPES, 50 mM KCl, 10 mM NaCl, 1 mM $MgSO_4x7H_2O$, 5 mM $NaHCO_3$, 1 mM $NaH_2PO_4.2H_2O$, pH 7.0) and resuspended at a density of $5x10^6$ cells/ml. Cells were mixed with linearised plasmids followed by direct exposure to two consecutive pulses of 0.65 kV with a capacitance of 25 μF with 5 seconds recovery between pulses in chilled 1 mm gap electroporation

cuvette (BDH). Cells were left on ice for 5 minutes and used for further experiments. After transformation with linearised plasmids, Blasticidin resistant mutants were screened by PCR using sequence-specific primers and genomic DNA of clonal isolates confirming each arm has been integrated into the expected position.

2.2.3.3 BsR cassette recycling for multiple gene disruptions

A bsR gene disruption cell line was chosen and transformed to transiently express NLS-cre, using a Cre recombinase expression plasmid. The cells were then clonally diluted into 96-well microtitre dishes at varying dilutions and grown in the absence of Blasticidin S. The Bsr cassette was removed but the in-frame stop codons and a single *loxP* site remained. This creates a nonsense mutation in the gene. The resulting cell line was unable to grow in either Blasticidin S or G418, indicating that neither bsR of pLPBLP nor Neo of the Cre expression plasmid were integrated into the genome.

Table 2.1. Oligonucleotides and primers used for the PCR. All sequences written from 5' to 3' end.

Forward primer	Sequence	Reverse primer	Sequence
TPC-5-F	GGTACCTCGAAATAGAGGGATTCTAACCTCA	**TPC-5-R**	AAGCTTCCAACAAATGTATCATCAAATTCCAA
TPC-3-F	CTGCAGTGAACTCAATGGAACTCAACATCAAA	**TPC-3R**	GGATCCCGTCAAAATGTTGTTGGGGATCTT
MCLN-5-F	GGTACCCAGTTGGAAAGATGCCACATGAAG	**MCLN-5-R**	AAGCTTACATCCCATAAATATGCAACTGGA
MCLN-3-F	CTGCAGTTCTCGTTCAATCGGTATCAAATCA	**MCLN-3-R**	GGATCCGATGGCGGTAAAGGAGGAGATTTT
IplAN28	GAGAAAAATGTTAATTTGAAAACCGGTGATTTGG	**IplAN29**	GGCTTTAGATGACCAAGGTAGAGTTTATACCTGG
5 IPLA Scn F1	TTTGAAAACCGGTGATTTGGTT	**5 IPLA Mid R**	ACACTAAATCACGACCTTCCAA
Centre IPLAF	TGGTTCATTTGTTCGTATTCAATCT	**Centre IPLAR**	GTAGTGGCACCAGCCAATGA
Centre IPLAF2	AAGACAAGGGTGATCGGTGG	**Centre IPLAR2**	ATGATGGTCCGACTGTTGGC
W3	AAAACACAACCCACACCACTATCAA	**W5**	TCACCAGTGACAGCACCAATTACA
5'BSR-Lox	ATGCTATACGAAGTTATCCGTGG	**3'BSR-Lox**	GAAGTTATCATATGCCGCATGG
MCLN5' screen	TTAAAAGTAGCAACAAGTTGGATGGA	**MCLN3' screen**	TTGAATCTCTTTGTTAAAGGCCAAT
KW56	GGTACCACCGCTAGTCCAGG	**KW57**	GTAAAGTACTATTGATAGTTGCAGGTGG
MCLN-middle-F	TGCTGGTGCCATTTTGGATT	**MCLN-middle-F**	AGCCTCACCAAATGAAGCGA
APL-1	CCATCATACTTAAAGAAAGC	**APL-2**	GAACTGTATTTTGTACTTTTGAACCTG

2.2.4 The *in vitro* Ca^{2+} store detection system

2.2.4.1 Vesicle preparation

Vesicle preparation was adapted from the method of Malchow *et al.* (Malchow *et al.*, 2008). Vegetatively growing *Dictyostelium* cells were washed twice with KK_2 buffer. 3.5 x 10^8 cells were resuspended at a density of 1.4 x 10^7 cells/ml in KK_2 containing 5 mM EGTA and shaken at 120 rpm for 4 hours pulsing with exogenous cAMP (50 nM every 6 minutes) (T4). Then they were washed with ice-cold Washing Buffer (20 mM HEPES, pH 7.2) twice and resuspended in 4 ml of Washing Buffer containing 1 x proteinase inhibitor; Roche. Samples were disaggregated, using 21 G and 23 G needles and then homogenized by passage through 3 μm nucleopore filters (Millipore Limited). Homogenate was immediately added to 4 ml of 2 x Buffer 1 (100 mM KCl, 2 mM $MgCl_2$, 6% sucrose, 2 x proteinase inhibitor; Roche). After centrifugation for 5 min at 200 g in 2 ml eppendorf tubes, to remove residue of intact cells, the supernatant was fractionated by centrifugation at 3,800 g for 5 min. Pellet P0 was resuspended in 30 μl/tube Buffer 2 (10 mM Tris.HCl, 50 mM KCl, 1 mM $MgCl_2$, 3% Sucrose, x2 Proteinase Inhibitor; Roche). Pellet P1 was obtained by centrifugation at 12,000 g for 20 min, and this pellet was resuspended in 25 μl/tube of Buffer 2. All procedures were carried out on ice in a cold room (4 °C). Samples were either used freshly or aliquot 10 μl in eppendorf tubes then snap frozen on dry ice then stored at -80 °C for up to 7 days.

2.2.4.2 Ca^{2+} uptake and release detection *in vitro*

100 μl ice-cold Ca^{2+} uptake buffer (10 mM HEPES, 50 mM KCl, 2 mM $MgCl_2$, 3% Sucrose) was aliquoted into 1.5 ml eppendorf tube before mixing with vesicles and

reaction chemicals (100 nM NaN_3, 6.6 μM Fluo-3, 0.4 mM Mg^{2+}-ATP, 12 μg/ml Oligomycin). The vesicles (10 μl, 200 - 400 μg protein) were mixed with Ca^{2+} uptake buffer and reaction chemicals in a 1.5 ml eppendorf. After mixing, the sample was monitored by detecting free ionized Ca^{2+} which was measured via Fluo-3 (490 nm excitation and 535 nm emission) in a 96 well plate, using a fluorometer (NovoStar, BMF Labtech Limited, Aylesbury, UK).

2.2.5 *Dictyostelium* development

Cells were developed on filters, agarose or under buffer. The development buffer (KK_2, LPS, HKC-LoCa and MM-LoCa) varied according to the experiment.

For filter development, harvested cells were washed twice with appropriate development buffer. This was followed by cell resuspension in the buffer at a density of 5 x 10^7 cells/ml and 100 μl placed on boiled 3.5 mm filters (black filter, pore size 0.45 μm; Millipore Limited), supported on buffer soaked blotting paper.

Similarly, for agarose and under buffer development, cells were washed twice with appropriate buffer and 3.84 x 10^6 cells plated either on 1% agarose HKC-LoCa buffer or directly on the plate surface in a 6 well plate (Greiner), which makes final cell density 4 x 10^5 cells/cm^2, incubated at 22 °C for the appropriate time. In fluorescence experiments μ-Dish 35 mm (ibidi), a 35 mm imaging dish with an ibidi Standard Bottom and low walls, were used for development for microscopy.

2.2.6 Microscopy

2.2.6.1 Light Microscopy

Developmental structures of *Dictyostelium* were observed by using a Leica MZ FL III Stereomicroscope and photographed with a Hamamatsu digital camera ORCA-05 or a Motic AE21 Inverted Phase microscope with a Coolpix P310 digital camera.

2.2.6.2 Fluorescence Microscopy

Fluorescence microscopy is capable of imaging the intracellular ions (such as H^+ and Ca^{2+}) detected by specific indicators. This is most commonly achieved using fluorescently labelled molecules that can subsequently be detected specifically. The technique is based on the fluorescence emitted from electronically excited states of the chemical or biological fluorophores. The fluorophore contains electrons that can enter an excited state when a photon ('excitation light') is absorbed; this energy can be subsequently emitted as a photon with lower energy (higher wavelength), generating emitted fluorescence that may be detected with suitable detectors. Imaging was carried out using a widefield fluorescence inverted microscope (DeltaVision™) with a 20x or 60x oil immersion objective. Excitation light was provided by an InsightSSI™ Solid State Illumination and appropriate excitation filters individually selected as required. Emitted fluorescence was reflected through the side port of the microscope and collected using an EMCCD camera. Images were analysed using Fiji-Image J downloaded from https://fiji.sc/.

2.2.6.3 Fluorescence Microscopy for pH indicator Lysosensor Yellow/Blue DND-160

Cells were washed twice with LPS buffer at pH 7.0 and plated with LPS buffer on a 35 mm imaging dish (ibidi μ-Dish). The cells were allowed to attached to the plate for 15 min or develop on a plate as appropriate. The buffer was loaded with LysoSensor Yellow/Blue DND-160 at final concentration of 2 μM for 15 min. The indicator undergoes a pH-dependent emission shift to longer wavelengths in acidic environments when illuminated near its excitation isosbestic point (~360 nm). The blue and green channel images and ratio images were acquired by using a widefield fluorescence inverted microscope (DeltaVision™ Elite) with two emission images at 438/48 nm (DAPI) and 525/48 nm (FITC), both excited at 390/18 nm (DAPI).

2.2.6.4 Fluorescence Microscopy for Calcium indicator YC-Nano 15

Cells were transformed with plasmid vectors containing the ultrasensitive Ca^{2+} indicator YC-Nano 15, which was kindly provided by Professor Takeharu Nagai (Horikawa *et al.*, 2010), via electroporation as described in Section 2.2.2 with selection by G418 (Invitrogen) at final concentration 10 μg/ml. The cells expressing YC-Nano 15 were washed twice with HKC development buffer before plating on a 35 mm imaging dish (ibidi μ-Dish). The cells were allowed to attach to the plate for 15 min or develop on the plate as appropriate. The $[Ca^{2+}]i$ changes were acquired using a widefield fluorescence inverted microscope (DeltaVision™ Elite) at wavelength 438/24 nm (CFP) excitation and captured the emitted fluorescence simultaneously at 548/22 nm (YFP) and 475/24 nm (CFP). The single and multiple sequential images for movies were captured every 15 seconds with an EMCCD camera.

2.2.6.5 Western blot analysis

Western blot analysis was performed by separating samples boiled in SDS loading buffer on SDS-PAGE gel (10%) using standard procedures (Orkin, 1990) followed by transferring to PVDF membrane. The membrane was then soaked in methanol followed by blocked with 5% milk for 30 min. After blocking, the membrane was subjected to a primary rabbit monoclonal [E385] antibody to GFP (Abcam), diluted 1:5,000 in 5% milk for 1 hour followed by 3x5 min washes with TBST buffer. Goat anti-rabbit IgG IR Dye® 800CW from LI-COR was used as a secondary antibody, diluted 1:10,000 in 5% milk for 1 hour followed by 3x5 min washes with TBST buffer. The loading control MCCC1 was detected by using Alexa 680-conjugated streptavidin, diluted 1:1,000 in 5% milk for 4 °C overnight followed by 3x5 min washes with TBST buffer. The blots were scanned on Odyssey Fc imaging system (LI-COR, Lincoln, NE, USA).

2.2.7. Statistics and bioinformatics analysis

Unless otherwise specified, for quantified data, the values represent the mean. The number of independent experiments is indicated by n, sample mean is indicated by $\overline{X}$. Statistical comparisons were conducted by using Student *t*-tests (two-tailed) or Wilcoxon rank-sum test by using Microsoft Excel or R (downloaded from https://www.r-project.org/). P values are quoted in the appendix, significance is defined as shown below and the asterisks system is displayed on relevant graphical figures.

P value	Significance	
< 0.001	Extremely significant	***
0.001 to 0.01	Very significant	**
0.01 to 0.05	Significant	*
≥ 0.05	Not significant	ns

Protein and DNA sequence analysis was conducted by using BioEdit biological sequence alignment editor (downloaded from http://www.mbio.ncsu.edu/bioedit/bioedit.html) and NCBI Blast (https://blast.ncbi.nlm.nih.gov/Blast.cgi). Plasmid maps were drawn using pDRAW32 (http://www.acaclone.com/). Protein domains analysis was conducted using HMMER (https://www.ebi.ac.uk/Tools/hmmer/search/hmmscan) and NCBI conserved domain (https://www.ncbi.nlm.nih.gov/Structure/cdd/wrpsb.cgi). Protein modification sites and motifs were analysed by using Predictprotein (https://www.predictprotein.org/), ScanProsite (http://prosite.expasy.org/scanprosite/) and Calmodulin Target Database (http://calcium.uhnres.utoronto.ca/ctdb/ctdb/home.html). Protein phylogenetic analysis was conducted by using the Environment for Tree Exploration (ETE), a Python programming based toolkit, available form website http://www.genome.jp/tools/ete/.

2.2.8. Quantitative real-time RT-PCR

For quantitative reverse transcriptional PCR (qRT -PCR), total RNA was isolated using the TRIzol® Reagent (Life Technologies), from which 10 µg total RNA was treated with TURBO DNA- free™ Kit (Life Technologies) to remove residual gDNA. 2 µg DNase-treated total RNA was reverse transcribed to cDNA using SuperScript™ IV

First-Strand Synthesis System (Invitrogen). qRT-PCR was performed with 100 fold diluted cDNA and the SensiFAST SYBR No-ROX Kit (Bioline) in a Rotor-Gene thermocycler (Corbett Research) using *ig7* for normalization (Vinet *et al.*, 2014). All primers were designed by using Primer-Blast on NCBI website (https://www.ncbi.nlm.nih.gov/tools/primer-blast/), except for *acaA* primers (Teo *et al.*, 2010; Vinet *et al.*, 2014) and *yakA* primers (Garige and Walters, 2015). Figure 2.1 shows all primers were validated for their specificity (panel A to C only shown for primers for *ig7* as an example) and high efficiency and linearity of detection (panel D). Primers used for qRT-PCR are listed in Table 2.2. The PCR program was set as follows: 95°C, 60 sec, 40× (95°C, 3 sec; 60°C, 8 sec; 72°C, 8 sec), followed by a melting curve analysis (55 to 95°C, rising by 0.7°C each step of 3 sec) to attest to amplification specificity.

Table 2.2 Oligonucleotides and primers used for the qRT-PCR. All sequences written from 5' to 3' end.

Forward primer	Sequence	Reverse primer	Sequence
Ig7-[2]-qpcr-Fwd	TCGATCAGAGACGCAAGTCG	**Ig7-[2]-qpcr-Rve**	CACCCCAACCCTTGGAAACT
yakA-[1]-qpcr-Fwd	GCACTCGGTCAAAGTCCATC	**yakA-[1]-qpcr-Rve**	AATTTGGTGTGGCAACTGGTG
carA-qpcr-02-Fwd	GCTGTCAATGGTGGTTTCCC	**carA-qpcr-02-Rve**	CTAATTGCAAGACATAAAGTCCACA
pdsA-qpcr-Fwd	TCCATCCTCTGTCGCTTGTG	**pdsA-qpcr-Fwd**	CTCTTGGACGGAGATGACCA
dscA-qpcr-02-Fwd	AAGGTTTAGTTCAACTCCTCGC	**dscA-qpcr-02-Rve**	ACACCAAGCTTCTGAACCATCA
aca-qpcr-Fwd	GGAGAAAATGTCTGATTTCGCTT	**aca-qpcr-Fwd**	CATTCTAGAGGCGGTATTGGC
csaA-qpcr-02-Fwd	AACCATGGGAACCTCAAGCC	**csaA-qpcr-02-Rve**	TGTGAGGTGCTTGAGTGACA
patA-qpcr-Fwd	TACAAACGATGGTCCTGCCC	**patA-qpcr-Rve**	ACGGCACGAACAATTGAAGC

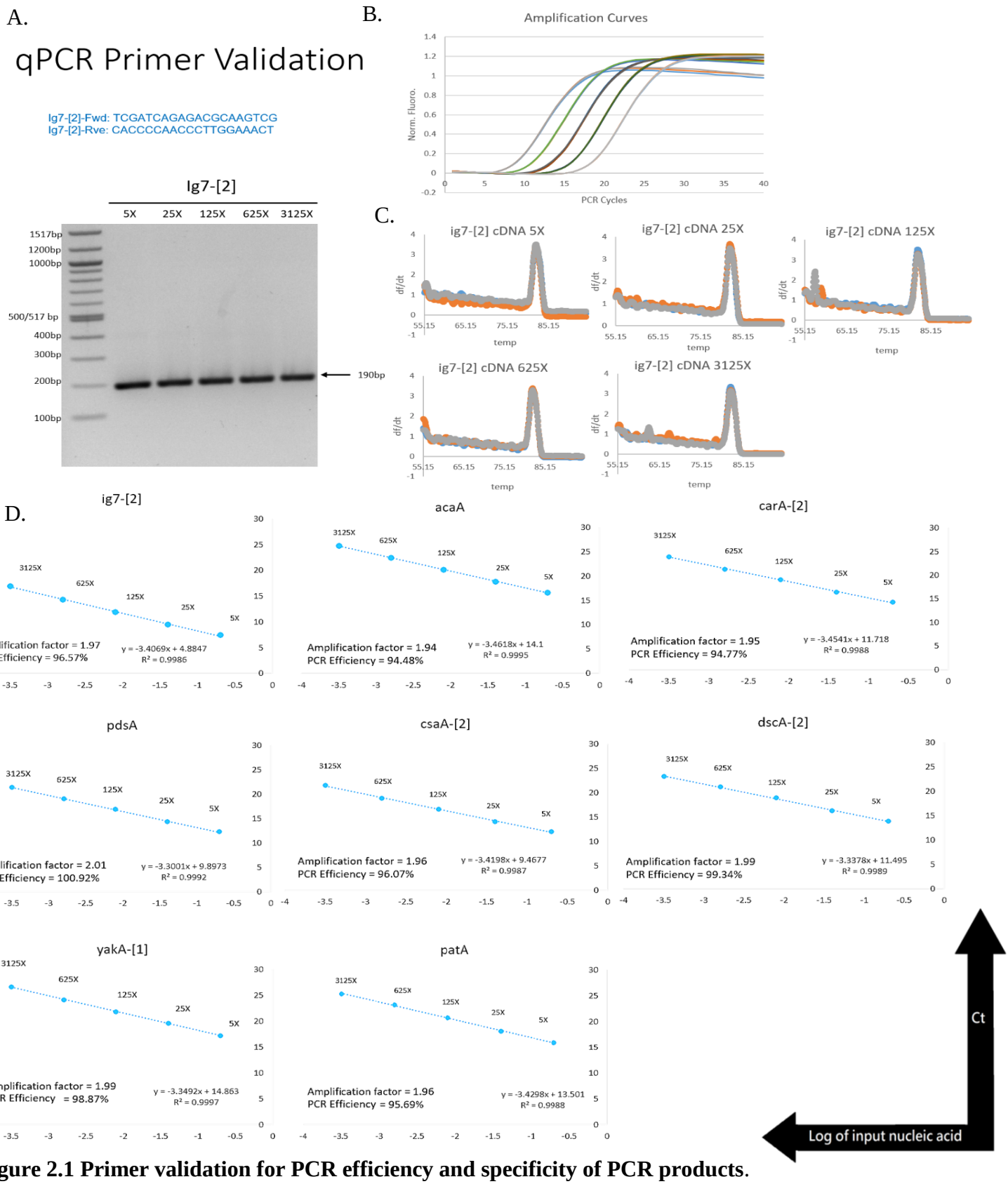

Figure 2.1 Primer validation for PCR efficiency and specificity of PCR products.
Ax2 cDNA was used as PCR template and serially diluted 5, 25, 125, 625, 3125 fold to check the quality of primers. The primers were validated for their specificity and efficiency. The single products are shown by agarose gel analysis (A) and melting curve analysis as in (C) illustrating the primers are specific. The PCR amplification curves rose with equal spacing shown in (B) and the Ct values plot with log of input nucleic acids (D) showed high PCR efficiency. The amplification factors and PCR efficiencies were calculated by using qPCR Efficiency Calculator. https://www.thermofisher.com/uk/en/home/brands/thermo-scientific/molecular-biology/molecular-biology-learning-center/molecular-biology-resource-library/thermo-scientific-web-tools/qpcr-efficiency-calculator.html

CHAPTER 3: The Role of *Dictyostelium* Two-Pore Channel 2 in Early Development

3.1. Introduction

Calcium has emerged as one of the most crucial and conserved second messengers for regulating a wide spectrum of cellular functions early in evolution (Berridge *et al.*, 2000; Plattner and Verkhratsky, 2013). It is essential for a number of cellular responses including cell division, cell growth, cell motility, differentiation and morphogenesis (Poloz and O'Day, 2012; Tu *et al.*, 2004). The calcium concentration in the cytosol is normally maintained at a low level, but transiently rises dramatically in response to a number of environmental stimuli such as hormones and stressors (Berridge *et al.*, 2000).

Maintaining a low level of intracellular Ca^{2+} requires a series of Ca^{2+} ATPases, including the plasma membrane Ca^{2+}-ATPase (PMCA) and sarco/endoplasmic reticulum Ca^{2+}-ATPase (SERCA), which act as pumps to remove Ca^{2+} from the cytosol (Carafoli, 1991) either by expelling Ca^{2+} to the extracellular space or sequestering Ca^{2+} into intracellular Ca^{2+} stores. On receipt of a signal Ca^{2+} can be released from intracellular stores via a number of calcium channels found on intracellular organelles, for example the inositol 1,4,5 triphosphate receptors and ryanodine receptors (IP_3R and RyR, respectively) on the endoplasmic reticulum (ER) (Berridge *et al.*, 2000), transient receptor potential – mucolipins (TRP-ML) channels on the endolysosomal system and plasma membrane (Puertollano and Kiselyov, 2009) and two-pore channels (TPCs) on acidic stores (Calcraft *et al.*, 2009; Davis and Galione, 2013).

Neutral Ca^{2+} stores such as the ER are by far the best studied and contain a well-defined repertoire of calcium pumps, channels and buffers (Berridge, 2002). Calcium, however, is also stored in a range of acidic organelles in eukaryotic cells (Patel and Docampo, 2010). These acidic Ca^{2+} stores are a group of organelles characterised by the presence of Ca^{2+} and their acidic interior or by being studded with vacuolar-type H^+-ATPase (Gross, 2009). They include acidocalcisomes, vacuoles, endosomes, lysosomes, lysosome-related organelles, secretory granules and the Golgi complex (Gross, 2009; Patel and Docampo, 2010). Their role in eukaryotic development has been recently appreciated especially in model organisms such as *Dictyostelium* (Gross, 2009).

Dictyostelium is an ideal system to characterise the role of calcium channels in development. Genes predicted to encode five classes of calcium channels have been found in *Dictyostelium*: IplA (*iplA*), TPC2 (*tpc2*), mucolipin (*mcln*), polycistin-2 (*pkd2*) and P2X receptors (Fountain *et al.*, 2007; Lima *et al.*, 2012; Sivaramakrishnan and Fountain, 2013; Wilczynska *et al.*, 2005) being homologous to mammalian IP_3R, TPC2, TRPML, Polycystin and P2X receptors, respectively. More importantly, acidic Ca^{2+} organelles, such as the acidocalcisome and contractile vacuole (CV), have been implicated in the early stages of development. Extracellular cAMP triggers an increase in cytosolic Ca^{2+} ($[Ca^{2+}]i$) and a link between acidic Ca^{2+} stores and cAMP oscillations was found using a calmodulin inhibitor W7, which has an inhibitory effect on the *Dictyostelium* vacuolar H^+-ATPase (Malchow *et al.*, 2004). However, an *iplA* disruption mutant aggregates and develops normally (Traynor *et al.*, 2000). Interestingly, during the later stages of development, prestalk and stalk cells accumulate more acidic Ca^{2+} stores (Davies *et al.*, 1993) and a slow sustained increase

of $[Ca^{2+}]i$ in monolayer cultures is sufficient to induce to stalk gene induction (Schaap *et al.*, 1996), suggesting a role for acidic Ca^{2+} stores in stalk cell differentiation.

3.2. Aims

The first aim of this chapter is to analyse the sequence of *Dictyostelium discoideum* TPC2, in comparison to predicted TPC2 proteins from other Dictyostelia and from plants and animals, for clues about its activity. The second aim is to determine the role of the putative TPC2 Ca^{2+} channels in development of *Dictyostelium*. Specifically, to generate strains of *Dictyostelium* in which the gene encoding for TPC2 has been disrupted to see if development is altered. The gene encoding the Ca^{2+} channel found on the neutral stores, IplA, was also deleted as a comparison for the role for the role of neutral stores, as was the gene encoding mucolipin, another channel predicted to lie on acidic stores.

3.3. Results

3.3.1. Putative Dictyostelid TPC2s

TPCs are highly conserved in animals and plants. *Dictyostelium discoideum* contains a single gene predicted to encode a TPC protein, most closely related to TPC2s of mammals (dictybase.org). The Dictyostelia family can be subdivided into four phylogenetic groups, with *D. discoideum* lying in group 4, the only group to use extracellular cAMP as a signalling molecule during early development (Schaap, 2016). Genome sequences are available for Dictyostelia from each of the four different phylogenetic groups (dictybase.org) so it is possible to determine if they all contain a gene predicted to encode a TPC2 protein. A BLAST search using *Dictyostelium*

discoideum TPC2 (DdTPC2) revealed one open reading frame with significant homology in each of the species of Dictyostelia except for *Actyostelium subglobosum*, which has an isoform of TPC2. Sequence alignment (Figure 3.1A) identified high homology between DdTPC2 (Group 4) and *D. lacteum* (Group 3) TPC2 (Identity 54%), *D. fasciculatum* (Group 1) TPC2 (Identity 62%), *Acytostelium subglobosum* (Group 2A) TPC2 (Identity 47%) and *Polysphondylium pallidum* (Group 2B) TPC2 (Identity 49%), which covers all four major clades of Dictyostelia. DdTPC2 also has homology with *Homo sapiens* TPC1 and TPC2 (Identity 25% and 29%, respectively), *Arabidopsis thaliana* TPC1 (Identity 27%) and *Oryza sativa* TPC1 (Identity 29%).

Protein sequence alignment of Dictyostelid TPC2s (DdTPC2, DlTPC2, DfTPC2, AsTPC2 and PpTPC2) with plants (AtTPC2 and OsTPC2) and animals (HsTPC1 and HsTPC2) reveals common conserved domains across organisms and Dictyostelid-specific domains. Figure 3.1A and B show two ion transport domains and a poly-cationic region (lysine and arginine-rich area) are conserved across animals, plants and Dictyostelia. A poly-anionic region (glutamic acid-rich area) in the C terminal domain (CTD) of plants is important for plant TPC function as deletion of the CTD results in inactive plant TPC1 channels (Kintzer and Stroud, 2016).

The non-ion transport regions of Dictyostelid TPC2s are quite different from those found in plants and animals. All of the Dictyostelid TPC2s have longer protein sequences than those of plants and animals, among which DdTPC2 (2060 amino acids) is the longest. It is interesting to note there are a number of areas of DdTPC2 that show no homology to other Dictyostelid TPC2s. Also there are at least four areas which are unique and conserved in Dictyostelia. The first are poly-asparagine (N) stretches that

can be found in the N-terminus of TPC2 and between the two ion transport domains. Such runs of poly-N are common in *D. discoideum* proteins due to the presence of AAC repeats in coding sequences of genes. The second is another poly-cationic region in the N-terminal region. Then there is a P-rich region and two RKDE-rich areas found towards the C-terminus of TPC2. The functions of these conserved regions in Dictyostelia are not known but could play important roles as proposed for the equivalent CTD (C-terminal domain) and NTD (N-terminal domain) of plant TPC1 (Kintzer and Stroud, 2016). By using the Predictprotein website (https://www.predictprotein.org/), clustered protein binding sites in the CTD were predicted in DdTPC2 and AsTPC2 suggesting that there might be a potential protein-protein interaction domain in the CTD of these proteins (Figure 3.2).

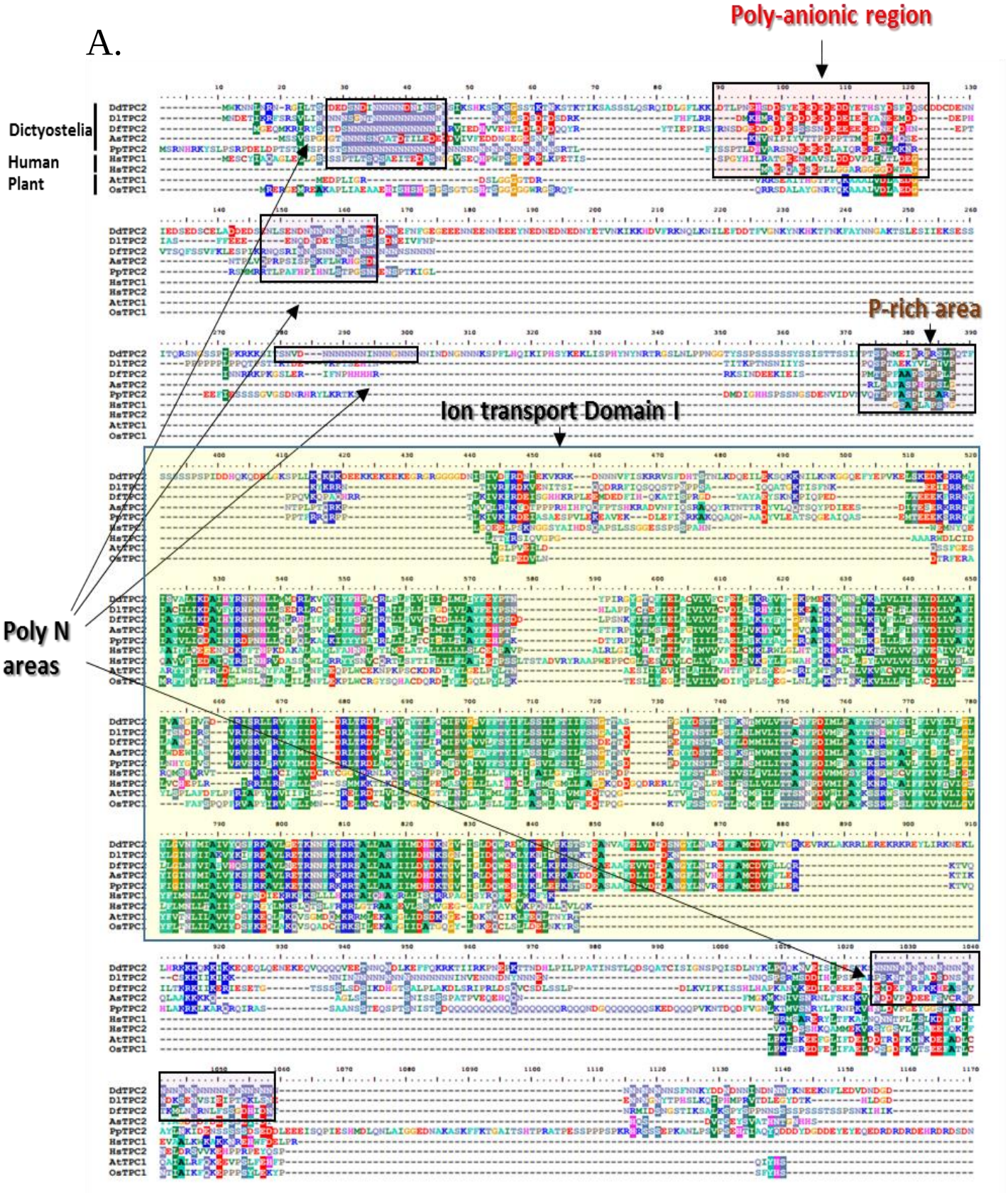

Figure 3.1. Protein alignment of TPCs in various organisms.
(A) Ion transport domain I of the predicted TPC2 protein sequences of five species of Dictyostelid TPC2, *Dictyostelium discoideum* (DdTPC2), *D. lacteum* (DlTPC2), *D. fasciculatum* (DfTPC2), *Acytostelium subglobosum* (AsTPC2) *and Polysphondylium pallidum* (PpTPC2) and sequences from *Homo sapiens* TPCs (HsTPC1 and HsTPC2), *Arabidopsis thaliana* TPC1 (AtTPC1) and *Oryza sativa*TPC1 (OsTPC1) were aligned using ClustalW built in BioEdit. Conserved domains and motifs are highlighted in boxes.

B.

Figure 3.1. Protein alignment of TPCs in various organisms.
(B) Ion transport domain II of the predicted TPC2 protein sequences of five species of Dictyostelid TPC2, *Dictyostelium discoideum* (DdTPC2), *D. lacteum* (DlTPC2), *D. fasciculatum* (DfTPC2), *Acytostelium subglobosum* (AsTPC2) *and Polysphondylium pallidum* (PpTPC2) and sequences from *Homo sapiens* TPCs (HsTPC1 and HsTPC2), *Arabidopsis thaliana* TPC1 (AtTPC1) and *Oryza sativa*TPC1 (OsTPC1) were aligned using ClustalW built in BioEdit. Conserved domains and motifs are highlighted in boxes.

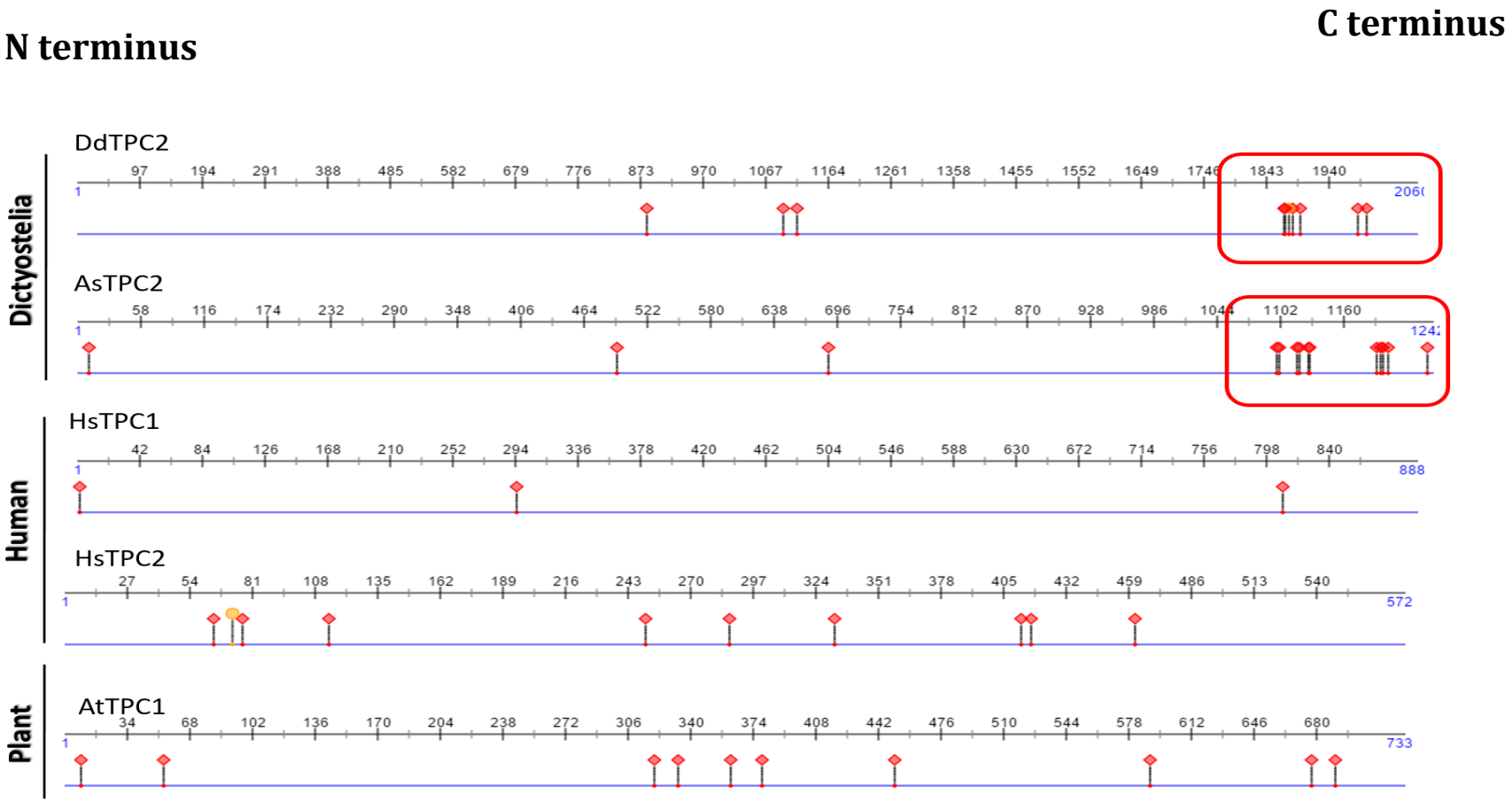

Figure 3.2. Predicted protein binding sites on TPC proteins.
The protein binding sites were predicted by using the Predictprotein website (https://www.predictprotein.org/). The clustered protein binding area is circled in red.

3.3.2. Domains, motifs and signal sequences of Dictyostelid TPC2s

Based on the sequence alignment, it seems that Dictyostelid TPC2s are quite different from those in plants and animals. Intriguingly, they seemed to have some unique sequences. In order to ask if these unique regions might serve specific functions, the sequences of Dictyostelid TPC2s were analysed using the NCBI Conserved Domain Database (NCBI DBB) (https://www.ncbi.nlm.nih.gov/Structure/cdd/wrpsb.cgi) and HMMER HMMSCAN website (https://www.ebi.ac.uk/Tools/hmmer/search/hmmscan). All Dictyostelid TPC2s are predicted to have two ion transporter domains and a pair of EF hands, which are predicted to bind Ca^{2+}, except for *D. lacteum*, which only has one predicted EF hand, which was predicted to be localised in the cytosolic side. This remaining EF hand sequence in DlTPC2 has lost a conserved alanine residue (A510S), making it lose the characteristics of an EF hand suggesting that there is no functioning EF hand in *D. lacteum*. The results are summarised in Figure 3.3 and Table 3.1. The six membrane-spanning helices within each 6-TM domain are labebed as IS1–IS6 and IIS1–IIS6, respectively.

It is interesting to note that unique domains were identified in PpTPC2 and DdTPC2. In PpTPC2, regions of homology were found, one of which is conserved with SpoIIM, a stage II sporulation protein. The most interesting conserved motifs were found in the sequence of DdTPC2. By using HMMER, two segments (position 1,311-1,479 and 652-793) were found to be related to sequences found in presenilin. Presenilins are a family of transmembrane proteins which constitute the catalytic subunits of the gamma-secretase intramembrane protease complex. Homology to another transmembrane protease was highlighted by using NCBI-DDB, in which a sequence in position 1,258-1,385 (overlapping with the presenilin-like domain) was found to be related to another

intramembrane protease, known as ClpG, a membrane associated serine protease of the rhomboid family. Both of the regions related to the proteases lacked the conserved residues required for catalytic activity. NCBI-DDB analysis also highlighted a region (aas 1,180-1,378) similar to one found in ProP, a permease, which is involved in carbohydrate, amino acid and inorganic ion transport and metabolism. It will be interesting to see if these regions are also conserved in TPC2 proteins of other group 4 Dictyostelia. As Group 4 is the only group use extracellular cAMP to aggregate, the proteins in *D. discoideum* might have evolved novel functions to achieve this.

The DdTPC2 sequence was analysed using the Predictprotein website (https://www.predictprotein.org/), which revealed three potential nuclear localization sequences (NLS) were predicted, located at 844-880, 1,897-1,904, 1,978-1,985.

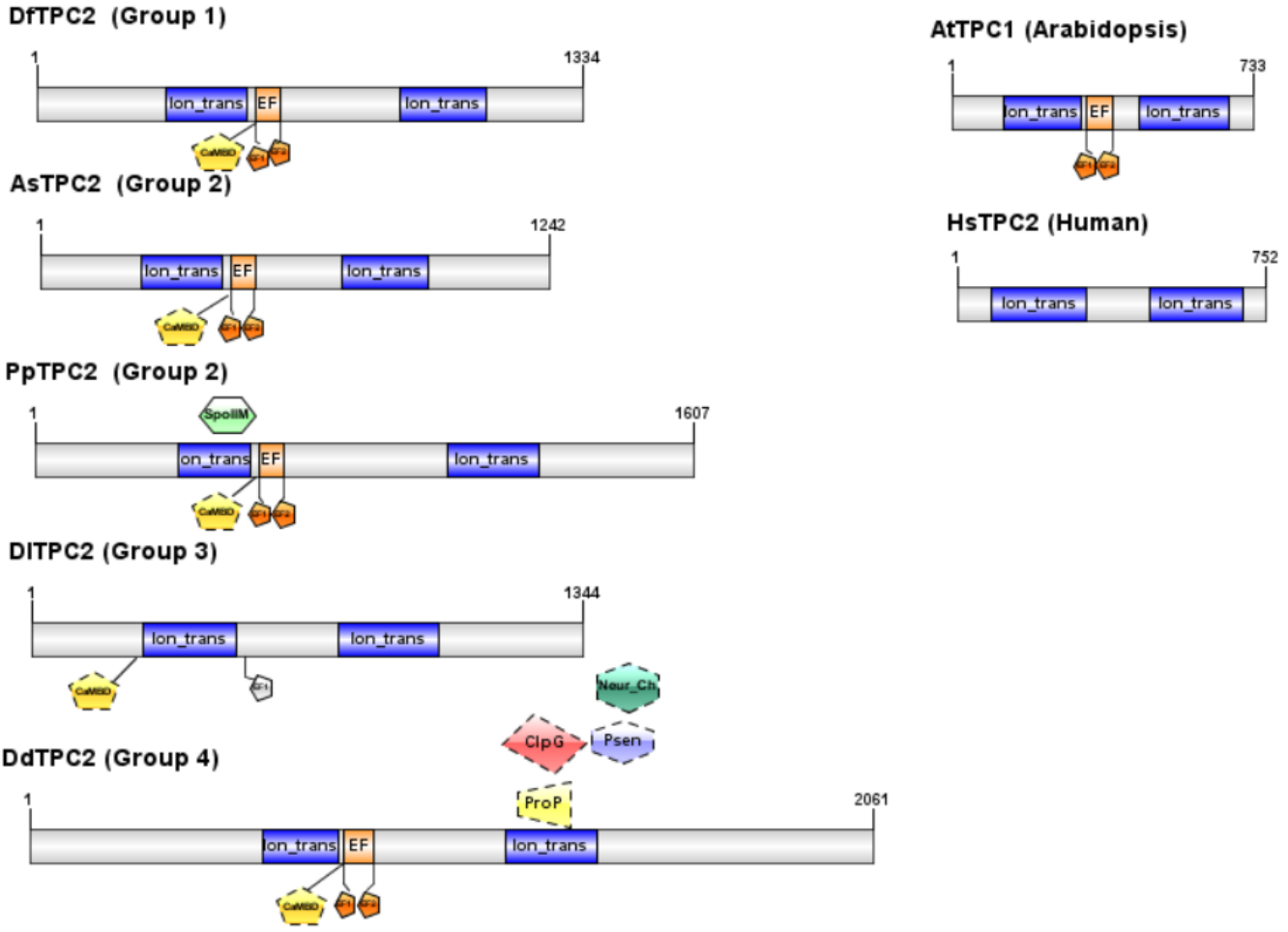

Figure 3.3. Illustration summarising the predicted domains and motifs of Dictyostelid TPC2s and other TPCs in plant and human.

The dashed shapes indicate putative conserved regions of unknown function. The solid shapes indicate known structures. Ion trans, ion transport domain: EF, EF hand, calcium binding motif: CaMBD, calmodulin binding domain: NLS, nucleus localization sequence: ClpG, a membrane associated serine protease, rhomboid family: ProP, a MFS family permease: Psen, presenilin, the catalytic subunit of the gamma-secretase intramembrane protease complex: Neur Ch, Neurotransmitter-gated ion-channel transmembrane region: SpoIIM, Stage II sporulation protein M.

Table 3.1. Conserved domains and motifs predicted in DdTPC2.

A.

Domains and motifs found on DdTPC2	Location	E-values
Ion transport protein	1140-1386	1.5e-26 (HMMER)/ 4.29e-25 (NCBI)
Ion transport protein	535-758	1.8e-12 (HMMER)/ 4.77e-13 (NCBI)
EF-hand domain pair	770-834	2.8e-08 (HMMER)/ 1.67e-05 (NCBI)
Presenilin	1311-1479 and 652-793	3.8e-07 (HMMER) and 0.051 (HMMER)
Neurotransmitter-gated ion-channel transmembrane region	1347-1490	3.9e-04 (HMMER)
GlpG, rhomboid super family	1258-1385	9.72e-03 (NCBI)
ProP, MFS family permease	1180-1378	2.96e-03 (NCBI)

B.

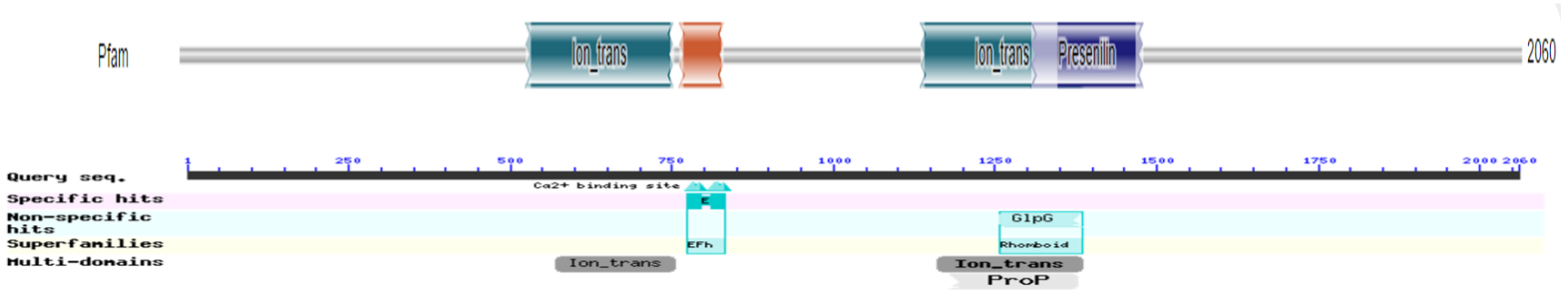

(A) Domains conserved between DdTPC2 and other proteins were identified by using NCBI Conserved Domain Database (https://www.ncbi.nlm.nih.gov/Structure/cdd/wrpsb.cgi) and HMMER HMMSCAN website (https://www.ebi.ac.uk/Tools/hmmer/search/hmmscan).
(B) The graphical results from HMMSCAN (upper) and NCBI CDD (lower) are shown.

3.3.3. Sequence analysis of Dictyostelid TPC2s

There are two recently published structures of Arabidopsis TPC1 (AtTPC1) (Guo *et al.*, 2016; Kintzer and Stroud, 2016). Therefore I carried out a detailed comparison of the TPC protein sequences between Arabidopsis and Dictyostelia, comparing the predicted ion channel domains of AtTPC1 and Dictyostelid TPC2s. Two groups of 6 transmembrane domains were well conserved in the sequence of Dictyostelid TPC2s (Figure 3.4). This suggests that Dictyostelid TPC2 proteins retain the classic structure of the two pore channels.

3.3.3.1 Ion conduction pores

An alignment of the sequences predicted to encode the ion conduction pores in Dictyostelid TPC2s (Figure 3.5) shows that for the ion conductivity filter 1 in the pore 1 region, most of the organisms including plants, animals and amoebae contain the consensus sequences TT[SA]N[NF]. However, *D. discoideum* and *D. fasciculatum* contain TTCNF, where the serine or alanine residue is replaced by a cysteine. It is not known if this difference is biologically significant, although the cysteine is chemically similar to serine (Figure 3.5). In filter 2 in the pore 2 region, all the proteins in amoebae and animals contain the consensus sequence VVNNW, in contrast to the sequence VMGNW found in plants. Plant TPC1s have been reported to be non-selective ion channels that conduct K^+, Ca^{2+}, Na^+ and ions, whereas human TPC1 is reported to be Na^+-selective and human TPC2 to conduct Na^+, Ca^{2+}, and H^+ ions (Pitt *et al.*, 2010a). The sequence differences in these regions could determine the ion-selectivity of the ion channel.

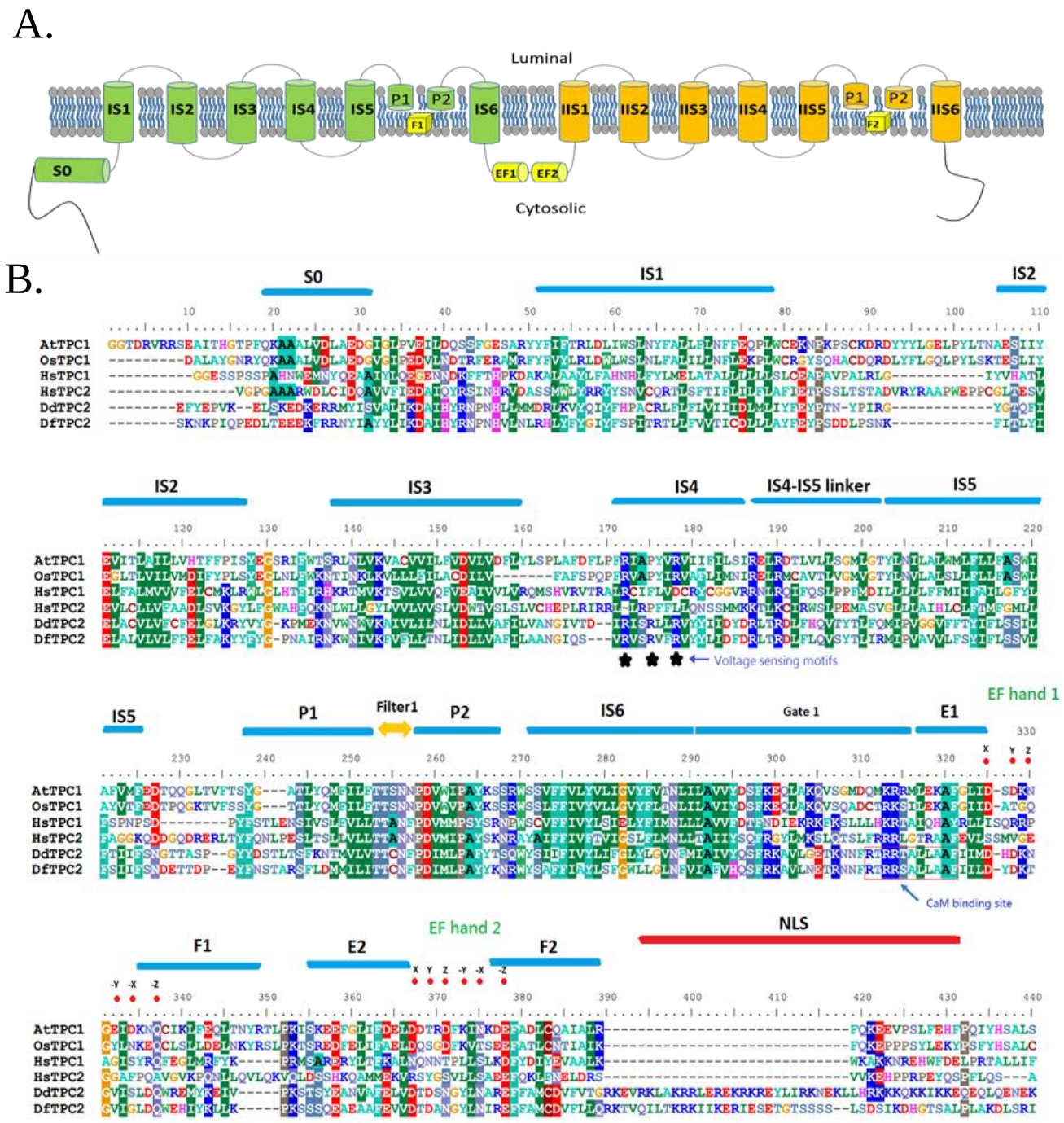

Figure 3.4. Domain sequence alignment of predicted TPC proteins.
A. Cartoon illustrating the domains of Arabidopsis TPC proteins, illustrating the 12 transmembrane domains (IS1-6 and IIS1-6), the pore regions (P1 and 2) the EF hands (EF1,2). B, C. Protein sequences from Arabidopsis AtTPC1 were aligned with TPC2 from *Dictyostelium discoideum* (DdTPC2), *D. fasciculatum* (DfTPC2), rice TPC1 (OsTPC1) and human TPCs (HsTPC1 and HsTPC2). The sequences were aligned using ClustalW built in BioEdit. Predicted transmembrane areas are labelled by blue lines. *Dictyostelid* specific motifs are labelled by red lines. B. Alignment of sequences from S0 to the second EF hand (EF2). C. Alignment of sequences from IIS1 to IIS6. EF hands, voltage sensing motifs and a potential calmodulin binding area are annotated in green, cyan and blue text, respectively.

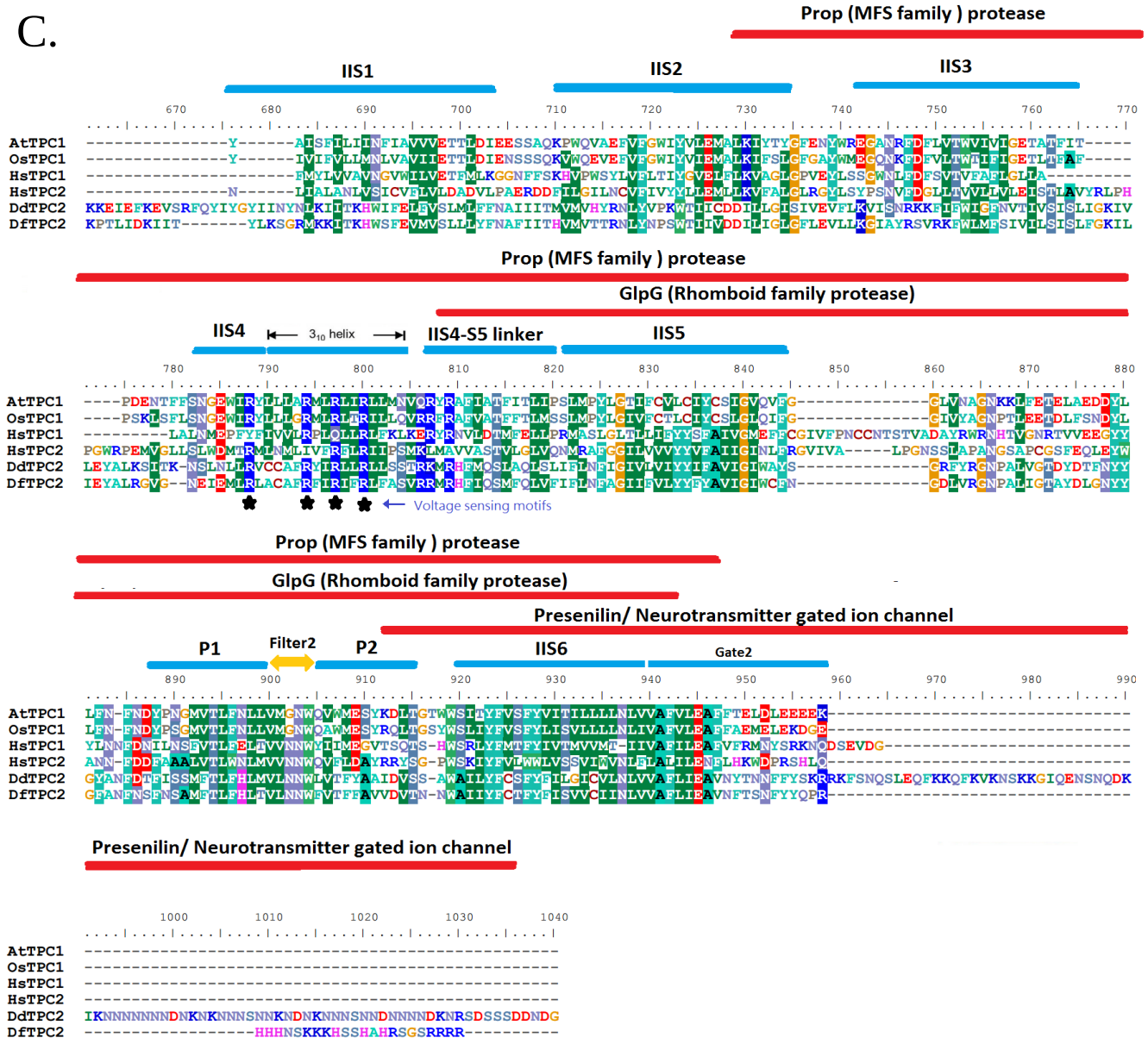

Figure 3.4. Domain sequence alignment of predicted TPC proteins.

A. Cartoon illustrating the domains of Arabidopsis TPC proteins, illustrating the 12 transmembrane domains (IS1-6 and IIS1-6), the pore regions (P1 and 2) the EF hands (EF1,2). B, C. Protein sequences from Arabidopsis AtTPC1 were aligned with TPC2 from *Dictyostelium discoideum* (DdTPC2), *D. fasciculatum* (DfTPC2), rice TPC1 (OsTPC1) and human TPCs (HsTPC1 and HsTPC2). The sequences were aligned using ClustalW built in BioEdit. Predicted transmembrane areas are labelled by blue lines. *Dictyostelid* specific motifs are labelled by red lines. B. Alignment of sequences from S0 to the second EF hand (EF2). C. Alignment of sequences from IIS1 to IIS6. EF hands, voltage sensing motifs and a potential calmodulin binding area are annotated in green, cyan and blue text, respectively.

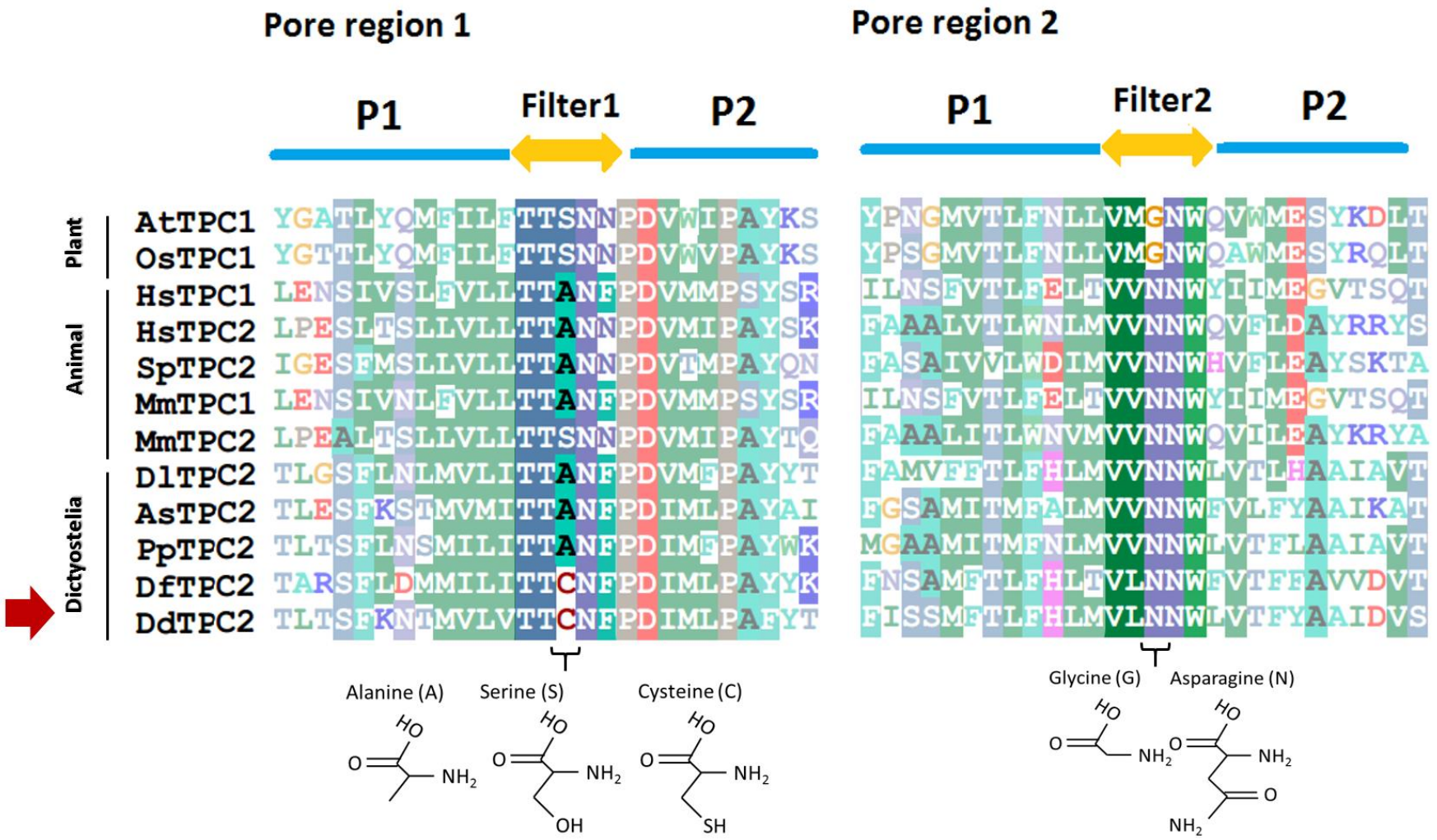

Figure 3.5. Pore domain sequence alignment.

Protein sequences forming the pore regions from Arabidopsis AtTPC1 are aligned with the predicted equivalent regions of TPC2 from Dictyostelia (*Dictyostelium discoideum, D. fasciculatum, D. lacteum, Acytostelium subglobosum and Polysphondylium pallidum*), rice TPC1 (*Oryza sativa* TPC1) and animal TPCs, including human (*Homo sapiens*), sea urchin (*Strongylocentrotus purpuratus*) and mouse (*Mus musculus*). The sequences were aligned using ClustalW built in BioEdit. Transmembrane pore areas are labelled with blue lines. Pore selectivity filters are labelled with yellow arrows. The structures of the relevant amino acids are shown for comparison.

3.3.3.2 Regulation by Ca^{2+}

In order to determine if Dictyostelid TPC2s could be regulated by Ca^{2+}, EF hands and Calmodulin binding motifs of Dictyostelid TPC2s were predicted using the Calmodulin Target Database (http://calcium.uhnres.utoronto.ca/ctdb/ctdb/home.html). Paired EF-hand motifs are known to serve as an important cytosolic Ca^{2+} activation site in plant TPC1, where cytosolic Ca^{2+} binds and potentiates voltage activation in the channel, and these motifs are conserved in Dictyostelid TPC2s. Although the EF-hand motifs are missing in animal TPCs, other Ca^{2+} binding proteins such as calmodulins retain conserved EF-hands motifs similar to plants and amoebae. Figure 3.6A shows conserved EF-hand motifs, EF1 and EF2, present in amoebae, plants and animals. It is interesting to note that *D. lacteum* is predicted to have lost the EF2 hand motif and the conserved AF sequence in the first helix region of EF1 is altered to SF (Figure 3.6A and Table 3.2). This suggests the functional EF-hand motifs in *D. lacteum* TPC2 are missing. In plants, only EF2 has been shown to have an essential role in Ca^{2+} sensing (Schulze *et al.*, 2011). Guo and colleagues (2016) found the tight protein packing around EF1 involving the S0 helix (Figure 3.4A) may explain the lack of EF1-dependent Ca^{2+} activation (Guo *et al.*, 2016). The S0 helix is also found in Dictyostelia (Figure 3.4B) so they might share a similar Ca^{2+} activation mechanism. Another mechanism by which Ca^{2+} may regulate proteins is via its interaction with Calmodulin (CaM), which is an important cytosolic Ca^{2+} binding protein that regulates many Ca^{2+} channels and pumps. The EF hands in CaM are highly conserved between plants, animal and amoebae: DdCaM is 89% identical to HsCaM and 82% identical to AtCaM (Figure 3.6B).

A conserved sequence "R-RR-ALLAAF" predicted to be a CaM-binding motif is located between the IS6 helix and an EF1 motif only in Dictyostelid TPC2s, but is not found in plants and animals (Table 3.2). In Dictyostelia, most of the predicted CaM binding sequences are found between IS6 and EF hand 1, except in *D. lacteum* the EF hand has lost one conserved alanine residue which is a serine labelled in red in Table 3.2. This means that this region has potentially lost both the characteristics of the CaM binding motif and the EF-hand, as the equivalent alanine is conserved in EF-hands in plants, animal and amoebae (Figure 3.6). However, a different CaM binding motif was predicted on IS0 in *D. lacteum*, which was predicted to be localised in the cytosolic side. This suggests that interaction between CaM and TPC2 might be functionally important in Dictyostelia.

Three conserved negatively charged amino acid residues, D, D and E in IS5, IIS1 and IIS4 respectively, have been shown to be important for luminal Ca^{2+} inhibition of the plant TPC1 ion channel activity (Guo *et al.*, 2016). However, sequence alignment shows these sites are not fully conserved in human TPC1 or TPC2 and are not conserved in Dictyostelid TPC2s (Figure 3.7).

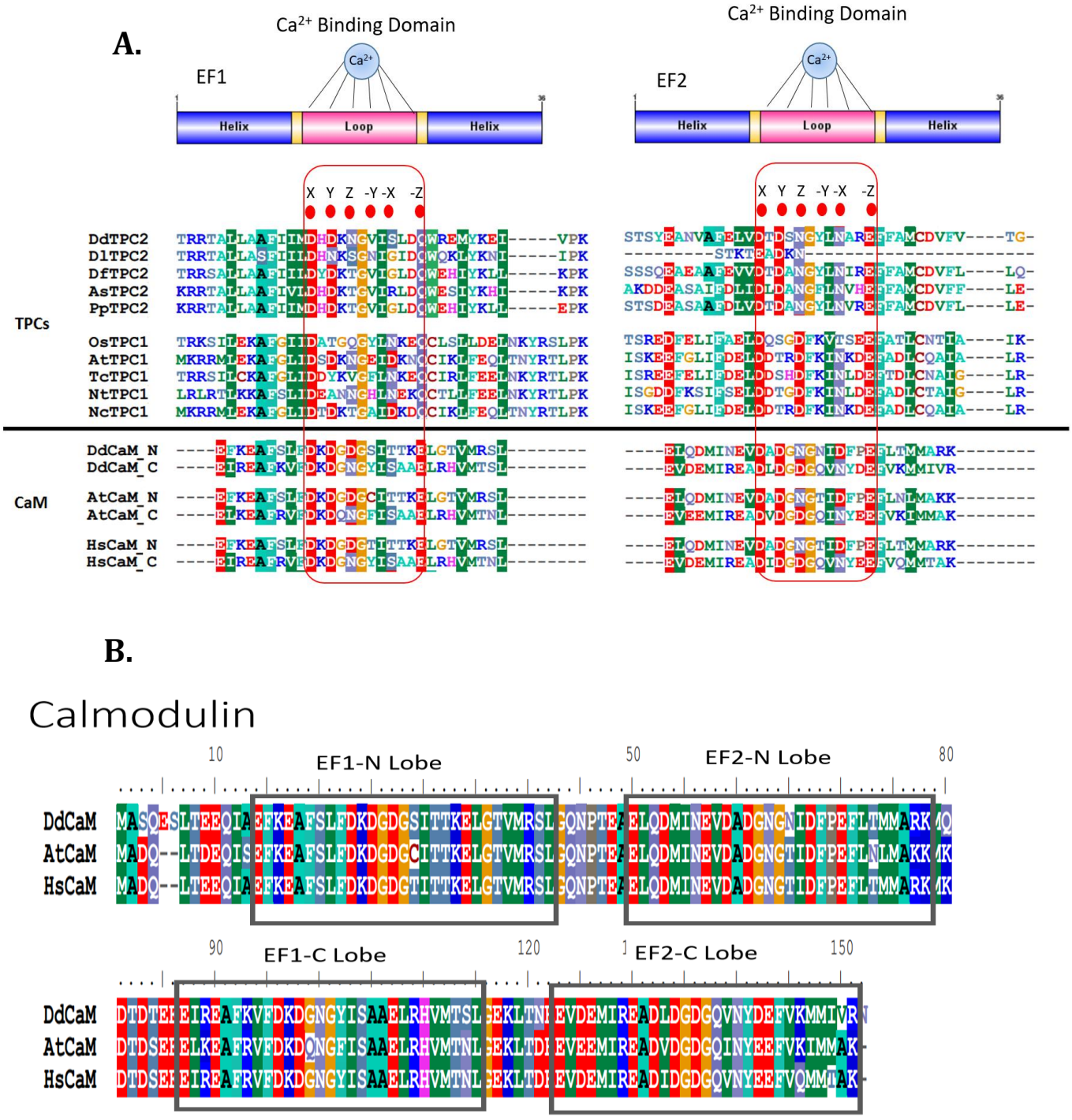

Figure 3.6. Calcium sensing/activation domain alignment.
(A) EF hand protein sequences from TPCs and calmodulins are aligned showing highly conserved sequences across organisms. The two EF hands of TPCs were aligned to compare sequences between plants (*Arabidopsis thaliana, Oryza sativa, Theobroma cacao, Nicotiana tabacum* and *Noccaea caerulescens*) and Dictyostelid (*Dictyostelium discoideum, D. lacteum, D. fasciculatum, Acytostelium subglobosum and Polysphondylium pallidum*). Animal TPCs do not have EF hands so the EF hand in calmodulin is used as a reference. N, N-lobe:C, C-lobe of EF hands. (B) Alignment of calmodulin sequences of *Dictyostelium (*DdCaM*)*, Arabidopsis (AtCaM) and human (HsCaM) illustrating highly conserved sequence overall. The sequences were aligned using ClustalW built in BioEdit.

Table 3.2. Predicted calmodulin binding motifs found on Dictyostelid TPC2 proteins.

	Organisms and TPCs	Predicted CaM binding motif on TPCs	Location	Correspondent EF hand sequences or nonfunctional EF hand residues
Dictyostelia	*Dictyostelium dicscoideum* TPC2	**RTRRTALLAAF**	767-777 IS6 - EF hand 1	**RTRRTALLAAF**IIMDHDKNGVISLDQWREMYKEIVPK
Dictyostelia	*Dictyostelium fasciculatum* TPC2	**RTRRSALLAAF**	531-541 IS6 - EF hand 1	**RTRRSALLAAF**IILDYDKTGVIGLDQWEHIYKLLKPK
Dictyostelia	*Acytostelium subglobosum* TPC2	**RKRRTALLAAF**	457-467 IS6 - EF hand 1	**RKRRTALLAAF**IVLDHDKTGVIRLDQWESIYKHIKPK
Dictyostelia	*Polysphondylium pallidum* TPC2	**RKRRTALLAAF**	540-550 IS6 - EF hand 1	**RKRRTALLAAF**IIMDHDKTGVIGLDQWEHIYKLLEPK
Dictyostelia	*Dictyostelium lacteum* TPC2	**IERRMNIACIL**	233-243 IS0	RTRRTALLA**S**FIILDHNKSGNIGIDQWQKLYKNIIPK
Plant	*Arabidopsis thaliana* TPC1	No matches	NA	QMKRRMLEKAFGLIDSDKNGEIDKNQCIKLFEQLTNYRTLPK
Plant	*Oryza sativa* TPC1	No matches	NA	CTRKSILEKAFGIIDATGQGYLNKEQCLSLLDELNKYRSLPK
Human	*Homo sapiens* TPC1	No matches	NA	LHKRTAIQHAYRLLISQRRPAGISYRQFEGLMRFYK
Human	*Homo sapiens* TPC2	No matches	NA	FRRRLGTRAAFEVLSSMVGEGGAFPQAVGVKPQNLL

The predicted calmodulin (CaM)-binding motifs were found by using the Calmodulin Target Database (http://calcium.uhnres.utoronto.ca/ctdb/ctdb/home.html). The CaM binding motifs were only found on the Dictyostelid TPC2 proteins. Most of the predicted sequences were located between IS6 and EF hand 1, except in *D. lacteum* the EF hand has lost one conserved residue (A to S, labelled in red) so it has lost both of the characteristics of the CaM binding motif and the EF hand. However, another predicted CaM binding motif was found on IS0 in *D. lacteum*. The EF hand sequences (underlined) are shown for reference. Predicted functional EF hands are coloured green, whereas the predicted non-functional EF hand sequences are black. The corresponding predicted CaM binding sequences are coloured blue.

Luminal Ca^{2+} inhibition site

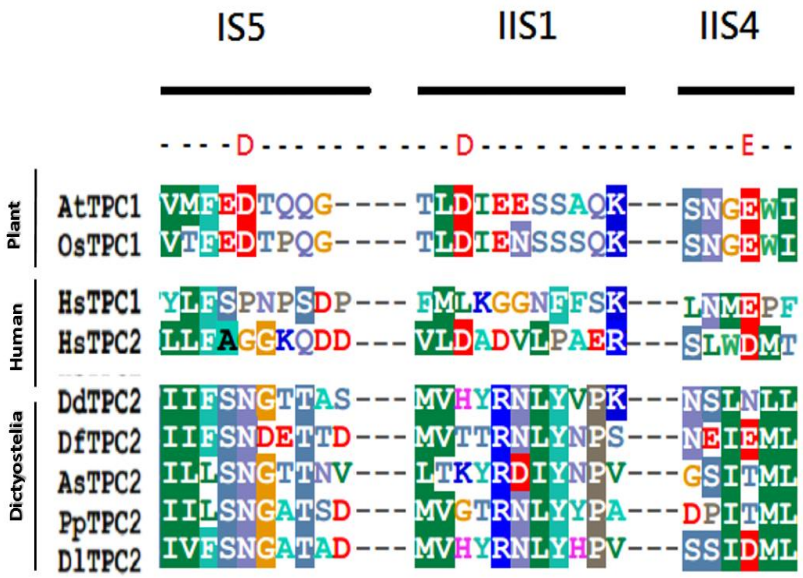

Figure 3.7. Luminal Calcium inhibition site alignment.
Plant TPCs are known to possess a luminal Calcium binding site (Kintzer and Stroud, 2016). The corresponding area of TPC sequences from plants (*Arabidopsis thaliana* and *Oryza sativa*,), Dictyostelia (*Dictyostelium discoideum, D. lacteum, D. fasciculatum, Acytostelium subglobosum and Polysphondylium pallidum*) and humans (*Homo sapiens*) were used for alignment. The sequences were aligned using ClustalW built in BioEdit.

3.3.3.3 Voltage sensing

Another important feature of TPC proteins is the voltage sensing domains, which are composed of a gating charge transfer centre on the S2 and S3 helices and a voltage sensing motif on S4 helix that responds to the transmembrane electric field. Movement of S4 is mechanically coupled to gating of the channel, which requires at least three regularly spaced positive charged residues in S4, and a counter anion region in S2 (Aggarwal and MacKinnon, 1996; Seoh *et al.*, 1996).

To check if the Dictyostelid TPC2s have classic voltage sensing motifs (VSM1 and VSM2), the sequences of the predicted voltage sensing motifs in Dictyostelid TPC2s were compared to the equivalent regions of plant, human TPC proteins and the regions from classic voltage sensitive channels, such as the *Drosophila* potassium channel, shaker and bacterial sodium channels, NavRh and NavAb. The consensus sequence of classic voltage sensing motifs features five conserved, regularly spaced, positively charged residues R1 to R5 (Figure 3.8).

For VSM1, all Dictyostelid TPC2s have three conserved residues R2, R3 and R4. The DlTPC2 even has retained R1 making it the most complete potential VSM1 relative to other amoebae, human and plants. The VSM1 of Dictyostelid TPC2s are more similar to human TPCs and are more closely related to the classic voltage sensing motif than plant TPC1s, which only have two of the arginine residues conserved, R2 and R4. It has been demonstrated that the VSM1 of plant TPC1 is not voltage sensitive (Guo *et al.*, 2016). For VSM2, all Dictyostelid TPC2s have four of the five conserved residues R1, R3, R4 and R5. This is similar to plant VSM2 and is more complete than VSM2 in

human TPCs. Only VSM2 in AtTPC1 is voltage sensitive, mediated by R3, R4 and R5, but not R1, and its S4 helix (IIS4) is the primary mobile component during voltage activation (Guo *et al.*, 2016).

A full functional VSM also requires a functional gating charge transfer centre on the S2 and S3 helices. The conserved sequence "Y--E-----" on S2 and a conserved D on the S3 helix are essential residues for the gating charge transfer centre based on the structure of plant TPC1 (Guo *et al.*, 2016; Kintzer and Stroud, 2016) (Figure 3.9). However this is not conserved in Dictyostelids, where they contain mostly "S--E-----"on the S2 and an N at the equivalent position on the S3 helix. DfTPC2 is even more diverged containing "G--E-----" on the S2 and an S on the S3 helix. With this sequence information we cannot determine if this diverged sequence is functioning as a gating transfer centre in Dictyostelia. To sum up, the Dictyostelid TPC2s have a set of residues required for the voltage sensing motif, but the gating transfer centres are atypical. Therefore it will be necessary to determine experimentally if the Dictyostelid TPC2s have functioning voltage sensing mechanisms.

A graphical illustration summarising the putative topology of DdTPC2 gathered from structure and sequence information in conjunction with predicted domains and motifs is shown in Figure 3.10.

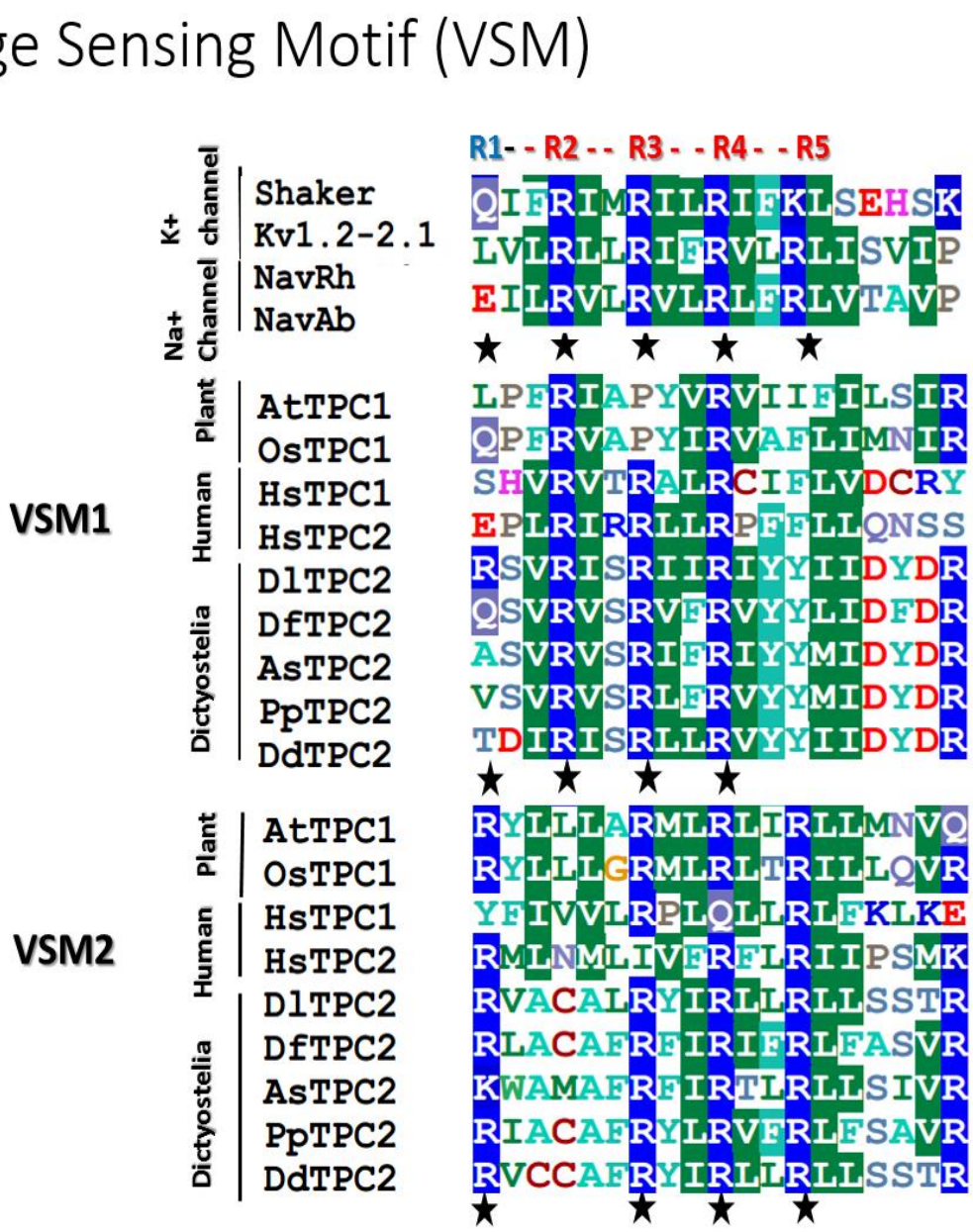

Figure 3.8. Voltage sensing motif alignment.
Sequences from classic voltage sensitive channels, the *Drosophila* potassium channel, shaker, bacterial sodium channels, NavRh and NavAb are compared to the equivalent region in TPCs from plants (*Arabidopsis thaliana* and *Oryza sativa*), Dictyostelia (*Dictyostelium discoideum, D. lacteum, D. fasciculatum, Acytostelium subglobosum and Polysphondylium pallidum*) and humans (*Homo sapiens*). The sequences were aligned using ClustalW built in BioEdit. Identical and /or similar sequences are shaded with the colour table function built in BioEdit. The conserved arginine residues required for voltage sensing, R1 to R5, are labelled with stars.

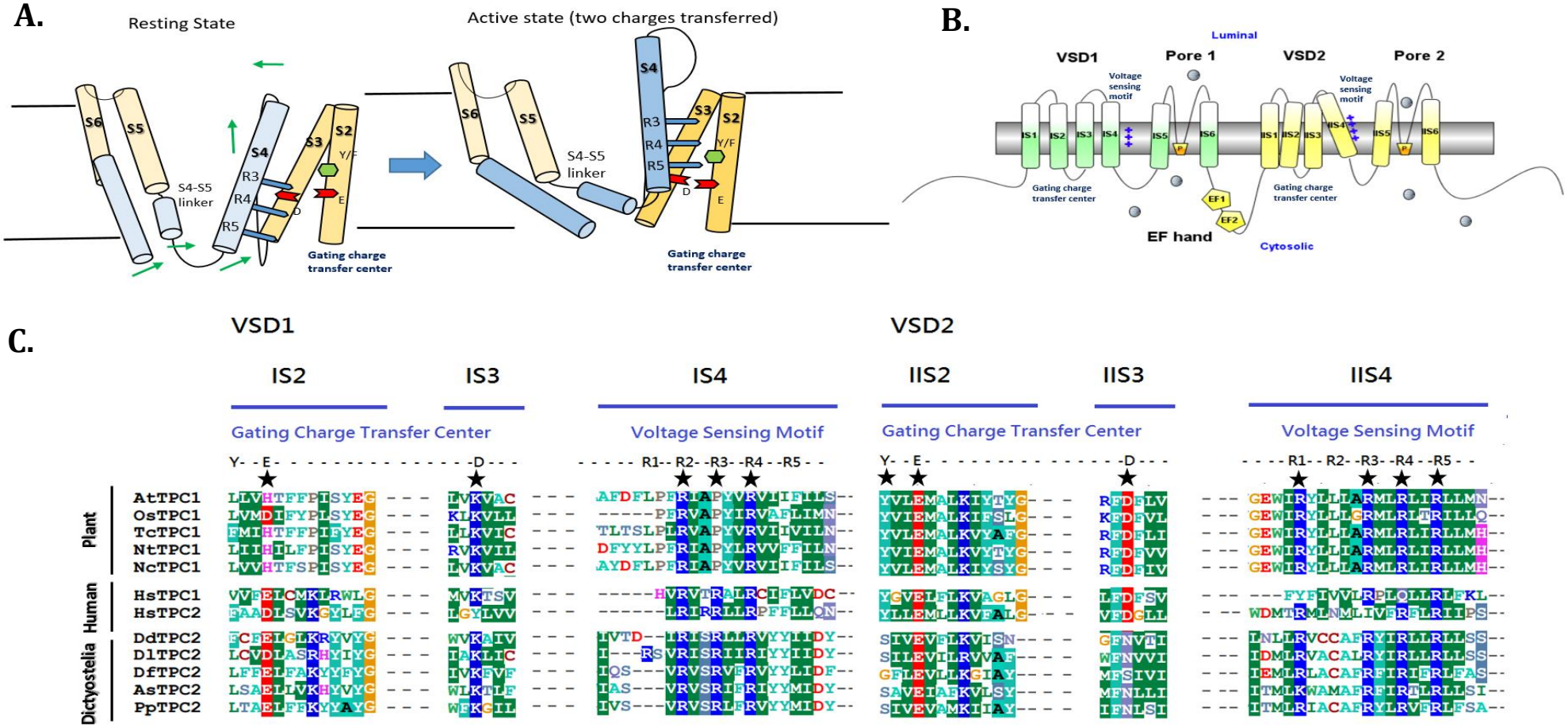

Figure 3.9. Voltage sensing mechanism alignment.

(A) Cartoon demonstrating the interaction between a classic gating charge transfer centre and 3 arginines on the voltage sensing motifs from resting state to active state adapted from (Guo *et al.*, 2016). (B) Cartoon showing the components of the voltage sensing motif and gating charge transfer centre. (C) The predicted voltage sensing regions from TPCs proteins from plants (*Arabidopsis thaliana*, *Oryza sativa*, *Theobroma cacao*, *Nicotiana tabacum* and *Noccaea caerulescen*,), Dictyostelids (*Dictyostelium discoideum, D. lacteum, D. fasciculatum, Acytostelium subglobosum and Polysphondylium pallidum*) and human (*Homo sapiens*) were aligned using ClustalW built in BioEdit. The consensus arginine residues are labelled with stars.

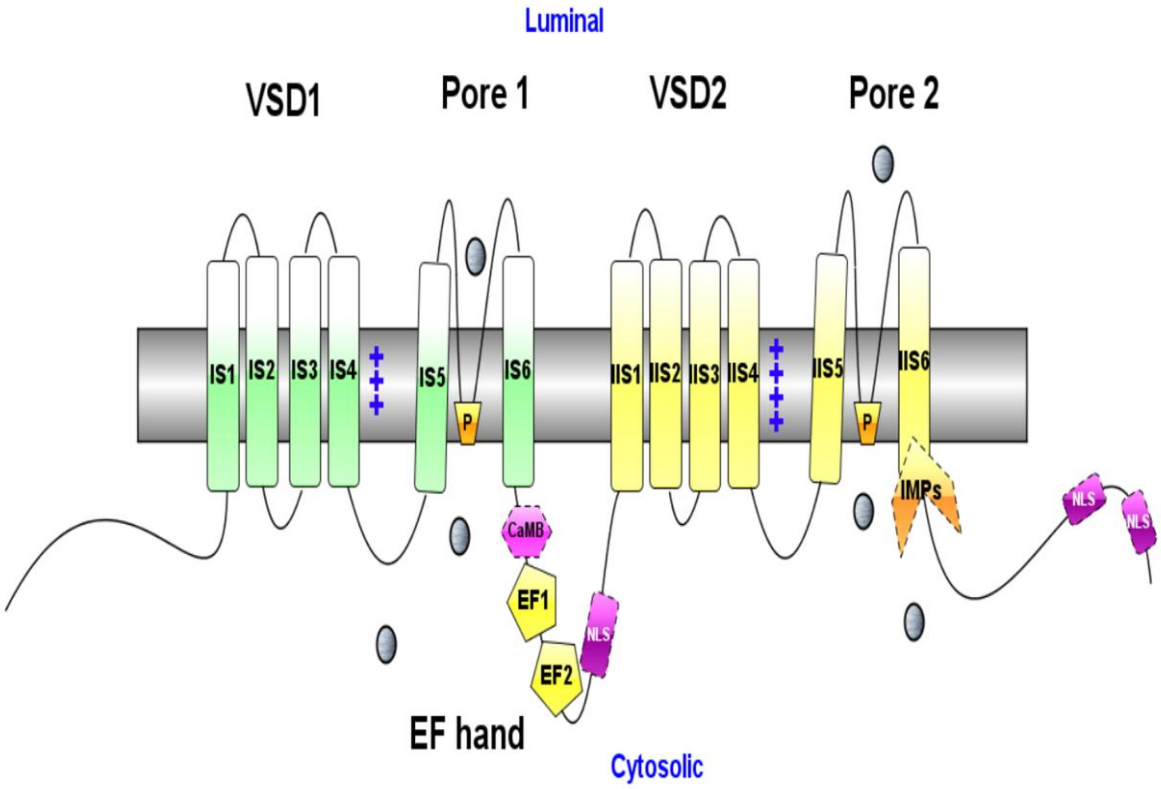

Figure 3.10. Illustration of the predicted topology of DdTPC2.
A summary gathered from sequence information in conjunction with predicted domains and motifs. The dashed shapes indicate conserved regions of unknown function. The solid shapes indicates more confident or known structures or functional regions. VSD, voltage sensing domain: IS, intramembrane sequence: P, pore domain: EF, EF hand, calcium binding motif: CaMB, calmodulin binding domain: NLS, nucleus localization sequence: IMPs, intramembrane protease sequences.

3.3.4. Predicted functional partners of DdTPC2.

In order to gain a further insight into the function of DdTPC2, I investigated the potential functional partners of TPCs using bioinformatics. Sequences of DdTPC2, AtTPC1, HsTPC2 and HsTPC2 were analysed using STRING (Search Tool for the Retrieval of Interacting Genes/Proteins (http://string-db.org/). Protein–protein interaction networks were analysed and visualized as in Figure 3.11 and Table 3.3. The coloured lines between functional partners represent different types of evidence used in predicting and\or summarising the associations, which are purple lines (experimental\ biochemical evidence), yellow lines (textmining evidence), green lines (neighbourhood in the genome evidence), blue lines (gene co-occurrence evidence), light blue lines (database evidence), black lines (co-expression evidence) and red lines (fusion evidence).

The results predict that the TPCs may have different functional partners in plants and animals and Dictyostelia. In *D. discoideum*, DdTPC2 was predicted to interact with ubiquitin domain containing proteins, calcineurin-related proteins and three different Ca^{2+} P-type ATPases, included the major Ca^{2+} pump in the *Dictyostelium* contractile vacuole, PAT1 (Figure 3.11 A). These results were predicted based on both experimental/biochemical data (purple lines) and textmining (yellow lines). The experimental/biochemical data indicates putative homologues of DdTPC2 were experimentally found to be interacting in another species (*Mus musculus*). The textmining indicates putative homologues of DdTPC2 from another species (*Rattus norvegicus*) were found mentioned together with these proteins in PubMed abstracts. *Dictyostelium* PAT1 is highly related to other Ca^{2+} ATPases of the plasma membrane (PMCA), and *patA* gene expression is up-regulated when cells are grown in a high Ca^{2+} environment (Coukell *et al.*, 1995; Moniakis *et al.*, 1995) Up-regulation of *patA*

expression is strongly reduced when the serine/threonine phosphatase calcineurin is inhibited, suggesting regulation of *patA* gene expression via a calcineurin-dependent pathway (Moniakis *et al.*, 1999).

In plants, the AtTPC1 was summarised and\or predicted to interact with proteins containing ATP binding cassettes, cyclic nucleotide gated channels (CNGCs), Ca^{2+} transporting ATPase, two pore K^{+} channels and vacuolar cation/proton exchanger (CAX), in which the evidences were gathered from experiments (purple lines), textmining (yellow lines), neighbourhood in the genome (green lines) and gene co-occurrence (blue lines).Similar to *Dictyostelium* TPC2 and *patA*, it is worth noting that plant TPC1 is also predicted to work with a Ca^{2+} transporting ATPase, suggested this might be an evolutionarily conserved relationship (Figure 3.11B and Table 3.3B).

Human TPCs were summarised and\or predicted to interact with mucolipin, sodium/potassium/calcium exchangers, HAX-1, MTOR, serine/threonine protein kinase and melanogenesis related proteins and other proteins, where the evidences were gathered from experiments (purple lines), textmining (yellow lines) and gene co-occurrence (blue lines) (Figure 3.11 C and D, Table 3.3C and D).

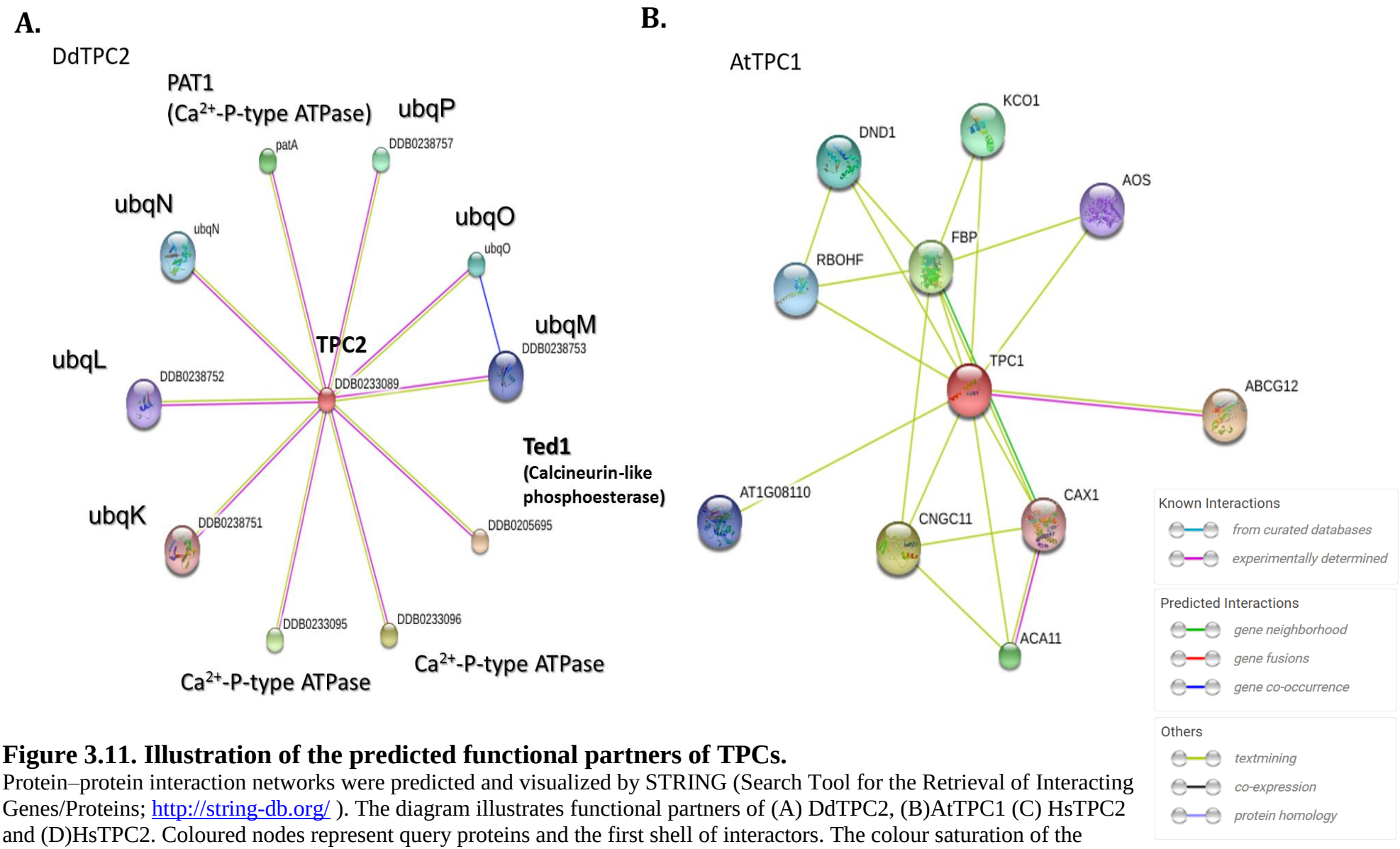

Figure 3.11. Illustration of the predicted functional partners of TPCs.
Protein–protein interaction networks were predicted and visualized by STRING (Search Tool for the Retrieval of Interacting Genes/Proteins; http://string-db.org/). The diagram illustrates functional partners of (A) DdTPC2, (B)AtTPC1 (C) HsTPC2 and (D)HsTPC2. Coloured nodes represent query proteins and the first shell of interactors. The colour saturation of the edges represents the confidence score of a functional association. Details of predicted protein partners are listed in Table 3.3.

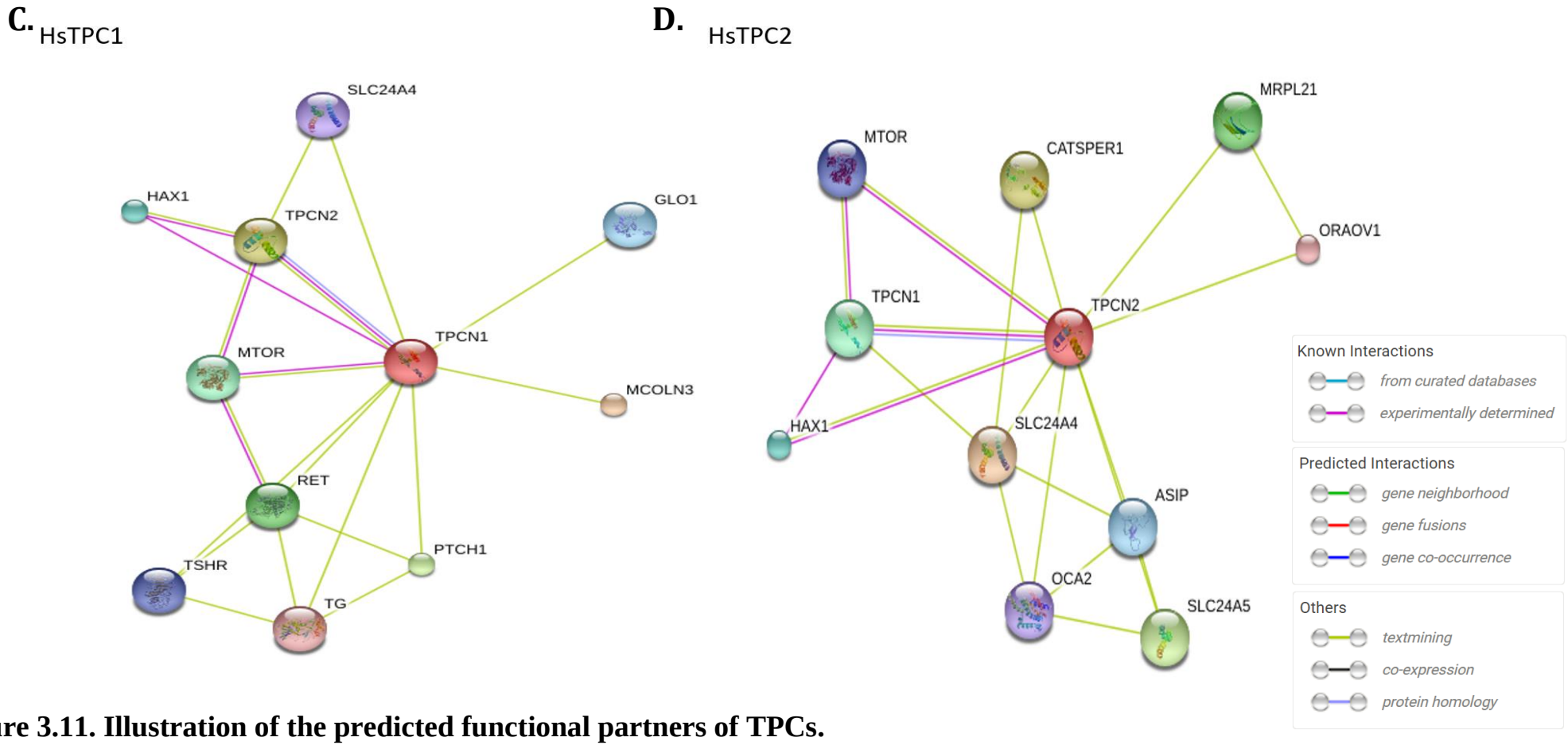

Figure 3.11. Illustration of the predicted functional partners of TPCs.
Protein–protein interaction networks were predicted and visualized by STRING (Search Tool for the Retrieval of Interacting Genes/Proteins; http://string-db.org/). The diagram illustrates functional partners of (A) DdTPC2, (B) AtTPC1 (C) HsTPC2 and (D)HsTPC2. Coloured nodes represent query proteins and the first shell of interactors. The colour saturation of the edges represents the confidence score of a functional association. Details of predicted protein partners are listed in Table 3.3.

Table 3.3. Predicted functional partners of TPCs.

A.

DdTPC2: Predicted Functional Partners	Annotation	Homology score
Calcineurin-like phosphoesterase	**Ted1, Calcineurin-like phosphoesterase (DDB0205695, 387aa).** Metallophosphoesterase 1; GPI anchor biosynthetic process; ER to Golgi vesicle-mediated transport	0.636
P-type ATPases	**Calcium-transporting P-type ATPase PAT1(1115 aa).** P-type ATPase that is up-regulated in calcium-adapted cells; contains 10 predicted transmembrane domains. Calcium ATPase involved in Ca(2+) homeostasis as a component of the contractile vacuole complex. **DDB0233096, P-type ATPase (927 aa).** Conserved plasma membrane calcium ATPases (PMCA), similar to *Dictyostelium* PAT1; contains 10 predicted transmembrane domains. **DDB0233095, P-type ATPase (1077 aa).** Orthologue of the conserved plasma membrane calcium ATPases (PMCA) such as *Dictyostelium* PAT1; contains at least 8 predicted transmembrane domains.	0.611
Ubiquitin domain-containing proteins.	**Ubiquitin domain-containing proteins.** UbqK (DDB0238751, 314aa) and UbqP(DDB0238757, 312 aa): NAD+ ADP-ribosyltransferase activity. UbqL (148aa), UbqM (275 aa) , ubqN (73 aa) and ubqO (77 aa):Putative uncharacterized protein	0.576

B.

AtTPC1: Predicted Functional Partners	Annotation	Homology score
ABCG12	**ATP-binding cassette G12**; Involved in the secretion of cuticular wax from epidermal cells to the cuticle (687 aa)	0.811
CNGC11	**Cyclic nucleotide-gated channels**; Putative cyclic nucleotide-gated ion channel (621 aa)	0.760
FBP	**Fructose-1,6-bisphosphatase** (341 aa)	0.635
ACA11	**Ca2+-transporting ATPase**; This magnesium-dependent enzyme catalyzes the hydrolysis of ATP coupled with the translocation of calcium from the cytosol out of the cell or into organelles (By similarity)	0.633
KCO1	**Two Pore K Channel**; Voltage-independent, large conductance and potassium- selective tonoplast ion channel. Regulated by cytoplasmic calcium and pH.	0.623
DND1	**DEFENSE NO DEATH 1**; Acts as cyclic nucleotide-gated ion channel. Permeable to K(+) and Ca(2+) in a cyclic nucleotide-dependent fashion (cAMP or cGMP). Could also transport lithium, cesium and rubium and displays a strong selectivity against sodium.	0.622
RBOHF	**Respiratory Burst Oxidase**; Calcium-dependent NADPH oxidase that generates superoxide. Generates reactive oxygen species (ROS) during incompatible interactions with pathogens and is important in the regulation of the hypersensitive response (HR).	0.598
AT1G08110	**Lactoylglutathione lyase**; Catalyzes the conversion of hemimercaptal, formed from methylglyoxal and glutathione, to S-lactoylglutathione (By similarity)	0.596
AOS	**Allene oxide synthase**	0.580
CAX1	**Cation exchanger 1**; Vacuolar cation/proton exchanger (CAX). Translocates Ca(2+) and other metal ions into vacuoles using the proton gradient formed by H(+)-ATPase and H(+)-pyrophosphatase.	0.542

The predicted functional partners found by STRING (Search Tool for the Retrieval of Interacting Genes/Proteins; http://string-db.org/). The table lists predicted functional partners of (A) DdTPC2, (B)AtTPC1 (C) HsTPC2 and (D)HsTPC2. The proteins are ranked according to the homology score.

Table 3.3. Predicted functional partners of TPCs.

C.

HsTPC1: Predicted Functional Partners	Annotation	Homology score
MCOLN3	**Mucolipin 3.**	0.852
TPCN2	**Two pore channel 2**; NAADP receptor that may function as one of the major voltage-gated Ca(2+) channels (VDCC) across the lysosomal membrane.	0.703
PTCH1	**Patched 1**.	0.689
RET	**Ret proto-oncogene**; Receptor tyrosine-protein kinase involved in numerous cellular mechanisms including cell proliferation, neuronal navigation, cell migration, and cell differentiation upon binding with glial cell derived neurotrophic factor family ligands.	0.650
MTOR	**Mechanistic target of rapamycin** (serine/threonine kinase); Serine/threonine protein kinase which is a central regulator of cellular metabolism, growth and survival in response to hormones, growth factors, nutrients, energy and stress signals. Activated mTORC1 up-regulates protein synthesis by phosphorylating key regulators of mRNA translation and ribosome synthesis.	0.629
HAX1	**HCLS1 associated protein X-1**; Promotes cell survival. Potentiates GNA13-mediated cell migration. Involved in the clathrin-mediated endocytosis pathway. May be involved in internalization of ABC transporters such as ABCB11. May inhibit CASP9 and CASP3. May regulate intracellular calcium pools.	0.576
GLO1	**Glyoxalase I**; Catalyzes the conversion of hemimercaptal, formed from methylglyoxal and glutathione, to S-lactoylglutathione. Involved in the regulation of TNF-induced transcriptional activity of NF- kappa-B	0.573
TG	**Thyroglobulin**.	0.439
SLC24A4	**Solute carrier family 24** (sodium/potassium/calcium exchanger), member 4; Transports 1 Ca(2+) and 1 K(+) in exchange for 4 Na(+).	0.439
TSHR	**Thyroid stimulating hormone receptor**.	0.457

The predicted functional partners found by STRING (Search Tool for the Retrieval of Interacting Genes/Proteins; http://string-db.org/). The table lists predicted functional partners of (A) DdTPC2, (B)AtTPC1 (C) HsTPC2 and (D)HsTPC2. The proteins are ranked according to the homology score.

Table 3.3. Predicted functional partners of TPCs.

D.

HsTPC2: Predicted Functional Partners	Annotation	Homology score
SLC24A4	**Solute carrier family 24** (sodium/potassium/calcium exchanger), member 4; Transports 1 Ca(2+) and 1 K(+) in exchange for 4 Na(+)	0.825
SLC24A5	**Solute carrier family 24**, member 5; Cation exchanger involved in pigmentation, possibly by participating in ion transport in melanosomes. Probably transports 1 Ca(2+) and 1 K(+) in exchange for 4 Na(+)	0.748
CATSPER1	**Cation channel, sperm associated 1**; Voltage-gated calcium channel that plays a central role in calcium-dependent physiological responses essential for successful fertilization, such as sperm hyperactivation, acrosome reaction and chemotaxis towards the oocyte.	0.749
MRPL21	**Mitochondrial ribosomal protein L21**.	0.712
TPCN1	**Two pore channel 1**; NAADP receptor that may function as one of the major voltage-gated Ca(2+) channels (VDCC) across the lysosomal and endosomal membrane	0.703
HAX1	**HCLS1 associated protein X-1**; Promotes cell survival. Potentiates GNA13-mediated cell migration. Involved in the clathrin-mediated endocytosis pathway. May be involved in internalization of ABC transporters such as ABCB11. May inhibit CASP9 and CASP3. May regulate intracellular calcium pools.	0.613
ASIP	**Agouti signaling protein**; Involved in the regulation of melanogenesis. The binding of ASP to MC1R precludes alpha-MSH initiated signaling and thus blocks production of cAMP, leading to a down-regulation of eumelanogenesis (brown/black pigment) and thus increasing synthesis of pheomelanin (yellow/red pigment). In higher primates, agouti may affect the quality of hair pigmentation rather than its pattern of deposition. Could well play a role in neuroendocrine aspects of melanocortin action. May have some functional role in regulating the lipid metabolism with adipocytes	0.608
MTOR	**Mechanistic target of rapamycin** (serine/threonine kinase); Serine/threonine protein kinase which is a central regulator of cellular metabolism, growth and survival in response to hormones, growth factors, nutrients, energy and stress signals. Activated mTORC1 up-regulates protein synthesis by phosphorylating key regulators of mRNA translation and ribosome synthesis.	0.593
OCA2	**Oculocutaneous albinism II**; Could be involved in the transport of tyrosine, the precursor to melanin synthesis, within the melanocyte. Regulates the pH of melanosome and the melanosome maturation. One of the components of the mammalian pigmentary system.	0.585
ORAOV1	**oral cancer overexpressed 1**	0.537

The predicted functional partners found by STRING (Search Tool for the Retrieval of Interacting Genes/Proteins; http://string-db.org/). The table lists predicted functional partners of (A) DdTPC2, (B)AtTPC1 (C) HsTPC2 and (D)HsTPC2. The proteins are ranked according to the homology score.

3.3.5. Generation of Calcium channel null strains

In order to determine if *Dictyostelium discoideum* TPC2 has a role in development and to examine and compare its function with that of other putative Ca^{2+} channels located on acidic stores (mucolipin) and neutral stores (IplA), I generated strains in which the genes coding for TPC2, mucolipin and IplA had been disrupted.

3.3.6. Construction of *tpc2*, *mcln* and *iplA* disruption vectorS

A strategy to disrupt the endogenous genes by homologous recombination was designed. To do this, two plasmids, pLPBLP–*tpc2* and pLPBLP–*mcln*, were constructed, designed to cause disruption of the corresponding loci on endogenous chromosomes by insertion of a blasticidin resistance (bsR) cassette through homologous recombination (Figures 3.12 and 3.13). The disruption plasmid for *iplA* (pTD5) previously used to successfully disrupt this gene (Traynor *et al.*, 2000) was obtained from the *Dictyostelium* Stock Center. The original bsR region of the pTD5 plasmid was replaced by the bsR cassette from pLPBLP flanked by two *loxP* sites, to generate pTLB (Figure 3.14).

3.3.7. Generation of *tpc2*$^-$, *mcln*$^-$ and *tpc2*$^-$*mcln*$^-$ strains

The pLPBLP–*tpc2* and pLPBLP–*mcln* disruption vectors were linearised using *Kpn*I and *BamH*I restriction enzymes and then electroporated into Ax2 cells (Figure 3.15A and Figure 3.16A). Electroporated cells were cultured at varying dilutions in 96 well plates in HL5 medium supplemented with 10 μg/ml blasticidin in order to yield clonal transformants. Blasticidin-resistant colonies formed a monolayer after approximately 14 days and transformants were screened via PCR to identify clones with integration of

the bsR cassette at the *tpc2* or *mcln* locus using appropriate primers (Figure 3.15A and Figure 3.16A). Cells in which targeted disruption has occurred were identified via a PCR screen (Figure 3.15B, Figure 3.16B-1). The 5 potential *tpc2*-disruption clones (T-II-1, T-II-23, T-I-10, T-I-16 and T-I-22) out of 100 screened showed successful insertion of both the 5' arm and 3'arm, indicating putative disruption of the *tpc2* gene (Figure 3.15B). The potential *mcln*-disruption clones (M47, M58, M62, M63, M68 and M70) which contained successful insertions of both the 5' arm and 3'arm, indicating disruption of the *mcln* gene (Figure 3.16B-1) were identified out of 72 colonies in the initial screen.

To generate *tpc2* and *mcln* double disruption mutants, the $tpc2^-$ strain (T-I-22) was electroporated with Cre expression plasmid pDEX-NLS-cre. The *loxP* sites flanking the bsR cassette allowed the resistance gene to be removed and blasticidin sensitive clones were isolated. The *mcln* gene was then disrupted in this strain as previously described (Figure 3.16A) and one potential double disruption ($tpc2^-mcln^-$) clone TM55 identified (Figure 3.15B-2) by PCR. The strain TM55 was further electroporated with Cre expression plasmid pDEX-NLS-cre and blasticidin sensitive colonies identified to facilitate generation of triple mutants.

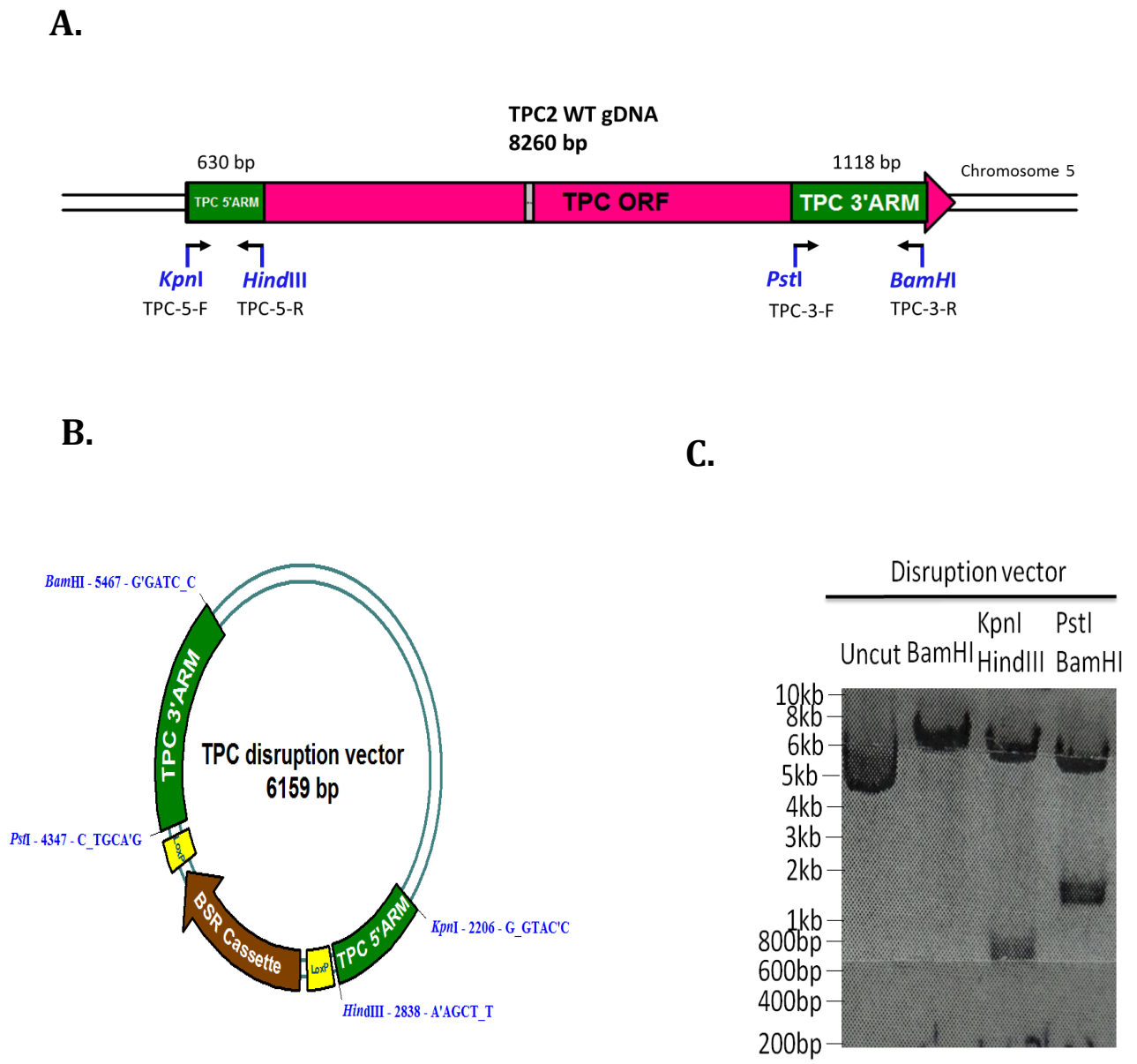

Figure 3.12. Construction of the *tpc2* disruption vector.

(A) 5' and 3' arms were amplified from genomic DNA using primers with restriction enzyme sites compatible with the vector pLPBLP. The purple region of the gene denotes the open reading frame (ORF) of TPC protein; the green fragments show the 5' arm and 3'arm used in the disruption cassette. The grey region denotes an intron. (B) The map of the TPC disruption vector. The yellow boxes denote the *lox p* sites facilitating construction of strains with multiple disrupted Ca^{2+} channels. (C) Diagnostic digestion of the disruption vector shows correct insertion of the 5' and 3'arms. Expected fragment sizes are 630 bp for the 5' arm and 1118bp for the 3' arm.

A.

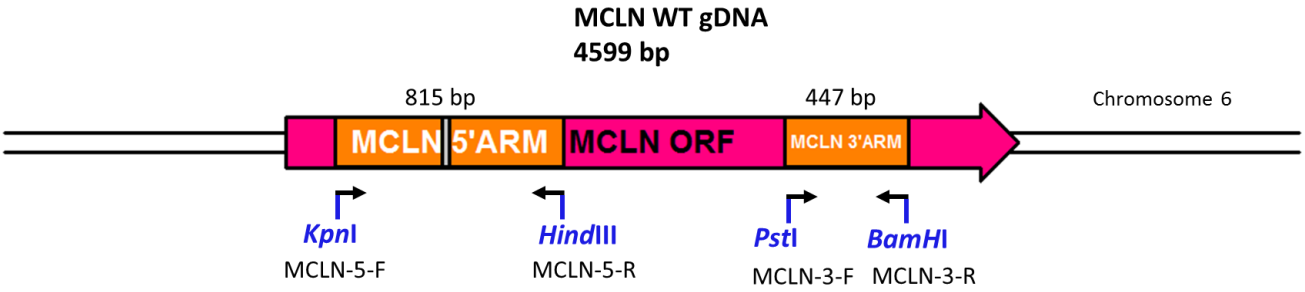

B.

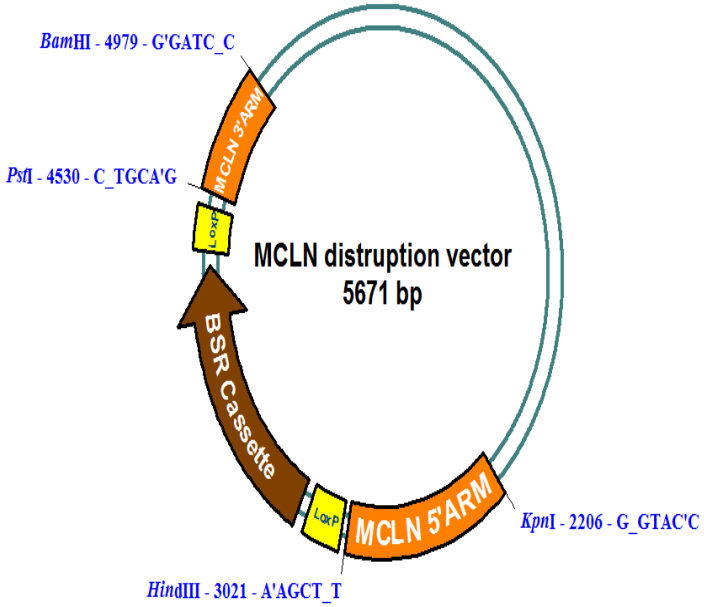

C.

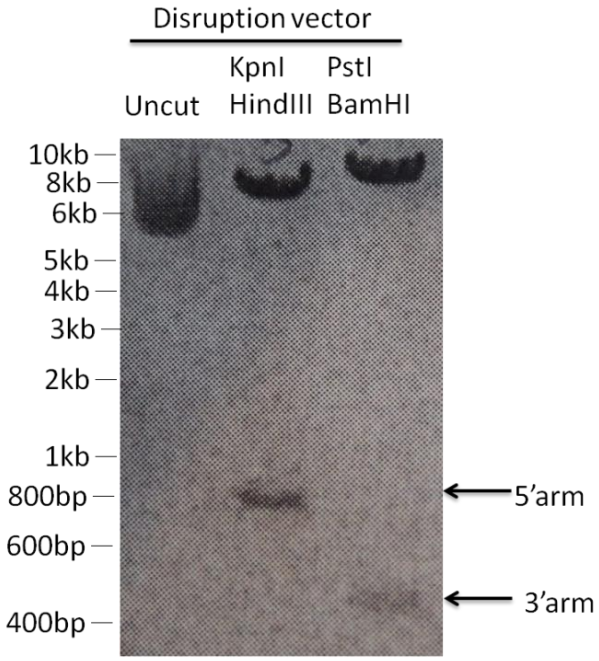

Figure 3.13. Cloning strategy for *mcln* disruption vector.
(A) 5' and 3' arms were amplified from genomic DNA using primers with restriction enzyme sites compatible with the vector pLPBLP. The pink region of the gene denotes the open reading frame (ORF) of mucolipin; the orange fragments show the 5' arm and 3'arm used in the disruption cassette. The grey region on 5' arm denotes an intron. (B) The map of the MCLN disruption vector. The yellow boxes denote the *lox p* sites facilitating construction of strains with multiple Ca^{2+} channels disruptions. (C) Diagnostic digestion of the disruption vector shows correct insertion of the 5' and 3'arms. Expected fragment sizes are 815 bp for the 5' arm and 447 bp for the 3' arm.

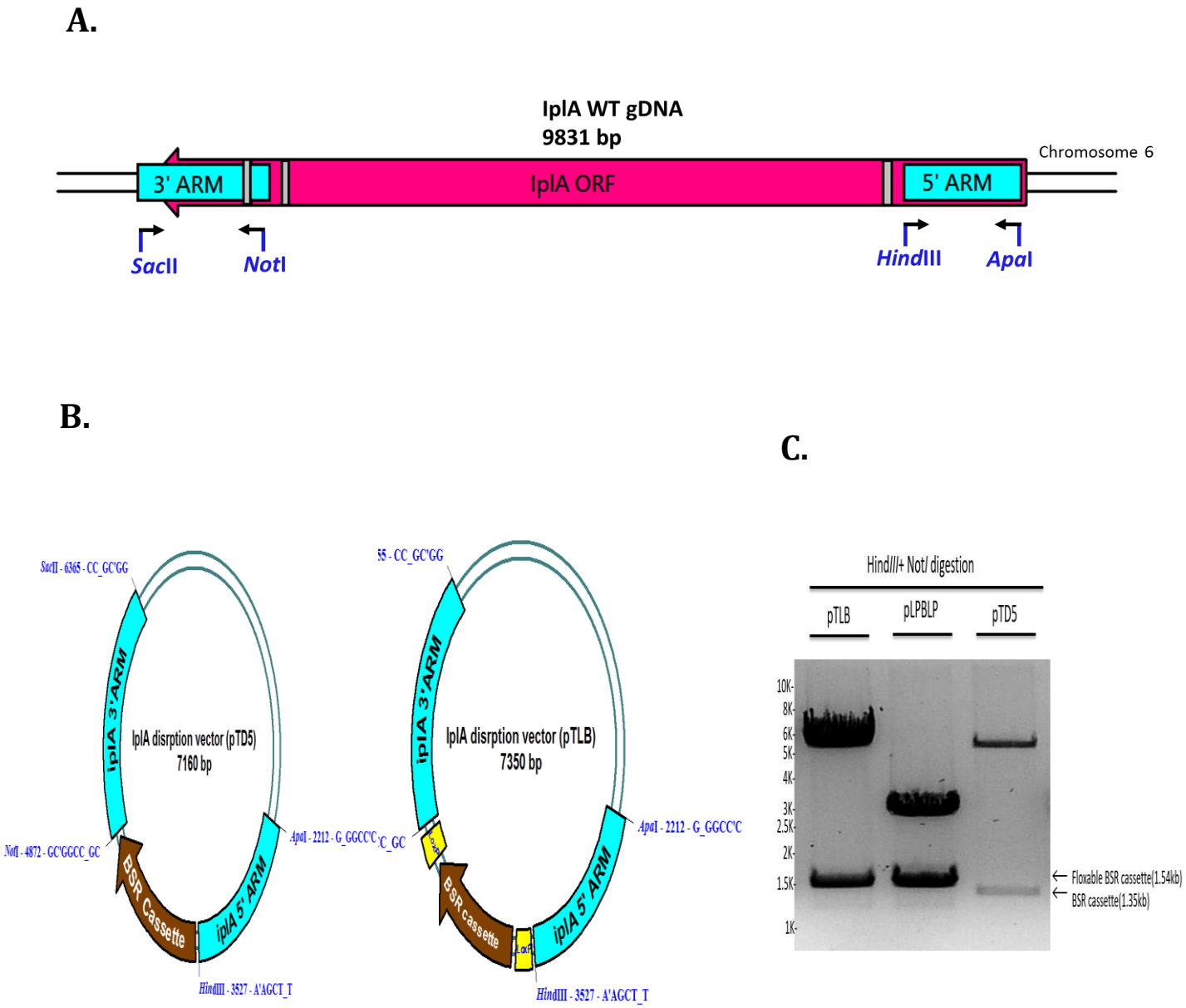

Figure 3.14. Cloning strategy for *iplA* disruption vector.
(A) Map of the positions of 5' and 3' arms in genomic DNA and corresponding primers introduced restriction enzyme sites used in the pTD5, an *iplA*- disruption vector (Traynor *et al.*, 2000), which was obtained from The *Dictyostelium* Stock Center. The pink region of the gene denotes the open reading frame (ORF); the cyan fragments show the 5' arm and 3'arm used in the disruption cassette. The grey regions denote introns. (B) The map of the original *iplA* disruption vector, pTD5 (left) and the modified vector, pTLB (right). The original pTD5, which was lacking *lox p* sites was replaced by a BSR cassette from pLPBLP by utilising *Hind*III and *Not*I restriction sites. The new cassette has two *lox p* sites allowing constructing multiple disruption strains in the future. (C) Diagnostic digestion of the pTLB vector by using *Not*I and *Hind*III shows correct insertion of the new BSR cassette from pLPBLP.

A.

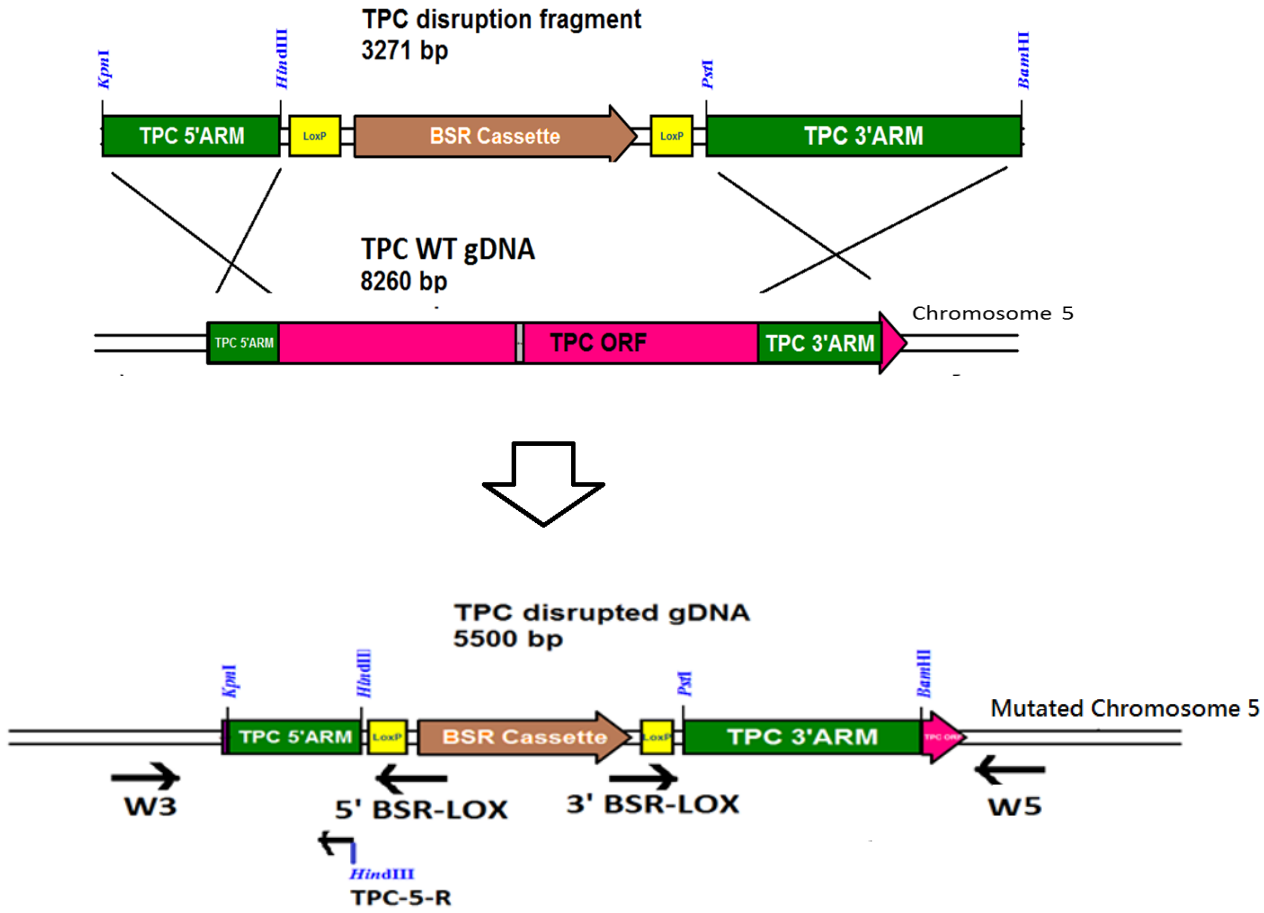

B.

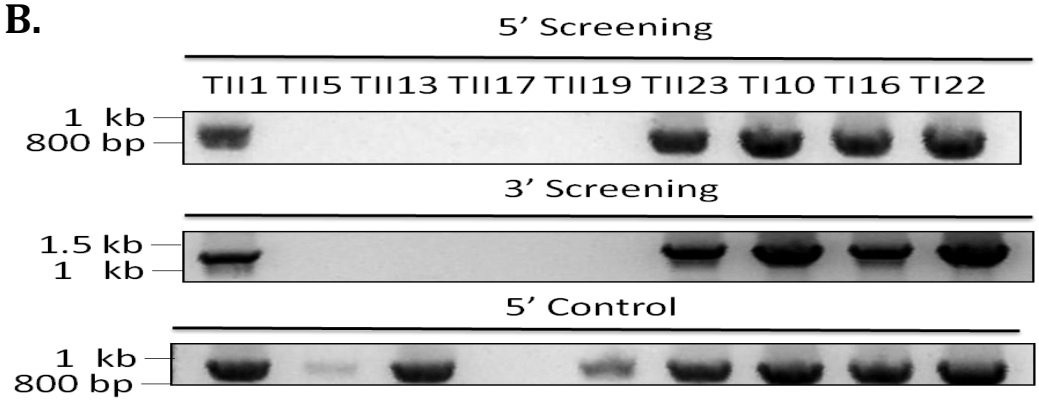

Figure 3.15. PCR screening of potential *tpc2*$^{-}$ disruptants.
(A) Schematic representation of the homologous recombination event. (B) Genomic DNA (gDNA) was prepared from each colony and used in a diagnostic PCR screen to confirm integration of the bsR cassette at the *tpc* locus. Two primer sets (W3, 5' BSR-LOX and 3' BSR-LOX, W5) were used in a PCR reaction to check for targeted insertion of the bsR cassette at the 5' and 3' ends, respectively. A primer set (W3 and TPC-5-R) was used as the positive control reaction. A random insertion of the bsR cassette would produce no PCR product for the screen, only targeted insertion of both arms would produce 938 bp and 1271bp bands. Clones T-II-1, T-II-23, T-I-10, T-I-16 and T-I-22 had successful insertions of both the 5' arm and 3'arm. The PCR bands were resolved on 1% agarose gels.

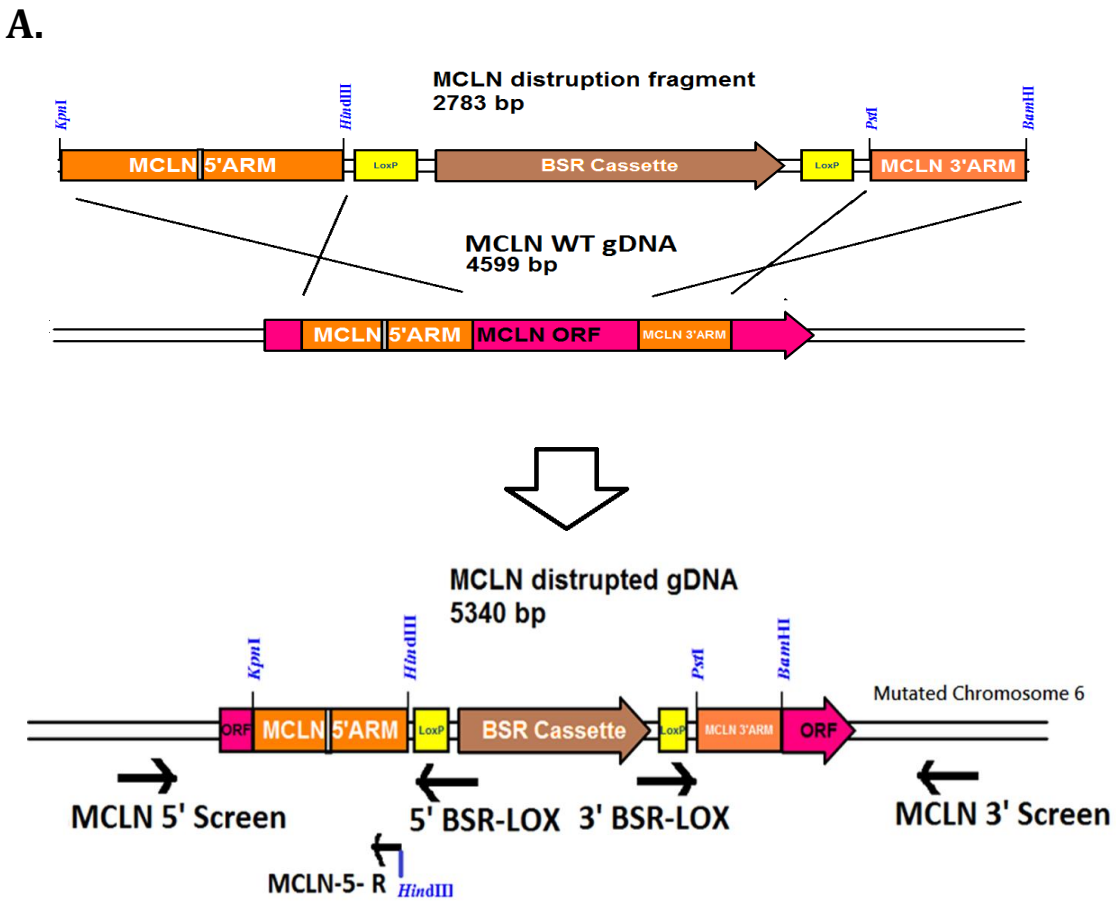

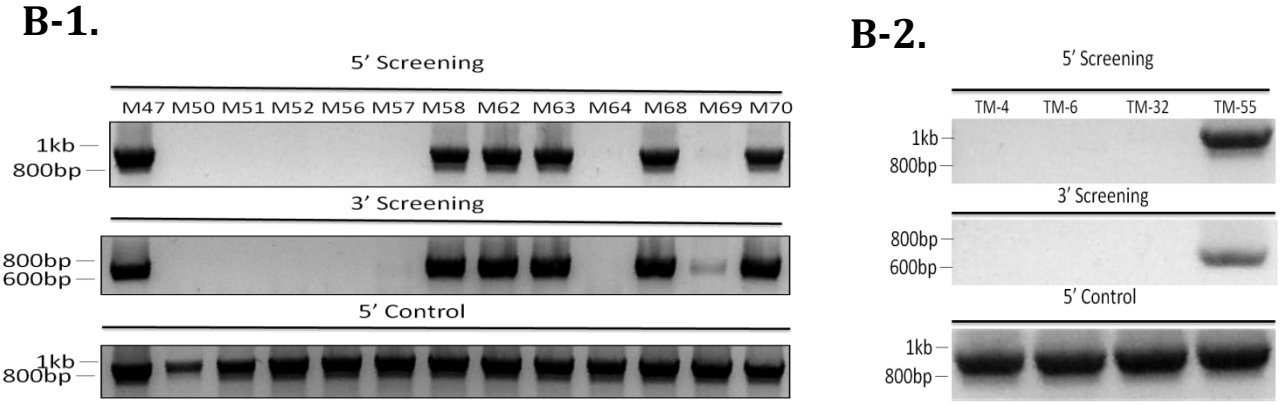

Figure 3.16. PCR screening of potential *mcln*$^-$ and *tpc2*$^-$*mcln*$^-$ double disruptants.
(A) Schematic representation of the homologous recombination event. (B) gDNA was prepared from each colony and used in a diagnostic PCR screen to confirm integration of the bsR cassette at the *mcln* locus. Two primer sets (MCLN 5'Screen, 5' BSR-LOX and 3' BSR-LOX, MCLN 5'Screen) were used in a PCR reaction to check for targeted insertion of the bsR cassette at the 5' and 3' ends, respectively. A primer set (MCLN 5'Screen and MCLN-5-R) was used as a positive control. A random insertion of the bsR cassette would produce no PCR product for the screen, only targeted insertion of both arms would produce a 956 bp and 633 bp bands. (B-1) *mcln*$^-$ clones M47, M58, M62, M63, M68 and M70 had successful insertions of both the 5' arm and 3'arm. (B-2) Double mutant (*tpc2*$^-$ *mcln*$^-$) clone TM-55 had successful insertion of both the 5' arm and 3'arm. Only one clone was identified out of 72 colonies in the initial screen. The PCR bands were resolved on 1% agarose gels.

3.3.8. Generation of *iplA*$^{-}$ and triple disruption strains

The pTLB disruption vector was linearised using *ApaI* and *SacII* restriction enzymes and then electroporated into Ax2 cells and cre-loxed cell lines TPC22B20 (*tpc2*$^{-}$) and TM55C (*tpc2*$^{-}$*mcln*$^{-}$) (Figure 3.17A). The procedures were carried out as above. In 14 days Blasticidin-resistant colonies formed a monolayer and were screened via PCR to identify clones with integration of the BSR cassette at the *iplA* locus using appropriate primers (Figure 3.17A). Cells in which targeted disruption has occurred were identified via a PCR screen and *SmaI* restriction diagnosis (Figure 3.17B-1 and B-2). The 3 potential *iplA*-disruption clones (IPLA-2, 7 and 14) out of 20 screened, 3 potential *tpc2-iplA* disruption mutants (TI-1-13, TI-2-8 and TI-2-19) out of 40 screened and 2 potential *tpc2*$^{-}$*mcln*$^{-}$*iplA*$^{-}$ triple mutants (TMI-55C and 67G) out of 100 screened showed successful insertion of both the 5' arm and 3'arm, indicating disruption of the *iplA* gene (Figure 3.17B-1 and B-2) (data not shown for other clones).

3.3.9. Confirmation of disruption strains

These potential disruption clones were plated on bacterial Ka plates at different dilutions (100, 1000 and 10,000 fold) to obtain single colonies, and the growing edges were harvested. PCR screening using primers in the deleted regions of the genes confirmed the loss of the coding sequences for *tpc2*, *mcln* or *iplA* as expected (shown for clones, 22B-20 (*tpc2*$^{-}$), M47E (*mcln*$^{-}$) and TM55A (*tpc2*$^{-}$*mcln*$^{-}$), (Figure 3.18) IPLA-1-2B, 1-2D, 1-7A, 1-7B, 1-14A, 1-14B (*iplA*$^{-}$), TI-1-13C, TI-2-8C and TI-2-19C (*tpc2*$^{-}$*iplA*$^{-}$) and TMI-67G (*tpc2*$^{-}$*mcln*$^{-}$*iplA*$^{-}$) (Figure 3.19) (data not shown for other clones)

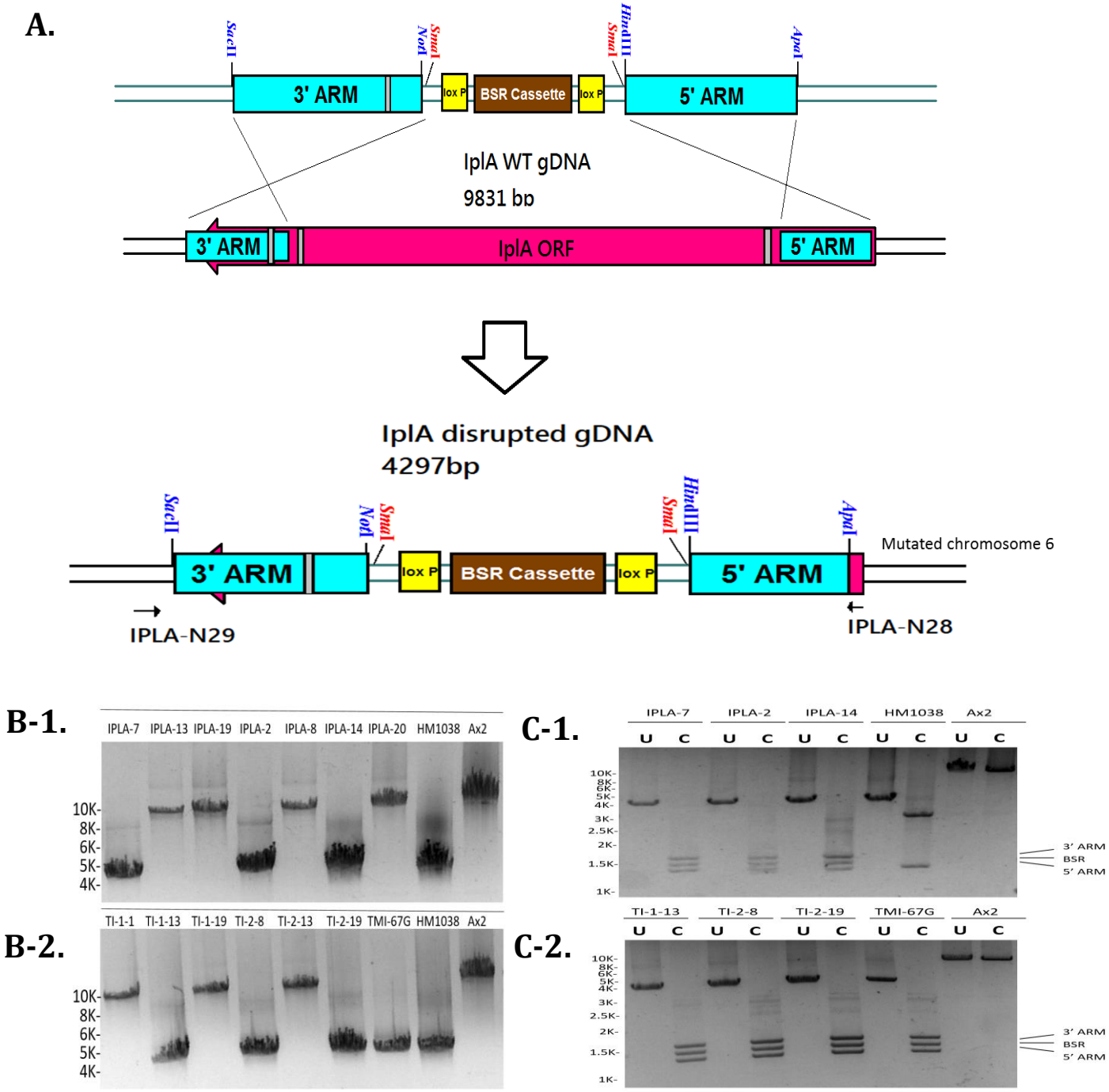

Figure 3.17. PCR screening of potential *iplA*$^-$, *tpc2*$^-$*iplA*$^-$ and *tpc2*$^-$*mcln*$^-$*iplA*$^-$ mutants.
(A) Schematic representation of the homologous recombination event. (B) gDNA was prepared from each colony and used in a diagnostic PCR screen to detect potential disruption clones that reduced size of fragment including the *iplA* gene. A primer set (IPLA-N28 and IPLA-N29) located outside of both arms was used in a PCR reaction to determine the genomic DNA size of the region containing the gene *iplA* according to previous research (Traynor *et al.*, 2000). Ax2 was used as a WT control with expected size of PCR product of 10,065 bp, whereas HM1038, an *iplA*$^-$ reference strain from *Dictyostelium* Stock Center with expected size of PCR product of 4,537bp, was used as a positive control. (B-1) *iplA*$^-$ clones (B-2) Double mutant (*tpc2*$^-$*iplA*$^-$) and triple mutant (*tpc2*$^-$*mcln*$^-$*iplA*$^-$) clones. The PCR bands were resolved on 1% agarose gels. (C-1 and C-2) PCR products of *iplA*$^-$ clones IPLA-2, 7, 14 and HM1038 were further cut with *SmaI* restriction enzyme showing all the putative KO clones have *SmaI* sites, where only those strains having a floxed BSR cassette have 2 *SmaI* sites flanking the BSR cassette to generate 3 fragments from the PCR product whereas the HM1038 PCR product only has one *SmaI* site and the Ax2 product remains uncut as there are no *SmaI* sites in the wild-type *iplA* gene.

A.

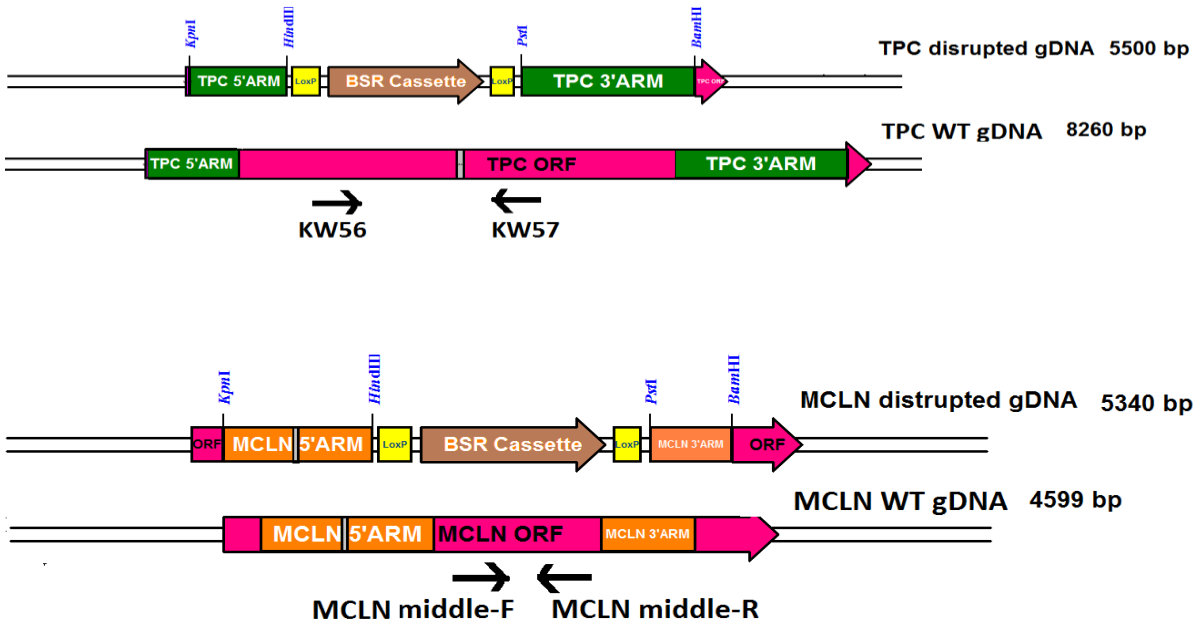

B.

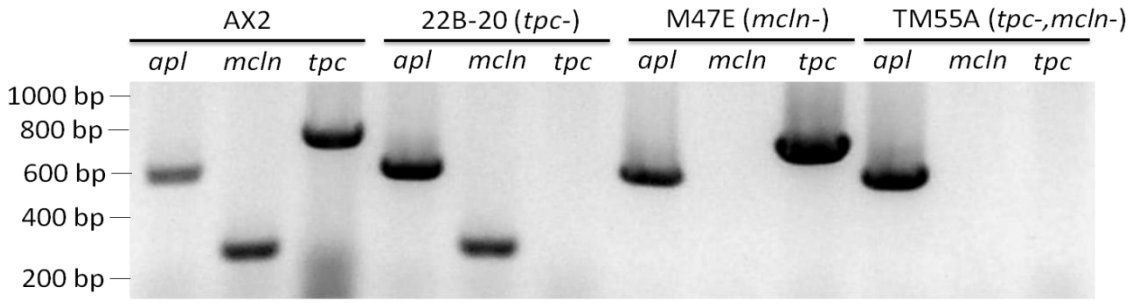

Figure 3.18. Confirmation of *tpc2*$^-$, *mcln*$^-$ and *tpc2*$^-$*mcln*$^-$ double disruption strains by PCR of genomic DNA.

(A) Schematic representation of the design of primers for detection of wild type gDNA. Primers amplifying the central region of TPC (KW56 and KW57), which is absent in the null strains of *tpc2*, were used to detect the presence of wild type *tpc2* gene. Similarly, primers amplifying the middle region of MCLN (MCLN middle-F and MCLN middle-R), which is absent in the null strains of *mcln* and in the double disruption strains of *tpc2* and *mcln*, were used to detect the presence of any wild type *mcln* gene. (B) Genomic DNA isolated from the parental strain AX2 and mutants, 22B-20 (*tpc*$^-$), M47E (*mcln*$^-$) and TM55A (*tpc2*$^-$*mcln*$^-$) was analysed by PCR using the above primers. Only strains containing wild type *mcln* or *tpc2* genes would produce a 280 bp or 775 bp band, respectively. PCR of the gene encoding *apl* was carried out (614 bp) as a positive control. The PCR products were resolved on a 0.8% agarose gel.

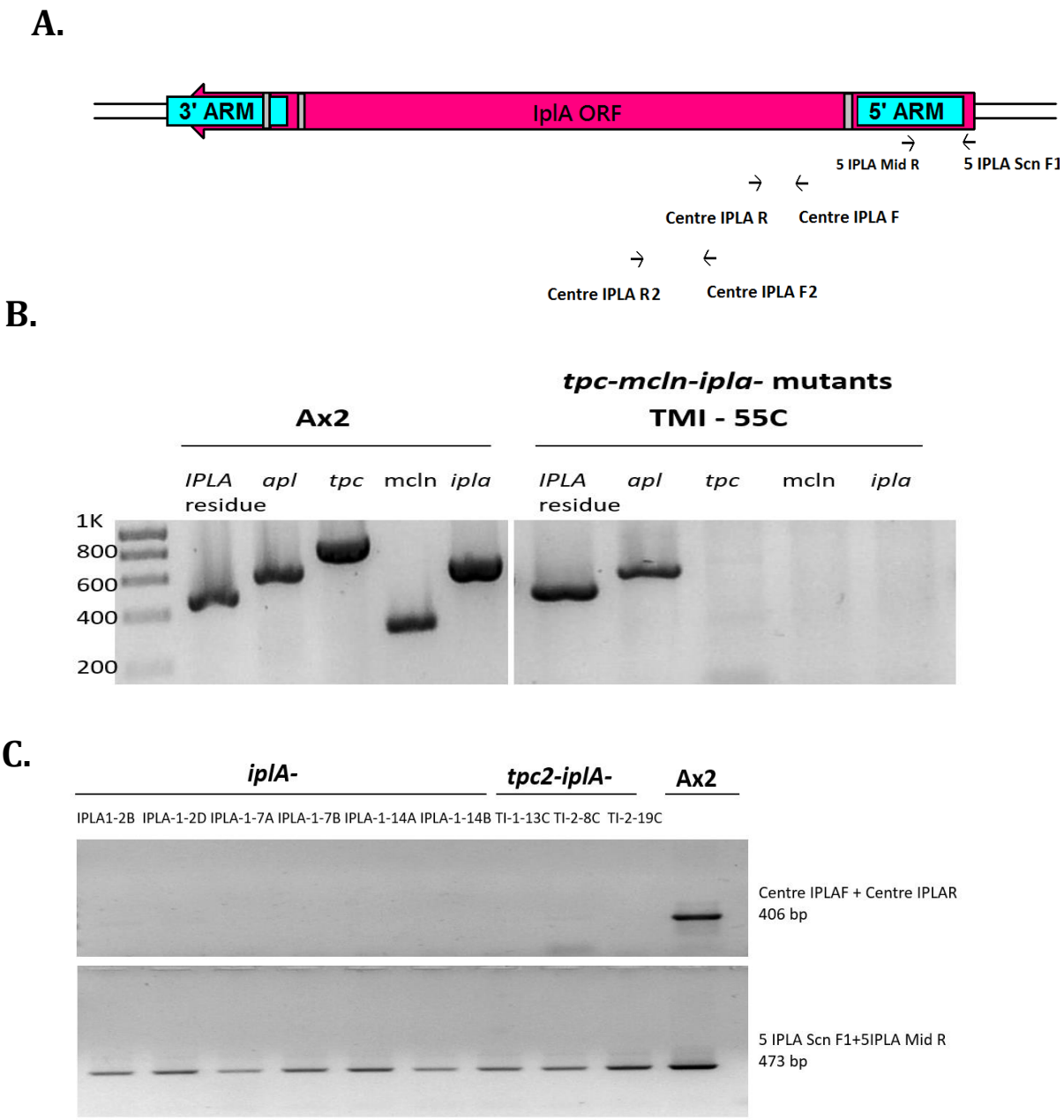

Figure 3.19. Confirmation of *iplA* gene disruption by PCR of genomic DNA.

(A) Schematic representation of the design of primers for detection of wild type gDNA. Primers amplifying the central region of *iplA* (Centre IPLAF and Centre IPLAR or Centre IPLAF2 and Centre IPLAR2), which is absent in the null strains of *iplA*, were used to detect the presence of wild type *iplA* gene. Similarly, primers amplifying the residual 5 'ARM region of IplA (5 IPLA Mid R and 5 IPLA Scn F1), which remains in both WT and mutants, were used as a positive control. (B) Genomic DNA isolated from the parental strain AX2 and mutants, IPLA-1-2B IPLA-1-2D, IPLA-1-7A, IPLA-1-7B, IPLA-1-14A and IPLA-1-14B (*iplA*$^-$), TI-1-13C and TI-2-8C and TI-2-19C (*tpc2*$^-$ *iplA*$^-$) were analysed by PCR using the above primers. Only strains containing wild type *iplA* gene would produce a 406 bp band. PCR of the residual part of *iplA* gene was carried out (473 bp) as a loading control. The PCR products were resolved on a 1% agarose gel. (C) Similarly, primers in the above diagrams were used to detect if the WT sequence of the central region of *iplA* (primer set: Centre IPLAF2 and Centre IPLAR2, product size 565 bp), *tpc2* and *mcln* were absent in a triple mutant TMI-55C. PCR amplification of the *apl* gene was used as a positive control.

3.3.10. Development of disruption strains

In order to determine whether TPC, mucolipin and IplA play roles in development, clones TPC22B-20 (*tpc2*$^-$) and MCLN47 (*mcln*$^-$) and iplA12D (*iplA*$^-$) and TMI67B (*tpc2*$^-$*mcln*$^-$*iplA*$^-$) were allowed to develop.

The strains were all developed initially at high cell density on filters. The results showed that all mutant strains were able to form fruiting bodies in a similar time to parental cells (Figure 3.20A, B and C). All the mutants did not show obvious phenotypic differences from the parental cells, despite increased expression of *tpc2* late in development (dictybase.org). However, the *tpc2*$^-$ and *tpc2*$^-$*mcln*$^-$*iplA*$^-$cells formed slightly smaller and broken aggregates comparing to other strains at the 10th hour of development (Figure 3.20A). Moreover, the *tpc2*$^-$ and *mcln*$^-$ cells tend to form slugs at the 12th hour of development, which was earlier than the wild type and other mutants (Figure 3.20A and B). This suggests the calcium channels on the acidic stores might play a role in this stage of development. However the fruiting bodies were phenotypically normal. Three repeats showed similar results (data not shown).

3.3.11. Early development of disruption strains

In order to observe if the Ca^{2+} channels have roles in early development, cells were developed on agarose (Figure 3.21) or under buffer (Figure 3.22) at lower cell densities as the cells developed more slowly during these early stages than on filters. Both the *tpc2*$^-$ and *tpc2*$^-$*mcln*$^-$*iplA*$^-$ disrupted mutants showed a developmental delay both on agarose and under buffer.

When cells were developed on agarose, although all cell lines had started aggregation by the 6th hr of development, the *tpc2*$^{-}$ and *tpc2*$^{-}$*mcln*$^{-}$*iplA*$^{-}$ cells aggregated more slowly than the other cell strains (Figure 3.21). This delay was most obvious at the 9th hr of development. At this stage Ax2, *mcln*$^{-}$ cells and *iplA*$^{-}$ cells had mostly finished aggregation whereas the *tpc2*$^{-}$ and *tpc2*$^{-}$*mcln*$^{-}$*iplA*$^{-}$ mutants were still making long streams of aggregating cells. The aggregation zones were usually larger and more streams were observed in the *tpc2*$^{-}$ and *tpc2*$^{-}$*mcln*$^{-}$*iplA*$^{-}$ cells (Figure 3.21A and B). At the 12th hr of development, streams were still observed in the *tpc2*$^{-}$ and *tpc2mcln-iplA*-disrupted cell lines. After the 12th hr of development, all strains could form slugs and later fruiting bodies. However, it is interesting to note that *mcln*$^{-}$ cells seemed to be slightly delayed in forming fruiting bodies since fewer fruiting bodies were found before the 24th hour.

The results of agarose development indicate that the *tpc2*$^{-}$ and *tpc2*$^{-}$*mcln*$^{-}$*iplA*$^{-}$ mutants were delayed in the early stage of development. To confirm this, the cells were further developed under buffer, where the early development process was prolonged but development halts after aggregate formation. All strains except *tpc2*$^{-}$ and *tpc2*$^{-}$*mcln*$^{-}$*iplA*$^{-}$ mutants started to form aggregates at the 6th hr of development (Figure 3.22). The *tpc2*$^{-}$ and *tpc2*$^{-}$*mcln*$^{-}$*iplA*$^{-}$ cells did not start aggregation until the 9th hr of development. In contrast, the Ax2, *mcln*$^{-}$ and *iplA*$^{-}$ cells had formed loose aggregates at this stage. At the 12th hr of development, all the cells except *tpc2*$^{-}$ and *tpc2*$^{-}$*mcln*$^{-}$*iplA*$^{-}$ cell lines had finished aggregation and formed tight aggregates, whereas the *tpc2*$^{-}$ and *tpc2*$^{-}$*mcln*$^{-}$*iplA*$^{-}$ cells were still making large and loose structures. At the 20th hr of development, the *tpc2*$^{-}$ and *tpc2*$^{-}$*mcln*$^{-}$*iplA*$^{-}$ cells were still streaming and forming small aggregates close

to each other. This was distinct from Ax2, *mcln*$^{-}$ and *iplA*$^{-}$ cells, which formed much larger, well separated aggregates (Figure 3.22A and B).

Another phenotype of interest was the presence of cells with multiple and irregular pseudopods surrounding the aggregates in later hours of development in strains lacking TPC2 (Figure 3.23). As the cells in these assays had been subjected to prolonged development, this was verified in cells after 10 hours under buffer. These cells were characterised by not being able to move efficiently but producing and withdrawing pseudopods in four or more directions at once (Figure 3.24 and Movies 3.1A and B) compared to the more polarised, elongated Ax2 cells, with fewer pseudopods visible at any one time. This phenotype was observed in three independent *tpc2*$^{-}$ strains.

3.3.12. Partial rescue of developmental delay in *tpc2*$^{-}$ cells by pulsing with exogenous cAMP.

One mechanism by which cells can be delayed in aggregation is if they show a delay or failure in expression of components of the cAMP relay system. In order to determine if this was the cause of delayed development in the absence of TPC2, it was determined if delayed aggregation can be rescued by exogenous pulses of cAMP. To do this the cells were starved by shaking in HKC-Buffer for two hours and then exogenously pulsed with 50 nM cAMP at 6 min intervals for a further 4 hours. The cells were then plated on a 35 mm imaging dish (ibidi µ-Dish) to observe aggregation. Aggregation is rescued to some extent, although not completely, by cAMP pulsing (Figure 3.25 and Movie 3.2). This suggests that developing *tpc2*$^{-}$ cells have a defect in the cAMP relay system.

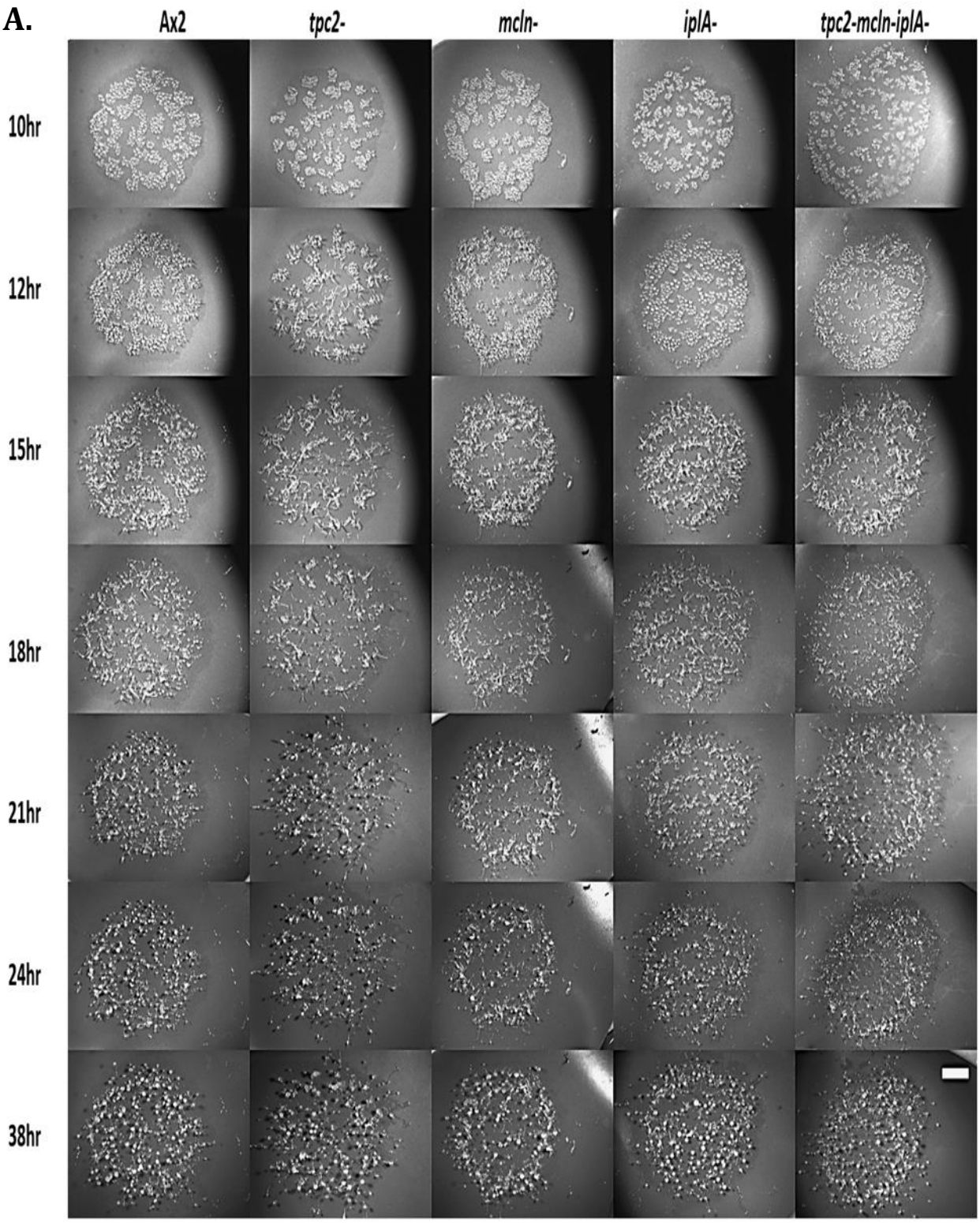

Figure 3.20. Filter development of Ax2, *tpc2*$^-$, *mcln*$^-$, *iplA*$^-$ and *tpc2*$^-$*mcln*$^-$*iplA*$^-$ cells

A. Ax2 (Parental strain), *tpc2*$^-$ (clone TPC22B20), *mcln*$^-$ (clone MCLN47), *iplA*$^-$ (clone IPLA1-2D) and *tpc2*$^-$*mcln*$^-$*iplA*$^-$ (clone TMI67B) cells were harvested during exponential growth. Cells were washed twice with HKC-LoCA buffer and 5 x 10^7 cells plated on 3.4 cm Millipore filter paper incubated on paper pre-soaked with KK2 at 22 °C. Developmental structures were observed at the times shown using a Leica MZ FL III Stereomicroscope and photographed using a Hamamatsu digital camera ORCA-05. Scale bar, 5 mm.

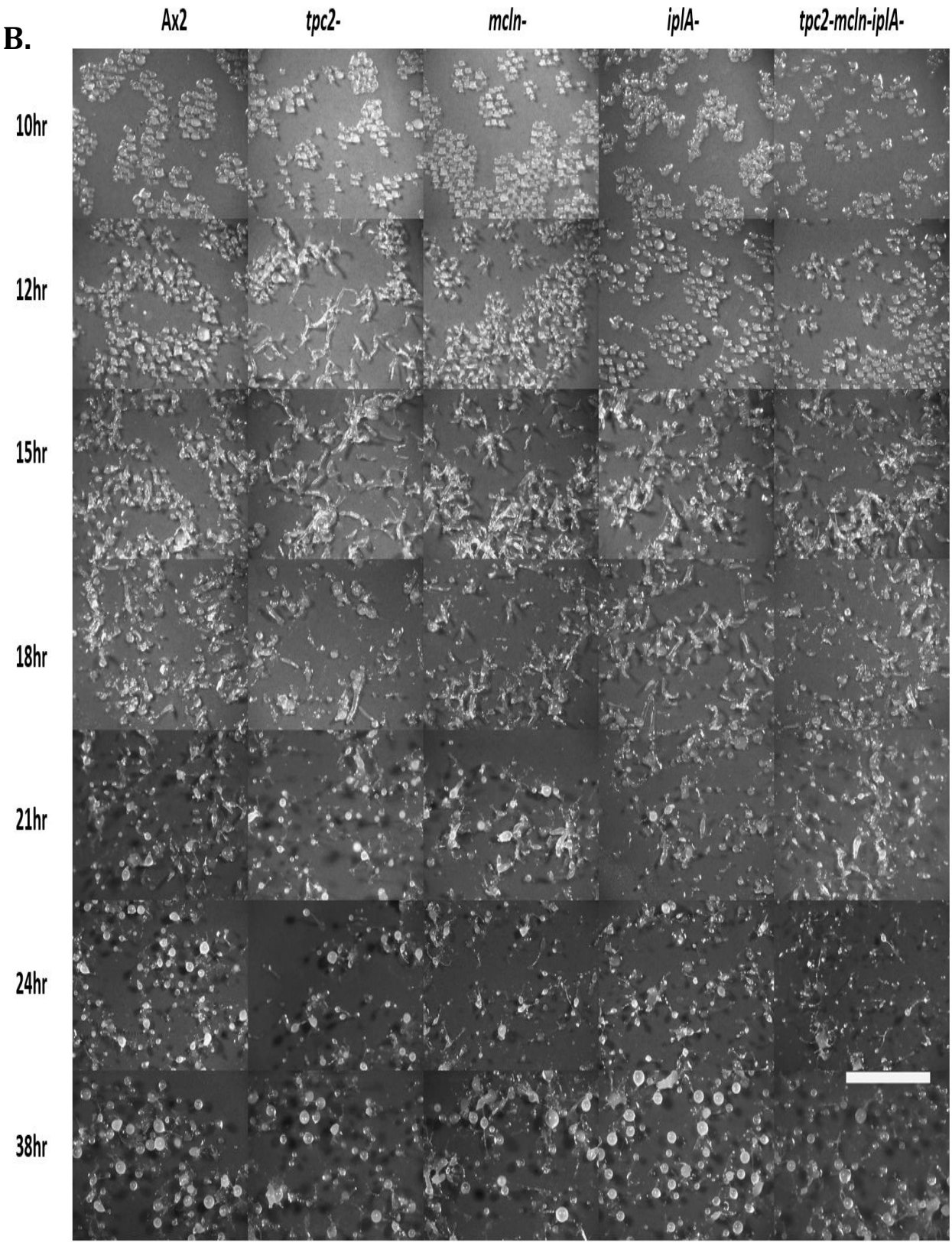

Figure 3.20. Filter development of Ax2, *tpc2*$^{-}$, *mcln*$^{-}$, *iplA*$^{-}$ and *tpc2*$^{-}$*mcln*$^{-}$*iplA*$^{-}$ cells

B. Features of development in Ax2 (Parental strain), *tpc2*$^{-}$ (clone TPC22B20), *mcln*$^{-}$ (clone MCLN47), *iplA*$^{-}$ (clone IPLA1-2D) and *tpc2*$^{-}$*mcln*$^{-}$*iplA*$^{-}$ cells (clone TMI67B) were developed as in A. Scale bar, 5 mm.

C.

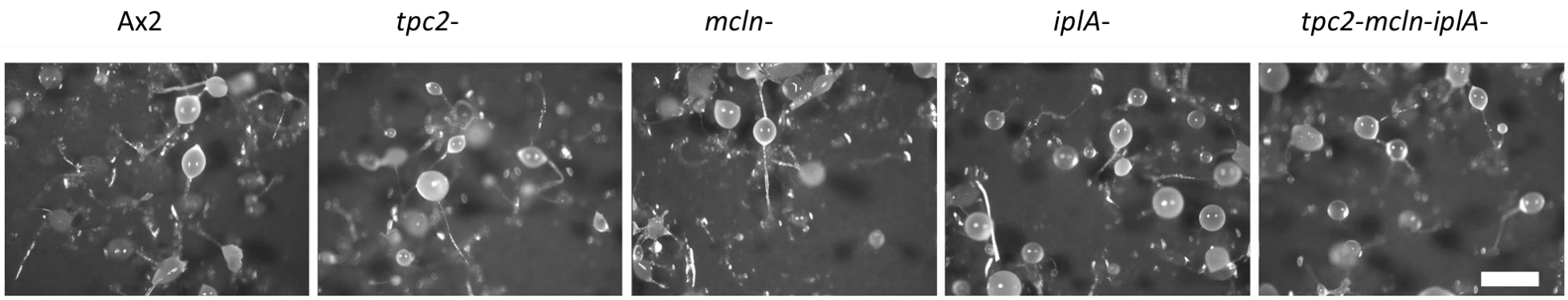

Figure 3.20. Filter development of Ax2, *tpc2*$^{-}$,*mcln*$^{-}$, *iplA*$^{-}$ and *tpc2*$^{-}$*mcln*$^{-}$*iplA*$^{-}$ cells

C. Final developmental structures of fruiting bodies were observed at the times shown using a Leica MZ FL III Stereomicroscope and photographed using a Hamamatsu digital camera ORCA-05. Scale bar, 1 mm.

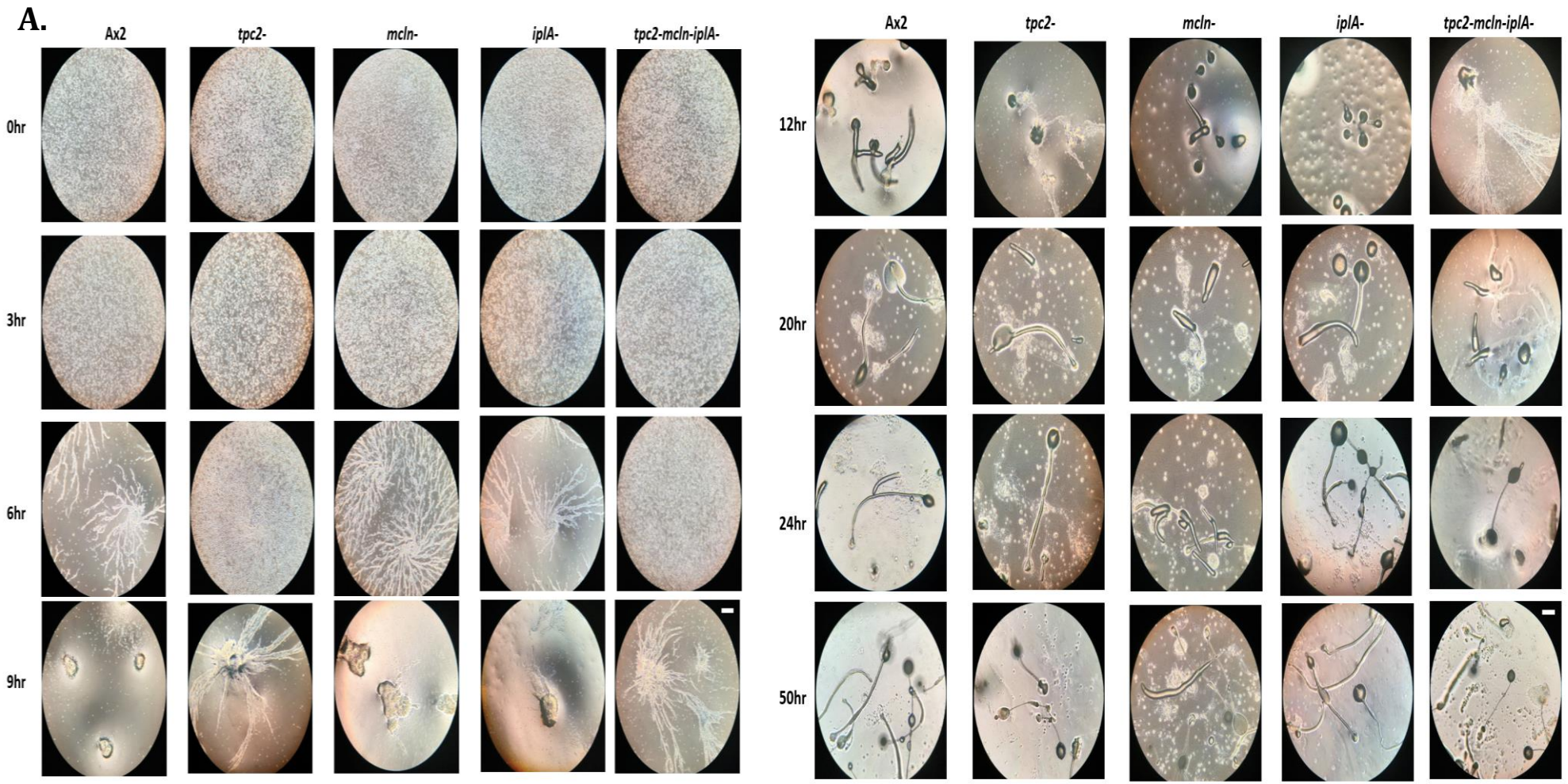

Figure 3.21. Agarose development of Ax2, *tpc2*$^{-}$, *mcln*$^{-}$, *iplA*$^{-}$ and *tpc*$^{-}$*-mcln*$^{-}$*iplA*-$^{-}$cells

A. Development of Ax2 (Parental strain), *tpc2*$^{-}$ (clone TPC22B20), *mcln*$^{-}$ (clone MCLN47), *iplA*$^{-}$ (clone IPLA1-2D) and *tpc2*$^{-}$*mcln*$^{-}$*iplA*$^{-}$ (clone TMI67B) cells were harvested from exponential growth. Cells were washed twice with HKC-LoCA buffer and 3.84 x 10^6 cells plated on 1% agarose HKC-LoCa buffer in a 6 well plate, (final cell density 4 x 10^5 cells/cm$^{2)}$, incubated at 22 °C. Developmental structures were observed at the times shown and photographed using a Coolpix P310 digital camera mounted on a light microscope (Motic AE21 Inverted Phase Microscope). Scale bars, 200 μm.

B.

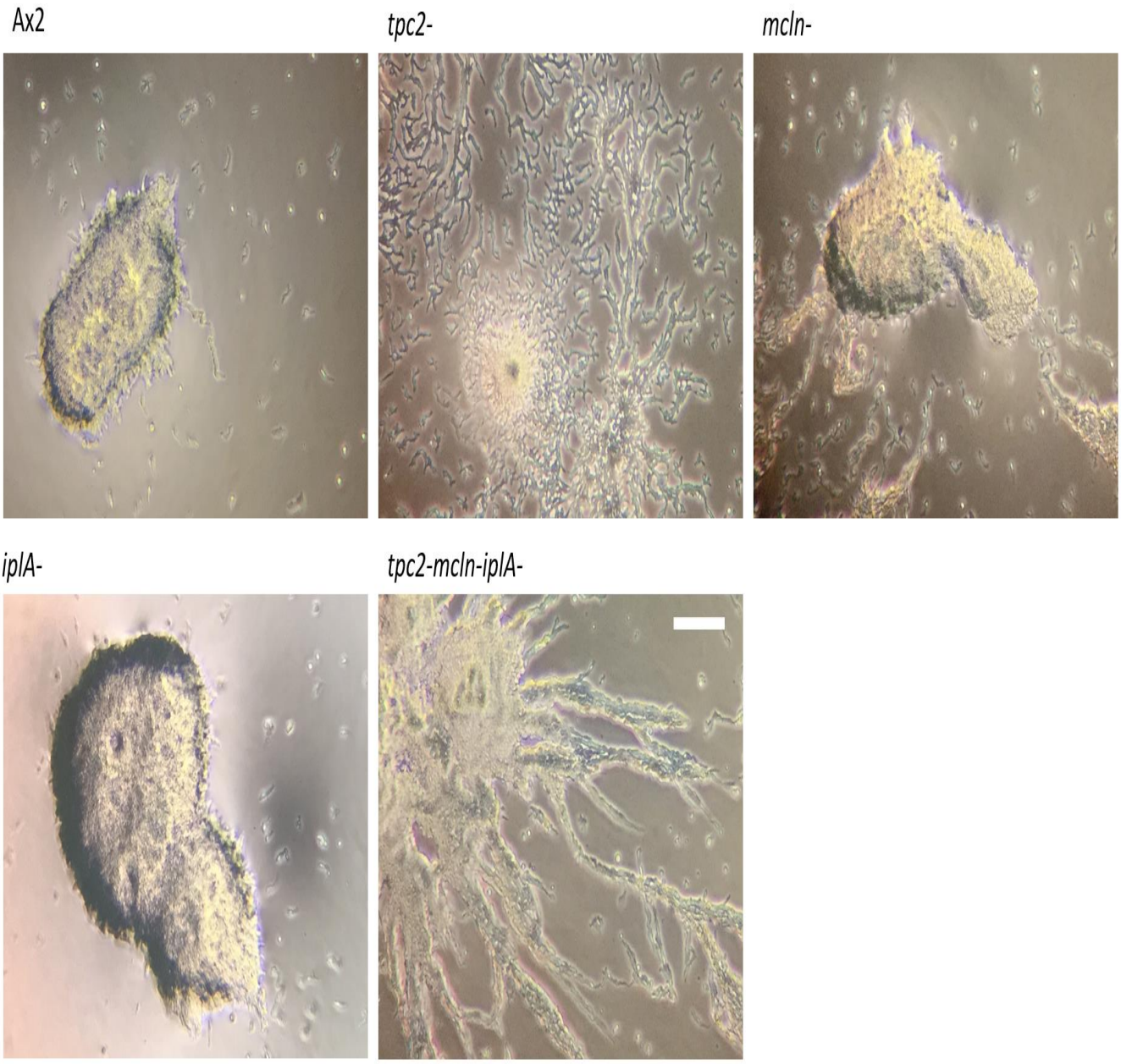

Figure 3.21. Agarose development of Ax2, *tpc2*$^-$, *mcln*$^-$, *iplA*$^-$ and *tpc2*$^-$*mcln*$^-$*iplA*$^-$ cells (9hr)

B. Developmental features of Ax2 (Parental strain), *tpc2*$^-$ (clone TPC22B20), *mcln*$^-$ (clone MCLN47), *iplA*$^-$ (clone IPLA1-2D) and *tpc2*$^-$*mcln*$^-$*iplA*$^-$ cells (clone TMI67B). Cells were developed as in A at 22 °C for 9 hr. Developmental structures were observed at the times shown and photographed using a Coolpix P310 digital camera mounted on a light microscope (Motic AE21 Inverted Phase Microscope). Scale bar, 100 μm.

A.

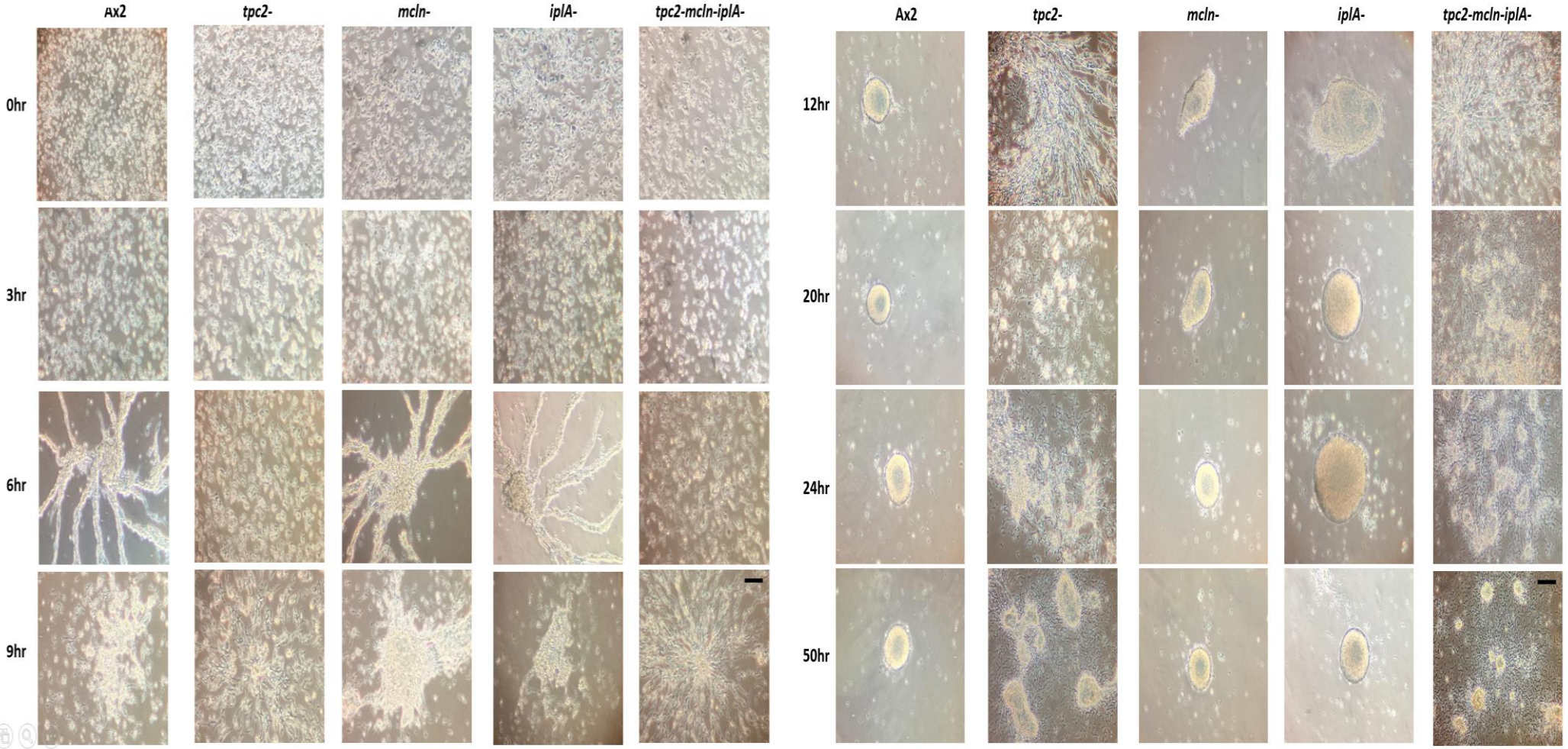

Figure 3.22. Under buffer development of Ax2, *tpc2*$^-$, *mcln*$^-$, *iplA*$^-$ and *tpc2*$^-$*mcln*$^-$*iplA*$^-$ cells

A. Ax2 (Parental strain), *tpc2*$^-$ (clone TPC22B20), *mcln*$^-$ (clone MCLN47), *iplA*$^-$ (clone IPLA1-2D) and *tpc2*$^-$*mcln*$^-$*iplA*$^-$ (clone TMI67B) cells were harvested from exponential growth. Cells were washed twice with HKC-LoCA buffer and plated in a 6 well plate, (final cell density at 4 x 10^5 cells/cm^2), under HKC-LoCA buffer and incubated at 22 °C. Developmental structures were observed at the times shown and photographed using a Coolpix P310 digital camera mounted on a light microscope (Motic AE21 Inverted Phase Microscope). Scale bars, 100 µm.

B.

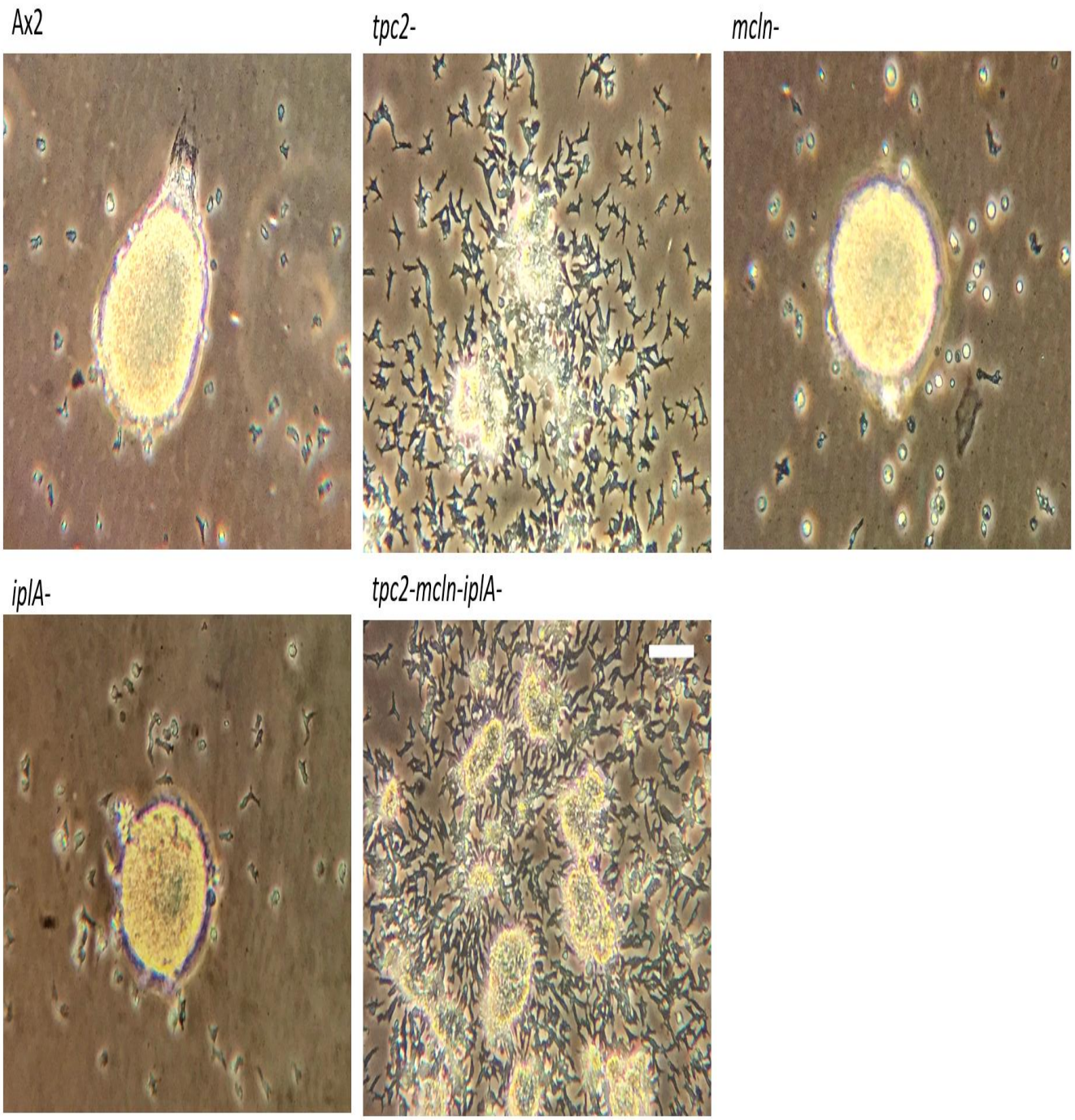

Figure 3.22. Under buffer development of Ax2, *tpc2*$^{-}$, *mcln*$^{-}$, *iplA*$^{-}$ and *tpc2*$^{-}$*mcl*$^{-}$*iplA*$^{-}$ cells (50 hr)

B Final developmental features. Ax2 (Parental strain), *tpc2*$^{-}$ (clone TPC22B20), *mcln*- (clone MCLN47), *iplA*$^{-}$ (clone IPLA1-2D) and *tpc2*$^{-}$*mcln*$^{-}$*iplA*$^{-}$ (clone TMI67B) cells were harvested from exponential growth. Cells were washed twice with HKC-LoCA buffer and 3.84 x 10^6 cells plated per well in a 6 well plate, (final cell density of 4 x 10^5 cells/cm^2), under HKC-LoCA buffer and incubated at 22 °C for 50 hr. Developmental structures were observed at the times shown and photographed using a Coolpix P310 digital camera mounted on a light microscope (Motic AE21 Inverted Phase Microscope). Scale bar, 50 μm.

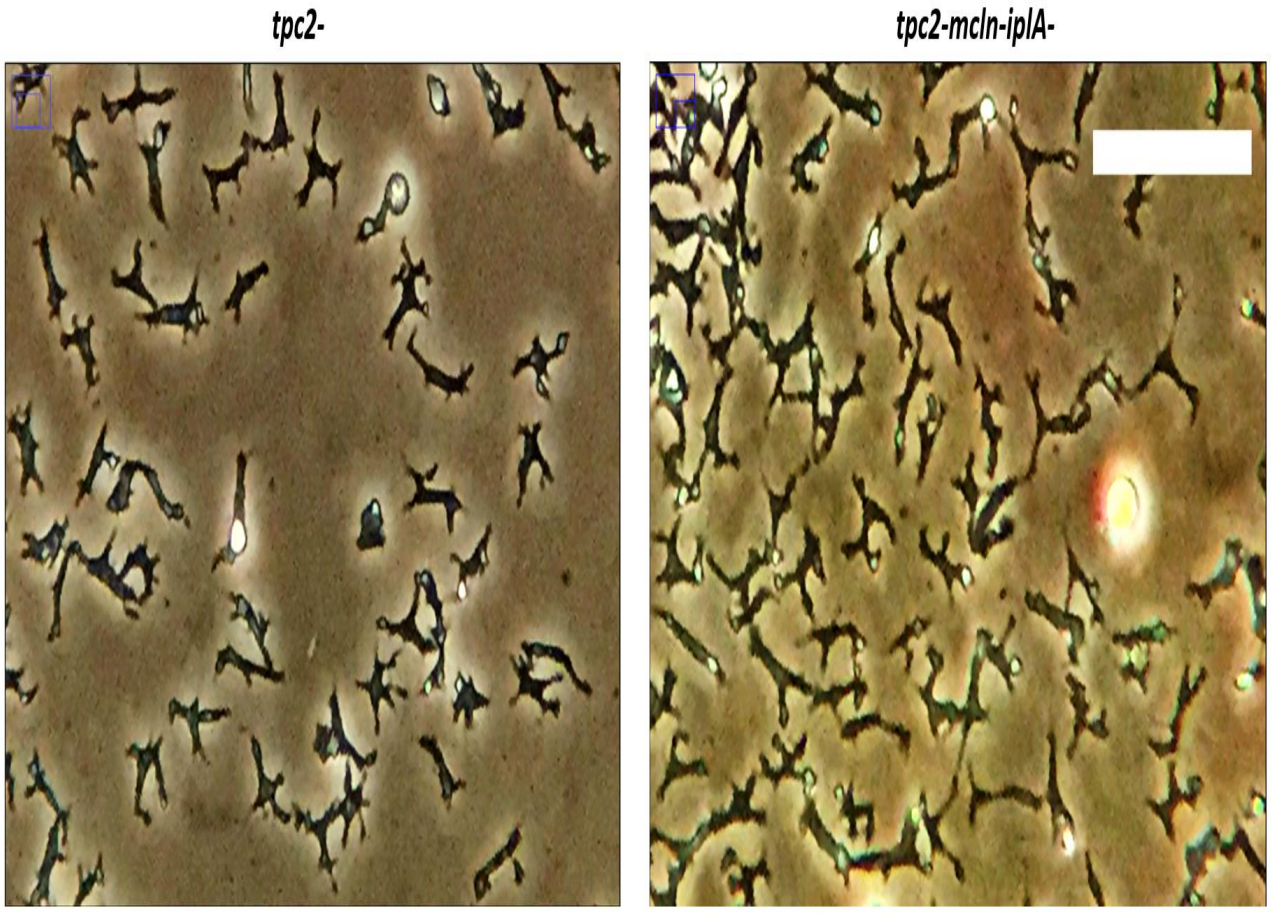

Figure 3.23. Morphology of *tpc2*$^-$ and *tpc2*$^-$*mcln*$^-$*iplA*$^-$ cells that fail to aggregate

tpc2$^-$ (clone TPC22B20), and *tpc2*$^-$*mcln*$^-$-*iplA*$^-$ cells (clone TMI67B) were harvested from exponential growth. Cells were washed twice with HKC-LoCA buffer and 3.84 x 10^6 cells plated per well in a 6 well plate, (final cell density of 4 x 10^5 cells/cm^2), under HKC-LoCA buffer and incubated at 22 °C for 50 hours. These strains both showed a high proportion of cells not joining aggregates after prolonged development and these cells photographed using a Coolpix P310 digital camera mounted on a light microscope (Motic AE21 Inverted Phase Microscope). There were no equivalent Ax2 cells outside aggregates for comparison. Scale bar, 50 μm.

A.

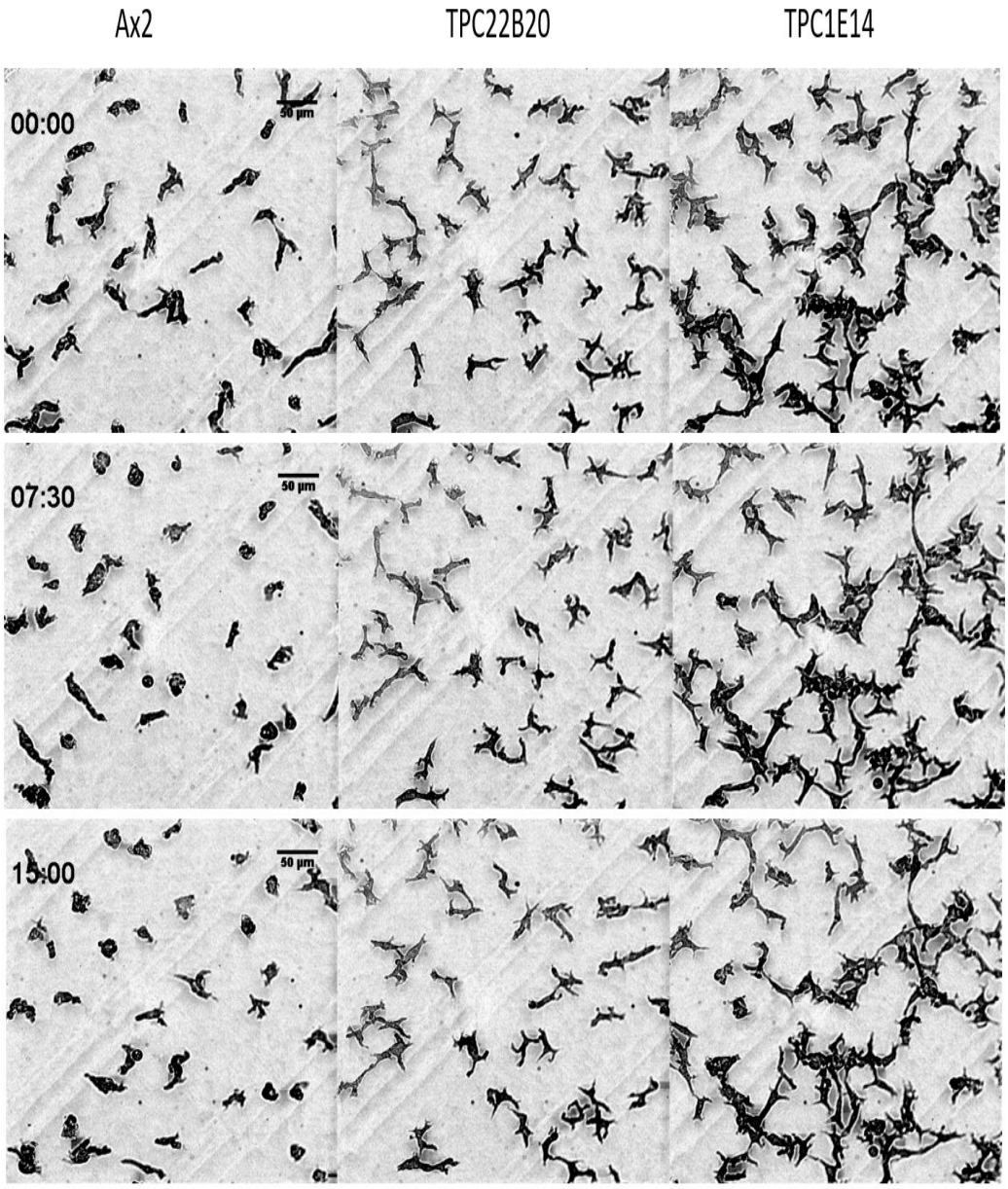

Figure 3.24. and Movie 3.1. Appearance of non aggregated *tpc2*$^-$ cells (10 hr)

A. Unusual morphology of two strains of *tpc2*$^-$ cells (independent clones TPC22B20 and TPC1E14). Cells were harvested from exponential growth. Cells were washed twice with HKC-LoCA buffer and 3.84 x 10^6 cells plated per well in a 6 well plate, (final cell density of 4 x 10^5 cells/cm^2), under HKC-LoCA buffer and incubated at 22 °C for 10 hr. Developmental structures were observed at the times shown using DeltaVision Elite microscope and photographed using a EMCCD camera mounted on the microscope. Scale bars, 50 µm. B. Comparison of unusual cellular movement of a *tpc2*$^-$ disruption cells (clones TPC22B20) and Ax2. Time is labelled in the upper right corner of each photograph. Scale bars, 20 µm.

B.

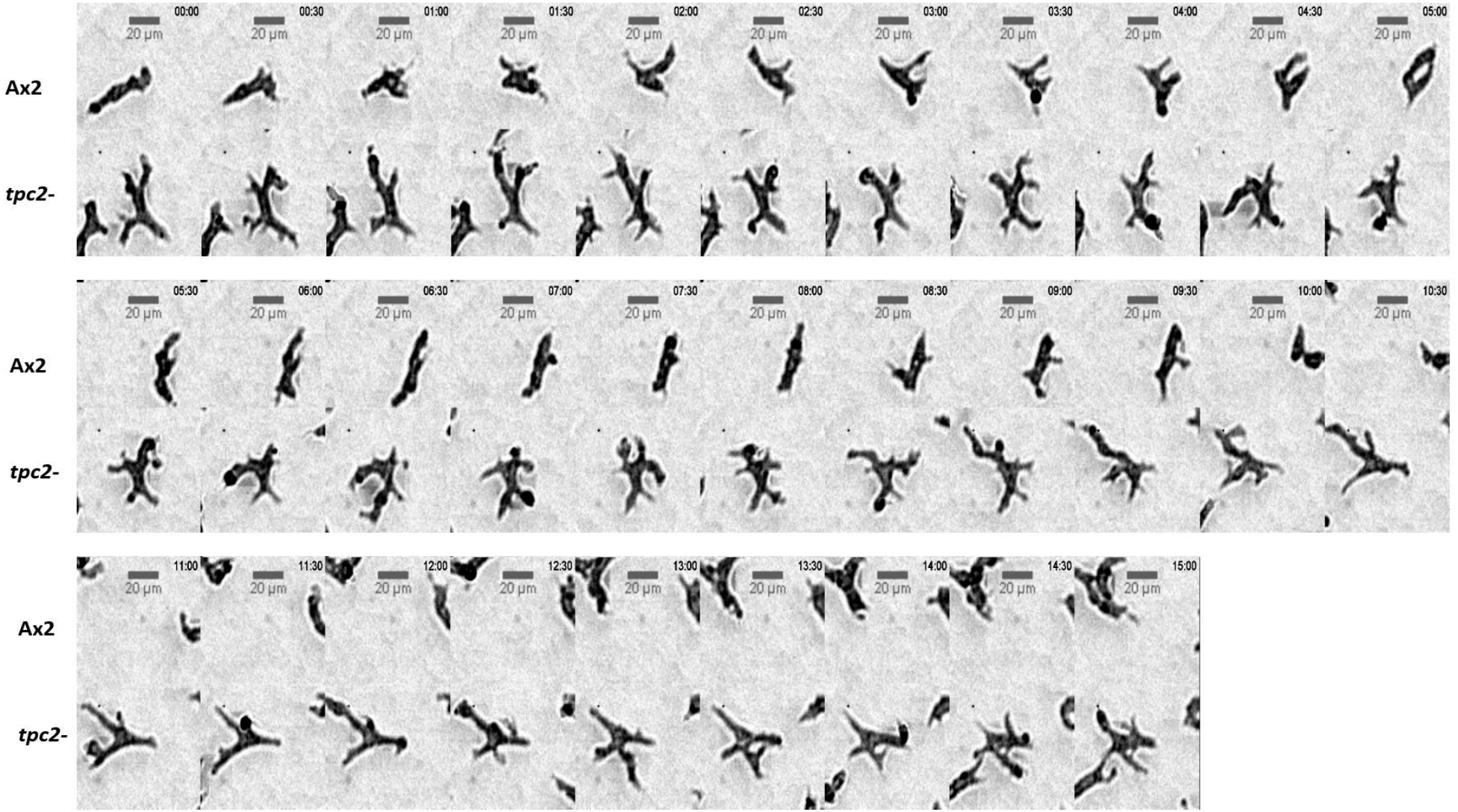
Ax2
tpc2-
00:00
00:30
01:00
01:30
02:00
02:30
03:00
03:30
04:00
04:30
05:00
05:30
06:00
06:30
07:00
07:30
08:00
08:30
09:00
09:30
10:00
10:30
11:00
11:30
12:00
12:30
13:00
13:30
14:00
14:30
15:00
20 µm

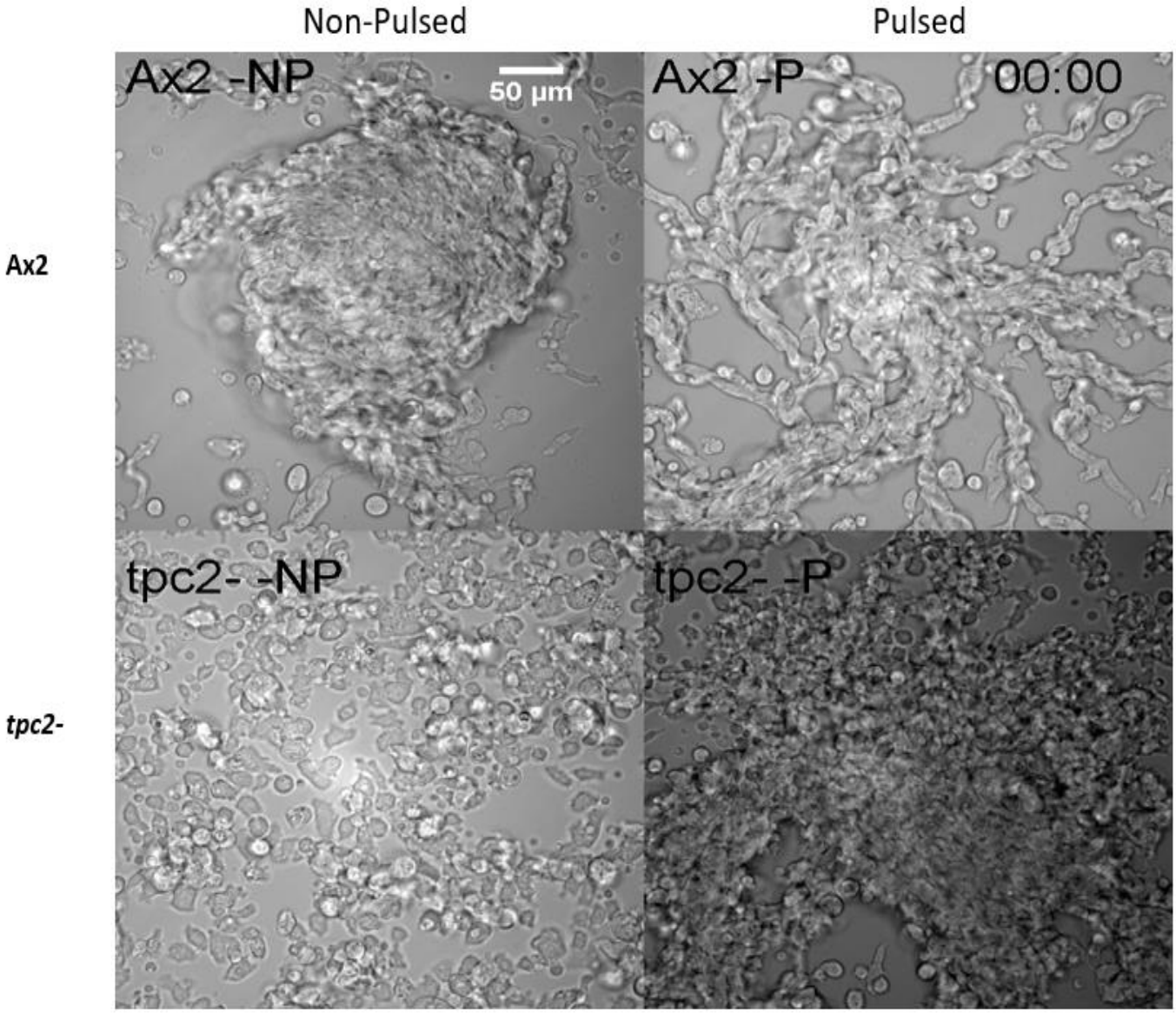

Figure 3.25. and Movie 3.2. Exogenous pulsing of cAMP partially rescues delayed aggregation of *tpc2*$^{-}$ cells.

Cells were harvested from exponential growth. Cells were washed twice with HKC-LoCA buffer and 7 x 10^7 cells shaken in 5 ml HLC-LoCa buffer for 2 hr then pulsed with (pulsed, P) or without (non-pulsed, NP) cAMP (50 nM every 6 mins) for 4hr, incubated at 22 °C. Cell were allowed to settle for 15 min then the aggregation was observed at the times shown using DeltaVision Elite microscope and photographed using a EMCCD camera mounted on the microscope. Scale bar, 50 µm.

3.3.13. Real-time PCR quantification of mRNA expression during early development of *tpc2*$^{-}$ and Ax2 cells.

In order to verify the concept that the phenotype observed in *tpc2*$^{-}$ cells is related to the cAMP relay system, the expression profile of genes induced in early development was determined. To do this, cells were developed as above either with (pulsed, P) or without (non-pulsed, NP) pulsing with exogenous cAMP (50 nM every 6 mins) from 2-6 hr, incubated at 22 °C. Every 2 hours mRNA was extracted and gene expression analysed by RT-PCR.

Three groups of genes were analysed: one was related to the prestarvation response (*yakA* and *dscA*), the second was genes whose induction is independent of extracellular cAMP (*carA* and *pdsA*) and the third group contains extracellular cAMP pulse-dependent genes (*acaA* and *csaA*) (Figure 3.26) (Loomis, 2014). In Ax2 cells the expression of all of these genes was induced during the first 6 hours of development. In *tpc2*$^{-}$ cells there was a general decrease in gene expression of the early developmental genes, consistent with a delay in early development. The genes showing the greatest reduction in expression were *dscA* and the pulse-independent genes *carA* and *pdsA*. Despite the partial rescue of the developmental phenotype by exogenous pulsing, pulse-induced genes, *acaA* and *csaA*, showed minimal reduction of expression in the absence of pulses. Pulsing with exogenous cAMP reduced expression of *dscA* by 6 hours of development, as expected for Ax2 cells, and this reduction was also apparent in *tpc2*$^{-}$ cells. Pulsing had little effect on the expression of *pdsA* or *carA* in both cell types, as expected for pulse-independent genes. However, pulsing increased expression of the pulse-induced genes in both strains. This suggested that the delay in early development might be due, at least in part to defects in pulse-independent pathways, and the

reduction in *dscA* expression suggests that this might include the prestarvation response. Despite the partial recue of the aggregation delay by exogenous pulses of cAMP, the expression of pulse-induced genes was not greatly reduced in the *tpc2*$^{-}$ cells (Figure 3.26).

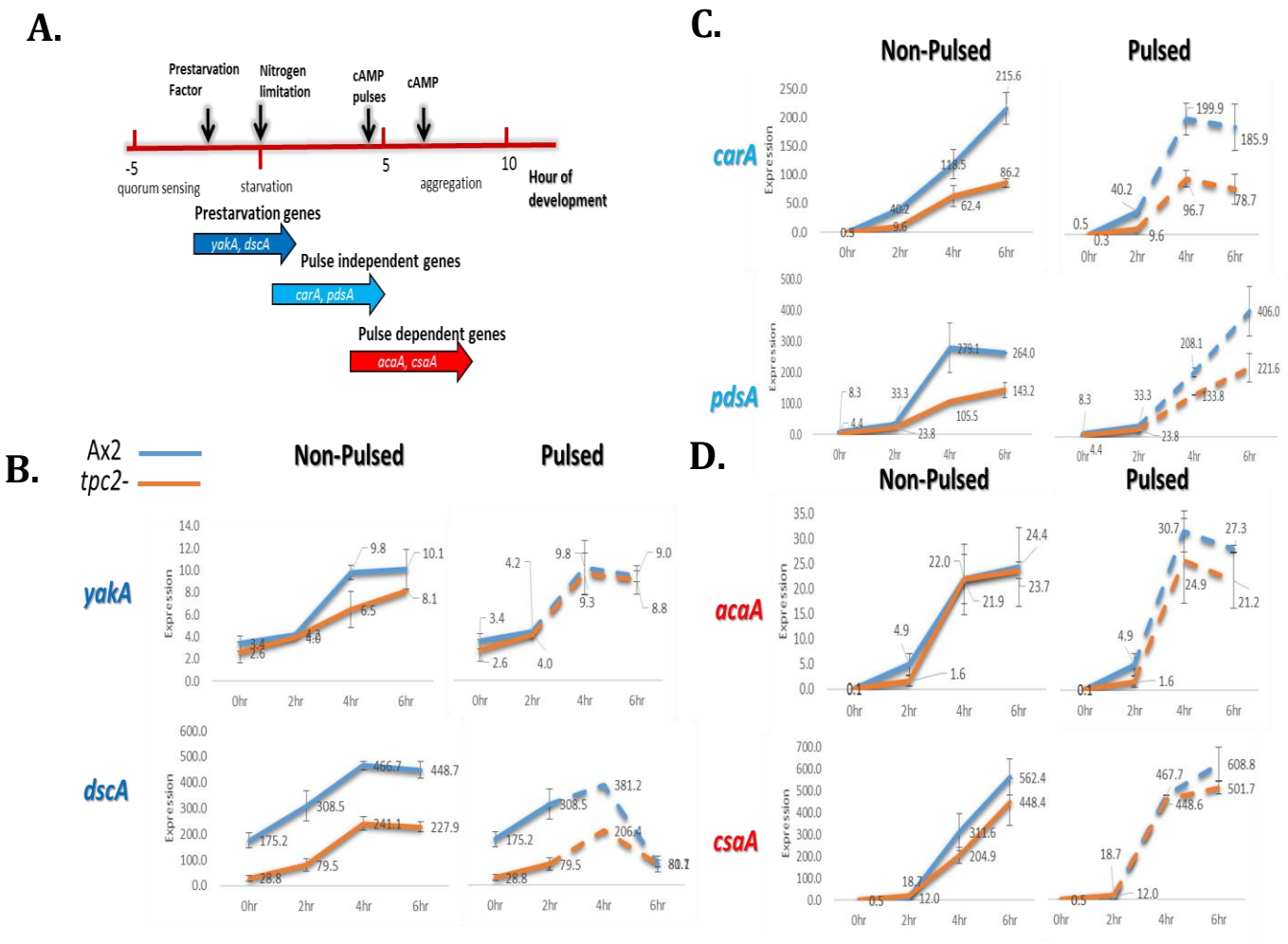

Figure 3.26. Real-time PCR quantification of mRNA by stage of development in Ax2 and *tpc2*$^{-}$ cells.

Cells were harvested from exponential growth. Cells were washed twice with HKC-LoCA buffer and 7 x 10^7 cells shaken in 5 ml HLC-LoCa buffer for 2 hr then pulsed with (pulsed, P) or without (non-pulsed, NP) cAMP (50 nM every 6 mins) for 4 hr, incubated at 22 °C. Every 2 hours 1.4x10^7 cells were sampled for mRNA extraction and RT-PCR. (A) Diagram shows genes related to specific stage of development, which are prestarvation genes (*yakA and dscA*), pulse-independent genes (*carA and pdsA*) and pulse-dependent genes (*acaA and csaA*). The mRNA expression profiles of development and the effect of cAMP pulsing (B) prestarvation genes (*yakA and dscA*). (C) pulse-independent genes (*carA and pdsA*). (D) pulse-dependent genes (a*caA and csaA*).

3.4. Discussion

The bioinformatics information and gene disruption experiments have shed some light on the roles of Dictyostelid TPC2s. The sequence alignment to the Arabidopsis AtTPC1 of known structure suggests that Dictyostelid TPC2s have a classic TPC structure, with two sets of six transmembrane domains and a paired EF hand domain. The sequence alignment reveals that voltage sensing motifs are quite conserved in Dictyostelia, however, the gating charge transfer centre motifs are not conserved. It will be necessary to determine experimentally, e.g. by using patch clamp experiments, whether Dictyostelid TPC2 are voltage sensitive. Dictyostelid TPC2s have a classic EF-hand domain and a potential non-canonical CaM binding site. No CaM binding sites have been previously reported in plant or animal TPCs. In *D. lacteum*, despite the lack of a potential CaM binding site at the equivalent position to the other Dictyostelia, another potential calmodulin interaction site was found in the IS0 cytosolic domain. This suggests that interaction with calmodulin might be functionally relevant for Dictyostelid TPC2s. DdTPC2 has the longest and most diverse sequences in the non-ion transporting regions. Conserved domain prediction information revealed conservation of sequences found in presenilin and another intramembrane protease in DdTPC2. Presenilin is the catalytic core of the gamma-secretase enzyme complex (De Strooper *et al.*, 2012), and has been implicated in regulating a number of Ca^{2+} channels and pumps, such as IP_3 and Ryanodine receptor channels, SERCA Ca^{2+} pumps, affecting capacitative Ca^{2+} entry and function of calcium leak conductance pores on the ER store (Honarnejad and Herms, 2012) and *Dictyostelium discoideum* cells lacking expression of presenilins show

altered Ca^{2+} responses (Ludtmann *et al.*, 2014). Therefore the presenilin-like domain could play a role in Ca^{2+} homeostasis.

It is noticeable that PpTPC2 and DdTPC2 encode a sequence related to that found in a transcription factor and a nuclear localization sequence (NLS), respectively. NLS motifs are present in a wide range of ion channels including voltage-gated Ca^{2+} channels, glycine receptors, and N-methyl-d-aspartate receptors (Gomez-Ospina *et al.*, 2006; Holmes *et al.*, 2002; Melzer *et al.*, 2010). It is also known that the C-terminus of the voltage-gated calcium channel Cav1.2 encodes a transcription factor. The NLS of Cav1.2 mediates transfer of the C-terminal channel fragment to the nucleus after proteolytic cleavage, where it acts as a transcriptional regulator (Gomez-Ospina *et al.*, 2013; Gomez-Ospina *et al.*, 2006). The co-existence of nuclear localization signals close to calmodulin binding motifs is reminiscent of cyclic nucleotide-gated channels (CNGCs). It will be interesting to discover if this is also found in other group 4 Dictyostelids (*Dictyostelium* spp) as these are the only group of Dictyostelids which use extracellular cAMP as a chemotactic signal for aggregation (Schaap, 2016), so DdTPC2 might have evolved a role similar to CNGC to cope with a new mechanism. However, all these predictions need experiments to validate their importance.

Functional partner prediction analysis links DdTPC2 with calcineurin related proteins and three Ca^{2+} P-type ATPases, including the major Ca^{2+} pump in *Dictyostelium*, PAT1. *Dictyostelium* PAT1 is related to plasma membrane Ca^{2+} ATPases (PMCA), and *patA* gene expression is up-regulated when cells are grown in

a higher Ca^{2+} environment (Coukell *et al.*, 1995; Moniakis *et al.*, 1995). Up-regulation of *patA* expression is strongly reduced when the serine/threonine phosphatase calcineurin is inhibited, suggesting gene regulation of PAT1 via a calcineurin pathway (Moniakis *et al.*, 1999). Interestingly, immunofluorescence analysis indicates that PAT1 co-localises with bound calmodulin to the contractile vacuole complex (Moniakis *et al.*, 1995). However, PAT1 itself does not have the highly conserved calmodulin-binding domain present in the C-terminal region of other PMCA family members. In this sense, it would be interesting to investigate if TPC2 functionally interacts with PAT1 and calmodulin on the contractile vacuole in future studies. It is also worth noting that plant TPC1 is also predicted to work with a Ca^{2+} transporting ATPase, suggested this might be a potential evolutionarily conserved relationship.

Dictyostelium is a good model to study the role of ion channels in development since the total number and complexity of putative ion channels is much reduced in *Dictyostelium* compared to other organisms. The *Dictyostelium* genome contains only three genes encoding putative calcium channels predicted to be expressed at the cell surface or in endocytic compartments (*mcln*, *pkd2*, *tpc2*), and a single mechanosensing-like channel (*mscS*) (Lima *et al.*, 2012; Lima *et al.*, 2014; Wilczynska *et al.*, 2005). In addition the genome encodes only one IP_3-like receptor (IplA) (potentially present in the ER), and five P2X receptors (p2xA-E) restricted to the contractile vacuole (Baines *et al.*, 2013; Fountain *et al.*, 2007; Parkinson *et al.*, 2014) and no orthologue of Ryanodine receptors. P2X receptors have been shown to

play a specific role in osmo-regulation via the contractile vacuole. This reduced complement of ion channels facilitates analysis of their role in development.

The first *Dictyostelium mcln*- and *tpc2*-deficient strains were generated in a uracil auxotroph strain DH1, which in turn is derived from the axenic strain Ax3. Lysosome exocytosis was profoundly increased in *mcln*$^{-}$ cells compared with DH1 cells. In addition, *mcln*$^{-}$ cells grew twice as fast in Ca^{2+}- depleted medium, suggesting they were more resistant to Ca^{2+} deprivation. Moreover, the Ca^{2+} concentration in their secretory lysosomes was decreased (Lima *et al.*, 2012). However, the role of mucolipin in development has not been reported. The same group also generated *tpc2*$^{-}$ cells in a DH1 background but only tested the strain for its response to mechanical stress, which was normal (Lima *et al.*, 2014).

Mammalian IP_3 receptors are implicated in cellular Ca^{2+} homeostasis by controlling Ca^{2+} release from neutral stores such as the ER. In *Dictyostelium,* disruption of the *iplA* gene does not impair overall development or chemotaxis (either towards cAMP or folic acid) (Lusche *et al.*, 2012; Traynor *et al.*, 2000), despite loss of Ca^{2+} influx in response to cAMP.

For the first time I have successfully generated *Dictyostelium* cells deficient in these three channels in the same genetic background and also strains deficient in two of the major Ca^{2+} channels on acidic stores (TPC2 and mucolipin) and a strain deficient in both of these and IplA predicted to be on neutral stores. Multiple independent clones of single and double disruptant strains were isolated and verified and phenotypes

confirmed in more than one clone. Only a single clone of triple deficient cells was tested so all results on these must be interpreted with some caution before verification on an independent clone, however this does reveal that these channels are not required in combination for cell viability.

TPC proteins, or NAADP, have been shown to play a role in cell differentiation, for example of neurons from embryonic stem cells and muscle (Aley *et al.*, 2010; Brailoiu *et al.*, 2006; Zhang *et al.*, 2013) although mice deficient in TPCs are viable (Ruas *et al.*, 2015). In *Dictyostelium* the *tpc2*$^-$, *mcln*$^-$, *tpc2*$^-$*mcln*$^-$ and *tpc2*$^-$*mcln*$^-$*iplA*$^-$ triple mutants all were able to aggregate and form fruiting bodies when developed at high density on filters, so these Ca^{2+} channels are not essential for *Dictyostelium* development. RNAseq data (dictybase.org) suggests that *tpc2* mRNA shows greatly increased expression from 16 hours of development and a role for acidic stores in late development has been hypothesized (Gross, 2009) but fruiting bodies were phenotypically normal. However, when cells were developed at lower cell densities on agarose or under buffer, cells with a disrupted *tpc2* gene showed a delay in early development. Cells lacking another Ca^{2+} channel on the acidic stores, mucolipin, also showed slightly delayed early development. This suggests that Ca^{2+} channels located on the acidic stores play a role in early development of *Dictyostelium*. A high proportion of *tpc2*$^-$ cells failed to aggregate even after many hours under buffer, and showed an unusual morphology. The delay could be partially, but not completely, rescued by exogenous pulsing with cAMP consistent with some deficiency in the endogenous cAMP relay.

Analysis of early developmental gene expression indicated a more pronounced reduction in expression of genes whose expression is independent of extracellular cAMP pulses and also one of the two prestarvation pathway genes investigated, *dscA*. Another marker of the prestarvation response *yakA* was slightly delayed in its up-regulation. Expression of the pulse-independent genes *pdsA* and *carA* was also reduced. Importantly, pulsing with cAMP could only partially rescue the gene expression levels of these pulse-independent genes. This suggested that loss of TPC2 led to defects in pulse-independent pathways and prestarvation responses. Three factors have been described to play a role in these early stages of development, the AprA/CfrD complex, prestarvation factor (PSF) and conditioned medium factor (CMF) (Gomer *et al.*, 2011; Loomis, 2014). Gene expression of *dscA* is known to be regulated by prestarvation factor (PSF) (Rathi *et al.*, 1991) as is expression of *yakA* (Souza *et al.*, 1998) so the reduced expression of both of these is consistent with a role for TPC2 in the PSF response. Expression of *dscA* is also known to be regulated by a number of other factors, including CMF (Blusch *et al.*, 1995), which might explain the more severe reduction in *dscA* expression. Expression of later genes is dependent on *yakA* expression as the protein kinase YakA inhibits PufA to relieve inhibition of translation of the catalytic subunit of cAMP-dependent protein kinase (PKA) (Souza *et al.*, 1998). PKA, in turn, is required for expression of genes such as *carA*, which encodes the major cAMP receptor involved in early development. Therefore any differences in later gene expression patterns may be secondary effects.

Loss of TPC2 expression leads to defects in early development, especially apparent at low cell densities, which are consistent with its involvement in early events

including, but not necessarily limited to the response to prestarvation factor PSF. PSF is continuously secreted by growing cells and used to sense cell density. A higher proportion of null cells which failed to aggregate also showed altered cell morphology suggesting other pathways may also be defective in these cells. This is the first description of a role for a putative Ca^{2+} channel in early development of *Dictyostelium.*

CHAPTER 4: The Role of *Dictyostelium* Two-Pore Channel2 in Acidic Vesicles

4.1. Introduction

Following disruption of the genes encoding three of the major Calcium channels, two, TPC2 and mucolipin, predicted to be found on the acidic stores and one, IplA, on the neutral stores, only strains lacking TPC2 showed an obvious phenotype in early development. The *iplA*$^{-}$ cells did not show an obvious phenotype in aggregation, in agreement with Traynor *et al.* (Traynor *et al.*, 2000) and there have been no previous reports on *Dictyostelium* development in the absence of mucolipin or TPC2. In order to try and understand the mechanism by which loss of TPC2 effects development, in this chapter, I investigated whether the *tpc2*$^{-}$ cells showed any phenotypes related to acidic stores. To do this, I have investigated Ca^{2+} uptake and release from *in vitro* vesicle preparations, sensitivity of development to weak bases and the *in vivo* vesicle pH in early development.

The acidic Ca^{2+} stores are a group of organelles characterised by the presence of Ca^{2+} and their acidic interior or by being studded with vacuolar-type H^{+}-ATPase (Gross, 2009). These organelles include acidocalcisomes, vacuoles, endosomes, lysosomes, lysosome-related organelles (LRO), secretory granules and the Golgi complex (Gross, 2009; Patel and Docampo, 2010). Their role in eukaryotic development has been recently appreciated especially in model organisms such as *Dictyostelium discoideum* (Gross, 2009).

Plant TPC1, also known as slow vacuolar (SV) channel, is localised to the vacuoles (Hedrich and Marten, 2011). In animal cells, TPC1 is distributed on recycling endosomes, early and late endosomes, and lysosomes, whereas TPC2 predominantly co-localises with markers for late endosomes, lysosomes and LROs with endocytic

dileucine motifs (Brailoiu *et al.*, 2010; Calcraft *et al.*, 2009). Interestingly, TPC2 has been recently reported to be involved in pH regulation of LROs such as platelet dense granules (PDGs) in platelet and melanosomes in melanocytes (Ambrosio *et al.*, 2016; Ambrosio *et al.*, 2015). TPCs are known for responding to and sensing a spectrum of cytosolic and luminal agents which regulate ion release from the endolysosome or the vacuole. These include Ca^{2+}, pH, and cellular redox potential (Carpaneto *et al.*, 1999; Hedrich and Neher, 1987; Pitt *et al.*, 2010b). In *Dictyostelium*, the acidic Ca^{2+} stores seem to be of two kinds, known as contractile vacuoles (CVs) and acidocalcisomes (Marchesini *et al.*, 2002). It is not known if TPCs play a role in regulation of pH in acidic stores in lower eukaryotes such as amoebae and if they have any role in development. However, acidic stores have been proposed to play a role in regulating development in *Dictyostelium* (Gross, 2009).

Upon starvation, *Dictyostelium* undergoes a great change in gene expression and protein content in response to development. These changes cause release of ammonia produced by metabolism of protein and RNAs. Ammonia functions as a weak base and is involved in a number of processes in *Dictyostelium* development, for example aggregation and culmination (Follstaedt *et al.*, 2003). An excess of ammonia causes inhibition of aggregation, increased slug migration, delay of culmination and the promotion of spore formation. Davies *et al.*, have confirmed that the endogenous weak base ammonia, and other weak bases including propylamine, chloroquine, and imidazole behave similarly by altering endolysosomal pH, while the cytosolic pH remains stable at 7.4. Their data indicates that inhibition of aggregation and culmination by weak bases is a consequence of neutralization of acidic compartments rather than a result of elevation of cytosolic pH (Davies *et al.*, 1993).

The properties of intracellular organelles have been studied in *Dictyostelium* using *in vitro* vesicle preparations. Malchow *et al*. reported two vesicle fractions isolated by differential centrifugation and suggested that P0 vesicles are enriched in membranes from the CV whereas P1 vesicles are enriched in ER (Malchow *et al.*, 2006), although the percentage of CV and ER were reported to be 42% and 34% for P0, and 34% and 43% for P1, respectively. Therefore these vesicle preparations both contain vesicles derived from both organelles.

Vesicles prepared from *Dictyostelium* cells starved for 4 hours, respond to both Ca^{2+} and arachidonic acid (AA) by releasing Ca^{2+}. This was monitored by increased fluorescence of Ca^{2+} sensitive dyes such as Fluo-3 in the medium outside the vesicles (Malchow *et al.*, 2008; Malchow *et al.*, 2006). Ca^{2+} release from intracellular Ca^{2+} stores induced by fatty acids, in particular AA, is relatively well characterized. AA is thought to release Ca^{2+} from acidic stores, for example the CV, which was supported by the observation that AA-induced Ca^{2+}-release was reduced in *lvsA*$^{-}$, a mutant strain where the CV is impaired (Malchow *et al.*, 2006). In other organisms, nicotinic acid adenine dinucleotide phosphate (NAADP) and the phospholipid phosphatidylinositol(3,5)bisphosphate ($PI(3,5)P_2$) also have been reported to mobilize calcium from acidic organelles possibly through TPCs (Calcraft *et al.*, 2009; Wang *et al.*, 2012).

4.2. Aims

The aim of this chapter is to determine the functional role of TPC2 as a Ca^{2+} channel found on acidic Ca^{2+} stores in *Dictyostelium*. By using an *in vitro* vesicle system, I investigated Ca^{2+} uptake and release in order to determine the effects of *tpc2* gene disruption. Then I investigated the effect of disruption of *tpc2* on vesicle pH *in vivo* by determining the sensitivity of development of *tpc2*$^{-}$ cells to inhibition by weak bases and using a pH indicator to explore the pH of acidic vesicles. This information sheds light on the role of TPC2 in regulation of acidic vesicles in *Dictyostelium*.

4.3. Results

4.3.1 Establishing a Calcium Release Detection System *in vitro*

A robust *in vitro* Ca^{2+} uptake and release detection system uses intracellular vesicles prepared from *Dictyostelium* starved for 4 hours (Malchow *et al.*, 2008; Malchow *et al.*, 2006). These vesicles have been reported to take up Ca^{2+} and respond to Ca^{2+} and arachidonic acid (AA) by releasing Ca^{2+}, monitored by fluorescence of Ca^{2+}-sensitive dyes such as Fluo-3. Vesicles sedimented at different densities have been proposed to be slightly enriched in ER (P1) or CV (P0) (Malchow *et al.*, 2006). Therefore vesicles were prepared from Ax2 cells starved for 4 hours (T4) in a shaking suspension following the protocol published. As *tpc2*$^{-}$ cells show a delay in development, the cells were developed in shaking suspension with exogenous cAMP pulses, conditions shown to partially rescue the delay (Chapter 3) to allow a more direct comparison between strains.

In our group, Watanabe previously reported by co-expression of dajumin-GFP fusion protein, a CV marker, and calnexin-GFP, an ER marker in *Dictyostelium*, that dajumin-GFP was mainly detected in the P1 fraction, with reduced levels in P0 fraction, whereas calnexin-GFP, was detected in both P0 and P1 fractions. Watanabe concluded that P1 is the fraction containing vesicles derived from both CVs and ER (Watanabe, DPhil thesis, 2011). Therefore, in this study, P1 was used in the Ca^{2+} release experiments.

4.3.1.1 Ca^{2+} uptake in P1 vesicles

In order to determine if P1 vesicles were capable of taking up Ca^{2+}, the vesicles were incubated with ATP in a buffer containing the Ca^{2+} sensitive dye Fluo-3. Monitoring fluorescence revealed that P1 vesicles showed robust uptake which levelled off over time (Figure 4.1) suggesting the presence of functional calcium pumps. *Dictyostelium* has at least three different P-type Ca^{2+} ATPases (Moniakis *et al.*, 1995; Moniakis *et al.*, 1999; Wilczynska *et al.*, 2005), which require ATP to drive the Ca^{2+} uptake. Ca^{2+} uptake in the vesicle preparation is ATP-dependent, as these vesicles showed a great increase in Ca^{2+} uptake when ATP was added (Figure 4.1).

4.3.1.2 The presence of a P-type Ca^{2+}-ATPase in P1 vesicles

Vanadate, a potent inhibitor of P-type Ca^{2+}-ATPases found on acidic stores (Rooney and Gross, 1992), and plasma membrane (PMCA), had an inhibitory effect on Ca^{2+} uptake (Figure 4.2). This result suggests that some of the Ca^{2+} uptake in P1 vesicles is dependent on Ca^{2+}-ATPases rather than a H^+/Ca^{2+} antiporter and is consistent with the presence of acidic stores.

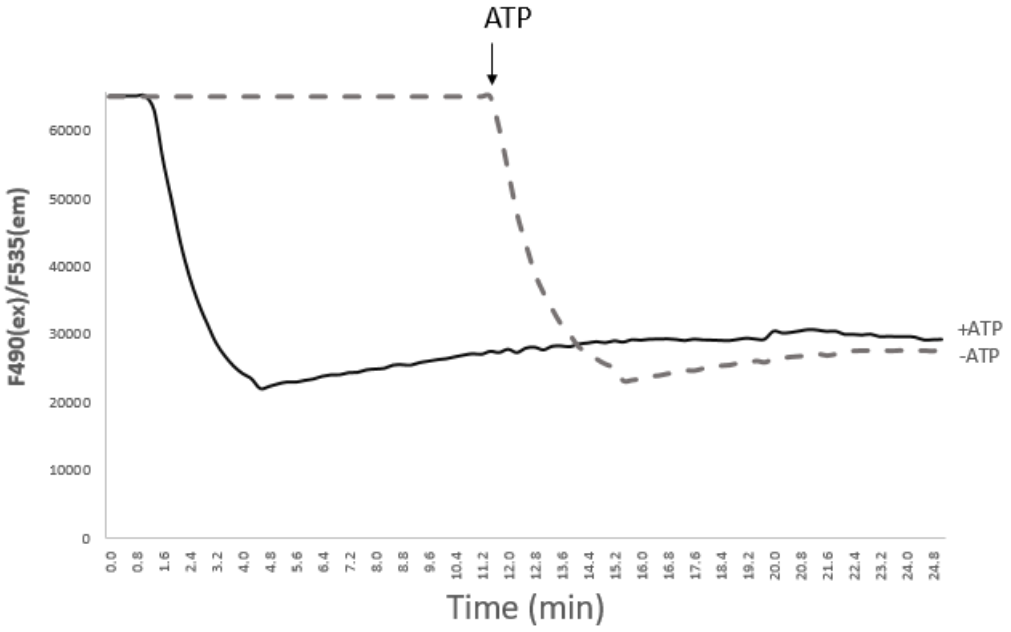

Figure 4.1 ATP-dependence of Calcium uptake by vesicles. Representative fluorimetric traces of Ca^{2+} uptake. 200 µg of the P1 fraction prepared from T4 Ax2 cells were added to 100 µl Ca^{2+} uptake buffer supplemented with 100 µM NaN_3 and 6 µg/ml oligomycin A with or without 1.5 mM ATP. Free ionized Ca^{2+} was measured by monitoring the fluorescence emission of 6.6 µM fluo-3 (490 nm excitation wavelength and 535 nm emission wavelength) using a Fluorometer (NovoStar). The Ca^{2+} uptake was observed by using vesicles incubated in buffer containing 1.5 mM ATP buffer is shown in black. The dotted grey line show the trace from vesicles initially incubated in the absence of ATP. Uptake was initiated by adding 1.5 mM ATP to the reaction as indicated.

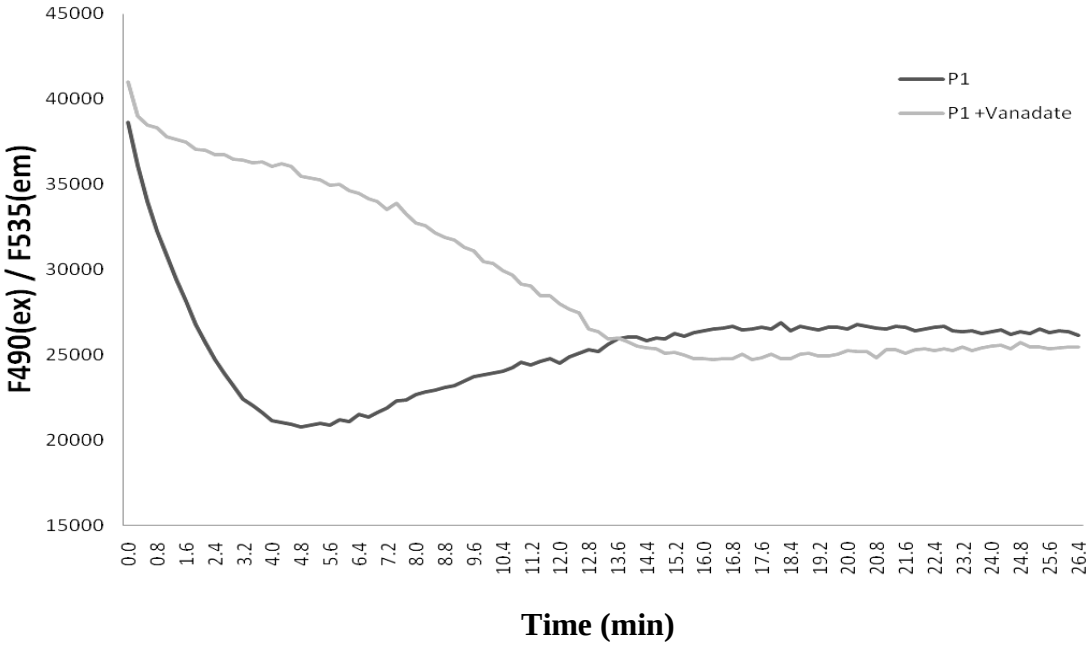

Figure 4.2 Inhibitory effect of a P-type ATPase inhibitor, vanadate, on Calcium uptake. Representative fluorimetric traces of Ca^{2+} uptake and its inhibition by pre-incubation with 60 μm sodium orthovanadate. 200 μg of the P1 fractions prepared from T4 Ax2 cells were added to 100 μl Ca^{2+} uptake buffer supplemented with 100 μM NaN_3, 1.5 mM ATP and 6 μg/ml oligomycin A. The dark trace denotes Ca^{2+} uptake without vanadate. The light grey trace denotes Ca^{2+} uptake following pre-incubation with vanadate for 5 minutes.

4.3.1.3 Increased vesicle Ca^{2+} uptake and *patA* expression in *tpc2*$^{-}$ cells

A higher rate of Ca^{2+} uptake was reproducibly observed in vesicles derived from T4 *tpc2*$^{-}$ cells, compared to those from Ax2 cells (Figure 4.3 shows representative traces of Ca^{2+} uptake). Ax2-derived vesicles uptake Ca^{2+} at -301.8 $\pm$ 27.2 absorbance units/sec, whereas those from *tpc2*$^{-}$ cells uptake Ca^{2+} at an average of -668.3 $\pm$ 67.2 absorbance units/sec, which is more than twice the speed of that in Ax2. In Chapter 3, bioinformatic analysis predicted that P-type Ca^{2+} ATPases are a potential functional partner of DdTPC2. An examination of mRNA expression via qRT-PCR for transcripts encoding the P-type Ca^{2+}ATPase PAT1, *patA*, showed that *patA* expression is higher in the second hour of development in *tpc2*$^{-}$ cells compared to Ax2 cells. This data is consistent with the higher rate of Ca^{2+} uptake in vesicles of *tpc2*$^{-}$ cells, although I did not investigate the expression level of other Ca^{2+} pumps and channels that may also be altered. The increased uptake would also be consistent with TPC2 normally playing a role as a Ca^{2+} leak channel in these vesicle preparations.

4.3.1.4 Ca^{2+} release studies in vesicle preparations from *Dictyostelium*

Arachidonic acid (AA) has been reported to induce Ca^{2+} release from these vesicle fractions (Malchow *et al.*, 2006) so the Ca^{2+} mobilizing ability of AA was examined. AA induced Ca^{2+} release from P0 (not shown) and P1 fractions prepared from T4 cells (T4P1) whereas the solvent, ethanol, induced less release (Figure 4.4). There have been previous reports of reduced AA-induced Ca^{2+} release in vesicle preparations from *tpc2*$^{-}$ cells in a DH1 background (Watanabe, 2011, DPhil thesis). However, I have found AA can induce Ca^{2+} release from P1 vesicles from *tpc2*$^{-}$ cells at a range of AA concentrations, at levels similar to parental Ax2 cells (Figure 4.4).

Figure 4.4B illustrates that vesicles from both cell types can be re-stimulated with AA to induce Ca^{2+} release, with no evidence for desensitisation. After treatment with vanadate, the Ca^{2+} uptake after stimulation by AA was reduced in P1 vesicles from both *tpc2*$^{-}$ and Ax2 cells.

4.3.1.5 The role of TPC2 in NAADP-induced Ca^{2+} release

AA and Ca^{2+} are the only molecules reported to release Ca^{2+} from intracellular vesicles in *Dictyostelium*. Therefore I tested whether NAADP could induce release in P1 fractions prepared from cells developed for 4 hours (T4P1 vesicles) from Ax2 cells (Figure 4.5A). NADP was used as a negative control to determine if any Ca^{2+} release observed was due to a specific interaction with an NAADP-binding protein. NAADP was able to induce Ca^{2+} release from T4P1 vesicles derived from Ax2 cells to a much greater extent than NADP. However, the dose required was much higher than reported in other organisms (Calcraft *et al.*, 2009), so further research still needs to verify whether this is an artefact. To determine if TPC has a role in NAADP-induced Ca^{2+} release in *Dictyostelium*, the T4P1 fraction from *tpc2*$^{-}$ cells was compared with the parental strain, Ax2 (Figure 4.5B and C) and found to be very similar. Therefore if the NAADP-induced release is genuine, it is not completely dependent on TPC2 in *Dictyostelium*.

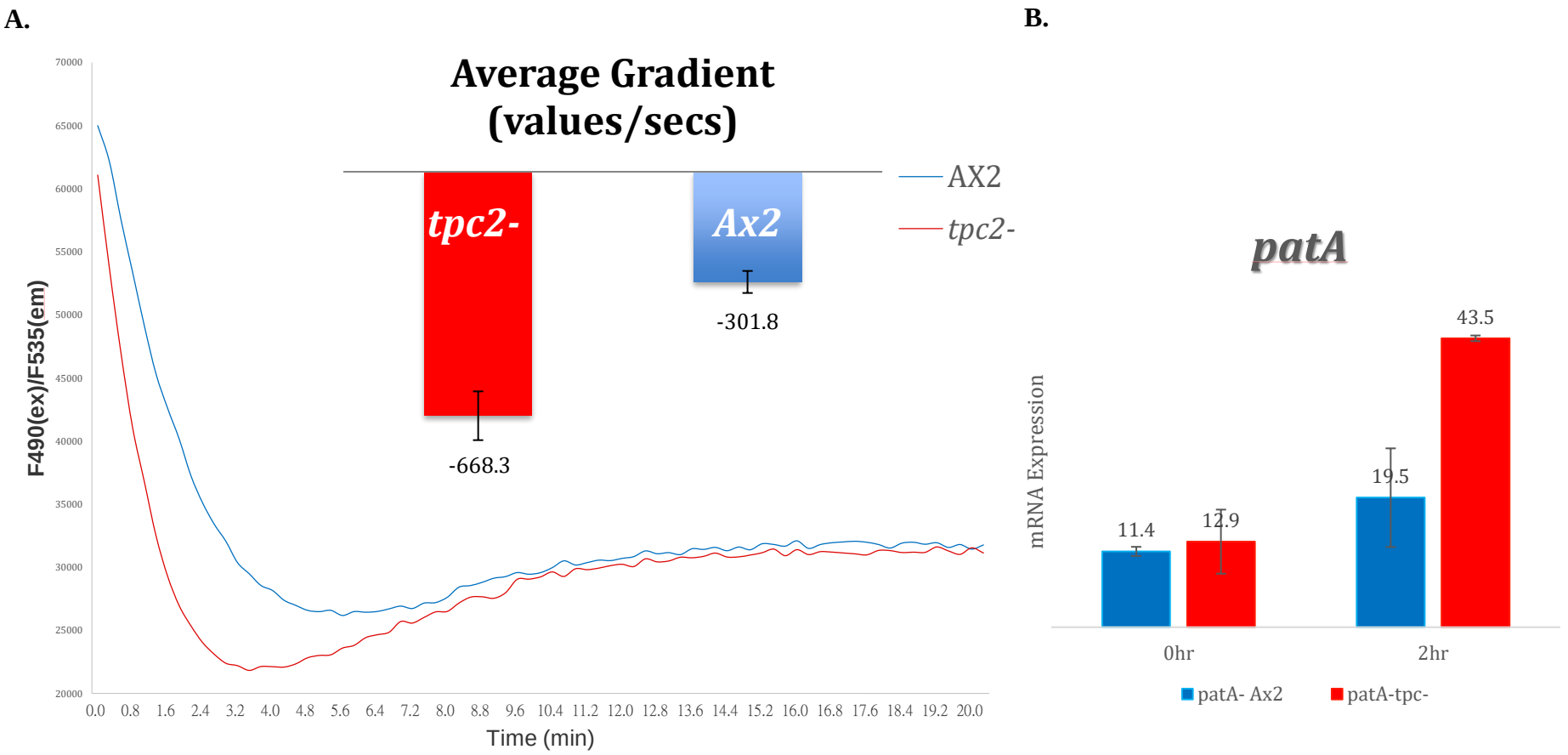

Figure 4.3 Higher initial uptake of Ca^{2+} by vesicles from *tpc2*$^-$ cells and up-regulation of mRNA levels of P-type ATPase, *patA*, in early development in *tpc2*$^-$ cells.

A. Representative trace showing calcium uptake by P1 vesicles made from Ax2 and *tpc2*$^-$ cells after 4 hours of development. In three independent experiments the average rate of uptake of Ca^{2+} in vesicles derived from *tpc2*$^-$ cells is -668.3 ± 67.2 absorbance units/sec compared to -301.8 ± 27.2 for those from Ax2 cells. Results are the average of 3 independent experiments. B. mRNA was extracted from Ax2 or *tpc2*$^-$ cells growing or developed in shaking suspension for 2 hours and levels of *patA* expression quantified by qRT-PCR relative to expression of *ig7*. Results are the average of 2 independent experiments.

A.

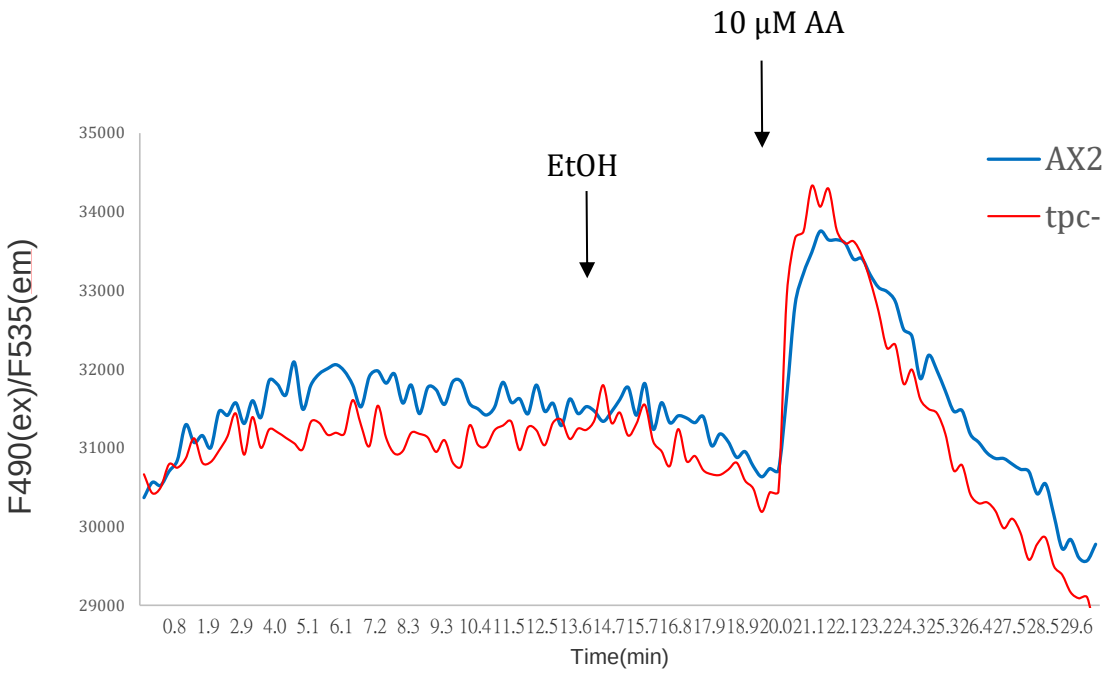

Figure 4.4A Arachidonic acid induced Ca^{2+} release from T4P1 vesicles of Ax2 and *tpc2*$^{-}$ cells. Representative trace showing calcium release by T4P1 vesicles made from Ax2 (blue trace) and *tpc2*$^{-}$ (red trace) cells. Vesicles were incubated in a buffer containing the Ca^{2+} sensitive dye fluo-3 and ATP. Ethanol (EtOH) or arachidonic acid (AA) were added as indicated.

B.

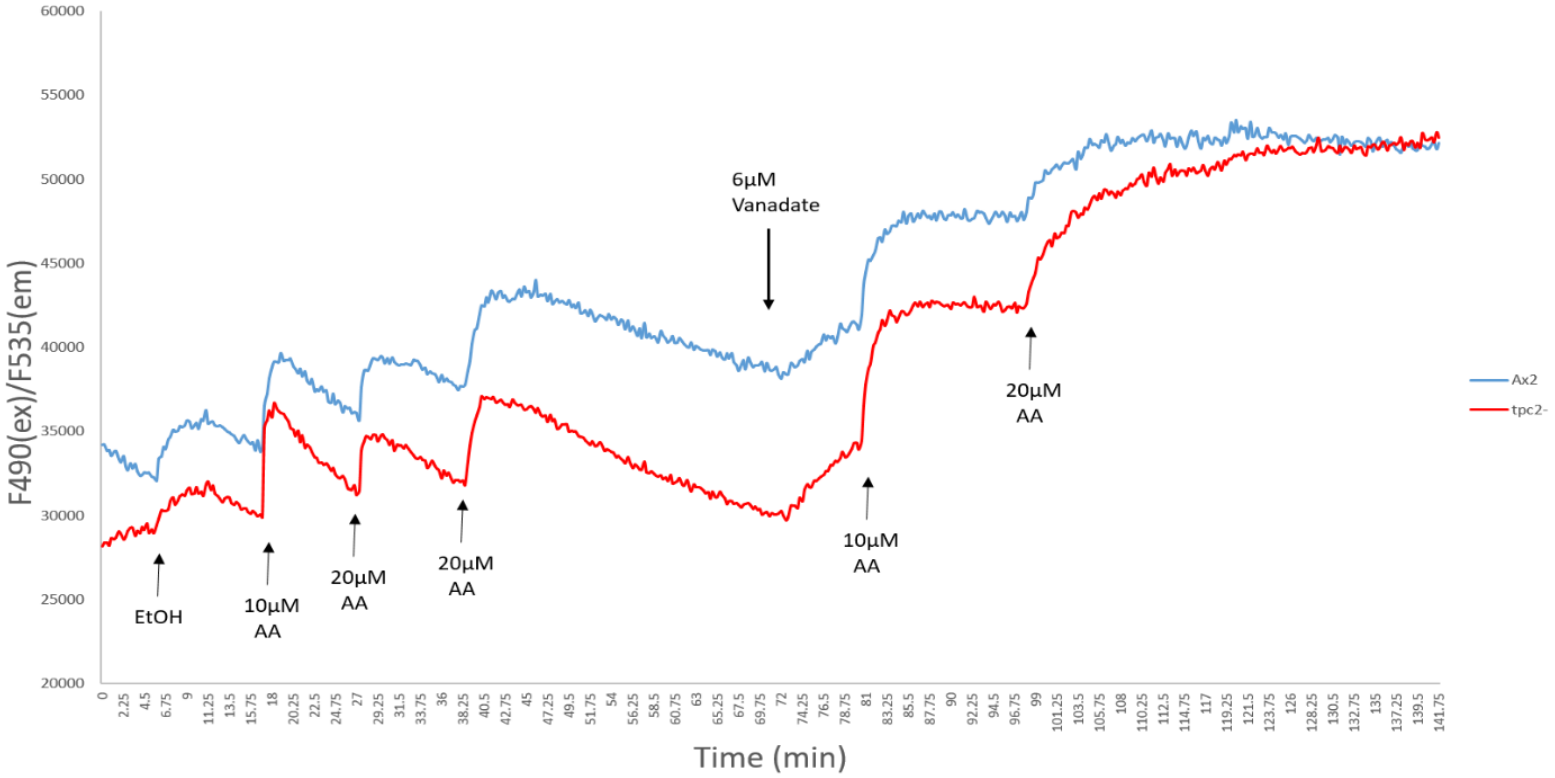

Figure 4.4B Arachidonic acid induced Ca^{2+} release from T4P1 vesicles of Ax2 and *tpc2*$^{-}$ cells.

Representative trace showing calcium release by T4P1 vesicles made from Ax2 (blue) and *tpc2*$^{-}$ (red) cells. Vesicles were incubated in a buffer containing the Ca^{2+} sensitive dye fluo-3 and ATP. Ethanol (EtOH), arachidonic acid (AA) and vanadate were added as indicated.

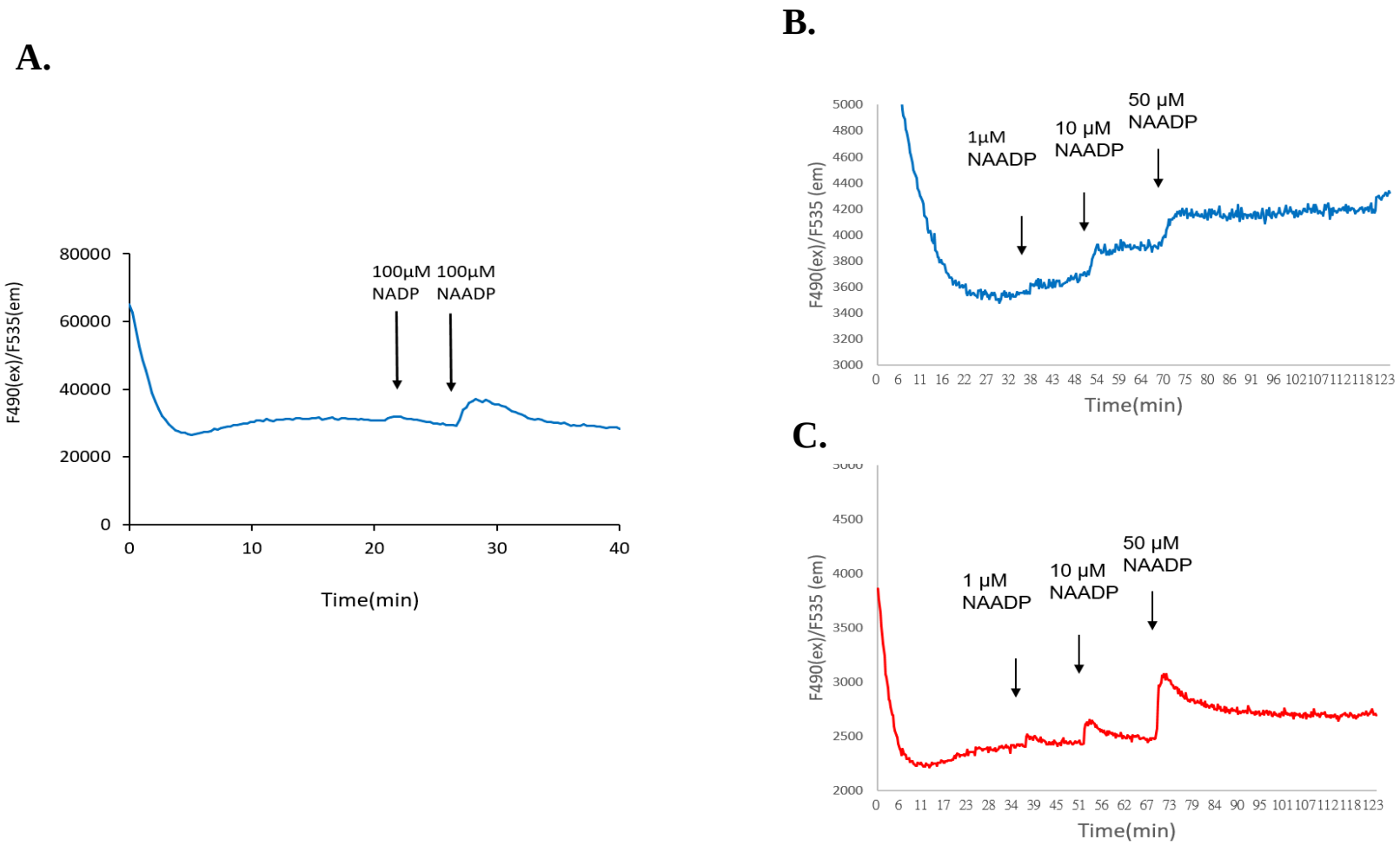

Figure 4.5 NAADP causes a larger Ca^{2+} release from T4P1 vesicles than NADP

Representative trace showing calcium release by T4P1 vesicles made from A. Ax2 (blue) and B. Ax2 (blue) and *tpc2*$^{-}$ (red) cells. Vesicles were incubated in a buffer containing the Ca^{2+} sensitive dye fluo-3 and ATP. NAADP or NADP were added as indicated.

4.3.2 The role of DdTPC2 in pH of acidic stores

Weak bases, such as ammonium chloride and imidazole, are effective in interfering with multicellular developmental processes, such as aggregation and culmination, by neutralizing the pH of acidic vesicles while having little or no effect on cytosolic pH (Davies *et al.*, 1993). If TPC2 plays a role in regulating the pH in acidic stores in *Dictyostelium*, then the *tpc2*$^{-}$ mutant would show different sensitivity to weak bases. To test if the *tpc2*$^{-}$ strains are sensitive to weak bases, development assays were conducted as below.

4.3.2.1 The effect of weak bases on under buffer development of *tpc2*$^{-}$ cells

To determine if TPC2 plays a part in regulating the pH of acidic stores in development, cells were developed under a buffer, in lower pad solution (LPS) at pH 7.0, suitable to study the effect of weak bases on intracellular pH and development. In these conditions un-protonated NH_3 can diffuse into acidic stores and become protonated whereas NH_4^+ cannot diffuse out again (Davies *et al.*, 1996). Figure 4.6 shows cells developed for 21 hours (A) and 38 hours (B) under LPS buffer at pH 7.0 in the presence of various concentrations of ammonium chloride (NH_4Cl) and sodium chloride (NaCl) as a control for osmotic effects. At the 21st hour, in the absence of weak bases most cells had aggregated although some large aggregating clusters of cells still can be seen in the absence of salt. Aggregation is disrupted in general with higher concentrations of ammonium chloride or sodium chloride, but at 20 mM it is clear that ammonium chloride has a greater effect. The *tpc2*$^{-}$ cells showed a delay in aggregation similar to that seen under HKC-LoCa buffer in Chapter 3. *Tpc2*$^{-}$ cells showed some resistance to

ammonium chloride most noticeable at 21 hours in 30 mM ammonium chloride where *tpc2*$^{-}$ cells formed larger clusters of cells compared to Ax2 cells. However, by 38 hours, no real difference was apparent. This suggests the difference in resistance to ammonium chloride between Ax2 and *tpc2*$^{-}$ cells might not be large although *tpc2*$^{-}$ cells seemed slightly more resistant to ammonium chloride in early development. To our surprise, the *tpc2*$^{-}$ cells showed a higher degree of resistance to sodium chloride. At the 21st hour, *tpc2*$^{-}$ cells formed clusters of aggregates whereas Ax2 cells could barely form aggregates in 30 mM of NaCl. This is more obvious after 38 hours of development, when *tpc2*$^{-}$ cells clearly formed larger aggregates in stark contrast to Ax2 cells which rarely formed aggregates above a concentration of 30 mM of sodium chloride.

4.3.2.2 The effect of weak bases on filter development of *tpc2*$^{-}$ cells

To determine if TPC2 has a role in later development cells were also developed on filters with various concentrations of weak bases (imidazole and NH_4Cl) and NaCl. Figure 4.7 shows filter development for 24 hours (A and B) and 42 hours (C) with LPS buffer at pH 7.0. Without any additions at the 24th hour, most structures have formed fruiting bodies. Development was delayed pronouncedly in the presence of weak bases, imidazole and NH_4Cl but not with the NaCl control and the number of aggregates was reduced in the presence of Imidazole, NH_4Cl and NaCl. Two independent *tpc2*$^{-}$ strains, TPC22B20 and TPC1E14, were more sensitive to weak bases, as the percentage of aggregates was greatly reduced (Figure 4.7 and Table 4.1). Both independent *tpc2*$^{-}$ strains showed reduction in number of aggregates, although TPC22B20 showed a greater reduction in the presence of weak bases and NaCl compared to TPC1E14. However, despite fewer aggregates forming, the *tpc2*$^{-}$ strains showed higher resistance to weak bases in terms of forming fruiting bodies (Figure 4.7A, B and C).

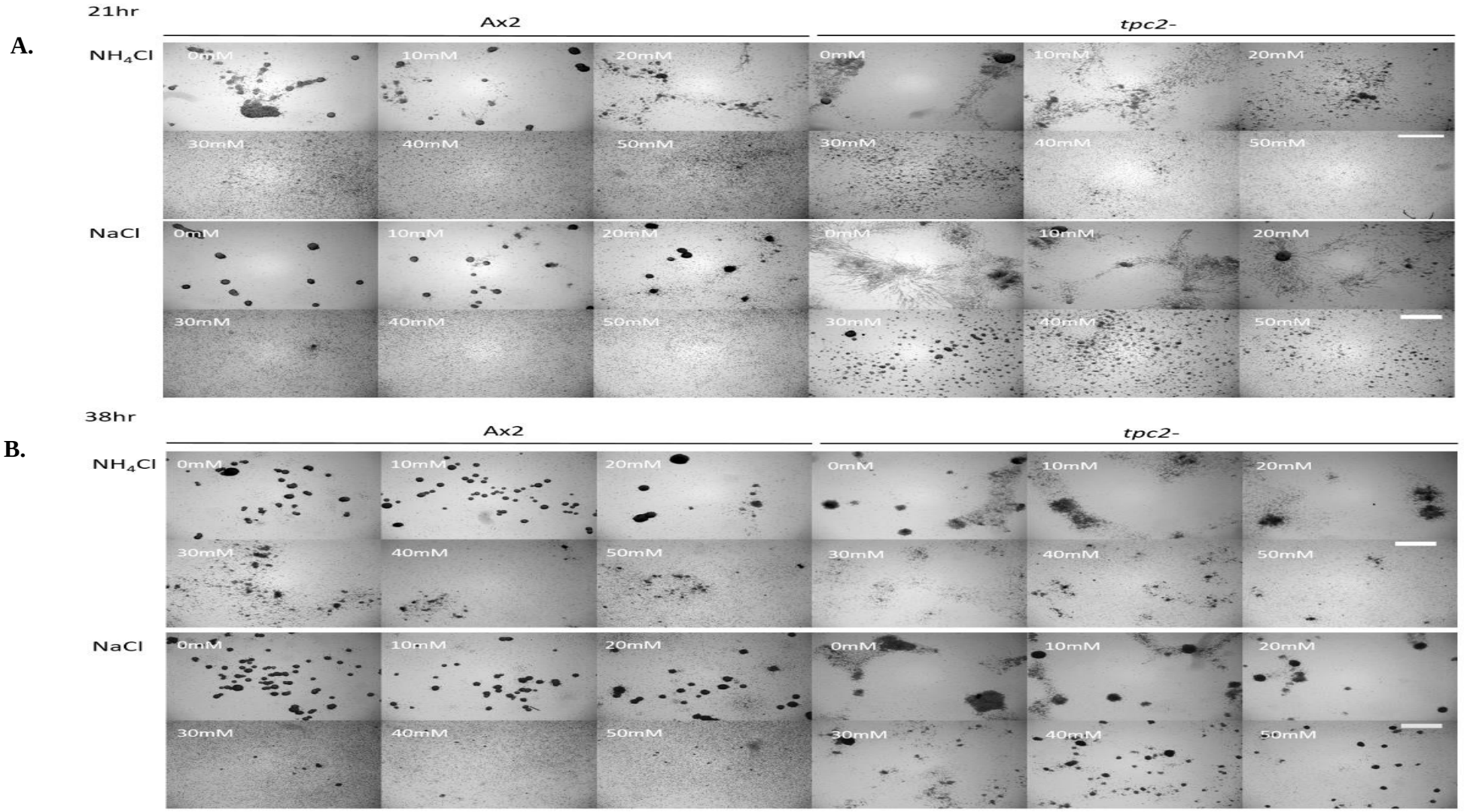

Figure 4.6 Sensitivity of Ax2 and *tpc2*$^{-}$ cells to ammonium and sodium chloride when developed under buffer

Ax2 and *tpc2*$^{-}$ (clone TPC22B20) cells were harvested from exponential growth. Cells were washed twice with LPS buffer and 3.84 x 10^6 cells plated in a 6 well plate, (final cell density of 4 x 10^5 cells/cm^2), under LPS buffer with various concentrations of ammonium chloride or sodium chloride and incubated at 22 °C. Developmental structures were observed at A. 21st and B. 38th hours using a Leica MZ FL III Stereomicroscope and photographed using a Hamamatsu digital camera ORCA-05. Scale bar, 1 mm.

A.

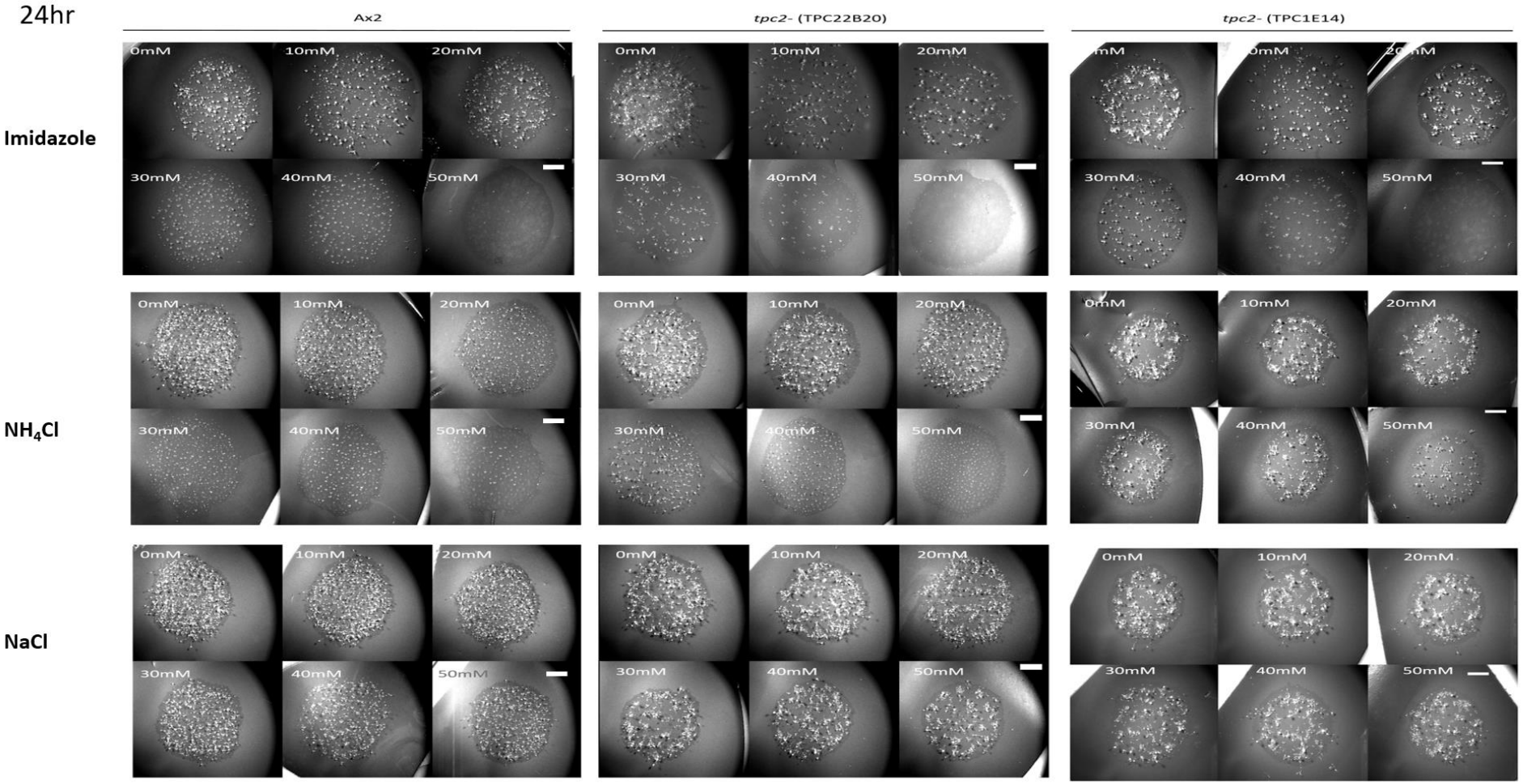

Figure 4.7. Sensitivity of Ax2 and *tpc2*$^{-}$ cells to weak bases when developed on filters.
A. Ax2 and *tpc2*$^{-}$ (clones TPC22B20 and TPC1E14) cells were developed on filters. 5 x 10^7 cells were plated on 3.4 cm Millipore filter paper incubated on paper pre-soaked LPS pH 7.0 in the presence of various concentrations of the weak bases (imidazole or ammonium chloride) or sodium chloride at 22 °C. Developmental structures were observed at 24th hour using a Leica MZ FL III Stereomicroscope and photographed using a Hamamatsu digital camera ORCA-05. Scale bar, 5 mm.

Table 4.1. Sensitivity of Ax2 and *tpc2*$^-$ cells to weak bases when developed on filters.

Condition	Ax2	TPC22B20	TPC1E14
Imidazole 0 mM	361	269	263
Imidazole 30 mM	324	115	143
% reduction	89.8%	42.8%	54.5%
NH_4Cl 0 mM	443	376	291
NH_4Cl 30 mM	397	203	201
% reduction	89.6%	54%	69.1%
NaCl 0 mM	469	300	292
NaCl 30 mM	324	211	221
% reduction	69.1%	70.3%	75.7%

Quantification of aggregate number per filter in the presence or absence of 30 mM salts. The reduction in aggregation is the number of aggregates in the presence of 30 mM of weak base or NaCl divided by the number formed in the absence of salts. One experiment representative of two.
.

B.

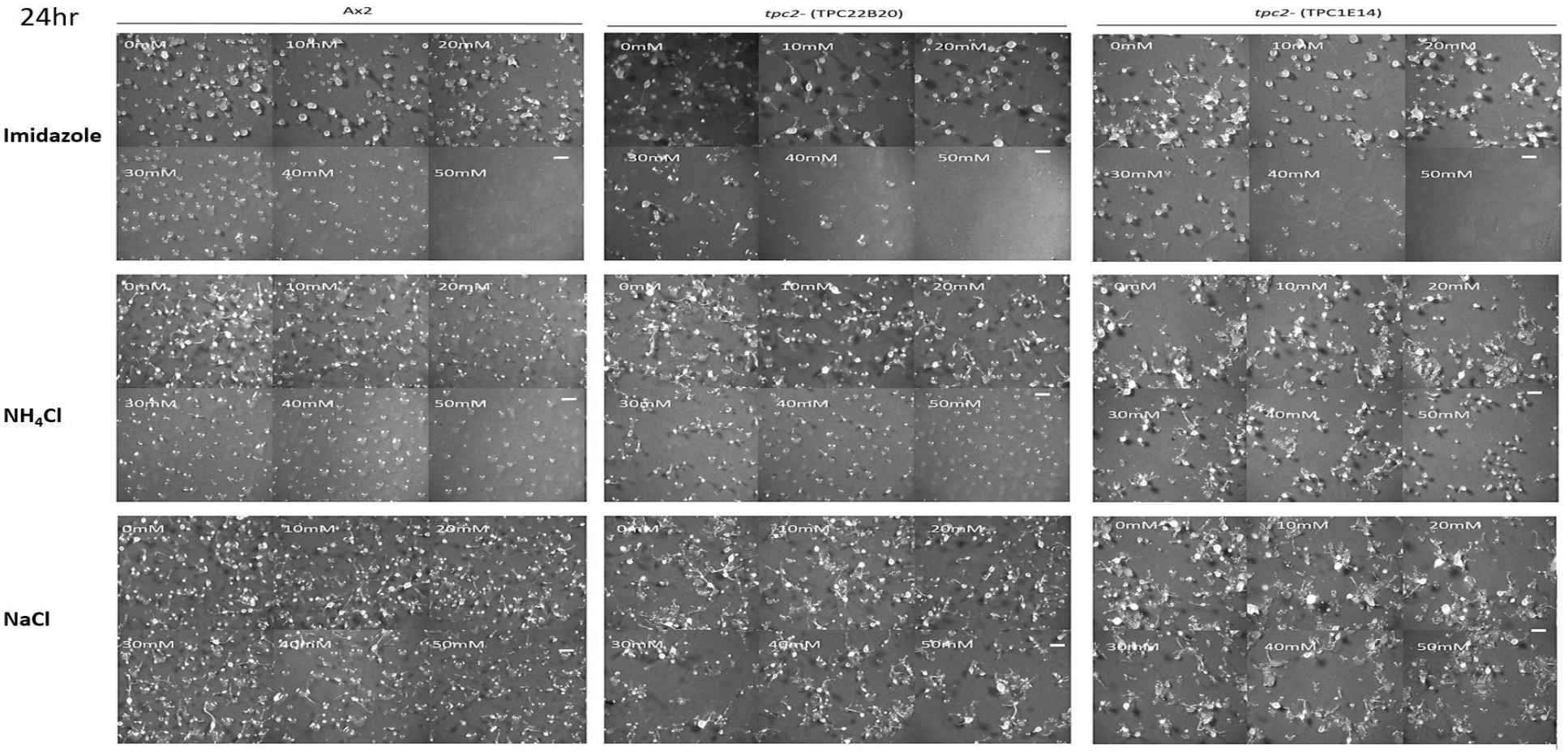

Figure 4.7. Sensitivity of Ax2 and *tpc2*$^{-}$ cells to weak bases when developed on filters.

(B) Ax2 and *tpc2*$^{-}$ (clone TPC22B20 and TPC1E14) cells were developed as in (A). Developmental structures were observed at 24th hour using a Leica MZ FL III Stereomicroscope and photographed using a Hamamatsu digital camera ORCA-05. Scale bar, 1 mm.

.

C.

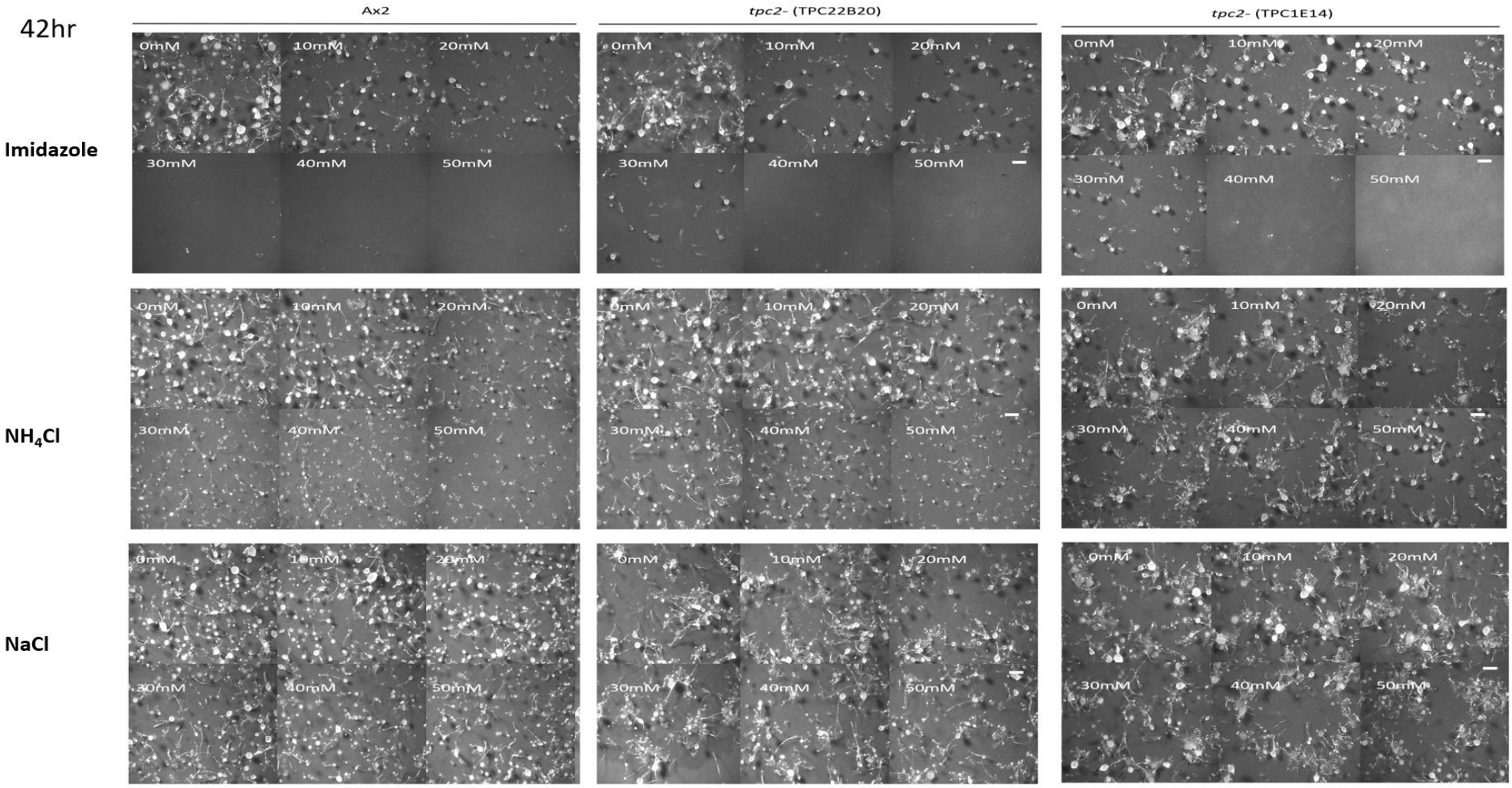

Figure 4.7. Sensitivity of Ax2 and *tpc2*⁻ cells to weak bases when developed on filters.

(C) Ax2 and *tpc2*- (clone TPC22B20 and TPC1E14) cells were developed as in (A). Developmental structures were observed at 42nd hour using a Leica MZ FL III Stereomicroscope and photographed using a Hamamatsu digital camera ORCA-05. Scale bar, 1 mm.

.

4.3.2.3 Acidic vesicle pH in *tpc2*$^-$ and Ax2 cells

To determine if TPC has a role in pH regulation of acidic stores, a pH sensitive indicator was used. Cells were grown in LoFlo medium to reduce auto-fluorescence and then allowed to develop under LPS buffer at pH 7.0 for 4 hours before staining with a pH sensitive indicator LysoSensor Yellow/Blue DND-160 (also known as PDMPO) at final concentration of 2 μM for 15 min. The indicator undergoes a pH-dependent emission shift to longer wavelengths in acidic environments (blue to green) when illuminated near its excitation isosbestic point (~360 nm). The blue channel (438/48 nm) and green channel (525/48 nm) images both excited at 390/18 nm allow ratiometric measuring of intracellular acidic vesicles *in vivo*. Figure 4.8 shows a striking general loss of green fluorescence (acidic compartments), where vesicles were in general less acidic shown as increased blue fluorescence in *tpc2*$^-$ cells compared to Ax2. Ratiometric images are also shown indicating the reduction of the green/blue ratio applied to the majority of vesicles observed in *tpc2*$^-$ cells. Mean ratio for Ax2 = 1.16 ; *tpc2*$^-$ cells = 0.92, two tailed Student *t*-test, $P \leq 0.0001$. This was also verified with two independent *tpc2*$^-$ strains and at different development time points (TPC1E14 and TPC1015, data not shown). This indicates the pH of acidic vesicles in *tpc2*$^-$ cells has been altered, with the vesicles being less acidic at 4 hours of development.

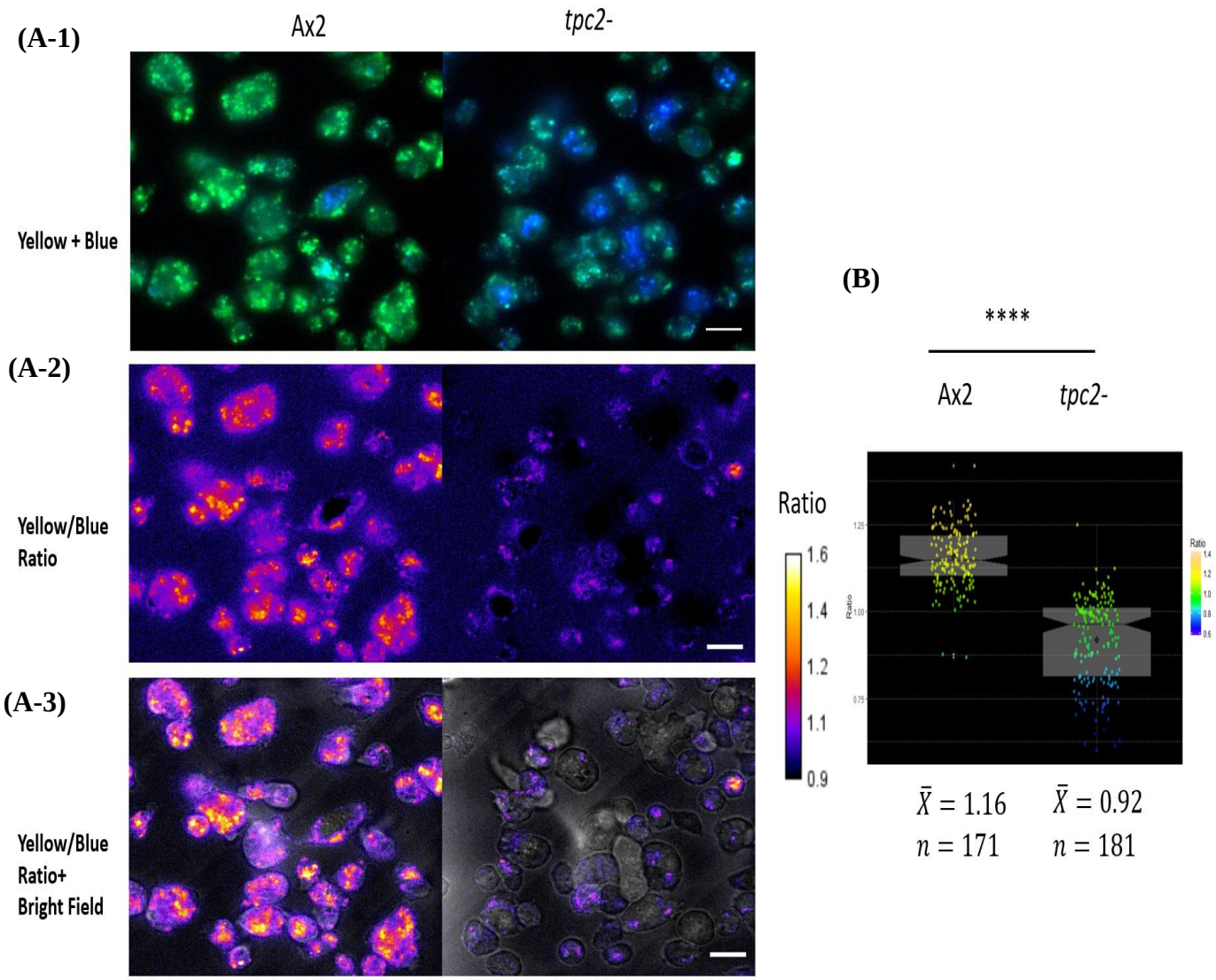

Figure 4.8. Alteration of pH in intracellular acidic organelles in *tpc2*$^-$ cells.

Intracellular acidic organelles were visualised using a fluorescent LysoSensor™ Yellow/Blue DND-160 (PDMPO) probe following incubation with 2 μM probe for 15 min. Panel (A-1) shows acidic organelle fluoresence. The LysoSensor™ emits predominantly yellow fluorescence, and in less acidic organelles it emits blue fluorescence (Diwu *et al.*, 1999). In (A-2), ratio images are shown and (A-3) merged with bright field images. Cells were observed at 4 hr of development using DeltaVision Elite microscope and photographed using an EMCCD camera mounted on the microscope. Scale bar, 10 μm. Panel B shows quantification and statistical analysis (Student *t*-test) of ratios as in A-3. $\bar{X}$, sample mean, n, sample numbers and ****, $P \leq 0.0001$.

4.4. Discussion

Intracellular levels of calcium ([Ca^{2+}]i) and protons ([H^{+}]i) both play important roles in cell fate decision of *Dictyostelium* development (Jang and Gomer, 2011). In this chapter, we aim to characterise the role of TPC2 in regulating acidic Ca^{2+} stores in development of *Dictyostelium*.

Vesicle preparations as described by Malchow *et al.*, contain vesicles from both neutral and acidic Ca^{2+} stores (Malchow *et al.*, 2008; Malchow *et al.*, 2006). In our group, Watanabe verified that P1 was the fraction enriched in vesicles derived from CVs compared to P0 which was enriched in vesicles from the ER by making vesicles from cells expressing either a CV marker, dajumin-GFP fusion protein, or calnexin-GFP, an ER marker in *Dictyostelium* (Watanabe, DPhil thesis, 2011). Therefore, in this study, P1 was used in the Ca^{2+} release experiments.

Vanadate is a potent inhibitor for some types of plasma membrane ATPases, which include P-type Ca^{2+}-ATPase (PMCA) and Na^{+}/K^{+}-ATPase. Importantly, vanadate does not inhibit other ATPases, such as SERCA (sarco/endoplasmic reticulum Ca^{2+}-ATPase), mitochondrial ATPase and actomyosin ATPase (Bowman and Slayman, 1979; Luo *et al.*, 2000). We have verified vanadate inhibition of Ca^{2+} uptake in P1 vesicles prepared from cells developed for 4 hours, which is ATP dependent, suggesting our P1 fraction contains vesicles with Ca^{2+} P-type ATPases. Vesicles from the *tpc2*$^{-}$ cells interestingly showed enhancement of Ca^{2+} uptake and up-regulated expression of the gene encoding for PAT1, *patA*, at the 2nd hour of development. This is of particular interest since PAT1 and calcineurin were predicted to be biological functional partners of TPC2 (Chapter 3). Moniakis *et al*. found that *Dictyostelium* PAT1 lacks the highly conserved

CaM-binding domain present in the C-terminal region of most PMCA type enzymes. However, intriguingly, PAT1 co-localised with calmodulin (CaM) on the contractile vacuoles in *Dictyostelium* (Moniakis *et al.*, 1995). They also confirmed *patA* expression in *Dictyostelium* is regulated by a Ca^{2+}/calcineurin pathway similar to yeast (Matheos *et al.*, 1997), thought to function in maintaining Ca^{2+} homeostasis (Moniakis *et al.*, 1999). *Dictyoselium* TPC2 and plant TPC1 have a CaM-like domain (EF-hand pair) which is absent in mammalian TPCs (Ishibashi *et al.*, 2000) and intriguingly *Dictyostelium* was predicted to have a putative CaM-binding domain (Chapter 3). All the information suggests a potential, but as-yet unidentified link between TPC2, PAT1 and possibly calcineurin. Further research is needed to investigate how these proteins and genes interact with each other. The increased Ca^{2+} uptake could also reflect a decrease in release if TPC2 proteins act as leak channels in these vesicle preparations.

I went on to study Ca^{2+} release from P1 vesicle preparations. In previous reports the calmodulin antagonist W7 as well as arachidonic acid (AA) caused Ca^{2+}-release from vesicles in *Dictyostelium* (Malchow *et al.*, 2006). *Dictyostelium* does not contain endogenous AA (Weeks, 1976) but a phospholipase A2, which could release related fatty acids, has been shown to play a role in aggregation (Chen *et al.*, 2007). AA has an inhibitory effect on plant TPC1. The addition of micromolar concentrations of AA reversibly inhibit plant TPC1 (SV channel) channel by decreasing the maximum open probability and shifting the half activation voltage to positive values (Gutla *et al.*, 2012). In *Dictyostelium* both AA and NAADP were able to cause Ca^{2+} release from vesicles with no pronounced differences between vesicles from Ax2 and *tpc2*$^{-}$ cells, suggesting that the TPC2 channel might not be the only channel responsive to these ligands. However, it is important to note that the doses of NAADP required to trigger Ca^{2+}

release from *Dictyostelium* P1 vesicles, ranging from 10 μM to 100 μM, was much higher than the nanomolar levels required in *in vitro* preparations from organisms such as sea urchin (Galione, 2011). Therefore it cannot be ruled out that this is an artefact, for example due to a contaminant in the preparation of NAADP, despite the control NADP causing a much lower response. One potential contaminant is Ca^{2+} itself. In preliminary experiments pre-incubation of NAADP with Ca^{2+}-chelating beads reduced, but did not abolish, Ca^{2+} release from vesicles but this requires verification (data not shown). In most eukaryotic cells, although not in yeast or plants, it has been proposed that NAADP triggers Ca^{2+} release from intracellular acidic stores, thereby causing transient increases in the cytosolic [Ca^{2+}] (Calcraft *et al.*, 2009; Cancela *et al.*, 1999). IP_3 receptors and ryanodine receptors (RyRs) further amplify these Ca^{2+} signals to a global level which is important for biological processes ranging from cardiac function to cell differentiation (Galione, 2015; Morgan *et al.*, 2015). NAADP triggers opening of human TPC2 channels through an indirect manner (Ruas *et al.*, 2015; Wang *et al.*, 2012), probably via a complex with a not yet unidentified NAADP-binding protein (Lin-Moshier *et al.*, 2014).

One intriguing question is whether acidic Ca^{2+} stores have a role in development and cell differentiation? It is known that a sustained increase in intracellular Ca^{2+} levels, [Ca^{2+}]i, mediates stalk gene induction by differentiation inducing factor (DIF) in *Dictyostelium* (Schaap *et al.*, 1996). Acidic Ca^{2+} stores have been postulated to be involved in cell differentiation in *Dictyostelium* (Gross, 2009). Traynor *et al.* (2000) and our study (Chapter 3) both showed that mutants lacking expression of IplA do not show obvious phenotypes in early or later development despite the fact that Ca^{2+} influx in response to extracellular cAMP is highly reduced in *iplA*$^-$ cells (Traynor *et al.*, 2000).

These results might suggest Ca^{2+} signalling in response to cAMP may be through the acidic Ca^{2+} store pathway with possibly a minor participation of IP_3-sensitive Ca^{2+} stores.

TPC2 has been found to play an important role in pH regulation of acidic stores in a range of organisms (Ambrosio *et al.*, 2016; Ambrosio *et al.*, 2015; Lu *et al.*, 2013). *Dictyostelium* strains that have defects in vacuolar H^+ ATPase, Hgr5 and Hgr8, show higher sensitivity to weak bases (Davies *et al.*, 1996), so this sensitivity can be used to examine vesicular pH. Therefore the effect of the weak base, ammonium chloride, on development under buffer was determined. Although it was not pronounced, the under buffer experiment showed that *tpc2*$^-$ cells seemed to have slightly higher resistance in forming small clusters of cells in the presence of 30 mM NH_4Cl. However, this might be influenced by higher resistance to osmosis or salt ions rather than a weak base effect as the *tpc2*$^-$ cells exhibited pronounced resistance to NaCl in these conditions as seen in Figure 4.6. This unexpected finding that mutants lacking expression of TPC2 are resistant to salinity is reminiscent of the plant TPC1 channel. Plant TPC1, known as slow vacuolar or slow-activating (SV) channels located on the tonoplast, are non-selective channels permeable to Na^+, K^+ and Ca^{2+} (Kintzer and Stroud, 2016). In order to confer salinity tolerance, toxic Na^+ ions have to be prevented from re-entering the cytosol. Therefore, the activity of a Na^+ permeable channel has to be reduced. It was observed in the 1990s that the probability of the tonoplast channels (SV and FV) opening dramatically decreased when plants were grown in a high salinity environment (Maathuis and Prins, 1990). Evidence suggests that reduced tonoplast TPC1 channel, as well as fast-activating channel, activity is essential for conferring salinity tolerance in plants (Bonales-Alatorre *et al.*, 2013). Although it is not known if *Dictyostelium* TPC2

is also Na^+ permeable, considering it is known that both plant and animal TPCs are sodium permeable and DdTPC2 has high sequence homology to TPC channels in plants and animals (Chapter 3), the salinity resistance of *Dictyostelium tpc2*$^-$ cells during aggregation under buffer might be related to this property.

Filter developments were also carried out in the presence of various concentrations of weak bases, such as imidazole and ammonium chloride. In these conditions there was no evidence of resistance of *tpc2*$^-$ cells to NaCl suggesting that the resistance seen under buffer is dependent on the conditions. Two independent *tpc2*$^-$ strains, TPC22B20 and TPC1E14, shown reduced numbers of aggregates compared to Ax2 cells, suggesting higher sensitivity to both weak bases in early development (aggregation). This is similar to the strains Hgr5 and Hgr8 that have defects in the vacuolar H^+ ATPase, where fewer aggregates were formed in mutants in the presence of weak bases suggesting higher sensitivity to weak bases (Davies *et al.*, 1996). However, to our surprise, both *tpc2*$^-$ strains showed pronounced resistance to both weak bases in later development, where more final fruiting bodies were formed in the presence of higher concentrations of weak bases despite fewer aggregates. The higher sensitivity to weak bases in early development in *tpc2*$^-$ cells might suggest the pH of acidic stores has been altered. The difference seen in late development might suggest a different role for TPC2 in regulating acidic stores at different stages of development.

In order to further verify if the phenotype of fewer aggregates formed by *tpc2*$^-$ cells in a higher weak base environment, is due to altered pH of acidic vesicles, a dual colour indicator, LysoSensor™ Yellow/Blue DND-160 (also known as PDMPO), was used to verify if the acidic compartments were altered in *tpc2*$^-$ cells. PDMPO undergoes a pH-

dependent emission shift to longer wavelengths in acidic environments when illuminated near its excitation isosbestic point (approximately 360 nm), so it is useful to examine the acidic compartments intracellularly (Diwu *et al.*, 1999). The results showed that when the cells were developed for 4 hours, which is comparable to the vesicle preparation experiments, the acidic compartments were in general less acidic in *tpc2*$^{-}$ cells than in Ax2. This is consistent with the aggregate number seen in filter development experiments where *tpc2*$^{-}$ cells were more sensitive to weak bases. In *Dictyostelium*, the acidic Ca^{2+} stores were found to be of two kinds, contractile vacuoles (CVs) and acidocalcisomes (Marchesini *et al.*, 2002). Further experiments are needed to verify if these PDMPO staining acidic compartments correspond to the CVs and acidocalcisomes.

TPCs have been reported to regulate pH in acidic Ca^{2+} stores in a number of types of cells. However, the effects of ablation of TPC2 channel expression seems to have a different effect on pH regulation of acidic stores depending on the cell type. Ambrosio *et al.* reported in melanocytes that TPC2-null cells had an increase in luminal pH (alkalinisation) of their acidic Ca^{2+} stores (melanosome) whereas TPC2 overexpression in wild-type cells (MNT-1 cells) caused a decrease in melanosomal pH (acidification) that could be blocked by the TPC2-specific inhibitor Ned19 (Ambrosio *et al.*, 2016). However, the same group also reported a completely different effect in platelets, in which TPC2 overexpression resulted in alkalisation of the lumen of acidic Ca^{2+} stores, platelet dense granules (PDGs). On the other hand, TPC2 knockdown and pharmacological inhibition of Ca^{2+} release resulted in PDG lumen acidification (Ambrosio *et al.*, 2015). Similarly, another group found that TPC2 overexpression raised lysosomal pH in HeLa cells and they suggested TPC2/NAADP/Ca^{2+} signalling

alkalinizes lysosomal pH to specifically inhibit the later stage of basal autophagy progression (Lu *et al.*, 2013). Our results demonstrated that ablation of TPC2 in *Dictyostelium* caused alkalisation of acidic vesicles at the fourth hour of development, which indicates less H^+ is stored in the acidic organelles. However the complexity of the sensitivity to weak bases in development suggests this may be more complicated, though the results are consistent with TPC2 playing a role in pH regulation of acidic stores in *Dictyostelium*.

CHAPTER 5: Imaging $[Ca^{2+}]c$ *in vivo*

5.1. Introduction

In order to determine whether TPC2 and other Ca^{2+} channels play a role in regulating cytosolic Ca^{2+} levels in *Dictyostelium* I have used an ultra-sensitive Ca^{2+} indicator, YC-Nano 15. I examined the basal cytosolic Ca^{2+} level of vegetative cells, in aggregates and in developed cells in response to extracellular cAMP, a molecule known to elicit a transient Ca^{2+} response (Abe *et al.*, 1988).

During the aggregation stage of development, cAMP is secreted by developing cells to both act as a chemoattractant and to trigger development in surrounding cells. The cAMP binds to cell surface G-protein coupled receptors (GPCRs), such as cAR1, that trigger, among other responses, release of more cAMP creating an autocatalytic feedback loop (Martiel and Goldbeter, 1987). Among the intracellular signalling molecules activated by these GPCRs (Firtel, 1991) there is a transient increase in cytosolic Ca^{2+} ($[Ca^{2+}]c$) concentration that occurs mainly in the rear of the cell where it fine-tunes chemotactic behaviour (Abe *et al.*, 1988; Yumura *et al.*, 1996). Cytosolic Ca^{2+} responses in *Dictyostelium* have been measured using the fluorescent Ca^{2+} indicator fura-2 (Abe *et al.*, 1988), influx of the radioisotope $^{45}Ca^{2+}$ (Schlatterer *et al.*, 1992; Sonnemann *et al.*, 1997; Traynor *et al.*, 2000), and by expression of a recombinant Ca^{2+}-sensitive chemiluminescent photoprotein, aequorin (Nebl and Fisher, 1997; Saran *et al.*, 1994) and a recombinant Ca^{2+}-sensitive fluorescent protein, yellow cameleon-Nano (YC-Nano) (Horikawa *et al.*, 2010).

Ca^{2+} imaging studies for intact *Dictyostelium* cells were initiated by using the chemical fluorescent dye, fura-2/AM (Abe *et al.*, 1988) and its relative conjugates such as fura-2-dextran (Schlatterer *et al.*, 1992) and fura-2-bovine serum albumin (BSA) (Yumura *et*

al., 1996). It is interesting to note that application of quin-2/AM and fura-2/AM to intact *Dictyostelium* cells was not successful until Abe and colleagues overcame this by using electroporation. By using this method, they provided direct evidence of a Ca^{2+} flux response triggered by chemoattractants (Abe *et al.*, 1988). Schlatterer *et al.* reported that the indicator was rapidly sequestered into intracellular vesicles. In order to overcome this drawback, it was found that it is necessary for fura-2 be covalently linked to dextran or BSA to prevent it being sequestered so quickly (Schlatterer *et al.*, 1992; Yumura *et al.*, 1996).

Electroporation to introduce the dye into cells is not desirable as cells are harmed by this method. If the condenser is charged at too high a voltage, the cells become rounded and unable to adhere to the substratum (Sonnemann *et al.*, 1997). On the other hand, using too low a voltage, such as 240 V as earlier suggested by Yumura and colleagues (Yumura *et al.*, 1995) did not allow cells to take up the dye. This was later improved by pulsing the cells at 850V (Sonnemann *et al.*, 1997). As an alternative to electroporation, the fluorescent dyes can be loaded into cells by using a scrape loading method, which involves tightly attaching cells to coverslips and scraping them with a rubber policeman to tear the cell membrane. This introduces macromolecules into the cell and the cell membranes are immediately repaired (Schlatterer *et al.*, 1992). However, these methods have led to inconsistent results reported by different groups. Abe *et al.* demonstrated that a submicromolar concentration of cAMP (20 nM) induced an increase in $[Ca^{2+}]c$ in cells into which fura-2/AM or quin-2/AM was introduced by electroporation (Abe *et al.*, 1988). Schlatterer *et al.*, who used the scrape loading method with fura-2-dextran, reported no detectable change in $[Ca^{2+}]c$ after stimulation with submicromolar concentrations of cAMP (Schlatterer *et al.*, 1994; Schlatterer *et al.*, 1992). Interestingly,

Sonnemann *et al.* who used both the electroporation and scrape loading methods successfully loaded cells with fura-2-dextran and measured [Ca^{2+}]c changes in response to 0.1–1 mM cAMP (Sonnemann *et al.*, 1997).

Measuring the uptake of the radioisotope $^{45}Ca^{2+}$ is an alternate approach, however this method only allows measurements of Ca^{2+} influx into the cell. Samples are taken at regular intervals over the course of the response and individually counted using a liquid scintillation counter. A useful protocol for $^{45}Ca^{2+}$ uptake assay was developed by Milne and Coukell who successfully measured Ca^{2+} accumulation in *Dictyostelium* in response to both cAMP and folic acid (Milne and Coukell, 1991). The Ca^{2+} responses reported were consistent with those later reported by Sonnemann and colleagues (Sonnemann *et al.*, 1997).

In order to solve the problems caused by measurements using both fura-2-dextran and $^{45}Ca^{2+}$, a non-perturbing method to measure [Ca^{2+}]c was developed. Saran *et al.* expressed the Ca^{2+}-sensitive recombinant chemiluminescent photoprotein, aequorin, in *Dictyostelium* (Saran *et al.*, 1994). However, there are several drawbacks of using aequorin. Firstly, the relatively low Ca^{2+} affinity of native aequorin hinders the accurate measurement of nanomolar level of fluxes in [Ca^{2+}]i in response to extracellular signals. Later a semisynthetic aequorin was developed (Nebl and Fisher, 1997) which showed some improvement in sensitivity to Ca^{2+} and light emission properties (Shimomura *et al.*, 1989). Secondly, the light emission intensity of aequorin is much less than fluorescent dyes or other proteins. Yumura and colleagues (1996) reported aequorin is much less sensitive for detection of Ca^{2+} responses than fura-2-BSA and could not be used for single cell observations (Yumura *et al.*, 1996). Another drawback is that

aequorin requires coelenterazine, a chemical cofactor that is consumed during the production of luminescence. Moreover, luminescence imaging lacks optical sectioning capabilities (Takai *et al.*, 2015). Fluorescent proteins emit signals only when illuminated with the specific excitation light. Therefore, the signals are stronger near the focal plane with fluorescence imaging. This optical sectioning character can be further enhanced by light-sheet illumination, multiphoton excitation or confocal optics. In stark contrast, all of the luciferases in the sample emit a light signal. The signals from thick samples are blurred by the haze from the out-of-focus luciferases (Takai *et al.*, 2015), also makes it difficult to compare subtle difference in single cells in detail.

Recent advances in fluorescence-based genetically encoded Ca^{2+} indicators (GECIs), such as cameleon and GCamP (Miyawaki *et al.*, 1997; Nakai *et al.*, 2001), have revolutionised Ca^{2+} imaging *in vivo*. In 2010, Horikawa *et al*. developed a series of ultrasensitive Ca^{2+} indicators, known as yellow cameleon-Nano (YC-Nano) and expressed these in *Dictyostelium* cells, successfully visualising Ca^{2+} signals as a rotating spiral wave in aggregation (Horikawa *et al.*, 2010). These indicators are adapted from a GFP-based Ca^{2+} probe known as cameleon (Miyawaki *et al.*, 1997), using a calmodulin (CaM) and CaM-binding peptide M13, joined by a linker, as Ca^{2+} sensor. Binding of Ca^{2+} causes the two to interact which in turn causes fluorescence resonance energy transfer (FRET) to occur between CFP and YFP which are present at the N and C termini of the protein. A number of variants of YC-Nano have been developed, characterised by having high Ca^{2+} affinities (K_d = 15 to 140 nM) and large signal change (1,450%) to enabled detection of subtle Ca^{2+} transients associated with intercellular signalling dynamics. The original experiments in *Dictyostelium* showed that expression of YC-Nano 15 was optimal for detecting Ca^{2+} release in aggregation

(Horikawa et al., 2010). They demonstrated that Ca^{2+} signalling shows a spiral pattern similar to cAMP production during multicellular aggregation and that it is possible to detect these low intracellular Ca^{2+} rises *in vivo*. The main advantage of YC-Nano is that it combines both advantages of ratiometric fluorescent indicators, such as fura-2, and GECIs, so it is used as a non-perturbing indicator. Its expression is driven by a promoter active in all developmental stages. Moreover, YC-Nano is a fluorescent protein that can be excited by external light, therefore the light emission is much brighter than that of luminescence. Ratiometric indicators can be calibrated very precisely and minimise the most common artefacts associated with chemical Ca^{2+} indicators including uneven dye loading, leakage, photobleaching and changes in cell volume (Paredes *et al.*, 2008), which is useful for determine the basal level of $[Ca^{2+}]c$ and subtle Ca^{2+} responses.

In this chapter, I have established an *in vivo* real-time Ca^{2+} imaging system with YC-Nano 15 (K_d = 15 nM). I show that YC-Nano15 is a useful Ca^{2+} indictor that can be used in single vegetative cells or developed aggregates. My data sheds some light on functional roles of TPC2 channels and other channels in *Dictyostelium*.

5.2. Aims

The aim of this chapter is to determine the functional roles of Ca^{2+} channels in *Dictyostelium* in regulating cytosolic Ca^{2+} levels in early development. I aimed to express the ultra-sensitive Ca^{2+} indicator, YC-Nano15 in Ax2 cells and cells lacking Ca^{2+} channels in order to establish an in *vivo* cytosolic $[Ca^{2+}]c$ detection system. I then characterised the $[Ca^{2+}]c$ responses in aggregates and single cells.

5.3. Results

5.3.1. The sensitive genetically encoded Ca^{2+} indicator, YC-Nano 15, is useful for detecting dynamics of cytosolic Ca^{2+} in live *Dictyostelium* cells.

A sensitive intracellular Ca^{2+} indicator allows the detection of changes in cytosolic Ca^{2+} levels, $[Ca^{2+}]c$, in live cells. Among the sensitive Ca^{2+} indicators, YC-Nano 15, which is a ratiometric GECI, has been shown to be useful to detect spontaneous changes of cytosolic Ca^{2+} during the early stages of development in *Dictyostelium* (Horikawa *et al.*, 2010). A great advantage of using GECIs is that the cells can be monitored in multicellular structures, throughout development. Moreover, the advantages of ratiometric indicators over single wavelength probes is that the ratio signal is independent of the indicator concentration, illumination intensity, and optical path length allowing the $[Ca^{2+}]c$ to be determined independently of these (Paredes *et al.*, 2008). A plasmid to drive expression of YC Nano15 was introduced in to Ax2 cells. It is important to test if the YC-Nano 15 protein responds to Ca^{2+} correctly. A protocol was used for monitoring the maximum and minimum Ca^{2+} response in *Dictyostelium* (Lima *et al.*, 2012). The cells were treated with ionomycin, a Ca^{2+} ionophore, in the presence of either 20 mM $CaCl_2$ or EGTA for 15 min, following the protocol published by Lima *et al.*, to confirm that the YC-Nano 15 responds specifically to a change of Ca^{2+} levels. The $[Ca^{2+}]c$ is detected by FRET which can be observed as the ratio of YFP/CFP emission. During incubation with ionomycin and EGTA, the ratio reduced and remained low for the duration of the experiment (15 min) (Figure 5.1 and Movie 5.1). In the presence of high Ca^{2+}, the ratio increased and peaked within 7.5 minutes,

remaining high for the duration of the incubation. These data suggest that the YC-Nano15 ratio of emissions is responding to changes of intracellular Ca^{2+} as expected. This validates that YC-Nano 15 is a useful tool to determine the basal level of $[Ca^{2+}]c$.

5.3.2. Basal cytosolic Ca^{2+} level in cells strains lacking Ca^{2+} channels.

In order to characterise any role of putative Ca^{2+} channels in regulating cytosolic Ca^{2+} levels, $[Ca^{2+}]c$, Ax2, *tpc2*-null, *mcln*-null, *iplA*-null and *tpc2-mcln-iplA*-null triple mutant cells were transfected with a plasmid to drive expression of YC-Nano 15.

To ensure that all the strains expressed YC-Nano 15 correctly and at a similar level, Western blotting of whole cell lysates using an anti-GFP monoclonal antibody antibody was conducted. Ax2 and all mutants expressed YC-Nano 15 protein at the expected size (73.5 kDa) and at similar levels (Figure 5.2B). MCCC1, detected by Alexa 680-conjugated streptavidin, was used as a loading control (Davidson *et al.*, 2013). For the remainder of this chapter I used pools of cells expressing YC-Nano 15, but they are referred to as Ax2, *iplA*$^{-}$, *tpc2*$^{-}$ and *mcln*$^{-}$ for convenience. To determine if these channels play a role in regulating basal cytosolic Ca^{2+} levels in growing cells, vegetative cells (T0) were incubated in low Ca^{2+} (HKC-LoCa) buffer for 15mins (Figure 5.2 and 5.3). All cell lines contained cells with a range of $[Ca^{2+}]c$ levels. The average YFP/CFP ratio for the basal $[Ca^{2+}]c$ levels in Ax2 cells is 2.03 ± 0.38. Interestingly, *iplA*-null, *tpc2*-null and *tpc2-mcln-iplA*-null cells have significantly lower average $[Ca^{2+}]c$ levels based on their mean YFP/CFP ratios, which were 1.87 ± 0.38 in *tpc2*-null, 1.86 ± 0.30 in *iplA*-null and 1.68 ± 0.30 in *tpc2-mcln-iplA*-null cells (mean ± SD, $p<0.0001$). It is noteworthy that *mcln*-null cells not only have slightly higher mean

ratio (2.09 ± 0.50) compared to Ax2 cells (2.03 ± 0.38) but also have a higher proportion of cells in both higher and lower ratio regions (Figure 5.3A and B) compared to other cell lines. All groups showed skewed peaks of distribution (Figure 5.3B) compared to the mean ratio of Ax2 (black dashed line) and the lowest mean ratio of *tpc2-mcln-iplA*-null cells (grey dashed line). The *tpc2-mcln-iplA*-null cells showed a pronounced positive-skew distribution and the *mcln*-null cells showed an unusual distribution indicating that the distributions in these groups may not be normal (Figure 5.3A and B). Therefore, a more appropriate statistics test, the Wilcoxon rank-sum test, analysed using the R statistical package (R Core Team, 2015, http://www.R-project.org/), which does not require the assumption of normal distributions like the Student's *t*- test, was conducted to confirm the significance of the differences although the *t*-test also showed similar results (not shown).

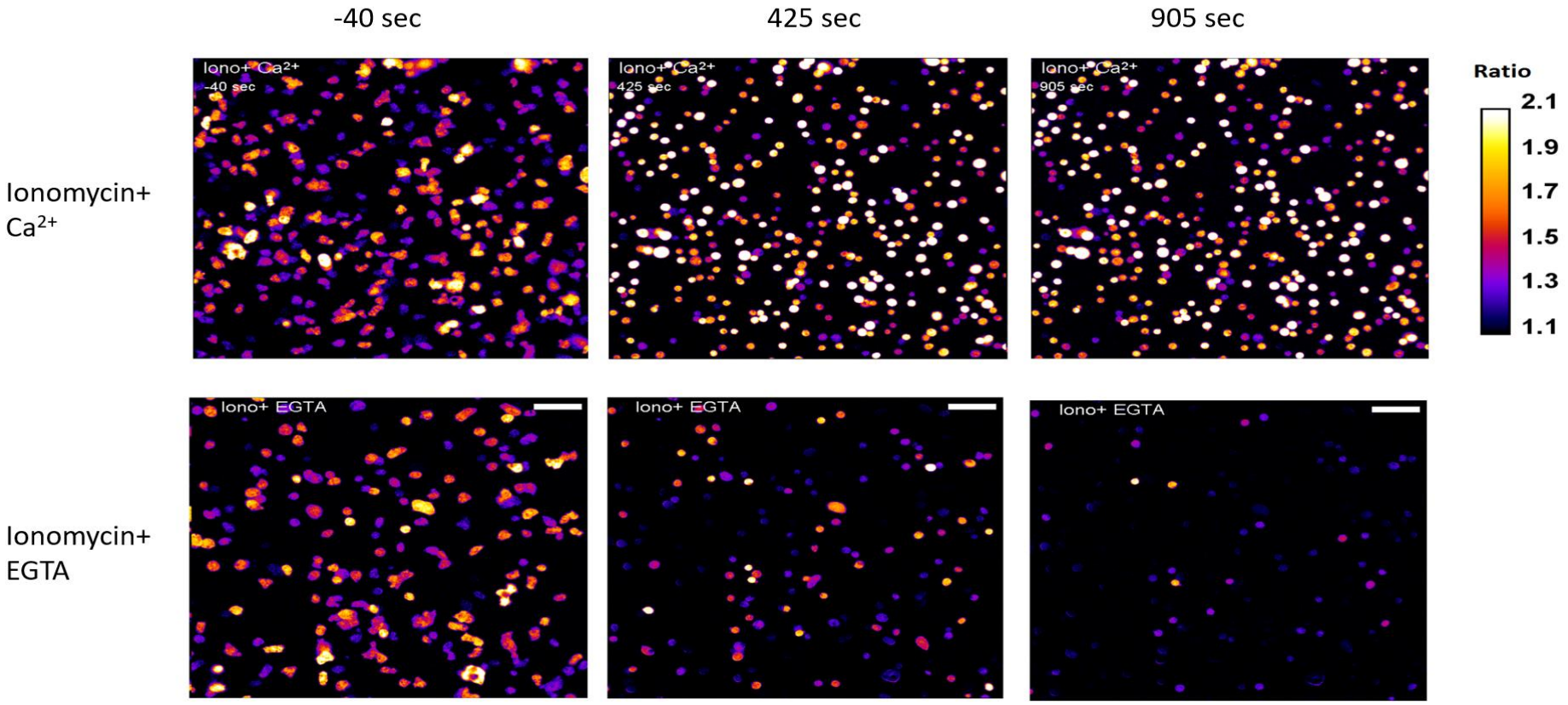

Figure 5.1 and Movie 5.1 The Ca^{2+} indicator, YC-Nano 15, responds to changes in Ca^{2+} in *Dictyostelium* Ax2 cells.
A representative Ca^{2+} imaging experiment shows Ax2 cells expressing the sensitive Ca^{2+} indicator, YC-Nano 15. Vegetative cells (T0) were washed twice with HKC-LoCa buffer and allowed to settle for 15 min. The $[Ca^{2+}]c$ level in response to 20 mM ionomycin and 20 mM Ca^{2+} or 20 mM EGTA, which was added at time zero, was visualised as the YFP/CFP ratio imaged through a widefield fluorescence inverted microscope (DeltaVision Elite) at wavelength (438 nm) excitation capturing emission simultaneously at 548 nm (YFP) and 475 nm(CFP). Scale bar, 50 μm. 425 seconds after adding Ca^{2+} with ionomycin the ratio reached the maximum whereas in the presence of EGTA the lower ratio continues until at least 905 seconds.

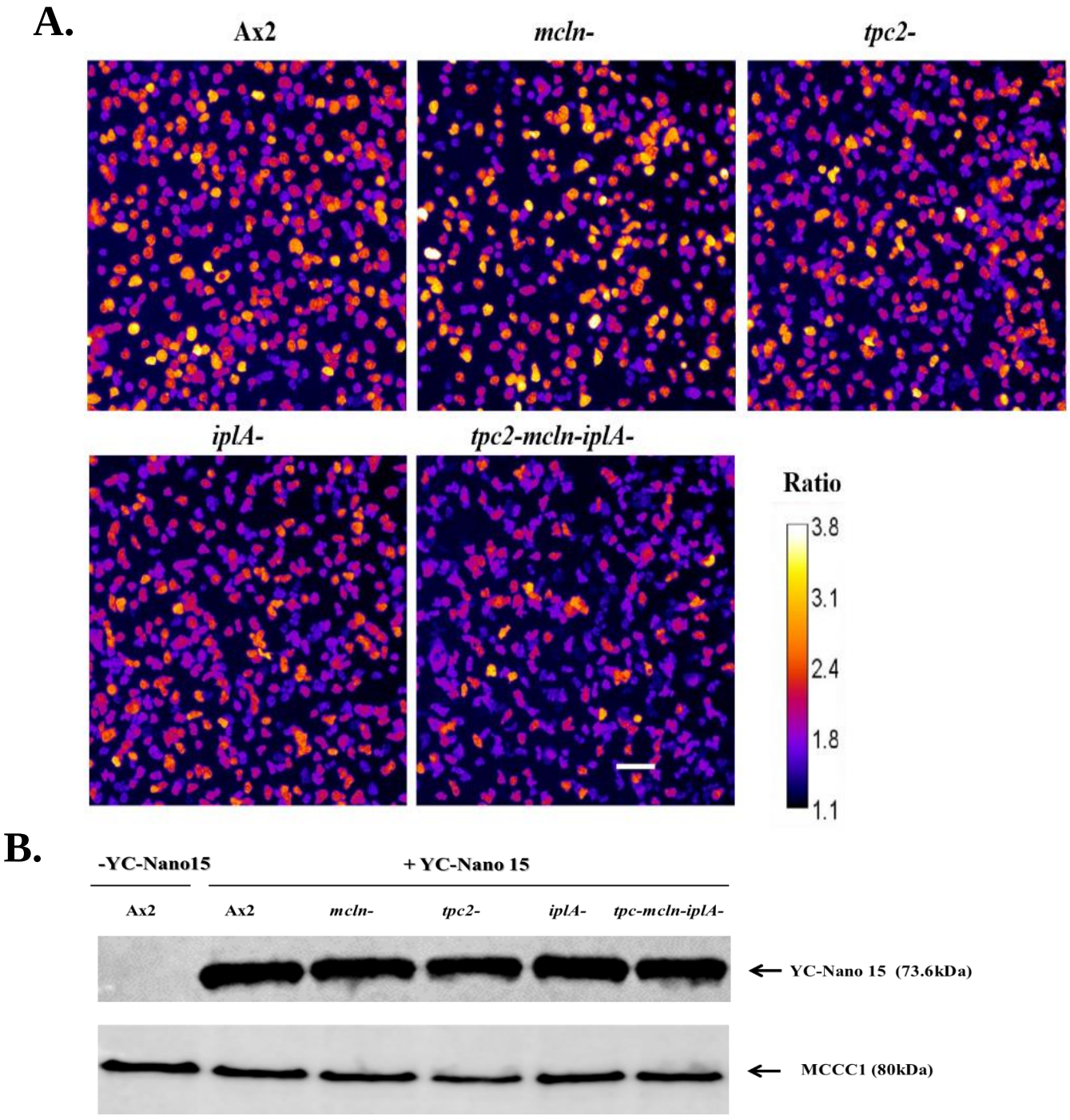

Figure 5.2 Difference in resting cytosolic Ca^{2+} levels in Ax2 cells and mutants lacking intracellular Ca^{2+} channels visualised using the sensitive Ca^{2+} indicator, YC-Nano 15.
(A) A representative Ca^{2+} imaging experiment shows Ax2 (parental strain) and cells lacking specific Ca^{2+} channels, *mcln*$^{-}$ (clone MCLN47), *tpc2*$^{-}$ (clone TPC22B20), *iplA*$^{-}$ cells (clone IPLA1-2D) and *tpc2*$^{-}$*mcln*$^{-}$ *iplA*$^{-}$ (clone TMI67B), expressing the sensitive Ca^{2+} indicator, YC-Nano 15. Vegetative cells (T0) were washed twice with HKC-LoCa buffer and allowed to settle for 15 min. The $[Ca^{2+}]c$ level was visualised as the YFP/CFP ratio imaged through a widefield fluorescence inverted microscope (DeltaVision Elite) at wavelength (438 nm) excitation capturing emission simultaneously at 548 nm (YFP) and 475 nm (CFP). Scale bar, 50 μm. (B) Whole cell lysates of the strains shown were resolved by SDS PAGE and expression of YC-Nano 15 (73.6 kDa) determined by western blot using anti-GFP antibody. MCCC1 (80 kDa) was used as a loading control.

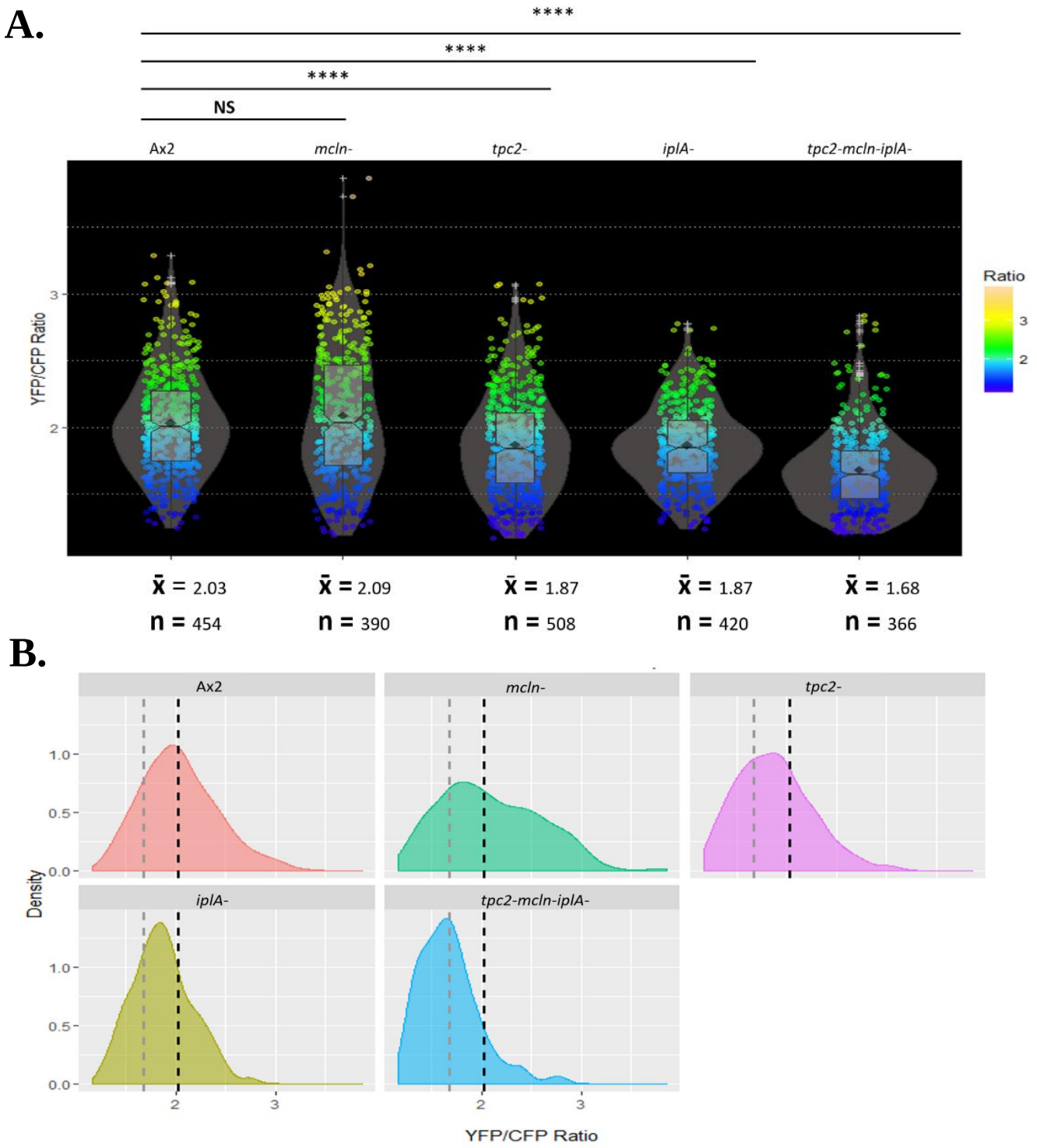

Figure 5.3 Analysis of the population distribution of basal [Ca^{2+}]c level in parental Ax2 vegetative cells and mutants lacking intracellular Ca^{2+} channels.

A. The dot plots illustrate the YFP/CFP ratios as described in Figure 5.1 representing the [Ca^{2+}]c in single cells. The violin plots overlaid with notched box-and-whisker plots illustrate the distribution and significance between each strain. The outliers, were also calculated, are shown as cross markers. The mean values were illustrated as diamonds. B. The density plot is shown to compare the highest density of ratios in each strain. The mean values of Ax2 are shown as black dashed lines and the mean values of triple mutant, *tpc2*$^{-}$*mcln*$^{-}$*iplA*$^{-}$ as grey dashed lines. The significance of the differences were analysed using the Wilcoxon rank-sum test, in which the [Ca^{2+}]c of *mcln*$^{-}$ does not significantly differ from wild type cells. *tpc2*$^{-}$, *iplA*$^{-}$ and *tpc2*$^{-}$*mcln*$^{-}$*iplA*$^{-}$ cells have significantly lower average [Ca^{2+}]c than that in Ax2 cells (NS= non-significant, ****P <0.0001).

5.3.3. Characterising spontaneous intercellular Ca^{2+} waves by using YC-Nano 15.

Previous studies have reported that spiral-shaped intercellular Ca^{2+} waves in early *Dictyostelium* development can be visualized successfully using YC-Nano15 (Horikawa *et al.*, 2010). In order to determine if we could visualise Ca^{2+} signalling in aggregates, Ax2 cells were developed under MM-HiCa buffer (5 mM MES, 5 mM $MgCl_2$, 5 mM $CaCl_2$, pH 6.5) as in Horikawa's paper at a density of 4 x 10^5 cells/cm^2 for 8 hr. The spontaneous intercellular signalling waves were visualised as the YFP/CFP ratio was imaged every 15 seconds (Figure 5.4 and Movie 5.2). Figure 5.4C shows a time course of the FRET signal change in the white box shown in Figure 5.4B. The mean period of wave is 4.75 ± 0.35 min (mean ± SD, n= 3 waves). The mean wave speed is 1.05 ± 0.19μm/sec (mean ± SD, n= 5 waves).

5.3.4. Intercellular Ca^{2+} waves are dependent on extracellular Ca^{2+}.

In order to determine if external Ca^{2+} is required for Ca^{2+} waves in aggregates, the cells harbouring YC-Nano 15 were developed under MM-HiCa with or without the presence of Ca^{2+} for 12 hours. Figure 5.5 and Movie 5.3 show that cells were able to successfully form aggregates with or without the addition of extra Ca^{2+} in the development buffer. However, without added Ca^{2+} in the buffer, the $[Ca^{2+}]c$ of cells in aggregates was much less than those developed in the presence of $CaCl_2$, which suggested a depletion of intracellular $[Ca^{2+}]c$ during development. More importantly, Ca^{2+} waves were not detectable under this condition, which indicated that detectable intercellular Ca^{2+} waves are dependent on external Ca^{2+} added in the buffer but the Ca^{2+} waves might not be essential for aggregation.

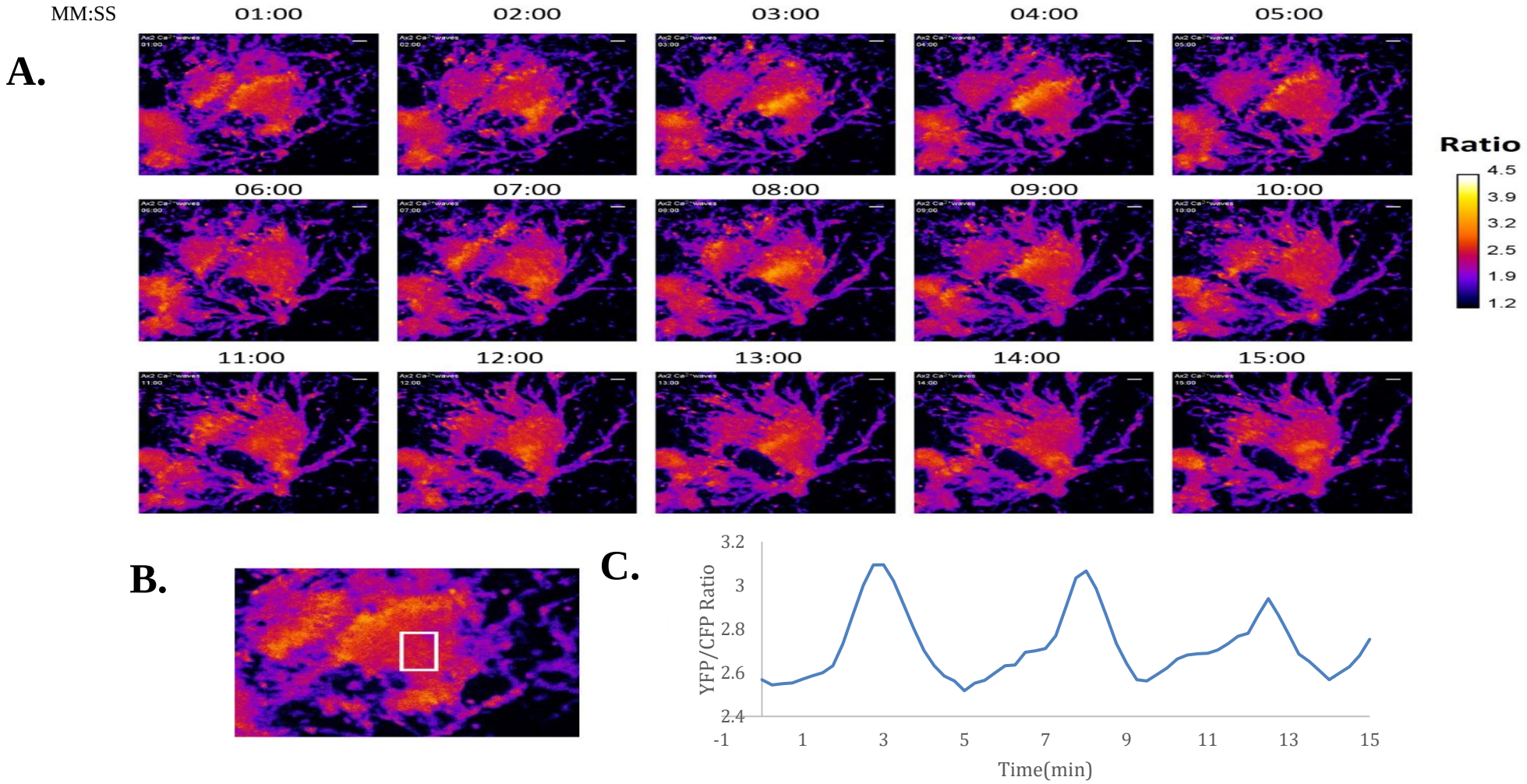

Figure 5.4 and Movie 5.2 Spontaneous Ca^{2+} waves in aggregates visualised by YC-Nano 15.
(A) A representative Ca^{2+} imaging experiment shows Ax2 (parental strain) expressing the sensitive Ca^{2+} indicator, YC-Nano 15. Cells washed twice with MM-HiCa buffer and allowed to develop at a density of 4 x 10^5 cells/cm^2 for 8 hr. The spontaneous intercellular signalling waves were visualised as the YFP/CFP ratio imaged through a widefield fluorescence inverted microscope (DeltaVision Elite) at wavelength (438 nm) excitation capturing emission simultaneously at 548 nm (YFP) and 475 nm (CFP). Scale bar, 50 µm. (B and C) C shows time course of the FRET signal change in the white box in B.

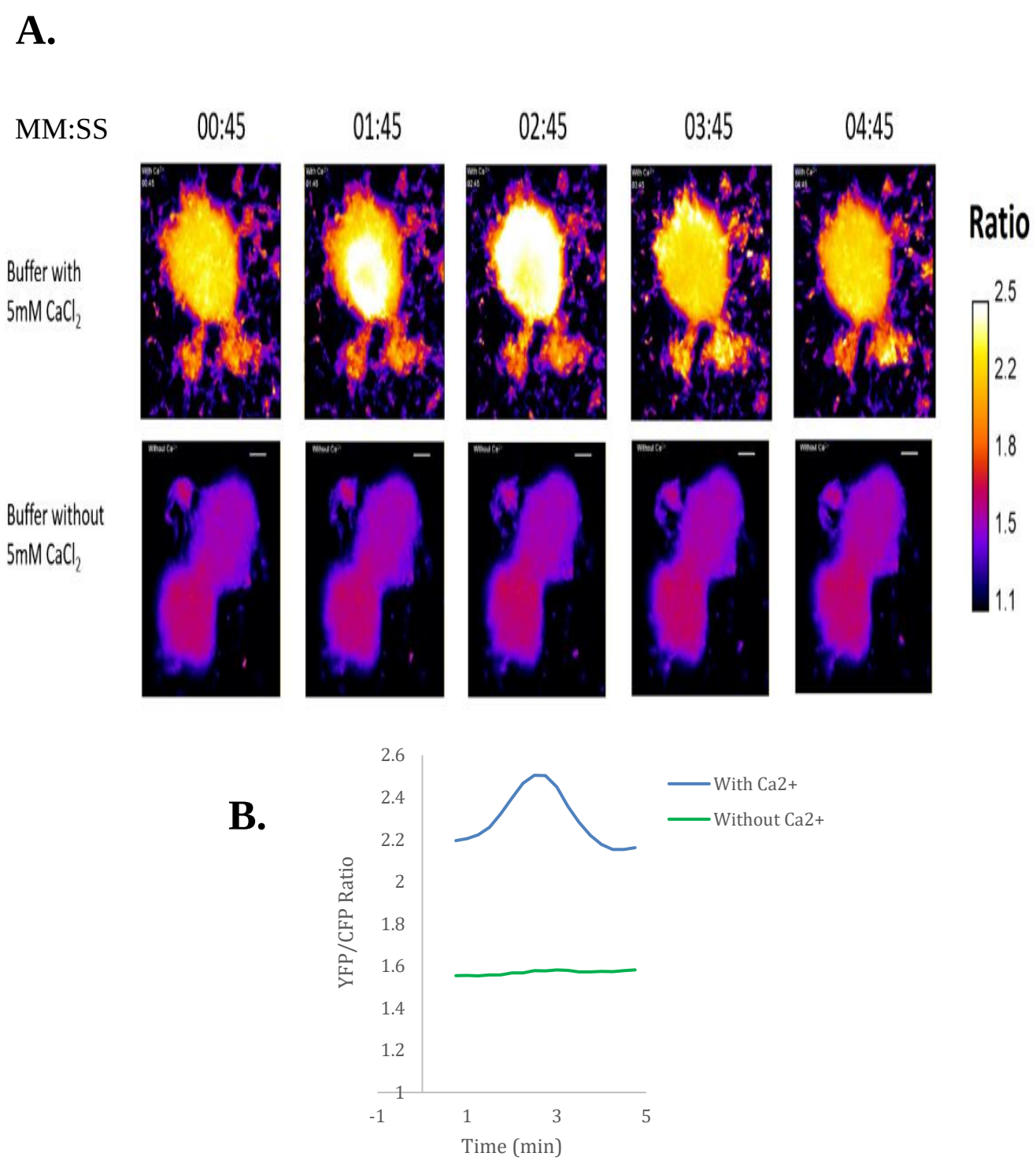

Figure 5.5 and Movie 5.3 Ca^{2+} waves in aggregates are dependent on the presence of extracellular Ca^{2+}.

(A) A representative Ca^{2+} imaging experiment for Ax2 cells expressing the sensitive Ca^{2+} indicator, YC-Nano 15. Cells were washed twice with MM-HiCa buffer and allowed to develop at a density of 4 x 10^5 cells/cm^2 for 12 hr with or without the presence of added 5 mM Ca^{2+} in the buffer. The spontaneous intercellular signalling waves were visualised as the YFP/CFP ratio imaged through a widefield fluorescence inverted microscope (DeltaVision Elite) at wavelength (438 nm) excitation capturing emission simultaneously at 548 nm (YFP) and 475 nm (CFP). Scale bar, 50 µm. (B) Time course of the FRET signal change in the average values acquired from whole aggregate areas shown in A.

5.3.5. The role of Ca^{2+} channels in intercellular Ca^{2+} waves during aggregation.

In order to determine if there are any roles for TPC2, mucolipin and IplA in the $[Ca^{2+}]c$ waves in aggregates Ax2 and *tpc2*$^{-}$, *mcln*$^{-}$ and *iplA*$^{-}$ cells expressing YC-Nano 15 were allowed to develop under MM-HiCa buffer for 10hr. Ca^{2+} waves are detectable in the Ax2, *mcln*$^{-}$ and *tpc2*$^{-}$ cells, however, interestingly, the waves were greatly reduced in *iplA*-null cells (Figure 5.6 A, C and E). The *tpc2*$^{-}$ cells show delayed development and might be at a different developmental stage (see Chapter 3) so they were also observed at the 16th hour of development (Figure 5.6 B) with similar results.

Figure 5. 6 C shows a typical time course of the FRET signal change from Ax2 in 10hr developed aggregates as shown by white boxes in Figure 5.6 D (mean amplitude 0.30 ± 0.09, n= 3). All aggregates lacking channels showed some differences in wave properties. The most striking was in the aggregates lacking IplA where increases in $[Ca^{2+}]c$ were barely detectable.

Figure 5.6 E shows the maximum amplitude in *iplA*$^{-}$ aggregates (mean amplitude 0.03 ± 0.01, n = 3) and *tpc2*$^{-}$ aggregates (mean amplitude 0.13 ± 0.03, n= 3) were both significantly reduced compared to Ax2 aggregates (waves) whereas *mcln*$^{-}$ aggregates (mean amplitude 0.45 ± 0.04, n = 3) showed a somewhat larger amplitude compared to Ax2. The period of waves for *tpc2*$^{-}$ aggregates, either developed for 10hr (loose aggregates, mean period length of wave 9.67 ± 2.02 min, n = 4) or 16hr (tight aggregates, period length of wave 11.5 min, n = 2), were both significantly longer than Ax2 (mean period length of wave 3.67 ± 0.88 min, n= 4) and *mcln*$^{-}$ aggregates (mean period length of wave 4.33 ± 0.88 min, n= 4). The period time of waves of *iplA*$^{-}$

aggregates (mean period length of wave 7.50 ± 3.53 min, n= 4) was also longer than Ax2 but it is not significant (P= 0.1) due to larger differences between waves. There is no significant difference in the velocity of wave propagation between parental Ax2 (1.24 ± 0.37 μm/sec, n=3) and mutants (*mcln*$^{-}$ =1.16 ± 0.25 μm/sec, n= 5; *tpc2*$^{-}$ = 0.89 ± 0.19 μm/sec, n= 3; *iplA*$^{-}$ = 0.93 ± 0.06 μm/sec, n= 3) although the *tpc2*$^{-}$ waves were the slowest (mean ± SD).

To conclude, the results suggest that TPC2 and IplA play roles in intercellular Ca^{2+} wave generation, directly or indirectly. In particular ablation of *iplA* reduced greatly the amplitude of Ca^{2+} waves and loss of TPC2 caused lower frequencies of Ca^{2+} waves. The *mcln*$^{-}$ aggregates also have slightly altered behaviour but show a reduced influence for the production of intercellular Ca^{2+} waves.

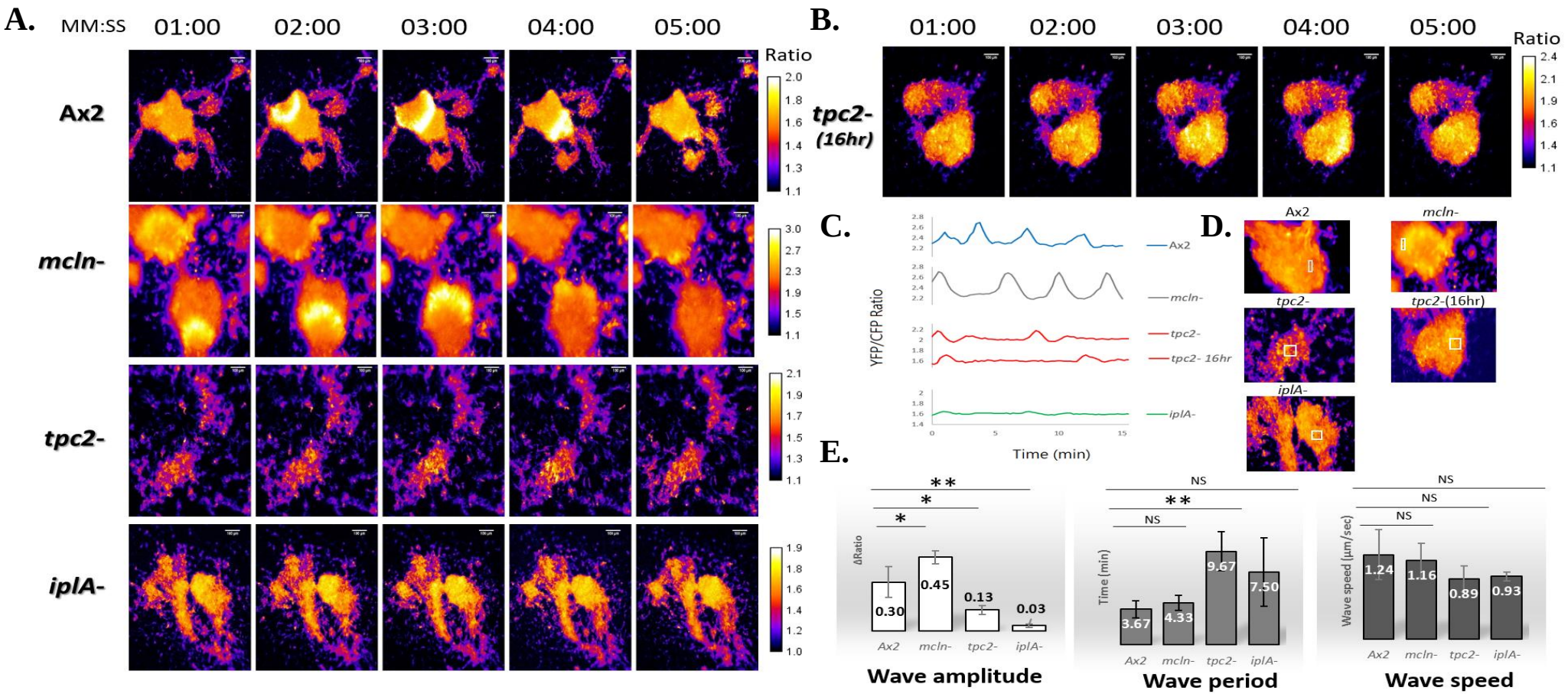

Figure 5.6 and Movie 5.4.1 to 5.4.4 Spontaneous Ca^{2+} waves in Ax2, *tpc2*$^-$, *mcln*$^-$ and *iplA*$^-$ cells.

(A.) A representative Ca^{2+}imaging experiment for Ax2 (parental strain. See movie 5.4.1), *mcln*$^-$ (clone MCLN47. See movie 5.4.2), *tpc2*$^-$ (clone TPC22B20. See movie 5.4.3.1 and movie 5.4.3.2), *iplA*$^-$ (clone IPLA1-2D. See movie 5.4.4) expressing the sensitive Ca^{2+} indicator, YC-Nano15. Cells were washed twice with MM-HiCa buffer and allowed to develop for 10 hr. The spontaneous intercellular signalling waves were visualised as the YFP/CFP ratio imaged through a widefield fluorescence inverted microscope (DeltaVision Elite) at wavelength (438 nm) excitation capturing emission simultaneously at 548 nm (YFP) and 475 nm(CFP). Scale bar, 100 μm. Figure B and movie 5.4.3.2 show aggregates of *tpc2*$^-$ cells as shown in A but allowed to develop for another 6 hr (total 16 hr). Figure C shows a typical time course of the FRET signal change from Ax2 and mutants in the 10 hr developed aggregates as shown white boxes in Figure D. Figure E shows quantification of the amplitude and period from four spontaneous Ca^{2+} waves as in C. The amplitudes of waves (Δratio) for *tpc2*$^-$ and *iplA*$^-$ cells were reduced compare to Ax2 and *mcln*$^-$ cells. The period time (minutes) of waves for *tpc2*$^-$ were significantly longer than Ax2 and *mcln*$^-$ cells. The difference of wave speed between Ax2 and mutants were not significant. (Student *t*-test, NS= non-significant, *P <0.05, **P <0.01).

5.3.6. The cAMP-induced Ca^{2+} response was not detectable in aggregates of *iplA*$^{-}$ cells.

Extracellular cAMP plays a key role in the process of aggregation and it is known that there is periodic release of cAMP to generate waves during aggregation. In order to determine if the cAMP signalling pathway is affected in the *iplA*$^{-}$ cells, it is necessary to determine if there is any difference in the cAMP-induced Ca^{2+} response. There is an increase in intracellular Ca^{2+} in response to cAMP in aggregation competent *Dictyostelium* cells (Saran *et al.*, 1994). Therefore to determine if YC-Nano15 expression could detect these changes, cells harbouring YC-Nano 15 were developed in shaking suspension of HKC-LoCa buffer for 2 hours and pulsed with 50 nM cAMP for another 4 hours. Then the aggregation competent cells were allowed to form aggregates that were treated with 10 μM cAMP to determine the maximum Ca^{2+} response caused by cAMP. In Ax2 aggregates, the exogenous cAMP caused a rapid spike in $[Ca^{2+}]c$. However no detectable cAMP-induced Ca^{2+} response was observed in the *iplA*$^{-}$ aggregates. ATP is also known to cause increased cytosolic Ca^{2+} in *Dictyostelium* cells so this was used as a positive control. The ATP-induced Ca^{2+} response was similar in *iplA*$^{-}$ and Ax2 aggregates (Figure 5.7A and B).

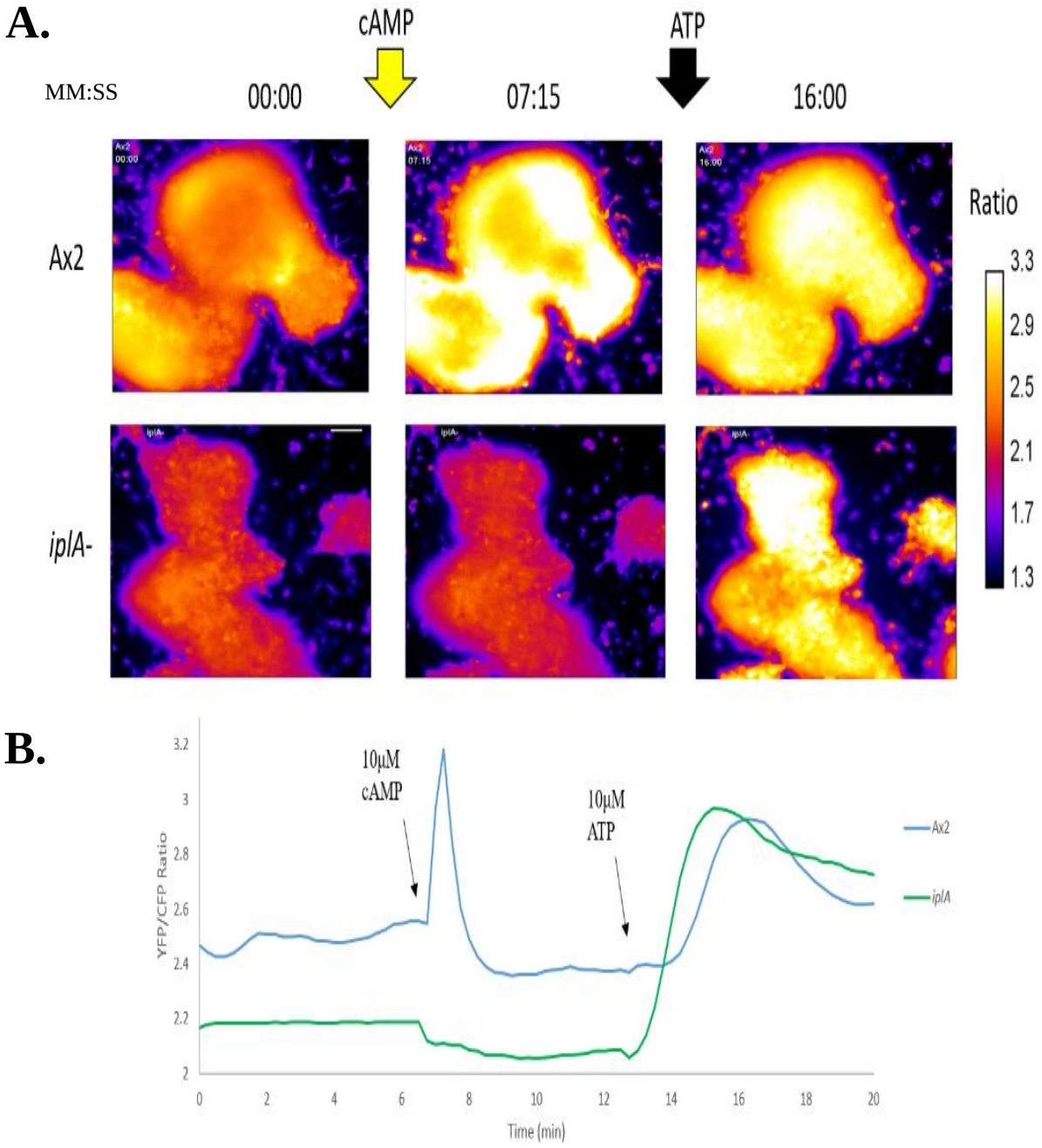

Figure 5.7 and Movie 5.5 cAMP-induced Ca^{2+} response is greatly reduced in *iplA*$^{-}$ aggregates.

(A) A representative Ca^{2+} imaging experiment shows Ax2 and *iplA*$^{-}$ cells (parental strain) expressing the sensitive Ca^{2+} indicator, YC-Nano 15. Cells were washed twice with HKC-LoCa buffer and 7 x 10^{7} cells shaken in 5 ml HLC-LoCa buffer for 2 hr then pulsed with cAMP (50 nM every 6 mins) for 4 hr, incubated at 22 °C. The developed cells were allowed to form aggregates for 15 min. The cytosolic Ca^{2+} was visualised as the YFP/CFP ratio imaged through a widefield fluorescence inverted microscope (DeltaVision Elite) at wavelength (438 nm) excitation capturing emission simultaneously at 548 nm (YFP) and 475 nm (CFP). Scale bar, 50 µm. Figure B shows a typical time course of the FRET signal change in the average values acquired from whole aggregate areas shown in A. One experiment representative of three.

5.3.7. The cAMP-induced Ca^{2+} response of *tpc2*$^{-}$ aggregates was similar to that of Ax2 aggregates but absent in caffeine treated cells.

Similar experiments were also conducted with *tpc2*$^{-}$ cells as described in section 5.3.6. The cAMP-induced Ca^{2+} responses observed in aggregates of Ax2 and *tpc2*$^{-}$ cells were very similar (Figure 5.8A and B). When the cells were treated with caffeine, a known inhibitor of the cAMP phosphodiesterase (PDE) in some organisms (Howell, 1993) but which serves as adenylyl cyclase inhibitor in *Dictyostelium* (Alvarez-Curto *et al.*, 2007; Brenner and Thoms, 1984), the levels of cytosolic Ca^{2+} decreased in both cell types over time. After caffeine incubation the cAMP-induced Ca^{2+} response was not detectable in *tpc2*$^{-}$ aggregates although it was still detected in Ax2 aggregates (Figure 5.8C and D). This is the first time it has been reported that caffeine causes a drop of intracellular Ca^{2+} levels in aggregates and loss of TPC2 interacts with this.

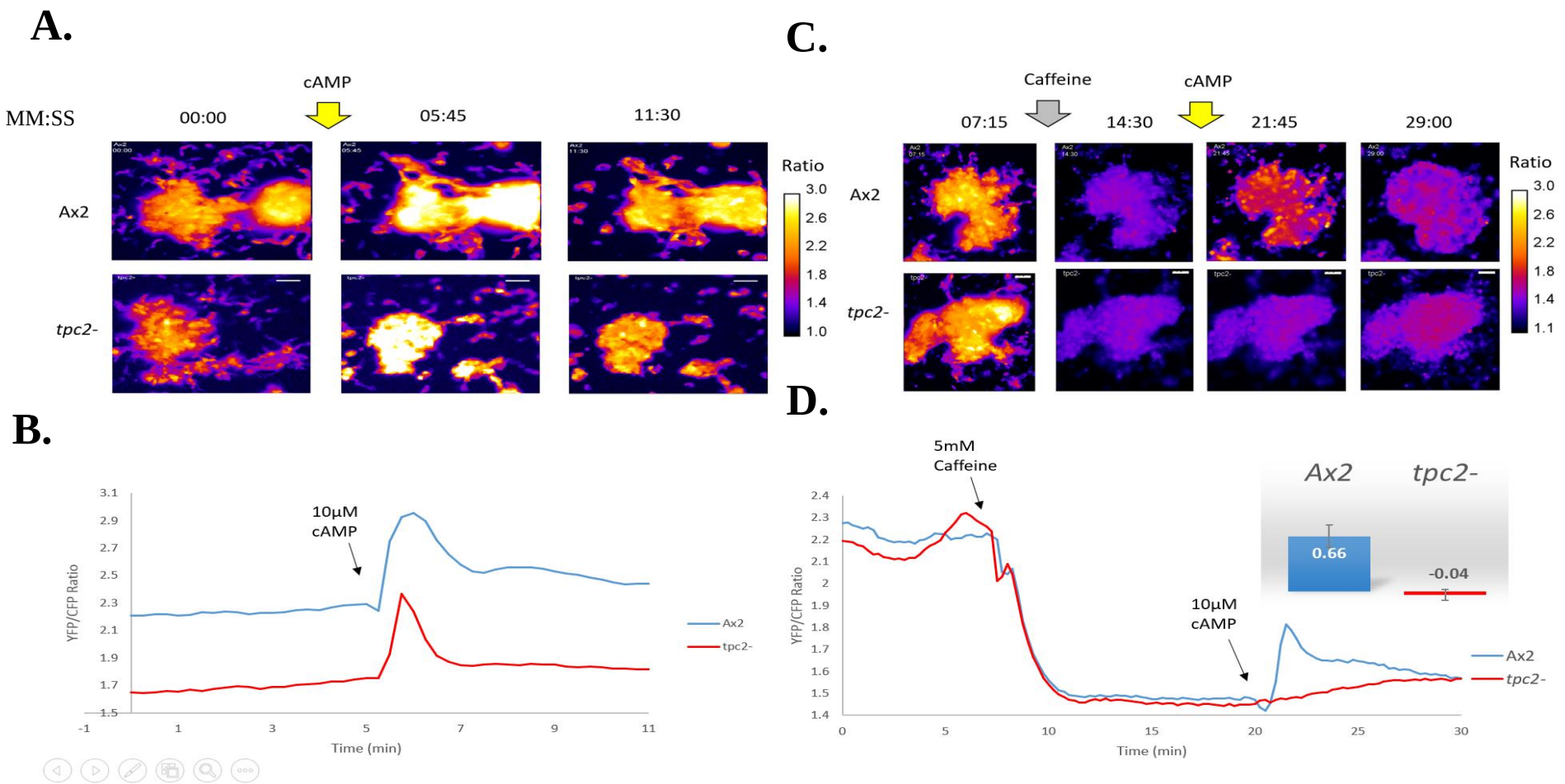

Figure 5.8 and Movie 5.6 to 5.7 Ca^{2+} response to exogenous cAMP in aggregates of *tpc2*-null cells is similar to Ax2 cells but is absent after caffeine treatment.

A. Representative Ca^{2+}imaging experiment with Ax2 (parental strain) and *tpc2*$^{-}$ cells (clone TPC22B20) expressing the sensitive Ca^{2+} indicator, YC-Nano 15. Cells were washed twice with HKC-LoCa buffer and 7 x 10^7 cells shaken in 5 ml HLC-LoCa buffer for 2 hr then pulsed with cAMP (50 nM every 6 min) for 4hr, incubated at 22 °C. The developed cells were allowed to form aggregates for 15 min. C. Developed cells were treated with 5 mM Caffeine, a known adenylyl cyclase inhibitor in *Dictyostelium*, at 7.5th min followed by stimulation of 10 µM cAMP at 20th min. B., D. Time course of the FRET signal change in the average values acquired from whole aggregate areas shown in A and C, respectively. Quantification of cAMP –induced Ca^{2+} responses from caffeine-treated aggregates from two independent experiments are shown in D. One experiment representative of two.

5.3.8. The cAMP-induced increase in cytosolic Ca^{2+} of single *tpc2*$^{-}$ cells is reduced and delayed compared to Ax2.

So far from previous sections in this chapter, I have shown that IplA and TPC2 seem to play a role in Ca^{2+} waves in aggregates and the response to exogenous cAMP is also affected in *iplA*$^{-}$ aggregates. In order to determine if there is any difference in cAMP-induced changes in cytosolic Ca^{2+} between *tpc2*$^{-}$ and Ax2 cells, it was decided to conduct experiments on single cells to exclude the possibility of minor differences that might be not visible in aggregates.

Cells were developed in shaking suspension with exogenous cAMP pulses added from T2, to overcome the developmental delay seen in *tpc2*$^{-}$ cells. After 6 hours (T6) cells were then allowed to settle and 50 nM cAMP was added at time 0. A transient increase in cytosolic Ca^{2+} was detectable by ratioing YFP/CFP emission (Figure 5.9).

A change in intracellular Ca^{2+} was detected with the Ca^{2+} response reaching its peak 20 to 35 seconds after adding cAMP. Ax2 reached a mean peak of 1.82 at the 20th second whereas *tpc2*-null cells reached a mean peak of 1.66 after 35 seconds (Figure 5.10). It is interesting to note that *tpc2*-null cells not only had a lower level of Ca^{2+} increase but also had a delayed time of peak response compare to Ax2 cells (Figure 5.11 A to E).

The maximum response values (MRV) were calculated by taking the highest ratio after the addition of cAMP (from time points= 5th second to 80th second) and subtracting the mean baseline fluorescence ratio (R0), which was defined as the mean ratio before cAMP was added (time points -40, -25 and -10 seconds) for individual cells. The values

are designated as Δratio. The maximum response rate (MRR) was calculated as MRV divided by the time difference, Δsec, in milliseconds, the time of the highest observed ratio minus the time of cAMP addition. The values are designated a unit as Δratio/millisecond (Figure 5.11A to E).

By examining the MRV and MRR with violin and box-and whisker plots, not only gives overall information about the difference of the average ratios but also visualises the distribution of the maximum response and its response rate in individual cells. The results indicate that the mean MRV of *tpc2*-null cells (mean = 0.23 Δratio) was significantly lower than that in the WT cells (mean = 0.36 Δratio), $p < 0.0001$ as analysed by the Wilcoxon rank-sum test (Figure 5.11 A). The mean MRV of *tpc2*-null cells was only 63.9% of that of Ax2 cells. It is interesting to note that the density plot showed that the MRV of Ax2 cells illustrates a bimodal distribution (peaks at 0.26 and 0.45) suggesting that there may be two types or developmental stages of cells in the population, in contrast to a single major peak in the *tpc2*-null cells (peak at 0.17) (Figure 5.11C).

The difference was more pronounced by including time as a factor. The mean response rate MRR of Ax2 is 15.8 Δratio/ms, whereas the *tpc2*-null cells is 7.2 Δratio/ms (Figure 5.11B). The mean MRR of *tpc2*-null cells was only 45.6% of that of Ax2 cells illustrating that the *tpc2*-null cells have a much slower response rate than Ax2 cells, $p<0.0001$. The bimodal distribution still persist in the rate distribution of Ax2 cells, with one peak at 13, and another at 22 Δratio/ms, in contrast to a single sharp peak of 5 Δratio/ms in *tpc2*-null cells (Figure 5.11D). All the information is summarised in Figure 5.11 E.

Analysing the distribution of sub-populations of higher and lower response rate groups of cells sheds more light on the heterogeneity of cellular responses to cAMP. The maximum response time was stratified into 5 categories: 5, 20, 35, 50, 65 and 80 Δsec (Figure 5.12A). It is clear that the majority of cells fall into the categories of 20 and 35 Δsec. A low value of Δsec means it takes a shorter time to reach the maximum response. The results show the distribution of populations in Ax2 and *tpc2*-null cells is quite different. The vast majority of Ax2 cells (74.7%) have a shorter response time of 20 Δsec, whereas for the *tpc2*-null cells, there are only 22% of cells classified in this category. On the contrary, the majority of *tpc2*-null cells (70.5%) are classified in the category of 35 Δsec, whereas only 19.5% of Ax2 cells fall into this category. It is also noteworthy that a slightly higher percentage of *tpc2*-null cells (total 7.5%) fall into the categories of slower response times (50, 65 and 80 Δsec) than Ax2 (total 5.1%). These results indicate that the vast majority of Ax2 cells respond more rapidly that the majority of *tpc2*-null cells.

It is interesting to know the correlation of response rate and the mean Ca^{2+} level of the sub-populations of cells. The question is, if cells have a higher response rate would they also have higher or lower maximum response level? To do this, the two groups containing the majority of cells by their response time, the categories of 20 and 35 Δsec, were analysed (Figure 5.12 B). The mean ratio in the faster response group (20 Δsec) in Ax2 is 0.35, which is slightly lower than the mean ratio 0.38 of the slower response group (35 Δsec). However, the difference is not statistically significant ($p= 0.4206$). The results indicate there is no difference in Ca^{2+} level between faster response and slower response groups in Ax2 cells. On the other hand, it is interesting that the

difference is significant for *tpc2*-null cells, as the mean ratio in the faster response group (20 Δsec) is 0.17, which is much lower than the mean ratio of 0.25 in slower response group (35 Δsec). This difference is statistically significant (**, p= 0.001) by Wilcoxon rank-sum test. This result indicates that in *tpc2*-null cells the faster response group has smaller increases in cytosolic Ca^{2+}, and the slower response group have bigger Ca^{2+} responses (Figure 5.12 B and C).

Analysis of the density plots shows that in both the faster and slower response groups, Ax2 cells show a similar bimodal distribution (Figure 5.12 B and C) as the data was stratified before (Figure 5.11). Peaking at 0.26 and 0.45 in the faster response group (20 Δsec), and 0.26 and 0.46 in slower response group (35 Δsec). This result indicates that the Ca^{2+} response levels might not be correlated with response time in Ax2 cells. However the difference is more pronounced in *tpc2*-null cells. The density plot shows the *tpc2*-null cells have a sharper density distribution, peak at 0.17, and a minor peak at 0.36 in the faster response group. The density distribution is changed in the slower response group, as the peak is increased slightly to 0.19, and the peak shape is broader, which means more of the higher response cells are included in the slower response group. The results indicate that Ca^{2+} response level might be different in terms of response time in *tpc2*-null cells, with the cells that have a lower Ca^{2+} response tending to have faster response times and vice versa (Figure 5.12 B and C).

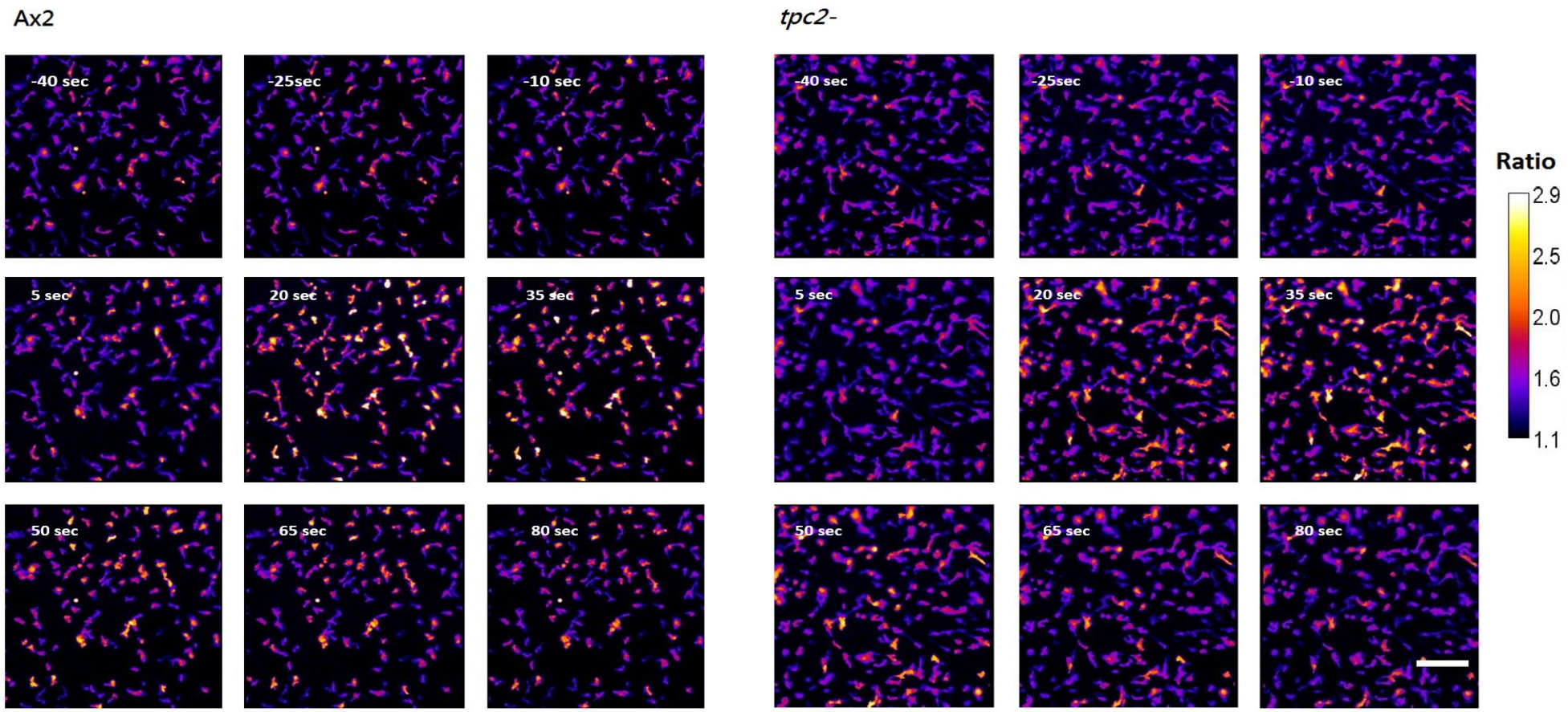

Figure 5.9 and Movie 5.8 Time-lapse photos illustrating exogenous cAMP-induced increase in cytosolic Ca^{2+} detected by YC-Nano 15 in individual Ax2 and *tpc2*-null cells.

Ax2 cells and *tpc2*$^{-}$ cells (clone TPC22B20) were developed at a density of 4 x 10^5 cells/cm^2 in HKC-LoCa buffer for 6 hours (T6) in order to generate aggregation competent cells and cells allowed to settle. The cells were stimulated with 50 nM cAMP at time zero to induce a Ca^{2+} response. The [Ca^{2+}]c level was recorded as YFP/CFP ratio images through a widefield fluorescence inverted microscope (DeltaVision Elite). Video timecode indicates the time (seconds) relative to cAMP addition. Scale bar, 50 μm.

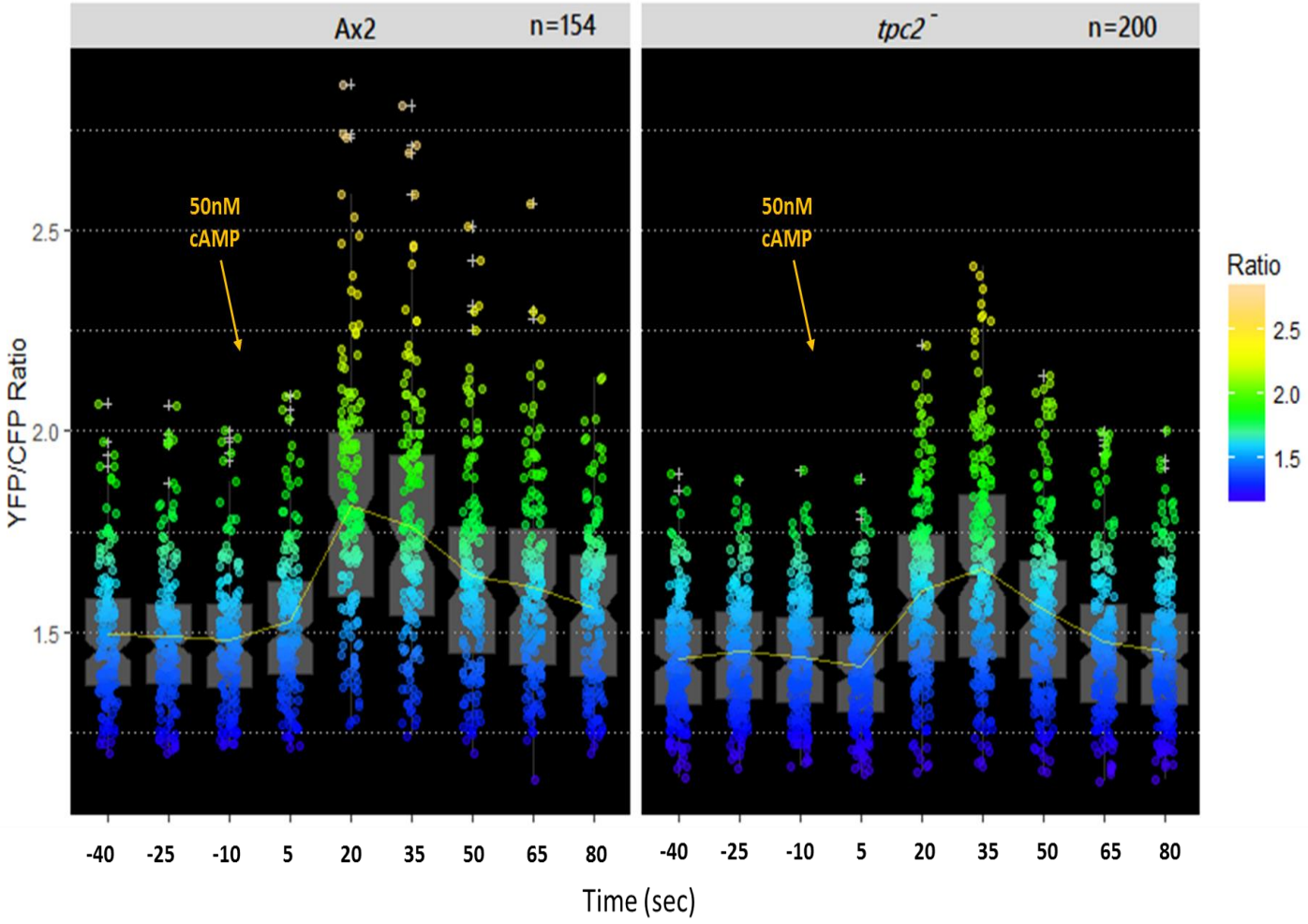

Figure 5.10 Analysis of exogenous cAMP-induced cytosolic Ca^{2+} responses in aggregation competent Ax2 and *tpc2*-null cells.

The cells described in Fig 5.9 were analysed. The dot plots illustrate a representative experiment of the YFP/CFP ratios representing the $[Ca^{2+}]c$ in single cells (A). 50 nM cAMP was added at time 0 second. The notched box-and- whisker plots illustrate the distribution and significance of difference between each time point. The outliers, were also calculated, are shown as cross markers. Cell numbers are labelled to the right side of each cell's strain name. Yellow lines indicate the mean values.

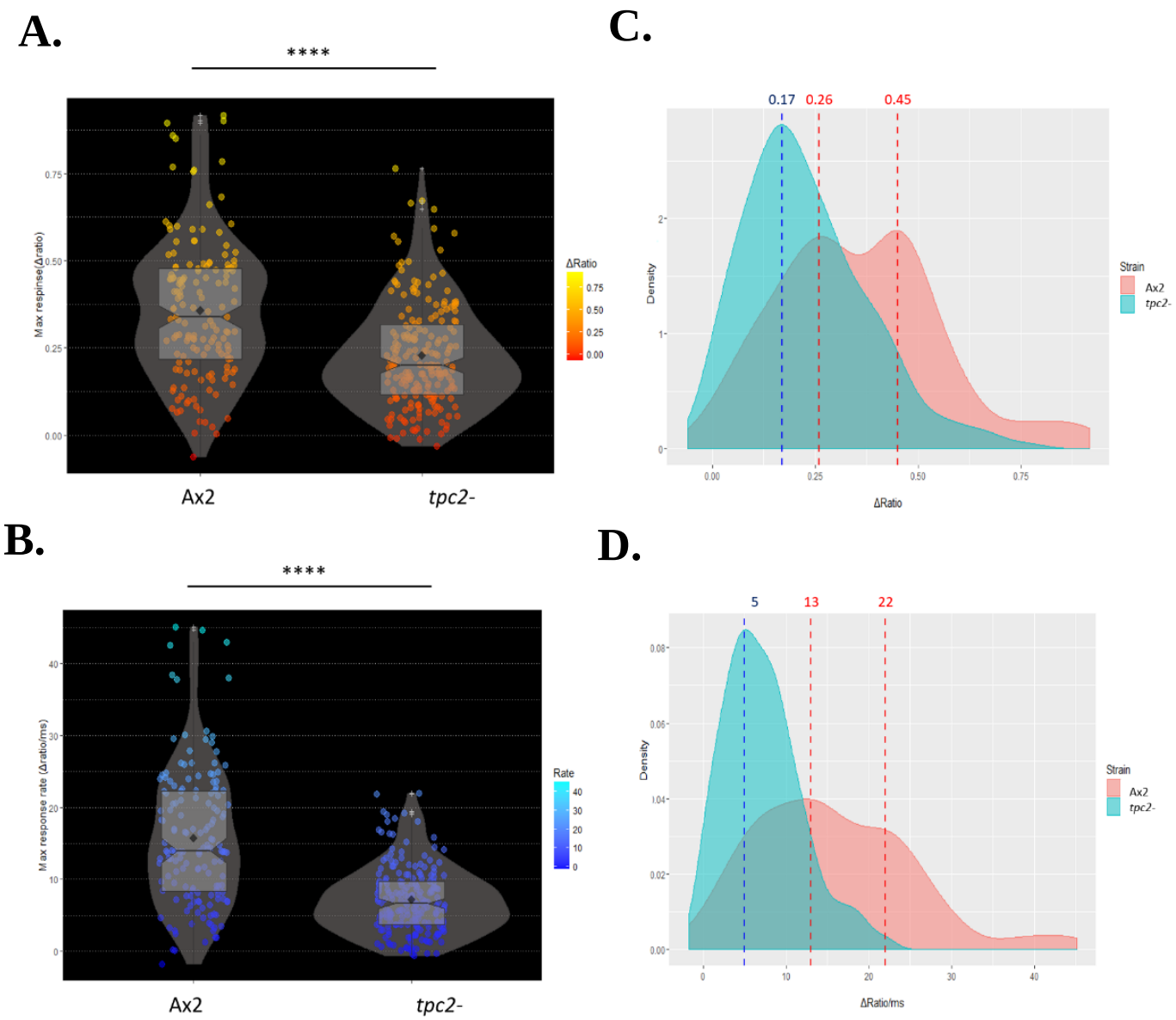

E.

	Max response values (Δratio)		Max response rate (Δratio/ms)	
	Mean	Major peaks	Mean	Major Peaks
Ax2 n=154	0.36	0.45, 0.26	15.8	22,13
tpc2- n=200	0.23	0.17	7.2	5

Fig. 5.11 Analysis of the population distributions of the maximum response and maximum response rate of exogenous cAMP-induced cytosolic Ca^{2+} increase in Ax2 and *tpc2*-null cells.

(A) For the cells shown in Fig 5.9 and 5.10, the dot plots represent the maximum response values (Δratio) and (B) shows response rate (Δratio/miliseconds) in individual cells with violin plots in conjunction with notched box-and-whisker plots. The maximum response values are the difference between the highest response ratio after adding cAMP (5^{th} sec to 80^{th} sec) and the mean ratio before adding cAMP (-40^{th} sec to -10^{th} sec). The maximum response rate is the maximum response value divided by the time taken to reach the peak. The mean values are illustrated as diamonds. The outliers, were also calculated, are shown as cross markers. The density plots (C and D) are shown to indicate the peak density areas in the Ax2 and *tpc2*-null cells. (E) Table summarises maximum response values and rate. The significance of the data was tested using the Wilcoxon rank-sum test (****P <0.0001).

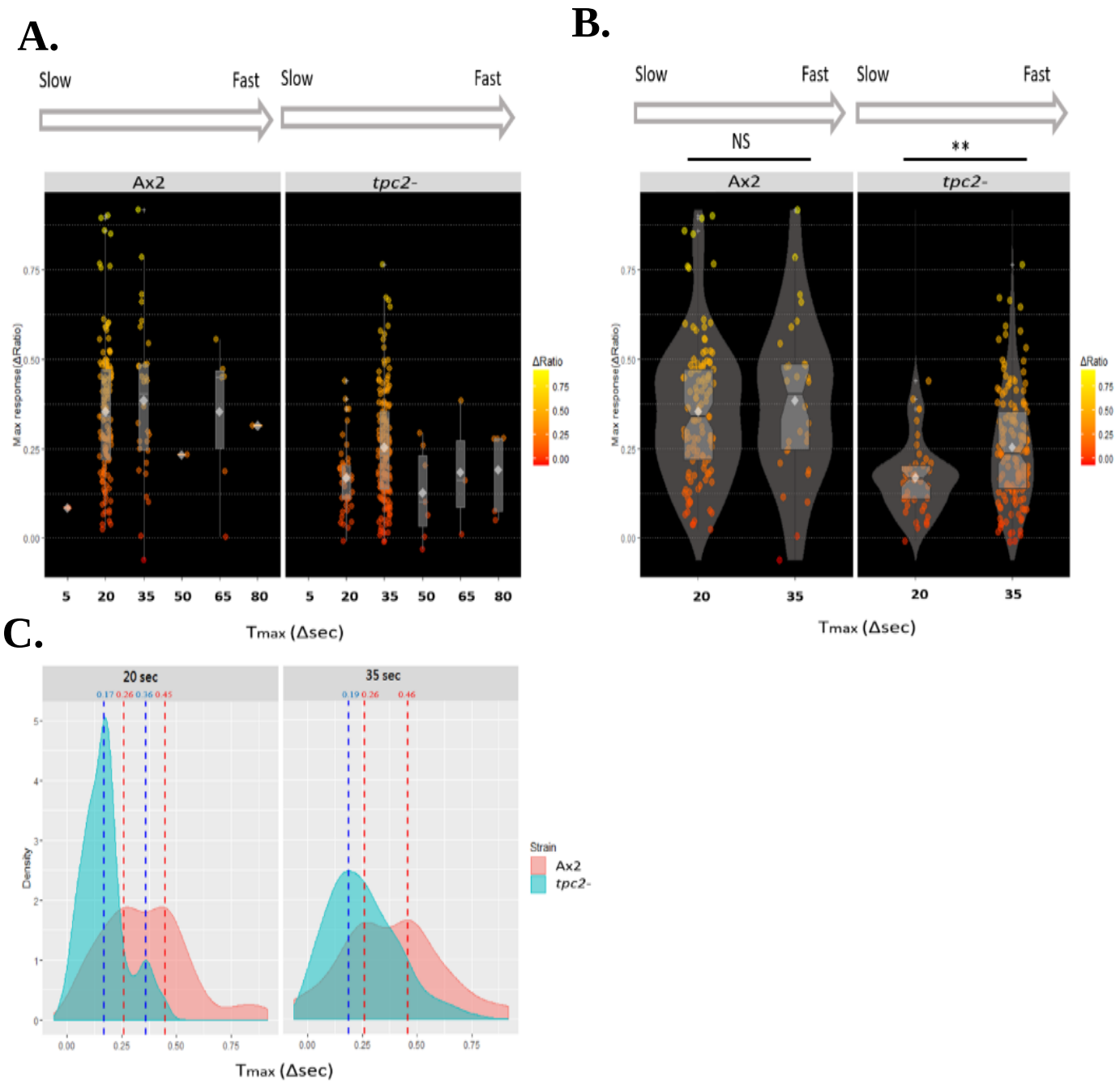

Fig. 5.12 Analysis of the population distributions of the maximum response to exogenous cAMP-induced Ca^{2+} response in Ax2 and *tpc2*- null cells stratified by response time.

For the cells shown in Figure 5.10, the dot plots show the maximum response values (Δratio) with box-and-whisker plot stratified by 5 categories of time to reach maximum response in individual cell (Tmax), which are 5, 20, 35, 50, 65 and 80 seconds (A) or the distribution of the major populations at their categories of Tmax 20 and 35 seconds (B) with violin plots in conjunction with notched box-and-whisker plots. The density plots (C) are shown to indicate the highest density areas in the WT cells and mutants at Tmax 20 and 35 seconds. The significance was analysed using the Wilcoxon rank-sum test (**, $p < 0.01$).

5.4. Discussion

The relative activity of Ca^{2+} channels and Ca^{2+}-ATPases fine tunes intracellular calcium concentrations (Berridge *et al.,* 2003). Activation of Ca^{2+} channels induces an increase in $[Ca^{2+}]c$, while Ca^{2+}-ATPases causes an influx of calcium into the intracellular Ca^{2+} stores or out of the cell and decreases $[Ca^{2+}]c$. In order to measure $[Ca^{2+}]c$ I expressed YC-Nano 15 in Ax2 cells and cells lacking Ca^{2+} channels. YC-Nano15 was expressed at a similar level in all the cell lines. In Ax2 cells the emission ratio was dependent on $[Ca^{2+}]c$ as it was reduced in cells incubated in the absence of Ca^{2+} and increased by the addition of the Ca^{2+} ionophore ionomycin in the presence of Ca^{2+} and changes could be monitored in response to extracellular cAMP, consistent with the appropriate sensitivity of YC-Nano 15.

In order to determine if TPC2, mucolipin and IplA play a role in regulating $[Ca^{2+}]c$ in *Dictyostelium*, I examined the basal level of Ca^{2+} in cells which lack these channels. Vegetative cells lacking TPC2 and/or IplA have significantly lower $[Ca^{2+}]c$ compared to parental cells. The observation that *tpc2*$^{-}$ cells have lower $[Ca^{2+}]c$ is in agreement with two studies conducted by Ambrosio *et. al*. (2015 and 2016) in which they found the cytosolic Ca^{2+} levels are significantly lower in both human megakaryocytic cells expressing a non-conducting pore mutant L265P TPC2 and *tpc2*-null derivatives of melanocytic MNT-1 cells monitored using a genetically encoded Ca^{2+} indicator GCamP6 (Ambrosio *et al.*, 2016; Ambrosio *et al.*, 2015). This information supports TPC2 playing a role in regulation of cytosolic Ca^{2+} levels.

The observation that *Dictyostelium* cells lacking IplA have significantly lower levels of $[Ca^{2+}]c$ is in agreement with Schaloske and colleagues, who reported that the basal

[Ca^{2+}]c level in *iplA*$^{-}$ amoebae was significantly lower than in wild type (an average of 36 ± 3 nM compared to 50 ± 2 nM in wild type cells) (Schaloske *et al.*, 2005). However, Traynor *et al.* observed *iplA*$^{-}$ cells had a resting [Ca^{2+}]c of 79 ± 15 nM, similar to the wild type which had 77 ± 29 nM (Traynor *et al.*, 2000). Both groups used fura-2-dextran and similar buffer conditions (5 mM Hepes, 5 mM KCl, 1 mM $CaCl_2$, pH 7.0) with developed cells. The discrepancy might be caused by the highly perturbing experimental procedures summarised in the introduction of this chapter. In the current study, we have used cells stably expressing a genetically encoded Ca^{2+} indicator to minimise potential perturbations caused by electroporation. Lower Ca^{2+} (0.25 mM) was also used in the buffer that might be closer to physiological concentration for *Dictyostelium* (David Traynor, personal communication). Moreover, vegetative cells were used in this experiment and differences in developmental stage or conditions might explain the reported discrepancies.

In contrast, the *mcln*-null cells exhibit an abnormal distribution of basal [Ca^{2+}]c in the total population, with more cells in both higher and lower ratio regions (Figure 5.3A and B) compared to other cells. Lima and colleagues observed that Ca^{2+} homeostasis is affected in *mcln*-null cells, where they found a decreased Ca^{2+} concentration in the lumen of the acidic stores (post-lysosomes) in *mcln*-null cells (Lima *et al.*, 2012). They observed that fusion of post-lysosomes with the cell surface was increased in *mcln*-null cells compared with parental cells. Based on this, they hypothesized that mucolipin actually transfers cytosolic Ca^{2+} into the post-lysosomes, and in doing so, reduces the fusion of post-lysosomes with the cellular membrane. Loss of mucolipin increases the fusion of post-lysosomes with the cell surface. They proposed mucolipin activity might decrease high local cytosolic Ca^{2+} concentrations in the vicinity of post-lysosomes thus

limiting their fusion with the cell surface. In the current study, we have observed an abnormal Ca^{2+} distribution in the population, which might be explained by this theory in which mucolipin transfers a high local cytosolic Ca^{2+} into acidic stores, therefore without the channel a high cytosolic Ca^{2+} cannot be regulated properly.

A Ca^{2+} wave is one of the most striking events that one can observe in Ca^{2+} signalling *in vivo*. The generation of YC-Nano 15 was a breakthrough for visualizing Ca^{2+} waves in *Dictyostelium* since spatiotemporal patterns had never been directly visualized using conventional Ca^{2+} indicators (Horikawa *et al.*, 2010). We have observed successfully spontaneous intercellular Ca^{2+} waves in aggregates of Ax2 cells (Figure 5.4, 5.5 and 5.6). These Ca^{2+} waves are dependent on extracellular Ca^{2+} (Figure 5.5) in the development buffer, indicating that Ca^{2+} is needed in the external environment to prevent the Ca^{2+} stores being depleted over the time of development. However, the cells still can aggregate without observable Ca^{2+} waves, suggesting that these waves are not essential for aggregation, although there might be residual Ca^{2+} responses below the level detectable in our system. This is reminiscent of the IplA channel disruptant study conducted by Traynor and colleagues, where they concluded that increased cytosolic Ca^{2+} is not required for chemotaxis in *Dictyostelium* (Traynor *et al.*, 2000).

The wave period of Ax2 cells is 4.75 ± 0.35 min at 8 hrs (Figure 5.4), 3.67 ± 0.88 min (Figure 5.6) at 10 hr. The period length of the cAMP waves starts at around 6 min (Gross *et al.*, 1976; Siegert and Weijer, 1989; Tomchik and Devreotes, 1981) but gradually decreases continuously until it settles at 2.5 min (Rietdorf *et al.*, 1996). Therefore, my data is consistent with the intercellular Ca^{2+} waves observed being caused by the waves of extracellular cAMP. This is supported by the increase in Ca^{2+}

seen on addition of exogenous cAMP to both aggregates and single cells. Aggregates of *tpc2*$^-$ cells had a significantly longer wave period than that of Ax2 cells either in loose aggregates (10 hr) 9.67 ± 2.02 min or tight aggregates (16 hr) 11.5 min, which suggests that TPC2 may have a role in propagation of intercellular Ca^{2+} waves. However, because of the developmental delay seen in *tpc2*$^-$ cells, it is not possible to be certain that the comparison is being made at equivalent developmental stages. The wave periods in aggregates of cells lacking IplA or mucolipin are not significantly different from Ax2 aggregates.

In aggregates of Ax2 cells Ca^{2+} waves propagate at a speed of approximately 1 μm/sec (Figure 5.4 and 5.6). This is in agreement with Lionel Jaffe's studies on Ca^{2+} waves, that categorised Ca^{2+} waves in *Dictyostelium* as "slow waves" which propagate at 1.1 μm/sec during mound formation (Jaffe, 2008). The wave information he gathered was based on optical density waves during aggregation as there were no ultra-sensitive Ca^{2+} indicators available (Rietdorf *et al.*, 1996). It was of great interest to determine if aggregates of cells lacking Ca^{2+} channels showed an altered propagation velocity. TPC channels have been reported to play an important part in regulating salt stress-triggered Ca^{2+} waves in plants (Choi *et al.*, 2014). By using YC-Nano 65, Choi *et al.* found that Ca^{2+} waves traveling at a high speed of approximately 400 μm/sec trigger changes in gene expression and require TPC1, for which a universal role had long been sought in plant vacuoles. Propagation of the wave was 25-fold slower in a *tpc1*$^-$ mutant, and significantly accelerated when the channel was overexpressed (Choi *et al.*, 2014). However, in our study, we did not see a significant difference wave speed in aggregates of *tpc2*$^-$ cells or cells lacking other channels. *tpc2*$^-$ and *iplA*$^-$ aggregates show slightly slower speeds (*tpc2*$^-$ = 0.89 ± 0.19 μm/sec, *iplA*$^-$ = 0.93 ± 0.06 μm/sec) than Ax2 (1.24 ±

0.37 μm/sec), but the difference is not significant. The *mcln*$^{-}$ aggregates show a similar speed of Ca^{2+} waves (1.16 ± 0.25 μm/sec) to Ax2 aggregates. The mechanism behind the plant Ca^{2+} waves was recently explained by a combined model of a reactive oxygen species (ROS)-assisted calcium-induced calcium-release (CICR) mechanism and TPC channels (Evans *et al.*, 2016), whereas in *Dictyostelium* the wave is most likely related to cAMP signalling and its receptor affinity (Dormann *et al.*, 2001).

Among the mutants I investigated only *iplA*$^{-}$ and *tpc2*$^{-}$ aggregates showed pronounced phenotypes in terms of amplitude and frequency of Ca^{2+} waves, respectively. The aggregates of cells lacking IplA showed a greatly decreased amplitude (Figure 5.6 and movie 5.4.4.4). It is known that cAMP signalling play an important part in the process of aggregation and Traynor and colleagues found the *iplA*$^{-}$ cells showed a lack of cAMP-stimulated Ca^{2+} influx (Traynor *et al.*, 2000). To make sure this is the case in our *iplA*$^{-}$ cells, I tested aggregates of *iplA*$^{-}$ cells with exogenous cAMP and the cAMP-stimulated Ca^{2+} response detected in Ax2 aggregates was missing (Figure 5.7) in agreement with Traynor *et al*. To confirm that the YC-Nano 15 was functioning when expressed in *iplA*$^{-}$ cells, I did see a response to exogenous ATP. ATP is known to cause a Ca^{2+} response in *Dictyostelium* cells and this is dependent on the polycystin-like channel Pkd2 (Traynor and Kay, 2016). In agreement with this, I have also found the ATP response to be intact in cells lacking TPC2 and mucolipin (data not shown).

Aggregates of *tpc2*$^{-}$ cells showed a lower frequency of waves either in loose or tight aggregates (Figure 5.6). To find if this is caused by a defect in the cAMP sensing system, we tested aggregates and single cells of *tpc2*$^{-}$. The aggregates did not show any difference in cAMP-induced Ca^{2+} response when challenged with cAMP. However the

response to extracellular cAMP was greatly reduced following treatment with caffeine. In *Dictyostelium*, caffeine is commonly used as an inhibitor for ligand-induced ACA (adenylyl cyclase A) activation (Brenner and Thoms, 1984). Caffeine not only blocks ACA function, but also inhibits cAMP accumulation by ACB and ACG (Alvarez-Curto *et al.*, 2007). I saw that treatment of aggregates with caffeine caused an overall drop of $[Ca^{2+}]c$ (Figure 5.8 and Movie 5.7) in Ax2 and *tpc2*$^{-}$ cells. However an increase in cytosolic Ca^{2+} was still detectable in caffeine-treated Ax2 aggregates when challenged with cAMP but was lost in the aggregates of *tpc2*$^{-}$ cells. One hypothesis to explain this increased Ca^{2+} uptake seen in vesicles, is that it is perhaps due to overexpression of PAT1 or loss of a leak channel, in *tpc2*$^{-}$ cells (see chapter 4). It is conceivable that in *tpc2*$^{-}$ cells, higher levels of uptake cause $[Ca^{2+}]c$ to continue to drop below a threshold for cAMP-mediated Ca^{2+} release as many channels show a dependence on cytosolic Ca^{2+}. However, it is also possible that caffeine causes pleiotropic effects on signalling by impairing the cAMP system and altering intracellular calcium levels. Further experiments in future should address this to clarify this pathway.

Single cell experiments are labour-intensive to analyse but useful and informative when characterising cell responses to ligand stimulation in detail. In order to look for any minor differences in *tpc2*$^{-}$ responses, hidden in aggregates, it was decided to conduct single cell experiments. Previous results documented that $[Ca^{2+}]c$ peaks 20 to 30 secs after cAMP stimulation, then declines due to sequestration by Ca^{2+}-ATPases (Bohme *et al.*, 1987; Rooney *et al.*, 1994), returning to basal levels about 40 to 60 sec post stimulation (Nebl and Fisher, 1997). My results are in agreement with this as in developed Ax2 single cell analysis $[Ca^{2+}]c$ peaks at 20^{th} sec after 50 nM cAMP stimulation, then declines to basal level after 64 to 80 sec. Interestingly, single *tpc2*$^{-}$

cells show a decreased and delayed cAMP-induced Ca^{2+} response (Figure 5.9 to 5.12). The cytosolic Ca^{2+} levels in *tpc2*$^{-}$ cells peak at 35th sec, which is 15 seconds later than Ax2 cells. A further analysis calculated max response and max response rate of individual cells and shows that *tpc2*$^{-}$ cells have a not significantly reduced mean response (Ax2 = 0.36 Δratio, *tpc2*$^{-}$= 0.23 Δratio) but a significantly slower mean response rate (Ax2 = 15.8 Δratio/ms, *tpc2*$^{-}$= 7.2 Δratio/ms) (Figure 5.11). The majority of individual *tpc2*$^{-}$ cells took a longer time to reach the maximum response (Tmax) compared to Ax2 cells (Figure 5.12). It is also noteworthy that the distribution of the Ax2 cell population shows two subpopulations of cells in contrast to only one major population in *tpc2*$^{-}$ cells.

Taken together, current results show that aggregates of *iplA*$^{-}$ cells show a dramatic loss of increased cytosolic Ca^{2+} responses in aggregates, both spontaneous and in response to extracellular cAMP. As development of these cells is phenotypically normal, this response is not required for development. Despite the delay in early development, *tpc2*$^{-}$ aggregates however, showed much more subtle defects in Ca^{2+} responses with a lower frequency of intercellular Ca^{2+} waves and somewhat reduced and delayed increase in cytosolic Ca^{2+} in response to cAMP in single cells. Aggregates of *tpc2*$^{-}$ cells showed a greatly reduced cAMP-induced Ca^{2+} response after treatment with caffeine. Further studies are required to clarify if differences in cAMP-induced increases in cytosolic Ca^{2+} are due to reduced expression of genes encoding proteins required for cAMP responses, such as cAMP receptors, (see Chapter 3) or a *bona fide* reduction of intracellular Ca^{2+} release due to lack of TPC2 channel.

Chapter 6: Summary and Future Work

6.1 Summary

1. I have generated strains of *Dictyostelium* in which genes encoding for the calcium channels TPC2, mucolipin and IplA have been disrupted in the same genetic background. Cells lacking expression of TPC2 showed a delay in early development which was most pronounced when developed under buffer. The delay could be partially rescued by pulsing with extracellular cAMP. Analysis of gene expression showed a reduced expression of a number of early-developmental genes (*dscA*) and pulse-independent genes (*carA* and *pdsA*). No obvious developmental phenotypes were observed in cells lacking IplA and a much less pronounced delay in cells lacking mucolipin.

2. To investigate the role of TPC2 in acidic vesicles of *Dictyostelium*, I have established and characterised a vesicle system to study Ca^{2+} uptake and release *in vitro* to determine the effects of gene disruption. Vesicles from *tpc2*$^{-}$ cells showed an increased uptake of Ca^{2+} relative to vesicles from parental Ax2 cells. Release of Ca^{2+} was seen in response to arachidonic acid and high levels of NAADP and both of these were preserved in vesicles from *tpc2*$^{-}$ cells. The *tpc2*$^{-}$ cells showed a complex behaviour with resistance to an aggregation defect caused by sodium chloride when developed under buffer and to ammonium chloride on filters. An increase pH of acidic vesicles and up-regulation of *patA* in early development in these cells are consistent with a role for TPC2 in regulating the ion content of acidic vesicles in early developing cells.

3. I have established a real-time Ca^{2+} detection system using living cells expressing ultrasensitive the Ca^{2+} indicator, yellow cameleon-Nano to analyse changes in cytosolic calcium levels *in vivo*. Vegetative cells showed heterogeneity in the level of cytosolic Ca^{2+} but the average level was reduced in cells lacking TPC2 or IplA. Spontaneous waves of increased cytosolic Ca^{2+} were detectable in aggregates of Ax2 cells, consistent with their generation in response to waves of extracellular cAMP, and also increases in response to addition of extracellular cAMP and ATP. Loss of IplA caused a great reduction in spontaneous Ca^{2+} waves during development and in response to extracellular cAMP suggesting this channel is necessary for the bulk of the cytosolic Ca^{2+} increase but that this increase is not required for aggregation. *tpc2*$^{-}$ aggregates showed subtle differences in wave period and a delayed, slightly reduced and delayed response to cAMP in single cells.

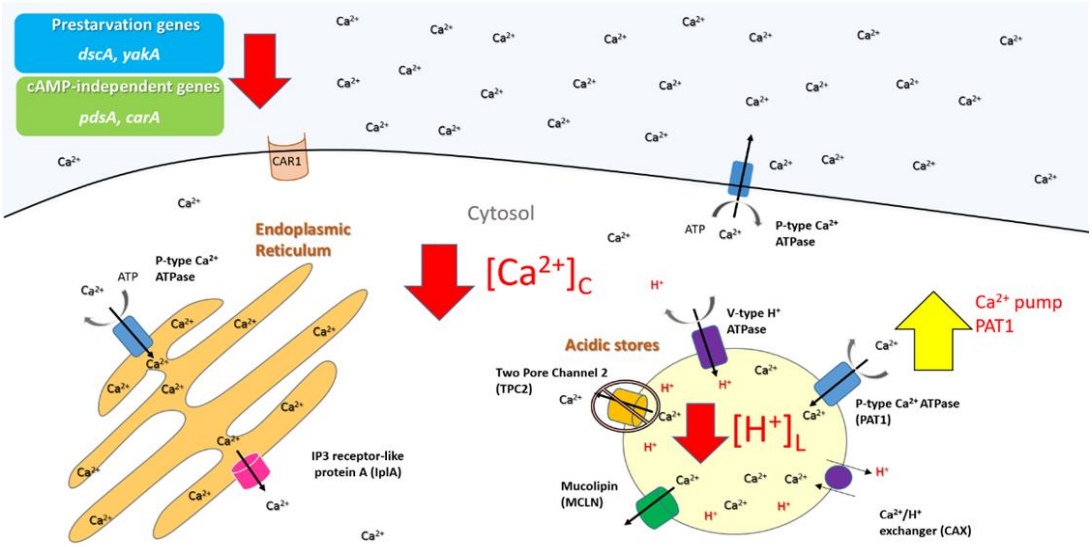

Figure 6.1 Summary of the cellular phenotypes of disrupting the gene encoding *Dictyostelium* TPC2.

Dictyostelium TPC2 located on acidic stores has a role in regulation of many functions based on the results presented in this research thesis. Ablation of the gene encoding TPC2 caused changes in developmental gene expression with up-regulation of mRNA encoding a Ca^{2+} pump, PAT1 and down-regulation of prestarvation genes (*dscA* and *yakA*) and cAMP-independent genes (*pdsA* and *carA*). Moreover, disrupting TPC2 also causes aberrant intracellular ion regulation, in which cytosolic Ca^{2+} and luminal protons of acidic stores are found to be at a lower level than parental cells. Links between the altered pH and/or Ca^{2+} levels with changes in gene expression and resulting developmental phenotypes remain to be determined.

6.2 Future directions

Possible Future Experiments:

1. Expression of TPC2 in *tpc1/tpc2*-null mouse embryo fibroblasts to analyse channel properties by determining if NAADP-dependent release is restored and by patch clamping of lysosomes as in (Ruas *et al.*, 2015).

2. Analysis of changes in cytosolic Ca^{2+} in Ax2, *tpc2*$^{-}$, *iplA*$^{-}$ and *mcln*$^{-}$ single cells in response to cAMP, and other extracellular factors, especially factors involved in early development such as PSF and CMF. PSF would have to be purified from conditioned media.

3. Expression of a fusion protein in *Dictyostelium* of TPC2 fused to a Ca^{2+} sensitive version of EGFP (e.g. GCamP). If channel opening allows Ca^{2+} flux through the channel, then this should be sensed as a change in fluorescence. This will allow me to determine whether Ca^{2+} ions pass through the channel and the circumstances that cause channel opening. A similar fusion protein has been used successfully in *Dictyostelium* to examine opening of a P2X receptor on the contractile vacuole (Parkinson *et al.*, 2014)

4. Development of a version of YC-Nano 15 that localises to acidic stores, by adding a signalling sequence for CV-targeting, to determine if loss of TPC2 alters the Ca^{2+} concentration within the stores.

5. Correlation of changes in cytosolic or vesicle pH or Ca^{2+} levels with changes in early developmental gene expression similar to those seen in the *tpc2*$^{-}$ cells. Ion levels can be manipulated chemically or by using genetic mutants.

6. Analysis of any cell fate bias in the cells lacking channels to see if the differences in cytosolic Ca^{2+} detected influence cell fate. Initial experiments suggest that *tpc2*$^{-}$ cells have a prestalk tendency (Warren, Chang and Pears, unpublished data). Mutant cells can be labelled with Cell Tracker and induced to form mixed aggregates with Ax2 and the proportion of labelled spores in the final fruiting body counted. Also the sensitivity of the cells to DIF-induced stalk cell differentiation in monolayer assay can be used to determine their propensity to differentiate into stalk cells as in (Thompson and Kay, 2000)

Reference

Abe T, Maeda Y and Iijima T (1988) Transient increase of the intracellular Ca^{2+} concentration during chemotactic signal transduction in *Dictyostelium discoideum* cells. *Differentiation* **39**:90-96.

Aggarwal SK and MacKinnon R (1996) Contribution of the S4 segment to gating charge in the Shaker K^+ channel. *Neuron* **16**:1169-1177.

Aley PK, Mikolajczyk AM, Munz B, Churchill GC, Galione A and Berger F (2010) Nicotinic acid adenine dinucleotide phosphate regulates skeletal muscle differentiation via action at two-pore channels. *Proc Natl Acad Sci U S A* **107**:19927-19932.

Alvarez-Curto E, Weening KE and Schaap P (2007) Pharmacological profiling of the *Dictyostelium* adenylate cyclases ACA, ACB and ACG. *Biochem J* **401**:309-316.

Ambrosio AL, Boyle JA, Aradi AE, Christian KA and Di Pietro SM (2016) TPC2 controls pigmentation by regulating melanosome pH and size. *Proc Natl Acad Sci U S A* **113**:5622-5627.

Ambrosio AL, Boyle JA and Di Pietro SM (2015) TPC2 mediates new mechanisms of platelet dense granule membrane dynamics through regulation of Ca^{2+} release. *Mol Biol Cell* **26**:3263-3274.

Aubry L, Klein G, Martiel JL and Satre M (1993) Kinetics of endosomal pH evolution in *Dictyostelium discoideum* amoebae. Study by fluorescence spectroscopy. *J Cell Sci* **105 (Pt 3)**:861-866.

Baines A, Parkinson K, Sim JA, Bragg L, Thompson CR and North RA (2013) Functional properties of five *Dictyostelium discoideum* P2X receptors. *J Biol Chem* **288**:20992-21000.

Bakthavatsalam D, Brazill D, Gomer RH, Eichinger L, Rivero F and Noegel AA (2007) A G protein-coupled receptor with a lipid kinase domain is involved in cell-density sensing. *Current Biology* **17**:892-897.

Bargal R, Avidan N, Ben-Asher E, Olender Z, Zeigler M, Frumkin A, Raas-Rothschild A, Glusman G, Lancet D and Bach G (2000) Identification of the gene causing mucolipidosis type IV. *Nat Genet* **26**:118-123.

Berridge MJ (2002) The endoplasmic reticulum: a multifunctional signaling organelle. *Cell Calcium* **32**:235-249.

Berridge MJ (2014) Module 3: Ion Channels. *Cell Signalling Biology* **6**.

Berridge MJ, Bootman MD and Roderick HL (2003) Calcium signalling: dynamics, homeostasis and remodelling. *Nat Rev Mol Cell Biol* **4**:517-529.

Berridge MJ, Lipp P and Bootman MD (2000) The versatility and universality of calcium signalling. *Nat Rev Mol Cell Biol* **1**:11-21.

Bewell MA, Maathuis FJ, Allen GJ and Sanders D (1999) Calcium-induced calcium release mediated by a voltage-activated cation channel in vacuolar vesicles from red beet. *FEBS Lett* **458**:41-44.

Bezprozvanny I, Scheller RH and Tsien RW (1995) Functional impact of syntaxin on gating of N-type and Q-type calcium channels. *Nature* **378**:623-626.

Blusch J, Alexander S and Nellen W (1995) Multiple signal transduction pathways regulate discoidin I gene expression in *Dictyostelium discoideum*. *Differentiation* **58**:253-260.

Bohme R, Bumann J, Aeckerle S and Malchow D (1987) A High-Affinity Plasma-Membrane Ca-$^{2+}$-Atpase in *Dictyostelium-Discoideum* - Its Relation to Camp-Induced Ca-$^{2+}$ Fluxes. *Biochimica Et Biophysica Acta* **904**:125-130.

Bonales-Alatorre E, Shabala S, Chen ZH and Pottosin I (2013) Reduced Tonoplast Fast-Activating and Slow-Activating Channel Activity Is Essential for Conferring Salinity Tolerance in a Facultative Halophyte, Quinoa. *Plant Physiology* **162**:940-952.

Bowman BJ and Slayman CW (1979) The effects of vanadate on the plasma membrane ATPase of Neurospora crassa. *J Biol Chem* **254**:2928-2934.

Brailoiu E, Churamani D, Pandey V, Brailoiu GC, Tuluc F, Patel S and Dun NJ (2006) Messenger-specific role for nicotinic acid adenine dinucleotide phosphate in neuronal differentiation. *J Biol Chem* **281**:15923-15928.

Brailoiu E, Rahman T, Churamani D, Prole DL, Brailoiu GC, Hooper R, Taylor CW and Patel S (2010) An NAADP-gated two-pore channel targeted to the plasma membrane uncouples triggering from amplifying Ca^{2+} signals. *J Biol Chem* **285**:38511-38516.

Brazill DT, Lindsey DF, Bishop JD and Gomer RH (1998) Cell density sensing mediated by a G protein-coupled receptor activating phospholipase C. *J Biol Chem* **273**:8161-8168.

Brenner M and Thoms SD (1984) Caffeine blocks activation of cyclic AMP synthesis in *Dictyostelium discoideum*. *Dev Biol* **101**:136-146.

Cai XJ and Lytton J (2004) The cation/Ca^{2+} exchanger superfamily: Phylogenetic analysis and structural implications. *Molecular Biology and Evolution* **21**:1692-1703.

Calcraft PJ, Ruas M, Pan Z, Cheng X, Arredouani A, Hao X, Tang J, Rietdorf K, Teboul L, Chuang KT, Lin P, Xiao R, Wang C, Zhu Y, Lin Y, Wyatt CN, Parrington J, Ma J, Evans AM, Galione A and Zhu MX (2009) NAADP mobilizes calcium from acidic organelles through two-pore channels. *Nature* **459**:596-600.

Cancela JM, Churchill GC and Galione A (1999) Coordination of agonist-induced Ca^{2+}-signalling patterns by NAADP in pancreatic acinar cells. *Nature* **398**:74-76.

Cang CL, Zhou YD, Navarro B, Seo YJ, Aranda K, Shi L, Battaglia-Hsu S, Nissim I, Clapham DE and Ren DJ (2013) mTOR Regulates Lysosomal ATP-Sensitive Two-Pore Na^{+} Channels to Adapt to Metabolic State. *Cell* **152**:778-790.

Carafoli E (1991) Calcium pump of the plasma membrane. *Physiol Rev* **71**:129-153.

Carpaneto A, Cantu AM and Gambale F (1999) Redox agents regulate ion channel activity in vacuoles from higher plant cells. *FEBS Lett* **442**:129-132.

Catterall WA (2011) Voltage-gated calcium channels. *Cold Spring Harb Perspect Biol* **3**:a003947.

Chen L, Iijima M, Tang M, Landree MA, Huang YE, Xiong Y, Iglesias PA and Devreotes PN (2007) PLA2 and PI3K/PTEN pathways act in parallel to mediate chemotaxis. *Dev Cell* **12**:603-614.

Chen W, Wang R, Chen B, Zhong X, Kong H, Bai Y, Zhou Q, Xie C, Zhang J, Guo A, Tian X, Jones PP, O'Mara ML, Liu Y, Mi T, Zhang L, Bolstad J, Semeniuk L, Cheng H, Zhang J, Chen J, Tieleman DP, Gillis AM, Duff HJ, Fill M, Song LS and Chen SR (2014) The ryanodine receptor store-sensing gate controls Ca^{2+} waves and Ca^{2+}-triggered arrhythmias. *Nat Med* **20**:184-192.

Chen Y, Rodrick V, Yan Y and Brazill D (2005) PldB, a putative phospholipase D homologue in *Dictyostelium discoideum* mediates quorum sensing during development. *Eukaryot Cell* **4**:694-702.

Choi WG, Toyota M, Kim SH, Hilleary R and Gilroy S (2014) Salt stress-induced Ca^{2+} waves are associated with rapid, long-distance root-to-shoot signaling in plants. *P Natl Acad Sci USA* **111**:6497-6502.

Chung KM, Jeong EJ, Park H, An HK and Yu SW (2016) Mediation of Autophagic Cell Death by Type 3 Ryanodine Receptor (RyR3) in Adult Hippocampal Neural Stem Cells. *Front Cell Neurosci* **10**:116.

Clapham DE (1995) Calcium signaling. *Cell* **80**:259-268.

Clapham DE (2007) Calcium signaling. *Cell* **131**:1047-1058.

Clarke M, Dominguez N, Yuen IS and Gomer RH (1992) Growing and Starving *Dictyostelium* Cells Produce Distinct Density-Sensing Factors. *Developmental Biology* **152**:403-406.

Clarke M and Gomer RH (1995) PSF and CMF, autocrine factors that regulate gene expression during growth and early development of *Dictyostelium*. *Experientia* **51**:1124-1134.

Clarke M, Kayman SC and Riley K (1987) Density-dependent induction of discoidin-I synthesis in exponentially growing cells of *Dictyostelium discoideum*. *Differentiation* **34**:79-87.

Clarke M, Yang J and Kayman SC (1988) Analysis of the prestarvation response in growing cells of *Dictyostelium discoideum*. *Dev Genet* **9**:315-326.

Collins SR and Meyer T (2011) Evolutionary origins of STIM1 and STIM2 within ancient Ca^{2+} signaling systems. *Trends in Cell Biology* **21**:202-211.

Coukell B, Moniakis J and Grinberg A (1995) Cloning and expression in Escherichia coli of a cDNA encoding a developmentally regulated Ca(2+)-binding protein from *Dictyostelium discoideum*. *FEBS Lett* **362**:342-346.

Cunningham KW and Fink GR (1996) Calcineurin inhibits VCX1-dependent H^+/Ca^{2+} exchange and induces Ca^{2+} ATPases in Saccharomyces cerevisiae. *Mol Cell Biol* **16**:2226-2237.

Davidson AJ, King JS and Insall RH (2013) The use of streptavidin conjugates as immunoblot loading controls and mitochondrial markers for use with *Dictyostelium discoideum*. *Biotechniques* **55**:39-41.

Davies L, Farrar NA, Satre M, Dottin RP and Gross JD (1996) Vacuolar $H(^+)$-ATPase and weak base action in *Dictyostelium*. *Mol Microbiol* **22**:119-126.

Davies L, Satre M, Martin JB and Gross JD (1993) The target of ammonia action in *Dictyostelium*. *Cell* **75**:321-327.

Davis LC and Galione A (2013) Cytolytic granules supply Ca(2+) for their own exocytosis via NAADP and resident two-pore channels. *Commun Integr Biol* **6**:e24175.

Davis LC, Morgan AJ, Chen JL, Snead CM, Bloor-Young D, Shenderov E, Stanton-Humphreys MN, Conway SJ, Churchill GC, Parrington J, Cerundolo V and Galione A (2012) NAADP activates two-pore channels on T cell cytolytic granules to stimulate exocytosis and killing. *Curr Biol* **22**:2331-2337.

De Strooper B, Iwatsubo T and Wolfe MS (2012) Presenilins and gamma-secretase: structure, function, and role in Alzheimer Disease. *Cold Spring Harb Perspect Med* **2**:a006304.

Deery WJ, Gao T, Ammann R and Gomer RH (2002) A single cell density-sensing factor stimulates distinct signal transduction pathways through two different receptors. *Journal of Biological Chemistry* **277**:31972-31979.

Deery WJ and Gomer RH (1999) A putative receptor mediating cell-density sensing in *Dictyostelium*. *J Biol Chem* **274**:34476-34482.

Diwu Z, Chen CS, Zhang C, Klaubert DH and Haugland RP (1999) A novel acidotropic pH indicator and its potential application in labeling acidic organelles of live cells. *Chem Biol* **6**:411-418.

Dong X-p, Shen D, Wang X, Dawson T, Li X, Zhang Q, Cheng X, Zhang Y, Weisman LS, Delling M and Xu H (2010) PI(3,5)P_2 controls membrane trafficking by direct activation of mucolipin Ca^{2+} release channels in the endolysosome. *Nature Communications* **1**:38.

Dormann D, Kim JY, Devreotes PN and Weijer CJ (2001) cAMP receptor affinity controls wave dynamics, geometry and morphogenesis in *Dictyostelium*. *J Cell Sci* **114**:2513-2523.

Esposito B, Gambara G, Lewis AM, Palombi F, D'Alessio A, Taylor LX, Genazzani AA, Ziparo E, Galione A, Churchill GC and Filippini A (2011) NAADP links histamine H1 receptors to secretion of von Willebrand factor in human endothelial cells. *Blood* **117**:4968-4977.

Europe-Finner GN and Newell PC (1986) Inositol 1,4,5-triphosphate induces calcium release from a non- mitochondrial pool in amoebae of *Dictyostelium*. *Biochim Biophys Acta* **887**:335-340.

Evans MJ, Choi WG, Gilroy S and Morris RJ (2016) A ROS-Assisted Calcium Wave Dependent on the AtRBOHD NADPH Oxidase and TPC1 Cation Channel Propagates the Systemic Response to Salt Stress. *Plant Physiol* **171**:1771-1784.

Feng X, Huang Y, Lu Y, Xiong J, Wong CO, Yang P, Xia J, Chen D, Du G, Venkatachalam K, Xia X and Zhu MX (2014) Drosophila TRPML forms PI(3,5)P2-activated cation channels in both endolysosomes and plasma membrane. *J Biol Chem* **289**:4262-4272.

Feske S and Prakriya M (2013) Conformational dynamics of STIM1 activation. *Nat Struct Mol Biol* **20**:918-919.

Finch EA, Turner TJ and Goldin SM (1991) Calcium as a Coagonist of Inositol 1,4,5-Trisphosphate Induced Calcium Release. *Science* **252**:443-446.

Firtel RA (1991) Signal transduction pathways controlling multicellular development in *Dictyostelium*. *Trends Genet* **7**:381-388.

Flaadt H, Jaworski E and Malchow D (1993) Evidence for two intracellular calcium pools in *Dictyostelium*: the cAMP-induced calcium influx is directed into a NBD-Cl- and 2,5-di-(tert-butyl)1,4-hydroquinone-sensitive pool. *J Cell Sci* **105 (Pt 4)**:1131-1135.

Fok AK, Clarke M, Ma L and Allen RD (1993) Vacuolar H(+)-ATPase of *Dictyostelium discoideum*. A monoclonal antibody study. *J Cell Sci* **106 (Pt 4)**:1103-1113.

Follstaedt SC, Kirsten JH and Singleton CK (2003) Temporal and spatial expression of ammonium transporter genes during growth and development of *Dictyostelium discoideum*. *Differentiation* **71**:557-566.

Fountain SJ, Parkinson K, Young MT, Cao L, Thompson CR and North RA (2007) An intracellular P2X receptor required for osmoregulation in *Dictyostelium discoideum*. *Nature* **448**:200-203.

Furuichi T, Yoshikawa S, Miyawaki A, Wada K, Maeda N and Mikoshiba K (1989) Primary structure and functional expression of the inositol 1,4,5-trisphosphate-binding protein P400. *Nature* **342**:32-38.

Galione A (2011) NAADP Receptors. *Csh Perspect Biol* **3**.

Galione A (2015) A primer of NAADP-mediated Ca(2+) signalling: From sea urchin eggs to mammalian cells. *Cell Calcium* **58**:27-47.

Garige M and Walters E (2015) Curcumin inhibits development and cell adhesion in *Dictyostelium discoideum*: Implications for YakA signaling and GST enzyme function. *Biochem Bioph Res Co* **467**:275-281.

Gomer RH, Armstrong D, Leichtling BH and Firtel RA (1986a) Camp Induction of Prespore and Prestalk Gene-Expression in *Dictyostelium* Is Mediated by the Cell-Surface Camp Receptor. *P Natl Acad Sci USA* **83**:8624-8628.

Gomer RH, Datta S and Firtel RA (1986b) Cellular and subcellular distribution of a cAMP-regulated prestalk protein and prespore protein in *Dictyostelium discoideum*: a study on the ontogeny of prestalk and prespore cells. *J Cell Biol* **103**:1999-2015.

Gomer RH, Jang W and Brazill D (2011) Cell density sensing and size determination. *Dev Growth Differ* **53**:482-494.

Gomez-Ospina N, Panagiotakos G, Portmann T, Pasca SP, Rabah D, Budzillo A, Kinet JP and Dolmetsch RE (2013) A promoter in the coding region of the calcium channel gene CACNA1C generates the transcription factor CCAT. *PLoS One* **8**:e60526.

Gomez-Ospina N, Tsuruta F, Barreto-Chang O, Hu L and Dolmetsch R (2006) The C terminus of the L-type voltage-gated calcium channel Ca(V)1.2 encodes a transcription factor. *Cell* **127**:591-606.

Grabel L and Loomis WF (1978) Effector controlling accumulation of N-acetylglucosaminidase during development of *Dictyostelium discoideum*. *Dev Biol* **64**:203-209.

Graham SM, Ding M, Luchowski R, Gryczynski Z and Ma R (2010) Promotion of Trafficking and Sensitivity to DAG are Involved in TRPC6 Channel Activation by Hydrogen Peroxide. *Faseb Journal* **24**.

Grimm C, Holdt LM, Chen CC, Hassan S, Muller C, Jors S, Cuny H, Kissing S, Schroder B, Butz E, Northoff B, Castonguay J, Luber CA, Moser M, Spahn S, Lullmann-Rauch R, Fendel C, Klugbauer N, Griesbeck O, Haas A, Mann M, Bracher F, Teupser D, Saftig P, Biel M and Wahl-Schott C (2014) High susceptibility to fatty liver disease in two-pore channel 2-deficient mice. *Nature Communications* **5**.

Gross JD (2009) Acidic Ca^{2+} stores, excitability, and cell patterning in *Dictyostelium discoideum*. *Eukaryot Cell* **8**:696-702.

Gross JD, Peacey MJ and Trevan DJ (1976) Signal Emission and Signal Propagation during Early Aggregation in *Dictyostelium-Discoideum*. *Journal of Cell Science* **22**:645-656.

Grynkiewicz G, Poenie M and Tsien RY (1985) A new generation of Ca^{2+} indicators with greatly improved fluorescence properties. *J Biol Chem* **260**:3440-3450.

Guo J, Zeng W, Chen Q, Lee C, Chen L, Yang Y, Cang C, Ren D and Jiang Y (2016) Structure of the voltage-gated two-pore channel TPC1 from Arabidopsis thaliana. *Nature* **531**:196-201.

Gutla PV, Boccaccio A, De Angeli A, Gambale F and Carpaneto A (2012) Modulation of plant TPC channels by polyunsaturated fatty acids. *J Exp Bot* **63**:6187-6197.

Gyorke I, Hester N, Jones LR and Gyorke S (2004) The role of calsequestrin, triadin, and junctin in conferring cardiac ryanodine receptor responsiveness to luminal calcium. *Biophys J* **86**:2121-2128.

Gyorke S and Terentyev D (2008) Modulation of ryanodine receptor by luminal calcium and accessory proteins in health and cardiac disease. *Cardiovasc Res* **77**:245-255.

Hardie RC (2007) TRP channels and lipids: from Drosophila to mammalian physiology. *J Physiol* **578**:9-24.

Hedrich R and Marten I (2011) TPC1-SV channels gain shape. *Mol Plant* **4**:428-441.

Hedrich R and Neher E (1987) Cytoplasmic Calcium Regulates Voltage-Dependent Ion Channels in Plant Vacuoles. *Nature* **329**:833-836.

Heuser J, Zhu Q and Clarke M (1993) Proton pumps populate the contractile vacuoles of *Dictyostelium* amoebae. *J Cell Biol* **121**:1311-1327.

Hirschi KD, Zhen RG, Cunningham KW, Rea PA and Fink GR (1996) CAX1, an H^+/Ca^{2+} antiporter from Arabidopsis. *Proc Natl Acad Sci U S A* **93**:8782-8786.

Holmes KD, Mattar P, Marsh DR, Jordan V, Weaver LC and Dekaban GA (2002) The C-terminal C1 cassette of the N -methyl-D-aspartate receptor 1 subunit contains a bi-partite nuclear localization sequence. *J Neurochem* **81**:1152-1165.

Honarnejad K and Herms J (2012) Presenilins: Role in calcium homeostasis. *Int J Biochem Cell B* **44**:1983-1986.

Horikawa K, Yamada Y, Matsuda T, Kobayashi K, Hashimoto M, Matsu-ura T, Miyawaki A, Michikawa T, Mikoshiba K and Nagai T (2010) Spontaneous network activity visualized by ultrasensitive Ca(2+) indicators, yellow Cameleon-Nano. *Nat Methods* **7**:729-732.

Hoth M and Penner R (1992) Depletion of intracellular calcium stores activates a calcium current in mast cells. *Nature* **355**:353-356.

Howell LL (1993) Comparative effects of caffeine and selective phosphodiesterase inhibitors on respiration and behavior in rhesus monkeys. *J Pharmacol Exp Ther* **266**:894-903.

Iino M (1987) Calcium dependent inositol trisphosphate-induced calcium release in the guinea-pig taenia caeci. *Biochem Biophys Res Commun* **142**:47-52.

Iino M (1990) Biphasic Ca^{2+} dependence of inositol 1,4,5-trisphosphate-induced Ca release in smooth muscle cells of the guinea pig taenia caeci. *J Gen Physiol* **95**:1103-1122.

Iranfar N, Fuller D and Loomis WF (2003) Genome-wide expression analyses of gene regulation during early development of *Dictyostelium discoideum*. *Eukaryot Cell* **2**:664-670.

Ishibashi K, Suzuki M and Imai M (2000) Molecular cloning of a novel form (two-repeat) protein related to voltage-gated sodium and calcium channels. *Biochem Biophys Res Commun* **270**:370-376.

Jaffe LF (2008) Calcium waves. *Philos Trans R Soc Lond B Biol Sci* **363**:1311-1316.

Jang W and Gomer RH (2011) Initial cell type choice in *Dictyostelium*. *Eukaryot Cell* **10**:150-155.

Kay RR (1982) cAMP and spore differentiation in *Dictyostelium discoideum*. *Proc Natl Acad Sci U S A* **79**:3228-3231.

Kintzer AF and Stroud RM (2016) Structure, inhibition and regulation of two-pore channel TPC1 from Arabidopsis thaliana. *Nature* **531**:258-262.

Kiselyov K, Chen J, Rbaibi Y, Oberdick D, Tjon-Kon-Sang S, Shcheynikov N, Muallem S and Soyombo A (2005) TRP-ML1 is a lysosomal monovalent cation

channel that undergoes proteolytic cleavage. *Journal of Biological Chemistry* **280**:43218-43223.

Knollmann BC, Chopra N, Hlaing T, Akin B, Yang T, Ettensohn K, Knollmann BE, Horton KD, Weissman NJ, Holinstat I, Zhang W, Roden DM, Jones LR, Franzini-Armstrong C and Pfeifer K (2006) Casq2 deletion causes sarcoplasmic reticulum volume increase, premature Ca^{2+} release, and catecholaminergic polymorphic ventricular tachycardia. *J Clin Invest* **116**:2510-2520.

Koch GL (1990) The endoplasmic reticulum and calcium storage. *Bioessays* **12**:527-531.

Kotturi MF and Jefferies WA (2005) Molecular characterization of L-type calcium channel splice variants expressed in human T lymphocytes. *Mol Immunol* **42**:1461-1474.

Kubohara Y and Okamoto K (1994) Cytoplasmic Ca^{2+} and H^{+} concentrations determine cell fate in *Dictyostelium discoideum*. *FASEB J* **8**:869-874.

Lam D, Kosta A, Luciani MF and Golstein P (2008) The inositol 1,4,5-trisphosphate receptor is required to signal autophagic cell death. *Molecular Biology of the Cell* **19**:691-700.

LaPlante JM, Falardeau J, Sun M, Kanazirska M, Brown EM, Slaugenhaupt SA and Vassilev PM (2002) Identification and characterization of the single channel function of human mucolipin-1 implicated in mucolipidosis type IV, a disorder affecting the lysosomal pathway. *FEBS Lett* **532**:183-187.

Larisch N, Kirsch SA, Schambony A, Studtrucker T, Bockmann RA and Dietrich P (2016) The function of the two-pore channel TPC1 depends on dimerization of its carboxy-terminal helix. *Cell Mol Life Sci* **73**:2565-2581.

Lemons RM and Thoene JG (1991) Mediated calcium transport by isolated human fibroblast lysosomes. *J Biol Chem* **266**:14378-14382.

Lima WC, Leuba F, Soldati T and Cosson P (2012) Mucolipin controls lysosome exocytosis in *Dictyostelium*. *J Cell Sci* **125**:2315-2322.

Lima WC, Vinet A, Pieters J and Cosson P (2014) Role of PKD2 in rheotaxis in *Dictyostelium*. *PLoS One* **9**:e88682.

Lin-Moshier Y, Keebler MV, Hooper R, Boulware MJ, Liu X, Churamani D, Abood ME, Walseth TF, Brailoiu E, Patel S and Marchant JS (2014) The Two-pore channel (TPC) interactome unmasks isoform-specific roles for TPCs in endolysosomal morphology and cell pigmentation. *Proc Natl Acad Sci U S A* **111**:13087-13092.

Liu CM and Hermann TE (1978) Characterization of Ionomycin as a Calcium Ionophore. *Journal of Biological Chemistry* **253**:5892-5894.

Loomis WF (2014) Cell signaling during development of *Dictyostelium*. *Dev Biol* **391**:1-16.

Lu Y, Hao BX, Graeff R, Wong CW, Wu WT and Yue J (2013) Two pore channel 2 (TPC2) inhibits autophagosomal-lysosomal fusion by alkalinizing lysosomal pH. *J Biol Chem* **288**:24247-24263.

Ludlow MJ, Durai L and Ennion SJ (2009) Functional characterization of intracellular *Dictyostelium discoideum* P2X receptors. *J Biol Chem* **284**:35227-35239.

Ludlow MJ, Traynor D, Fisher PR and Ennion SJ (2008) Purinergic-mediated Ca^{2+} influx in *Dictyostelium discoideum*. *Cell Calcium* **44**:567-579.

Ludtmann MH, Otto GP, Schilde C, Chen ZH, Allan CY, Brace S, Beesley PW, Kimmel AR, Fisher P, Killick R and Williams RS (2014) An ancestral non-

proteolytic role for presenilin proteins in multicellular development of the social amoeba *Dictyostelium discoideum*. *J Cell Sci* **127**:1576-1584.

Luo DL, Nakazawa M, Yoshida Y, Cai JQ and Imai S (2000) Effects of three different Ca^{2+} pump ATPase inhibitors on evoked contractions in rabbit aorta and activities of Ca^{2+} pump ATPases in porcine aorta. *Gen Pharmacol-Vasc S* **34**:211-220.

Lusche DF, Wessels D, Scherer A, Daniels K, Kuhl S and Soll DR (2012) The IplA Ca^{2+} channel of *Dictyostelium discoideum* is necessary for chemotaxis mediated through Ca^{2+}, but not through cAMP, and has a fundamental role in natural aggregation. *J Cell Sci* **125**:1770-1783.

Lyfenko AD and Dirksen RT (2008) Differential dependence of store-operated and excitation-coupled Ca^{2+} entry in skeletal muscle on STIM1 and Orai1. *J Physiol* **586**:4815-4824.

Lytton J (2007) Na^{+}/Ca^{2+} exchangers: three mammalian gene families control Ca^{2+} transport. *Biochem J* **406**:365-382.

Maathuis FJM and Prins HBA (1990) Patch Clamp Studies on Root Cell Vacuoles of a Salt-Tolerant and a Salt-Sensitive Plantago Species - Regulation of Channel Activity by Salt Stress. *Plant Physiology* **92**:23-28.

Maeda N, Niinobe M, Nakahira K and Mikoshiba K (1988) Purification and characterization of P400 protein, a glycoprotein characteristic of Purkinje cell, from mouse cerebellum. *J Neurochem* **51**:1724-1730.

Malchow D, Lusche DF, De Lozanne A and Schlatterer C (2008) A fast Ca^{2+}-induced Ca^{2+}-release mechanism in *Dictyostelium discoideum*. *Cell Calcium* **43**:521-530.

Malchow D, Lusche DF and Schlatterer C (2004) A link of Ca^{2+} to cAMP oscillations in *Dictyostelium*: the calmodulin antagonist W-7 potentiates cAMP relay and transiently inhibits the acidic Ca^{2+}-store. *BMC Dev Biol* **4**:7.

Malchow D, Lusche DF, Schlatterer C, De Lozanne A and Muller-Taubenberger A (2006) The contractile vacuole in Ca^{2+}-regulation in *Dictyostelium*: its essential function for cAMP-induced Ca^{2+}-influx. *BMC Dev Biol* **6**:31.

Marchesini N, Ruiz FA, Vieira M and Docampo R (2002) Acidocalcisomes are functionally linked to the contractile vacuole of *Dictyostelium discoideum*. *J Biol Chem* **277**:8146-8153.

Marshall IC and Taylor CW (1993) Biphasic effects of cytosolic Ca^{2+} on Ins(1,4,5)P3-stimulated Ca^{2+} mobilization in hepatocytes. *J Biol Chem* **268**:13214-13220.

Martiel JL and Goldbeter A (1987) A Model Based on Receptor Desensitization for Cyclic AMP Signaling in *Dictyostelium* Cells. *Biophys J* **52**:807-828.

Marx SO, Reiken S, Hisamatsu Y, Jayaraman T, Burkhoff D, Rosemblit N and Marks AR (2000) PKA phosphorylation dissociates FKBP12.6 from the calcium release channel (ryanodine receptor): defective regulation in failing hearts. *Cell* **101**:365-376.

Matheos DP, Kingsbury TJ, Ahsan US and Cunningham KW (1997) Tcn1p/Crz1p a calcineurin-dependent transcription factor that differentially regulates gene expression in Saccharomyces cerevisiae. *Gene Dev* **11**:3445-3458.

Mehdy MC and Firtel RA (1985) A secreted factor and cyclic AMP jointly regulate cell-type-specific gene expression in *Dictyostelium discoideum*. *Mol Cell Biol* **5**:705-713.

Melzer N, Villmann C, Becker K, Harvey K, Harvey RJ, Vogel N, Kluck CJ, Kneussel M and Becker CM (2010) Multifunctional basic motif in the glycine receptor

intracellular domain induces subunit-specific sorting. *J Biol Chem* **285**:3730-3739.

Mignery GA, Sudhof TC, Takei K and De Camilli P (1989) Putative receptor for inositol 1,4,5-trisphosphate similar to ryanodine receptor. *Nature* **342**:192-195.

Milne JL and Coukell MB (1991) A Ca^{2+} transport system associated with the plasma membrane of *Dictyostelium discoideum* is activated by different chemoattractant receptors. *J Cell Biol* **112**:103-110.

Miyawaki A, Llopis J, Heim R, McCaffery JM, Adams JA, Ikura M and Tsien RY (1997) Fluorescent indicators for Ca^{2+} based on green fluorescent proteins and calmodulin. *Nature* **388**:882-887.

Moniakis J, Coukell MB and Forer A (1995) Molecular cloning of an intracellular P-type ATPase from *Dictyostelium* that is up-regulated in calcium-adapted cells. *J Biol Chem* **270**:28276-28281.

Moniakis J, Coukell MB and Janiec A (1999) Involvement of the Ca^{2+}-ATPase PAT1 and the contractile vacuole in calcium regulation in *Dictyostelium discoideum*. *J Cell Sci* **112 (Pt 3)**:405-414.

Moreno C and Vaca L (2011) SOC AND NOW ALSO SIC: Store-operated and Store-inhibited Channels. *Iubmb Life* **63**:856-863.

Morgan AJ, Davis LC, Ruas M and Galione A (2015) TPC: the NAADP discovery channel? *Biochem Soc Trans* **43**:384-389.

Morgan AJ and Galione A (2014) Two-pore channels (TPCs): current controversies. *Bioessays* **36**:173-183.

Muñoz-Braceras S, Mesquita A and Escalante R (2013) *Dictyostelium discoideum* as a Model in Biomedical Research, in *Dictyostelids: Evolution, Genomics and Cell Biology* (Romeralo M, Baldauf S and Escalante R eds) pp 1-34, Springer Berlin Heidelberg, Berlin, Heidelberg.

Nakai J, Ohkura M and Imoto K (2001) A high signal-to-noise Ca^{2+} probe composed of a single green fluorescent protein. *Nature Biotechnology* **19**:137-141.

Nakamura T, Barbara JG, Nakamura K and Ross WN (1999) Synergistic release of Ca^{2+} from IP3-sensitive stores evoked by synaptic activation of mGluRs paired with backpropagating action potentials. *Neuron* **24**:727-737.

Navedo MF and Santana LF (2013) CaV1.2 sparklets in heart and vascular smooth muscle. *J Mol Cell Cardiol* **58**:67-76.

Nebl T and Fisher PR (1997) Intracellular Ca^{2+} signals in *Dictyostelium* chemotaxis are mediated exclusively by Ca^{2+} influx. *J Cell Sci* **110 (Pt 22)**:2845-2853.

Nguyen N, Biet M, Simard E, Beliveau E, Francoeur N, Guillemette G, Dumaine R, Grandbois M and Boulay G (2013) STIM1 participates in the contractile rhythmicity of HL-1 cells by moderating T-type Ca(2+) channel activity. *Biochim Biophys Acta* **1833**:1294-1303.

Nolta KV, Padh H and Steck TL (1993) An immunocytochemical analysis of the vacuolar proton pump in *Dictyostelium discoideum*. *J Cell Sci* **105 (Pt 3)**:849-859.

Ohashi R, Sakata S, Naito A, Hirashima N and Tanaka M (2014) Dendritic differentiation of cerebellar Purkinje cells is promoted by ryanodine receptors expressed by Purkinje and granule cells. *Dev Neurobiol* **74**:467-480.

Orkin S (1990) Molecular-Cloning - a Laboratory Manual, 2nd Edition - Sambrook,J, Fritsch,Ef, Maniatis,T. *Nature* **343**:604-605.

Palmer CP, Aydar E and Djamgoz MB (2005) A microbial TRP-like polycystic-kidney-disease-related ion channel gene. *Biochem J* **387**:211-219.

Paredes RM, Etzler JC, Watts LT, Zheng W and Lechleiter JD (2008) Chemical calcium indicators. *Methods* **46**:143-151.

Park CY, Shcheglovitov A and Dolmetsch R (2010) The CRAC channel activator STIM1 binds and inhibits L-type voltage-gated calcium channels. *Science* **330**:101-105.

Parkinson K, Baines AE, Keller T, Gruenheit N, Bragg L, North RA and Thompson CR (2014) Calcium-dependent regulation of Rab activation and vesicle fusion by an intracellular P2X ion channel. *Nat Cell Biol* **16**:87-98.

Parys JB, Sernett SW, DeLisle S, Snyder PM, Welsh MJ and Campbell KP (1992) Isolation, characterization, and localization of the inositol 1,4,5-trisphosphate receptor protein in Xenopus laevis oocytes. *J Biol Chem* **267**:18776-18782.

Patel S (2015) Function and dysfunction of two-pore channels. *Sci Signal* **8**:re7.

Patel S and Cai XJ (2015) Evolution of acidic Ca^{2+} stores and their resident Ca^{2+}-permeable channels. *Cell Calcium* **57**:222-230.

Patel S and Docampo R (2010) Acidic calcium stores open for business: expanding the potential for intracellular Ca^{2+} signaling. *Trends Cell Biol* **20**:277-286.

Perez CA, Huang L, Rong M, Kozak JA, Preuss AK, Zhang H, Max M and Margolskee RF (2002) A transient receptor potential channel expressed in taste receptor cells. *Nat Neurosci* **5**:1169-1176.

Petersen OH, Gerasimenko OV, Gerasimenko JV, Mogami H and Tepikin AV (1998) The calcium store in the nuclear envelope. *Cell Calcium* **23**:87-90.

Pitt SJ, Funnell TM, Sitsapesan M, Venturi E, Rietdorf K, Ruas M, Ganesan A, Gosain R, Churchill GC, Zhu MX, Parrington J, Galione A and Sitsapesan R (2010a) TPC2 is a novel NAADP-sensitive Ca^{2+} release channel, operating as a dual sensor of luminal pH and Ca^{2+}. *J Biol Chem* **285**:35039-35046.

Pitt SJ, Funnell TM, Sitsapesan M, Venturi E, Rietdorf K, Ruas M, Ganesan A, Gosain R, Churchill GC, Zhu MX, Parrington J, Galione A and Sitsapesan R (2010b) TPC2 Is a Novel NAADP-sensitive Ca^{2+} Release Channel, Operating as a Dual Sensor of Luminal pH and Ca^{2+}. *Journal of Biological Chemistry* **285**:35039-35046.

Pitt SJ, Lam AKM, Rietdorf K, Galione A and Sitsapesan R (2014) Reconstituted Human TPC1 Is a Proton-Permeable Ion Channel and Is Activated by NAADP or Ca^{2+}. *Science Signaling* **7**.

Plattner H and Verkhratsky A (2013) Ca^{2+} signalling early in evolution--all but primitive. *J Cell Sci* **126**:2141-2150.

Poloz Y and O'Day DH (2012) Ca^{2+} signaling regulates ecmB expression, cell differentiation and slug regeneration in *Dictyostelium*. *Differentiation* **84**:163-175.

Pottosin II, Tikhonova LI, Hedrich R and Schonknecht G (1997) Slowly activating vacuolar channels can not mediate Ca^{2+}-induced Ca^{2+} release. *Plant Journal* **12**:1387-1398.

Proenza C, O'Brien J, Nakai J, Mukherjee S, Allen PD and Beam KG (2002) Identification of a region of RyR1 that participates in allosteric coupling with the alpha(1s) (Ca(V)1.1) II-III loop. *Journal of Biological Chemistry* **277**:6530-6535.

Puertollano R and Kiselyov K (2009) TRPMLs: in sickness and in health. *Am J Physiol Renal Physiol* **296**:F1245-1254.

Putney JW, Jr. (1986) A model for receptor-regulated calcium entry. *Cell Calcium* **7**:1-12.

Rahman T, Cai X, Brailoiu GC, Abood ME, Brailoiu E and Patel S (2014) Two-pore channels provide insight into the evolution of voltage-gated Ca^{2+} and Na^{+} channels. *Sci Signal* **7**:ra109.

Rathi A, Kayman SC and Clarke M (1991) Induction of gene expression in *Dictyostelium* by prestarvation factor, a factor secreted by growing cells. *Dev Genet* **12**:82-87.

Ray S, Chen Y, Ayoung J, Hanna R and Brazill D (2011) Phospholipase D controls *Dictyostelium* development by regulating G protein signaling. *Cell Signal* **23**:335-343.

Raychowdhury MK, Gonzalez-Perrett S, Montalbetti N, Timpanaro GA, Chasan B, Goldmann WH, Stahl S, Cooney A, Goldin E and Cantiello HF (2004) Molecular pathophysiology of mucolipidosis type IV: pH dysregulation of the mucolipin-1 cation channel. *Hum Mol Genet* **13**:617-627.

Rietdorf J, Siegert F and Weijer CJ (1996) Analysis of optical density wave propagation and cell movement during mound formation in *Dictyostelium discoideum*. *Developmental Biology* **177**:427-438.

Rizzuto R, De Stefani D, Raffaello A and Mammucari C (2012) Mitochondria as sensors and regulators of calcium signalling. *Nat Rev Mol Cell Bio* **13**:566-578.

Rooney EK and Gross JD (1992) ATP-driven Ca^{2+}/H^{+} antiport in acid vesicles from *Dictyostelium*. *Proc Natl Acad Sci U S A* **89**:8025-8029.

Rooney EK, Gross JD and Satre M (1994) Characterisation of an intracellular Ca^{2+} pump in *Dictyostelium*. *Cell Calcium* **16**:509-522.

Roos J, DiGregorio PJ, Yeromin AV, Ohlsen K, Lioudyno M, Zhang S, Safrina O, Kozak JA, Wagner SL, Cahalan MD, Velicelebi G and Stauderman KA (2005) STIM1, an essential and conserved component of store-operated Ca^{2+} channel function. *J Cell Biol* **169**:435-445.

Ruas M, Chuang KT, Davis LC, Al-Douri A, Tynan PW, Tunn R, Teboul L, Galione A and Parrington J (2014) TPC1 Has Two Variant Isoforms, and Their Removal Has Different Effects on Endo-Lysosomal Functions Compared to Loss of TPC2. *Molecular and Cellular Biology* **34**:3981-3992.

Ruas M, Davis LC, Chen CC, Morgan AJ, Chuang KT, Walseth TF, Grimm C, Garnham C, Powell T, Platt N, Platt FM, Biel M, Wahl-Schott C, Parrington J and Galione A (2015) Expression of Ca(2)(+)-permeable two-pore channels rescues NAADP signalling in TPC-deficient cells. *EMBO J* **34**:1743-1758.

Ruas M, Rietdorf K, Arredouani A, Davis LC, Lloyd-Evans E, Koegel H, Funnell TM, Morgan AJ, Ward JA, Watanabe K, Cheng X, Churchill GC, Zhu MX, Platt FM, Wessel GM, Parrington J and Galione A (2010) Purified TPC isoforms form NAADP receptors with distinct roles for Ca(2+) signaling and endolysosomal trafficking. *Curr Biol* **20**:703-709.

Rybalchenko V, Ahuja M, Coblentz J, Churamani D, Patel S, Kiselyov K and Muallem S (2012) Membrane potential regulates nicotinic acid adenine dinucleotide phosphate (NAADP) dependence of the pH- and Ca^{2+}-sensitive organellar two-pore channel TPC1. *J Biol Chem* **287**:20407-20416.

Saran S, Nakao H, Tasaka M, Iida H, Tsuji FI, Nanjundiah V and Takeuchi I (1994) Intracellular free calcium level and its response to cAMP stimulation in developing *Dictyostelium* cells transformed with jellyfish apoaequorin cDNA. *FEBS Lett* **337**:43-47.

Schaap P (2016) Evolution of developmental signalling in Dictyostelid social amoebas. *Curr Opin Genet Dev* **39**:29-34.

Schaap P, Nebl T and Fisher PR (1996) A slow sustained increase in cytosolic Ca^{2+} levels mediates stalk gene induction by differentiation inducing factor in *Dictyostelium*. *EMBO J* **15**:5177-5183.

Schaloske R, Sonnemann J, Malchow D and Schlatterer C (1998) Fatty acids induce release of Ca^{2+} from acidosomal stores and activate capacitative Ca^{2+} entry in *Dictyostelium discoideum*. *Biochem J* **332 (Pt 2)**:541-548.

Schaloske RH, Lusche DF, Bezares-Roder K, Happle K, Malchow D and Schlatterer C (2005) Ca^{2+} regulation in the absence of the iplA gene product in *Dictyostelium discoideum*. *BMC Cell Biol* **6**:13.

Schatzle J, Bush J, Dharmawardhane S, Firtel RA, Gomer RH and Cardelli J (1993) Characterization of the signal transduction pathways and cis-acting DNA sequence responsible for the transcriptional induction during growth and development of the lysosomal alpha-mannosidase gene in *Dictyostelium discoideum*. *J Biol Chem* **268**:19632-19639.

Schatzle J, Rathi A, Clarke M and Cardelli JA (1991) Developmental Regulation of the Alpha-Mannosidase Gene in *Dictyostelium-Discoideum* - Control Is at the Level of Transcription and Is Affected by Cell-Density. *Molecular and Cellular Biology* **11**:3339-3347.

Schlatterer C, Gollnick F, Schmidt E, Meyer R and Knoll G (1994) Challenge with high concentrations of cyclic AMP induces transient changes in the cytosolic free calcium concentration in *Dictyostelium discoideum*. *J Cell Sci* **107 (Pt 8)**:2107-2115.

Schlatterer C, Knoll G and Malchow D (1992) Intracellular calcium during chemotaxis of *Dictyostelium discoideum*: a new fura-2 derivative avoids sequestration of the indicator and allows long-term calcium measurements. *Eur J Cell Biol* **58**:172-181.

Schulze C, Sticht H, Meyerhoff P and Dietrich P (2011) Differential contribution of EF-hands to the Ca(2)(+)-dependent activation in the plant two-pore channel TPC1. *Plant J* **68**:424-432.

Seoh SA, Sigg D, Papazian DM and Bezanilla F (1996) Voltage-sensing residues in the S2 and S4 segments of the Shaker K^+ channel. *Neuron* **16**:1159-1167.

Shigaki T, Rees I, Nakhleh L and Hirschi KD (2006) Identification of three distinct phylogenetic groups of CAX cation/proton antiporters. *J Mol Evol* **63**:815-825.

Shimomura O, Musicki B and Kishi Y (1989) Semi-synthetic aequorins with improved sensitivity to Ca^{2+} ions. *Biochem J* **261**:913-920.

Shuttleworth TJ (2009) Arachidonic acid, ARC channels, and Orai proteins. *Cell Calcium* **45**:602-610.

Siegert F and Weijer C (1989) Digital Image-Processing of Optical-Density Wave-Propagation in *Dictyostelium-Discoideum* and Analysis of the Effects of Caffeine and Ammonia. *Journal of Cell Science* **93**:325-335.

Sivaramakrishnan V and Fountain SJ (2012) A mechanism of intracellular P2X receptor activation. *J Biol Chem* **287**:28315-28326.

Sivaramakrishnan V and Fountain SJ (2013) Intracellular P2X receptors as novel calcium release channels and modulators of osmoregulation in *Dictyostelium*: a comparison of two common laboratory strains. *Channels (Austin)* **7**:43-46.

Sonnemann J, Knoll G and Schlatterer C (1997) cAMP-induced changes in the cytosolic free Ca^{2+} concentration in *Dictyostelium discoideum* are light sensitive. *Cell Calcium* **22**:65-74.

Souza GM, Lu S and Kuspa A (1998) YakA, a protein kinase required for the transition from growth to development in *Dictyostelium*. *Development* **125**:2291-2302.

Soyombo AA, Tjon-Kon-Sang S, Rbaibi Y, Bashllari E, Bisceglia J, Muallem S and Kiselyov K (2006) TRP-ML1 regulates lysosomal pH and acidic lysosomal lipid hydrolytic activity. *J Biol Chem* **281**:7294-7301.

Spat A, Bradford PG, McKinney JS, Rubin RP and Putney JW, Jr. (1986) A saturable receptor for 32P-inositol-1,4,5-triphosphate in hepatocytes and neutrophils. *Nature* **319**:514-516.

Sun M, Goldin E, Stahl S, Falardeau JL, Kennedy JC, Acierno JS, Bove C, Kaneski CR, Nagle J, Bromley MC, Colman M, Schiffmann R and Slaugenhaupt SA (2000) Mucolipidosis type IV is caused by mutations in a gene encoding a novel transient receptor potential channel. *Human Molecular Genetics* **9**:2471-2478.

Supattapone S, Worley PF, Baraban JM and Snyder SH (1988) Solubilization, purification, and characterization of an inositol trisphosphate receptor. *J Biol Chem* **263**:1530-1534.

Takai A, Nakano M, Saito K, Haruno R, Watanabe TM, Ohyanagi T, Jin T, Okada Y and Nagai T (2015) Expanded palette of Nano-lanterns for real-time multicolor luminescence imaging. *Proc Natl Acad Sci U S A* **112**:4352-4356.

Taylor CW, da Fonseca PCA and Morris EP (2004) IP3 receptors: the search for structure. *Trends in Biochemical Sciences* **29**:210-219.

Teo R, Lewis KJ, Forde JE, Ryves WJ, Reddy JV, Rogers BJ and Harwood AJ (2010) Glycogen synthase kinase-3 is required for efficient *Dictyostelium* chemotaxis. *Mol Biol Cell* **21**:2788-2796.

Thompson CR and Kay RR (2000) The role of DIF-1 signaling in *Dictyostelium* development. *Mol Cell* **6**:1509-1514.

Tomchik KJ and Devreotes PN (1981) Adenosine 3',5'-monophosphate waves in *Dictyostelium discoideum*: a demonstration by isotope dilution--fluorography. *Science* **212**:443-446.

Touchberry CD, Bales IK, Stone JK, Rohrberg TJ, Parelkar NK, Nguyen T, Fuentes O, Liu X, Qu CK, Andresen JJ, Valdivia HH, Brotto M and Wacker MJ (2010) Phosphatidylinositol 3,5-bisphosphate (PI(3,5)P2) potentiates cardiac contractility via activation of the ryanodine receptor. *J Biol Chem* **285**:40312-40321.

Traynor D and Kay RR (2016) A polycycstin-type transient receptor potential (Trp) channel that is activated by ATP. *Biol Open*.

Traynor D, Milne JL, Insall RH and Kay RR (2000) Ca(2+) signalling is not required for chemotaxis in *Dictyostelium*. *EMBO J* **19**:4846-4854.

Tsien RY, Pozzan T and Rink TJ (1982) T-cell mitogens cause early changes in cytoplasmic free Ca^{2+} and membrane potential in lymphocytes. *Nature* **295**:68-71.

Tu CL, Oda Y, Komuves L and Bikle DD (2004) The role of the calcium-sensing receptor in epidermal differentiation. *Cell Calcium* **35**:265-273.

Tuluc P and Flucher BE (2011) Divergent biophysical properties, gating mechanisms, and possible functions of the two skeletal muscle Ca(V)1.1 calcium channel splice variants. *J Muscle Res Cell Motil* **32**:249-256.

van Haastert PJ, Keizer-Gunnink I and Kortholt A (2007) Essential role of PI3-kinase and phospholipase A2 in *Dictyostelium discoideum* chemotaxis. *J Cell Biol* **177**:809-816.

Venkatachalam K and Montell C (2007) TRP channels. *Annu Rev Biochem* **76**:387-417.

Vinet AF, Fiedler T, Studer V, Froquet R, Dardel A, Cosson P and Pieters J (2014) Initiation of multicellular differentiation in *Dictyostelium discoideum* is regulated by coronin A. *Mol Biol Cell* **25**:688-701.

Walseth TF, Lin-Moshier Y, Jain P, Ruas M, Parrington J, Galione A, Marchant JS and Slama JT (2012) Photoaffinity labeling of high affinity nicotinic acid adenine dinucleotide phosphate (NAADP)-binding proteins in sea urchin egg. *J Biol Chem* **287**:2308-2315.

Wang X, Zhang X, Dong XP, Samie M, Li X, Cheng X, Goschka A, Shen D, Zhou Y, Harlow J, Zhu MX, Clapham DE, Ren D and Xu H (2012) TPC proteins are phosphoinositide- activated sodium-selective ion channels in endosomes and lysosomes. *Cell* **151**:372-383.

Wang Y, Deng X, Mancarella S, Hendron E, Eguchi S, Soboloff J, Tang XD and Gill DL (2010) The calcium store sensor, STIM1, reciprocally controls Orai and CaV1.2 channels. *Science* **330**:105-109.

Ward JM and Schroeder JI (1994) Calcium-Activated K^+ Channels and Calcium-Induced Calcium Release by Slow Vacuolar Ion Channels in Guard Cell Vacuoles Implicated in the Control of Stomatal Closure. *Plant Cell* **6**:669-683.

Weeks G (1976) The manipulation of the fatty acid composition of *Dictyostelium discoideum* and its effect on cell differentiation. *Biochim Biophys Acta* **450**:21-32.

Wilczynska Z, Happle K, Muller-Taubenberger A, Schlatterer C, Malchow D and Fisher PR (2005) Release of Ca^{2+} from the endoplasmic reticulum contributes to Ca^{2+} signaling in *Dictyostelium discoideum*. *Eukaryot Cell* **4**:1513-1525.

Yamaguchi S, Jha A, Li Q, Soyombo AA, Dickinson GD, Churamani D, Brailoiu E, Patel S and Muallem S (2011) Transient receptor potential mucolipin 1 (TRPML1) and two-pore channels are functionally independent organellar ion channels. *J Biol Chem* **286**:22934-22942.

Yuen IS and Gomer RH (1994) Cell density-sensing in *Dictyostelium* by means of the accumulation rate, diffusion coefficient and activity threshold of a protein secreted by starved cells. *J Theor Biol* **167**:273-282.

Yuen IS, Jain R, Bishop JD, Lindsey DF, Deery WJ, Van Haastert PJ and Gomer RH (1995) A density-sensing factor regulates signal transduction in *Dictyostelium*. *J Cell Biol* **129**:1251-1262.

Yumura S, Furuya K and Takeuchi I (1996) Intracellular free calcium responses during chemotaxis of *Dictyostelium* cells. *J Cell Sci* **109 (Pt 11)**:2673-2678.

Yumura S, Matsuzaki R and Kitanishi-Yumura T (1995) Introduction of macromolecules into living *Dictyostelium* cells by electroporation. *Cell Struct Funct* **20**:185-190.

Zhang F, Jin S, Yi F and Li PL (2009) TRP-ML1 functions as a lysosomal NAADP-sensitive Ca^{2+}release channel in coronary arterial myocytes. *Journal of Cellular and Molecular Medicine* **13**:3174-3185.

Zhang F and Li PL (2007) Reconstitution and characterization of a nicotinic acid adenine dinucleotide phosphate (NAADP)-sensitive Ca^{2+} release channel from liver lysosomes of rats. *J Biol Chem* **282**:25259-25269.

Zhang SL, Yeromin AV, Zhang XHF, Yu Y, Safrina O, Penna A, Roos J, Stauderman KA and Cahalan MD (2006) Genome-wide RNAi screen of Ca^{2+} influx identifies genes that regulate Ca^{2+} release-activated Ca^{2+} channel activity. *P Natl Acad Sci USA* **103**:9357-9362.

Zhang SYL, Yu Y, Roos J, Kozak JA, Deerinck TJ, Ellisman MH, Stauderman KA and Cahalan MD (2005) STIM1 is a Ca^{2+} sensor that activates CRAC channels and migrates from the Ca^{2+} store to the plasma membrane. *Nature* **437**:902-905.

Zhang ZH, Lu YY and Yue J (2013) Two pore channel 2 differentially modulates neural differentiation of mouse embryonic stem cells. *PLoS One* **8**:e66077.

Zhu MX, Evans AM, Ma J, Parrington J and Galione A (2010) Two-pore channels for integrative Ca signaling. *Commun Integr Biol* **3**:12-17.

Zhu Q, Liu T and Clarke M (1993) Calmodulin and the contractile vacuole complex in mitotic cells of *Dictyostelium discoideum*. *J Cell Sci* **104 (Pt 4)**:1119-1127.